Fluorine and Fluorinated Motifs in the Design and Application of Bioisosteres for Drug Design

Nicholas A. Meanwell*

Discovery Chemistry and Molecular Technologies Bristol-Myers Squibb Research and Development P.O. Box 4000, Princeton, New Jersey 08543-4000, United States

ABSTRACT: The electronic properties and relatively small size of fluorine endow it with considerable versatility as a bioisostere and it has found application as a substitute for lone pairs of electrons, the hydrogen atom, and the methyl group while also acting as a functional mimetic of the carbonyl, carbinol, and nitrile moieties. In this context, fluorine substitution can influence the potency, conformation, metabolism, membrane permeability, and P-gp recognition of a molecule and temper inhibition of the hERG channel by basic amines. However, as a consequence of the unique properties of fluorine, it features prominently in the design of higher order structural metaphors that are more esoteric in their conception and which reflect a more sophisticated molecular construction that broadens biological mimesis. In this Perspective, applications of fluorine in the construction of bioisosteric elements designed to enhance the in vitro and in vivo properties of a molecule are summarized.
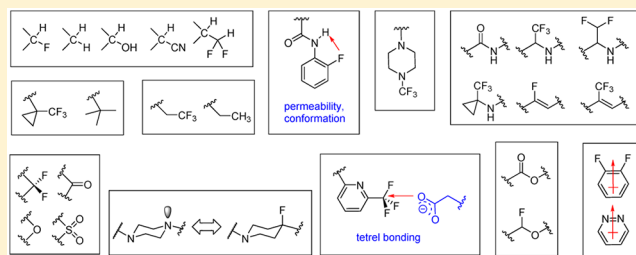
INTRODUCTION

The design of bioisosteres is a useful principle in drug design that, although widely practiced, is contextual in application. Thus, the design of bioisosteres requires detailed insight into the physicochemical properties of an element, heterocycle, or functional group if effective emulation is to be achieved and, ideally, complemented by a similar level of understanding of the binding site of a molecule.[1] Bioisosterism has its origins in the concept of isosterism between relatively simple functionality and small molecules that was advanced by Moir and Langmuir a century ago.[1] However, contemporary interpretations of structural metaphors in a biological setting accommodate a much broader range of bioisosteric structural motifs that can vary considerably in size and shape from the functionality being emulated.[1,2] Thus, modern bioisosteric relationships are rooted far more in functional reproduction of biochemical pharmacological properties that reflect aspects of molecular recognition that are often unique to a specific environment.[1] Consequently, the relationship between shape and/or aspects of physicochemical properties of a bioisostere can be oblique. Fluorine has played a prominent role in drug design since the approval of the first fluorinated drug, the synthetic 9α-fluoro-substituted corticosteroid fludrocortisone (**1**), on August 18, 1955.[3] The applications of fluorine in the design of drugs and agricultural chemicals continues to grow as our knowledge and understanding of how to take full advantage of the unique properties of this element matures.[4−6] This has been fostered by the development of innovative synthetic methodology which is providing access to new fluorinated motifs with interesting topographies and physicochemical attributes.[7] While early applications of fluorine as a bioisostere focused on the relatively simple replacement of hydrogen atoms in drug molecules, often as a means of influencing metabolism, the last 20 years has seen broader deployment of fluorine and

fluorinated motifs in the construction of more sophisticated structural arrangements that are able to emulate and influence a number of more traditional functionalities. In this Perspective, I provide a synopsis of some of the practical applications of fluorine as a bioisostere in drug design, ranging from the simple substitution of the hydrogen atom in the setting of alkyl and aromatic moieties to examples that utilize fluorine in conjunction with additional functionalities to explore bioisosteric relationships that are more esoteric in nature and which are, in some cases, less well developed.

1
(fludrocortisone)
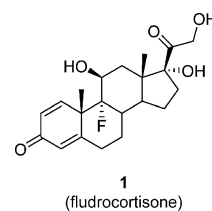
KEY PROPERTIES OF FLUORINE OF RELEVANCE TO BIOISOSTERE DESIGN

The effective application of fluorine in drug design requires an understanding of its key physicochemical properties, and those of relevance to the design of bioisosteres are summarized in Table 1.[4,8] Fluorine is approximately 20% larger than hydrogen based on comparison of the van der Waals radii, while the length and size of a C−F bond is more closely aligned with a C=O bond than either the shorter C−H or longer C−OH, C−C≡N, or S=O bonds. The electronegativity of fluorine is closer to that of oxygen, which is reflected in the dipole moment of the C−F

Table 1. Key Properties of the C−F Bond Compared to the C−H, C=O, C−OH, C−C≡N, and S=O Bonds

bond	bond length (Å)	van der Waals radius (Å)	van der Waals volume of atom (Å^3)	total size (Å^3)	electronegativity of the element	dipole moment μ (D)	π	bond dissociation energy (kcal/mol)
C−H	1.09	1.20	7.24	2.29	2.20	~−0.4	0	98.8
C−F	1.35	1.47	13.31	2.82	3.98	1.41	0.14	105.4
C−Cl	1.77	1.75	22.45		3.16	1.87 (CH_3Cl)	0.71	78.5
C=O	1.23	1.52	14.71	2.73	3.44	2.33 ($H_2C=O$)	CHO: −0.65	85 (π bond)
C−OH	1.43 (CH_3OH)	1.52	14.71		3.44	2.87 (CH_3OH)	−0.67	84.0
	1.48 ($CH_3 CH_2OH$)					1.66 ($CH_3 CH_2OH$)		
C−C≡N	2.22 (HCN)					3.92 (CH_3CN)	−0.57	
S=O	1.44 ($CH_3SO_2 CH_3$)	1.52	14.71		3.44	4.44 ($CH_3SO_2 CH_3$)[9]	CH_3SO: −1.58	
							CH_3SO_2: −1.63	

Table 2. Comparisons of the Size of Alkyl and CF$_3$ Groups Based on Van Der Waals Volume, *A* Values, Taft Es Values, Biphenyl Interference Values, and the Activity of the Two Structurally-Related Series of MMP-9 Inhibitor Probes 2 and 3

	vdW volume (Å^3)	*A* value (kcal/mol)	Taft Es value	biphenyl rotational interference value (kcal/mol)[14]	experimental biphenyl rotational *B* value ($\Delta G^{\ddagger}_{rot}$, kcal/mol)[15]	inhibition of MMP-9 by **2/3** IC$_{50}$ (nM)[16]
H	1.20		0			
F	13.3	0.15	−0.46	4.6	4.4	
Me	21.6	1.70	−1.24	9.7	7.4	1/10
Et	38.9	1.70	−1.31		8.7	2/27
CF$_3$	39.8	2.10	−2.40	12.1	10.5	87/22
iPr	56.2	2.15	−1.71	12.6	11.1	1800/4500
tBu		>4.50	−2.78	18.3	15.4	

bond being larger and in the opposite direction of a C−H but less than that of C=O, S=O, C−OH, and C−C≡N moieties. Fluorine is modestly more lipophilic than a hydrogen atom and significantly more lipophilic than OH, C=O, C≡N, or sulfoxide and sulfone substituents. Unlike chlorine, bromine, and iodine, fluorine does not engage in halogen bonding and is nonpolarizable, a property that underlies strong electrostatic interactions which can be attractive or repulsive.[4] These properties confer fluorine with considerable versatility such that it has been explored as a potential bioisostere of the hydrogen atom, carbonyl and sulfonyl functionalities, the carbinol moiety, and the nitrile, with effective functional mimicry very much dependent upon the biochemical context.

■ FLUORINE AS A BIOISOSTERE OF THE HYDROGEN ATOM IN ALKYL MOIETIES

Developability Aspects Associated with Fluorination and the Size of the CF$_3$ Moiety. Replacing hydrogen atoms with fluorine has been explored extensively in drug design, most commonly to replace those bound to an aromatic ring or in the context of a CF$_3$ for CH$_3$ replacement where these substitutions can modulate potency or interfere with metabolic modification.[10] The replacement of a hydrogen atom by fluorine would be expected to add to the physical size, modestly increase the lipophilicity of a molecule based on the π coefficient of 0.14 determined for fluorine, but more significantly increase molecular weight (MW) (Table 1). Thus, the replacement of a CH$_3$ by CF$_3$ would be expected to increase the overall lipophilicity of a molecule (cLog *P*) by 0.42 and add 54 Da to the MW, parameters that would be anticipated to negatively affect ligand efficiency metrics.[11] However, fluorination of a molecule does not necessarily lead to an increase in lipophilicity, and several structural motifs are associated with increased polarity based on a matched molecular pairs (MMP) analyses.[4d,12] Fluorine atoms that are deployed in a molecule such that they are proximal to an oxygen atom, separated by a distance of <3.1 Å, can exhibit a lower measured Log *P* value, while vicinal alkyl fluorides offer increased polarity as a function

of C−F dipole alignment that is favored by the gauche effect, stabilizing a more polar conformation (vide infra). Adding to these observations, concerns around the effect of fluorination on ligand efficiency metrics has been addressed by a careful MMP analysis of the performance of a large data set of compounds evaluated in in vitro developability assays.[13] This study, in which fluorine was present in a range of environments but most commonly incorporated as an aryl-F, aryl-CF$_3$, or an aryl-CF$_2$H motif, concluded that polyfluorination may not necessarily represent a deleterious modification. On the basis of an analysis of P-glycoprotein (P-gp) recognition, lipophilicity, metabolic stability, and membrane permeability using assays conducted in vitro, fluorine was found to behave more like a hydrogen atom, leading to the contention that up to five fluorine atoms can be introduced into a molecule without a significant impact on performance in these assays.[13] As a consequence, it was suggested that the MW increase associated with the introduction of fluorine may be ignored in efficiency metric calculations and that the fluorine-corrected molecular weight MW$_{FC}$ (MW$_{FC}$ = total MW − MW of the fluorine atoms present in the molecule) should be used as a more suitable and relevant descriptor for this purpose.[13]

The size of the CF$_3$ moiety has also been somewhat challenging to definitively assess and this moiety has often been considered to be isosteric with an iso-propyl substituent, although it is clearly of a different shape.[4g] The calculated van der Waals volumes, the *A* values, and both experimental measures of biphenyl rotational interference compiled in Table 2 all indicate that the CF$_3$ is a smaller than an iso-propyl substituent with the exception of the Taft Es value which uniquely indicates the reverse, although the differences projected by several of these measurements are relatively modest.[14,15] Under some circumstances, the CF$_3$ moiety has been found to sterically dominate a phenyl or *tert*-butyl substituent in defining the stereochemical outcome of an aldol reaction.[15d−f] Assessing the size of the CF$_3$ moiety in biochemical applications is unlikely to simplify the inherent complexity associated with this question given the context-dependent nature of drug−target interactions. Nevertheless, an experiment designed

to compare the size of the CF_3 and an iso-propyl substituent in a biological context has been conducted with matrix metalloprotease-9 inhibitors where the alkyl side chains of **2** and **3** project into the well-defined lipophilic S1′ pocket of the enzyme.[16] In both series, an alkyl chain terminating in CH_3 or CH_3CH_2 was associated with potent inhibitory activity, while the respective iso-propyl homologues were over 1000-fold weaker; however, the two CF_3-substituted derivatives largely retained the potency of the smaller alkyl groups, data captured in Table 2. These results indicate that, in this specific context, the CF_3 moiety could be considered to be bioisosteric with an ethyl rather than an iso-propyl substituent.[16]

R = CH_3, CH_3CH_2, iPr, CF_3

2: R_1 = H
3: R_1 = OCH_3
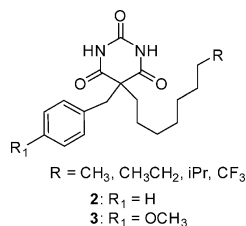
**Fluorination as an Approach to Reducing Metabolism.** Because the introduction of fluorine can lead to resistance toward oxidative metabolism, fluorination has developed into a popular approach to addressing the poor pharmacokinetic performance of compounds in vitro and in vivo.[10,17] Under some circumstances, a CH_3 substituent can be replaced directly by a fluorine atom despite being 40−50% smaller, although metabolically labile alkyl groups are more commonly addressed by more sophisticated motifs in which the CF_3 moiety plays a prominent role. While the introduction of fluorine is often directed specifically toward a metabolic soft spot, the effects of fluorination can be indirect and complex. As a consequence, the effect can range from negative or null, possibly due to redirecting metabolism to an alternative site, to global protection toward metabolic modification, while the effects exerted on the metabolic stability of proximal functionality can be positive or negative dependent upon context.[18−20]

Examples where replacing hydrogen atoms with fluorine exerts a positive effect on metabolism are provided by the taxoids **4** and **5**, which are related to paclitaxel (**6**) and the GPR119 agonists **7** and **8**.[21,22] For the taxoid derivatives, CYP 3A4 oxidation of the C-3′ iso-butenyl CH_3 groups of **4** represented an important metabolic pathway that prompted replacement of the allylic methyl substituents by fluorine, affording **5**. Fluorinated derivative **5** exhibited highly potent cytotoxicity toward a series of human cancer cell lines, with a 10−1000-fold advantage over **6**.[21] Remarkably, **5** was quite resistant to metabolic modification in the presence of CYP 450 enzymes, with the introduction of the two fluorine atoms providing protection against metabolic modification

at the C-3′ N-t-Boc and C-6 methylene moieties known to be the major sites of metabolic lability in the homologue **6**.[21]

4: R = CH_3
5: R = F

6
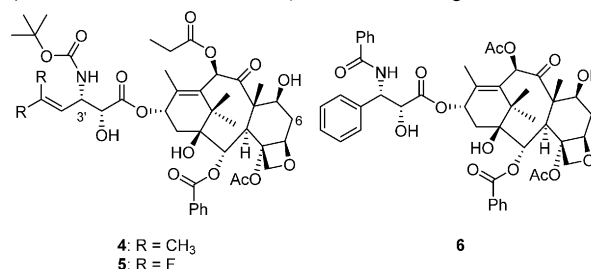
In the example provided by GPR119 agonists, compound **7** displayed poor metabolic stability in vitro which was attributed to its high lipophilicity, ELog D = 4.3.[22] Replacing of the CH_3 substituent β- to the amide N atom with fluorine afforded **8**, which exhibited enhanced metabolic stability while also illuminating aspects of the bound conformation. This was the result of the N-β-fluoroethylamide adopting a preferred conformation in which the two elements were in a gauche relationship (vide infra), which constituted about 75% of the conformer population on the NMR time scale.[22]
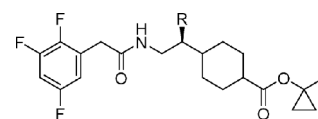
7: R = CH_3
EC_50 (h-cAMP) = 44 nM; IA = 124%
Cl_int (HLM) = >300 mL/min/kg

8: R = F
EC_50 (h-cAMP) = 80 nM; IA = 107%
Cl_int (HLM) = 42.44 mL/min/kg

In a study seeking replacements for a *tert*-butyl moiety that would offer improved metabolic stability, systematic modifications to the 3 methyl groups were explored in the context of the simple biphenyl derivative 6-(4-(*tert*-butyl)phenyl)nicotinonitrile (**9**) (Table 3).[23,24] The effects of structural modification were compared with compound persistence when incubated in rat and human liver microsomes (RLM and HLM), respectively, with the results summarized in Table 3. While some success was achieved with the polar substituents found in **10−13**, these were viewed as potential liabilities in the context of a drug target where the *tert*-butyl group may be accommodated in a hydrophobic binding pocket. The CF_3-susbstitued cyclopropyl (Cp-CF_3) moiety exemplified in **17** emerged as the optimal lipophilic substituent, with higher metabolic stability in both RLM and HLM preparations than **14−16**.

To further demonstrate the utility of the Cp-CF_3 substituent, comparison of liver microsomal stability data for six matched

**Table 3. RLM and HLM Half-Life Values Associated with a Series of 6-(4-Substituted-phenyl) Nicotinonitrile Derivatives 9−17**
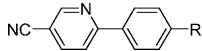
	9	10	11	12	13	14	15	16	17
R		OH	CN	CO_2H	O		CF_3		F_3C
RLM t_{1/2} (min)	30	125	70	135	37	7	25	11	>400
RLM t_{1/2} (min)	51	202	122	274	38	9	66	35	150

pairs of biphenyl amide derivatives was probed, where the outcome was a positive result in each case, and as a replacement for the metabolically labile *tert*-butyl moiety in the steroid 5α-reductase inhibitor finasteride (**18**).[24] The Cp-CF$_3$ analogue **19** exhibited a $t_{1/2}$ in HLM of 114 min which compared to 63 min for **18**, with recognition that in this particular example, the modification may not protect against metabolism at other sites of the molecule and may cause a redirection of metabolism to alternative sites.


18: R = *t*Bu   **19**: R = Cp-CF$_3$
HLM $t_{1/2}$ = 63 min   HLM $t_{1/2}$ = 114 min
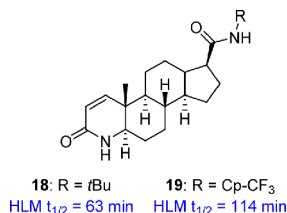
The Cp-CF$_3$ moiety featured prominently in a complementary study in which a series of *tert*-butyl isosteres were the subject of detailed in vitro profiling when installed in the background of the dual endothelin A and B antagonist bosentan (**20**) and the CCR-9 antagonist vercirnon (**21**), both of which contain a 4-(*tert*-butyl)benzenesulfonamide moiety.[25] In this analysis, the profiles of the *tert*-butyl progenitors were compared with the Cp-CF$_3$, CF$_3$, SF$_5$, and [1.1.1]-bicyclopentane (BCP) homologues, with the calculated relative sizes of these substituents compiled in Table 4. With the exception of Cp-CF$_3$, all of the substituents are smaller than a *tert*-butyl, and Log D measurements indicated that lipophilicity increased in the order of CF$_3$ < SF$_5$ < Cp-CF$_3$ < tBu < BCP while the pK_a of the sulfonamide N−H increased in the order of SF$_5$ < CF$_3$ < Cp-CF$_3$ < tBu ≈ BCP.
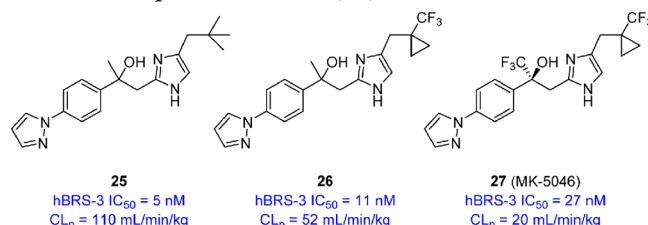

20   **21**
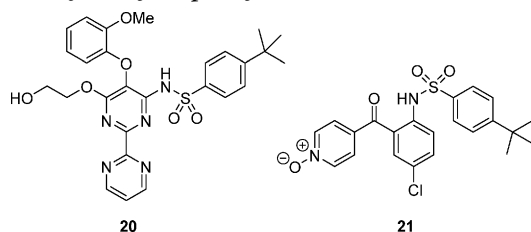
In the context of **20**, the Cp-CF$_3$- and BCP-substituted analogues performed similarly to the parent molecule as antagonists at the endothelin A and B receptors, while the CF$_3$- and SF$_5$-substituted derivatives were 10-fold less potent.[25] When incorporated as *tert*-butyl replacements in **21**, all of the substituents performed similarly to the prototype in a CCR9 functional assay.

In both series of compounds, there was a trend toward enhanced metabolic stability in liver microsomes for these substituents compared to the *tert*-butyl-substituted prototypes, with CF$_3$ and SF$_5$ the most effective. No significant CYP inhibitory effects were observed with either series, but the effects on solubility were varied in analogues of **20** while all of the modifications led to reduced solubility in the context of **21**.

These general observations have support from examples harvested from studies conducted across a range of compound structures with widely varying biochemical mechanisms, although there are unique contextual variations in individual performance. For example, the FMS-like tyrosine kinase 3 (FLT3) inhibitor quizartinib (**22**), which is in phase 3 clinical trials for the treatment of acute myeloid leukemia (AML), is metabolized at the *tert*-butyl moiety in humans to afford alcohol **23**.[26,27] This lability was addressed in a related series of compounds by replacing the *tert*-butyl substituent with Cp-CF$_3$, with **24** characterized as a potent FLT3 inhibitor, K_d = 0.6 nM, with improved metabolic stability compared to its *tert*-butyl progenitor.[28]

22: R = H (quizartinib)   **24**
23: R = OH
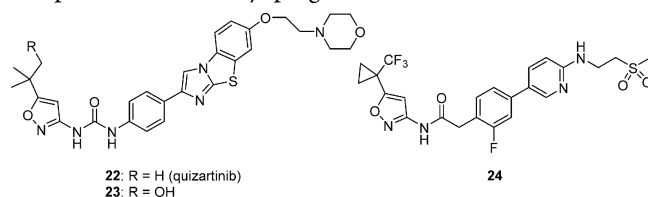
The Cp-CF$_3$ moiety in the human bombesin receptor subtype-3 (hBRS-3) agonist **26** provided a partial solution to the high metabolic turnover rate observed with the prototype **25**, with further refinement of the carbinol CH$_3$ to a CF$_3$ affording the more advanced compound MK-5046 (**27**).[29]

25
hBRS-3 IC$_{50}$ = 5 nM
CL$_p$ = 110 mL/min/kg

26
hBRS-3 IC$_{50}$ = 11 nM
CL$_p$ = 52 mL/min/kg

**27** (MK-5046)
hBRS-3 IC$_{50}$ = 27 nM
CL$_p$ = 20 mL/min/kg

The 1,1,1-trifluoro-2-methylpropan-2-yl moiety addressed the metabolic lability of the *tert*-butyl substituent of the selective phosphatidylinositol-3 kinase-α (PI3Kα) inhibitor **28**, a precursor to alpelisib (NVP-BYL719, **29**) which is currently in phase 3 clinical trials for the treatment of breast cancer (Table 5).[30]

Table 4. Calculated Volumes of a Series of Substituents Normalized to the *tert*-Butyl Moiety

substituent	-CF$_3$	-SF$_5$			
relative size normalized to the tert-butyl moiety	-34.9 Å^3	-11.1 Å^3	-4.1 Å^3	0	+4.14 Å^3

Table 5. SARs, Metabolic Stability, and in Vivo Clearance Associated with the PI3Kα Inhibitors 28 and 29
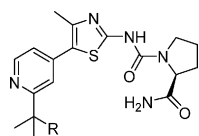
	R	P110α IC$_{50}$ (nM)	P110β IC$_{50}$ (nM)	P110δ IC$_{50}$ (nM)	P110γ IC$_{50}$ (nM)	RLM clearance (µL/min/mg)	rat clearance in vivo (mL/min/kg)
28	CH$_3$	14	4400	330	430	77	39
29	CF$_3$	5	1200	290	250	29	10

The main metabolic pathways for **28** were determined to be hydroxylation of one of the CH$_3$ moieties of the *tert*-butyl element and hydrolysis of the primary amide. The design of **29** was inspired by an examination of an X-ray cocrystal structure which indicated scope to slightly enlarge the size of *tert*-butyl moiety in order to more completely fill the pocket of the enzyme into which it projected. In the event, the CF$_3$ analogue not only retarded metabolism at this site, leading to lower clearance in vivo and excellent oral bioavailability (F = 106% in mouse, F = 58% in rat, and F = 140% in dog) but also enhanced potency by 2-fold. In the cocrystal structure of **28** with PI3Kα, one fluorine atom of the CF$_3$ moiety was described as engaging in a hydrogen-bonding interaction with the protonated amine of Lys$_{802}$, while the bound conformation of the inhibitor was stabilized by an intramolecular interaction between one of the lone pairs of electrons on the urea oxygen atom and the low lying C−S σ^* of the sulfur atom of the thiazole, interactions depicted in Figure 1.[30,31]
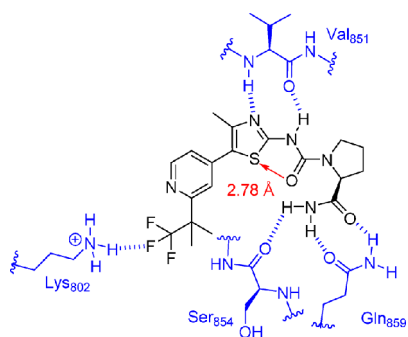

Figure 1. Key drug−target interactions between **29** and the PI3Kα enzyme and conformational bias provided by an intramolecular O to S interaction.

Similarly, in a series of inhibitors of V-RAF murine sarcoma viral oncogene homologue B1 (BRAF) that led to the discovery of CEP-32496 (**30**), the 1,1,1-trifluoro-2-methylpropan-2-yl substituent was a more effective bioisostere of a *tert*-butyl substituent that adequately addressed the metabolic lability associated with the prototype, preserving potency in this example more effectively than a Cp-CF$_3$ substituent which was a 2-fold weaker enzyme inhibitor.[32]
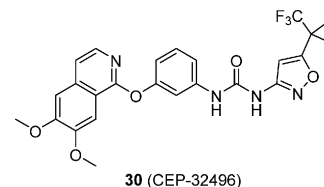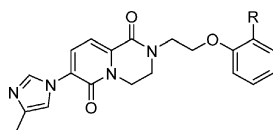

30 (CEP-32496)

In a series of γ-secretase modulators based on the *tert*-butyl-substituted lead compound **31**, which combined modest potency with poor metabolic stability, substituting one of the CH$_3$ moieties with a CF$_3$ gave **32**, which significantly improved both parameters (Table 6).[33] This result allowed further refinement of the structure by pruning of the substituent which revealed that both potency and metabolic stability were dependent upon the absolute configuration of the trifluoroethyl moiety. The (R)-isomer **33** was found to be superior to the (S)-antipode **34** and it was this motif that was retained in the optimized molecule **35** where the addition of a CH$_3$ moiety to the linker element was found to improve potency by a further 3-fold. More recently the CF$_3$ oxetane was evaluated as a *tert*-butyl replacement in the context of **36**, a modification that retained biological potency while lowering E Log P, enhancing LipE, and improving metabolic stability in HLM compared to **31**.[34]

The triazole-based CF$_3$ substituent in sitagliptin (**40**), a potent dipeptidyl peptidase-4 (DPP-4) inhibitor marketed for the treatment of type 2 diabetes, is an important determinant of both its in vitro and in vivo profile.[35] In this example, the CF$_2$H (**38**) and CF$_3$ (**40**) moieties performed more effectively as bioisosteres

Table 6. SARs, Lipophilicity, and Metabolic Stability Associated with a Series of γ-Secretase Modulators 31−36[a]

|	R	R	IC$_{50}$ (Aβ42, nM)	cLog P	LipE*	HLM clearance (mL/min/kg)
31	H	(tert-butyl)	128	3.3	3.6	95.7
32	H	CF$_3$	30	3.2	4.3	24.3
33	H	CF$_3$	20	2.8	4.9	12.3
34	H	CF$_3$	85	2.8	4.3	23.4
35	F	CF$_3$	20	2.8	4.9	12.3
36	F	CF$_3$ (oxetane)	74	1.9	5.2	37.1

[a]*LipE = pIC$_{50}$ − Log P.

Table 7. SAR, Metabolic Stability, and Oral Bioavailability of the Series of DPP-4 Inhibitors 37–40
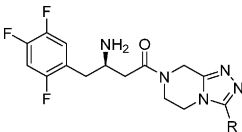
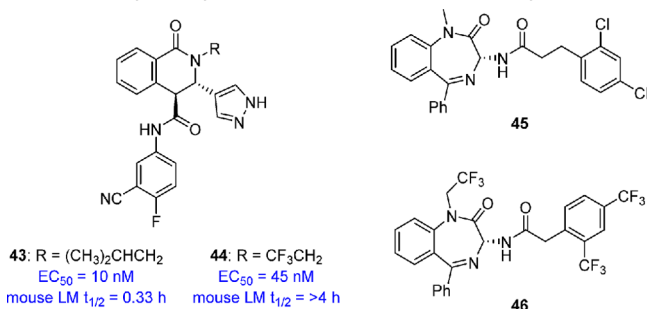|	R	DPP-4 IC$_{50}$ (nM)	rat clearance (mL/min/kg)	oral bioavailability (F, %)^a
37	CH$_2$CH$_3$	37	70	2
38	CF$_2$H	29	66	39
39	CF$_2$CF$_3$	71	58	61
40	CF$_3$	18	60	76

^{a}Dose = 1 mg/kg IV; 2 mg/kg PO.

of the CH$_3$ in prototype **37**, while the CF$_2$CF$_3$ substituent in **39** resulted in 2-fold lower enzyme inhibitory potency (Table 7). Strikingly, while the oral bioavailability of each of the 3 fluorinated **38**–**40** derivatives in the rat was significantly improved compared to **37**, this was not the result of significant changes in clearance in vivo.

Fluorination of the terminal CH$_3$ groups of the γ-secretase inhibitor **41** was examined as an approach to address the metabolic modification that had been determined to occur at this site.[36] By replacing the CH$_3$ groups with CF$_3$, intrinsic enzyme inhibitory activity was improved marginally from an IC$_{50}$ value of 25 nM for **41** to 16 nM for begacestat (**42**), while the $t_{1/2}$ in RLM increased from 1 to 8 min. This effect extended to mouse LM, where the $t_{1/2}$ increased from 2 to 24 min, but not to HLM, where the measured $t_{1/2}$ values for **41** and **42** were comparable at 8 min. The improved metabolic stability in mouse LM translated to enhanced exposure and better efficacy at lowering Aβ$_{42}$ levels in mice in vivo, leading to **42** being selected for clinical evaluation.
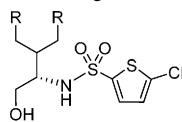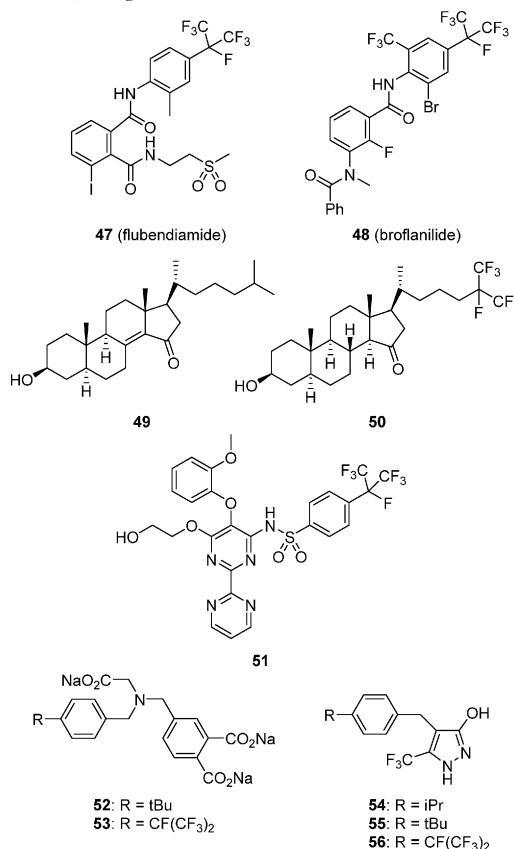

41: R = CH$_3$
42: R = CF$_3$

Fluorination of amide-bound alkyl groups has been shown to interfere with oxidative N-dealkylation processes.[37,38] For example, replacing the iso-butyl amide substituent of the tetrahydroisoquinolinone-based antimalarial agent **43** with the trifluoroethyl moiety found in **44** resulted in only a modest reduction in cell-based potency while metabolic stability in mouse LM was substantially increased.[37] Similarly, the CF$_3$CH$_2$ substituent in the slowly activating cardiac delayed rectifier potassium current (I_{Ks}) inhibitor **46** (L-768,673) was designed to interfere with the N-dealkylation observed with the N-methyl analogue **45**, a known metabolic pathway for benzodiazepine derivatives, and this compound exhibited long lasting effects on the QT interval in dogs in vivo.[38]


43: R = (CH$_3$)$_2$CHCH$_2$
EC$_{50}$ = 10 nM
mouse LM $t_{1/2}$ = 0.33 h

44: R = CF$_3$CH$_2$
EC$_{50}$ = 45 nM
mouse LM $t_{1/2}$ = >4 h

45

46

The heptafluoroisopropyl substituent was originally explored in the agricultural chemistry arena and is found in the pesticides flubendiamide (**47**), which activates insect ryanodine (Ry)-sensitive intracellular Ca^{2+} release channels, and broflanilide (**48**), a noncompetitive insect γ-aminobutyric acid (GABA) receptor antagonist.[39] This moiety has also found application in drug design campaigns where it has been evaluated as a substitute for the iso-propyl and tert-butyl substituents, most notably in the context of the hypocholesterolemic steroid **50** and the bosentan analogue **51**, both of which offer improved metabolic stability compared to their progenitors **49** and **20**, respectively.[40,41] While **50** demonstrated higher potency toward lowering serum cholesterol levels in rats in vivo following oral dosing, **51** bound to the ET$_A$ receptor with 16-fold reduced affinity (IC$_{50}$ = 75.4 nM) compared to **20** (IC$_{50}$ = 4.7 nM) although the selectively index over the ET$_A$ receptor was enhanced.

47 (flubendiamide)

48 (broflanilide)

49

50

51

52: R = tBu
53: R = CF(CF$_3$)$_2$

54: R = iPr
**55**: R = tBu
56: R = CF(CF$_3$)$_2$

The selective aspartate semialdehyde dehydrogenase inhibitor **53** offers enzyme inhibitory potency comparable to the tert-butyl derivative **52**, while substitution of the iso-propyl moiety in the hypoglycemic agent **54** with either tert-butyl (**54**) or heptafluoroisopropyl (**56**) led to reduced effects on sugar levels in vivo.[42,43]

In a series of inhibitors of aryl urea-based soluble epoxide hydrolase (SEH) inhibitors, fluorination of the phenyl substituent group conferred increased potency with the CF$_3$ (**59**) and CF$_3$O (**60**) analogues 3- and 6-fold more potent than the iso-propyl (**57**) and tert-butyl (**58**) prototypes, respectively (Table 8).[44] However, the heptafluorisopropyl substituent in **61** provided a uniquely potent inhibitor, with an almost 20-fold advantage over **59** and **60**. Interestingly, while the aqueous solubility of **61** was 15-fold lower than **59**, the CF$_3$O-substituted derivative **60** was 8-fold more soluble than both **57** and **59**, an observation not anticipated by the predicted lipophilicity values.

Table 8. Structure and Inhibitory Potency of a Series of Soluble Epoxide Hydrolase (SEH) Inhibitors
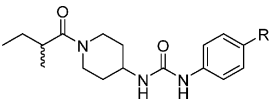
|	R	SEH IC$_{50}$ (nM)	solubility (μg/mL)
57	iPr	1.17	2.60
58	tBu	2.44	0.02
59	CF$_3$	0.37	2.60
60	CF$_3$O	0.36	22.5
61	(CF$_3$)$_2$CF	0.02	0.17

One word of caution with respect to the taking advantage of the heptafluoroisopropyl moiety as an aromatic substituent is the potential for it to exist as atropisomers when there is a large ortho- substituent. This has been observed with **62**, where the ^{1}H NMR spectrum indicated a 60:40 ratio of rotamers, with **62a** identified as the major component (Figure 2).[45]
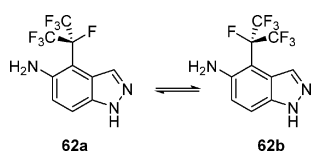
**Figure 2.** Atropoisomerism associated with 4-(perfluoropropan-2-yl)-1H-indazol-5-amine.

The coalescence temperature, as determined from monitoring the C-6 proton in Cl$_2$DCCDCl$_2$, was 108 °C, corresponding to an energy barrier of 19.4 kcal/mol. A similar observation was made with the naphthalene and benzofuran analogues in which the pyrazole ring of **62** is replaced by benzene and furan, respectively.

**Scheme 1. Metabolism of 63 and the Release of 66**
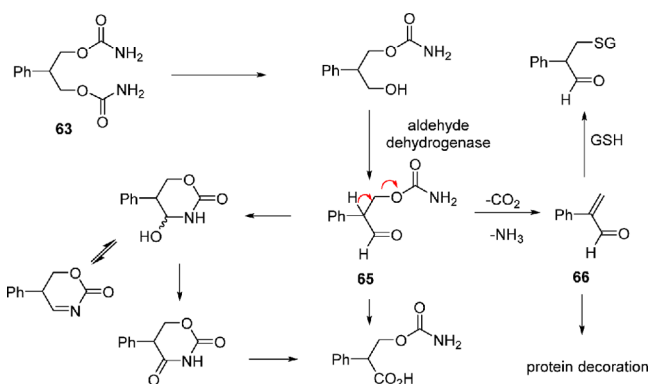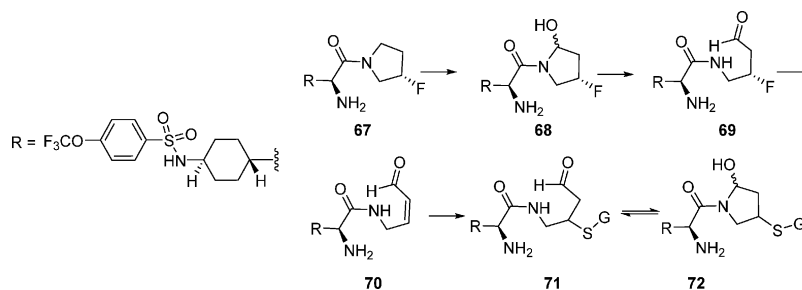
The strategic deployment of a fluorine atom can exert an effect on drug metabolism and toxicity in a less direct fashion, as exemplified by the design of the fluoro analogue **64** of the anticonvulsant felbamate (**63**).[46] Clinical use of **63** is associated with aplastic anemia and hepatotoxicity that is idiosyncratic in frequency and which has been suggested to be due to metabolic release of atropaldehyde (**66**), a bivalent electrophile capable of cross-linking proteins.[46,47] The mechanism of release of **66** is postulated to occur by the metabolic process depicted in Scheme 1 and is believed to be the consequence of an irreversible retro-Michael reaction that results in the elimination of H$_2$O and CO$_2$ from **65**. The formation of **66** is efficiently blocked by the fluorine atom present in **64**, which prevents the fluorinated metabolite analogous **65** from undergoing the retro-Michael reaction.[47] The preclinical anticonvulsant profile of **64** compares favorably to **63** and is, in some circumstances, superior, and this compound has been advanced into clinical trials.[48,49]

63: R = H
64: R = F
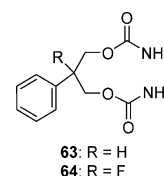
Metabolic Activation of Fluoro-alkyl Derivatives. Despite the high strength of the C−F bond (Table 1) and the relatively poor ability of fluoride to act as a leaving group, circumstances have been documented where an alkyl fluoride derivative undergoes metabolic activation that sets the stage for the elimination of HF from sp^3-hybridized carbon centers.[8,50] Fluorine atoms are introduced into the ring of pyrrolidine derivatives as an isostere of hydrogen designed to interfere with metabolism, moderate the basicity of the nitrogen atom if so configured, or modulate ring conformation (vide infra). However, one circumstance where this structural configuration presented problems is exemplified by the DPP-IV inhibitor **67**, which was observed to generate protein adducts when incubated in RLMs.[50] The protein covalent binding associated with **67** was irreversible and dependent on both time and NADPH but could be abrogated by including GSH or N-acetyl cysteine in the incubation medium. Trapping experiments using semicarbazide, a hard nucleophile that reacts with aldehydes, helped to elucidate the metabolic pathway depicted in Scheme 2. Metabolic activation is believed to be initiated by α-hydroxylation adjacent to the nitrogen atom of the pyrrolidine ring to give the hemiaminal **68** that, upon ring opening to the aldehyde **69**, is configured for the elimination of HF to form the Michael acceptor **70**. The unsaturated aldehyde **70** is an electrophile with dual sites of reactivity and thus has the potential to cause protein crosslinking. However, the addition of a soft nucleophile like GSH

Scheme 2. Metabolic Activation Pathway Deduced for the DPP-4 Inhibitor 67
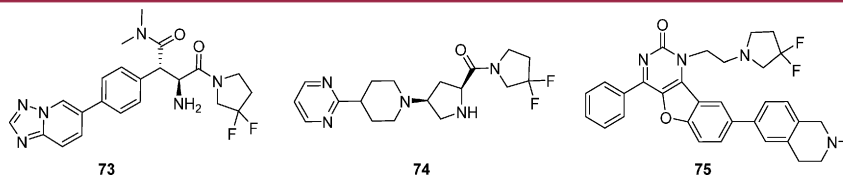
would provide **71**, which is presumably in equilibrium with the ring closed form **72**.
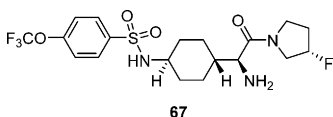

Although this example provides a cautionary note with respect to the bioisosteric replacement of hydrogen by fluorine in pyrrolidine and, presumably, the homologous piperidine rings, detailed studies with the difluorinated pyrrolidine-based DPP-IV inhibitors **73** and **74** have indicated that for these molecules, this specific metabolic pathway is not followed.[51] The HIV-1 non-nucleoside reverse transcriptase inhibitor **75** exhibits a short life in RLM and HLM, and while the difluoro-pyrrolidine ring was determined to be the site of metabolism by an undetermined pathway, there was no apparent indication of reactive metabolite formation.[52]

2,2-Difluoro-1,3-benzodioxole Derivatives. The 1,3-benzodioxole moiety is a structural element in prevalent natural products found, for example, in the papaverine alkaloids, camptothecins, and several constituents of kava-kava.[53] However, this functionality is susceptible to metabolism by CYP 450 enzymes following a pathway that leads to the formation of a carbene intermediate that binds tightly to the Fe atom of the enzyme (Scheme 3). This carbene-bound intermediate is referred to as a

Scheme 3. Cytochrome P450-Mediated Metabolism of the 1,3-Benzodioxole Moiety to a MI Complex
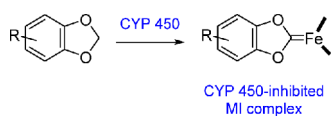

metabolite intermediate (MI) complex that inactivates the enzyme until the complex degrades, which relieves the inhibition, with the methylenedioxy carbon atom released as carbon monoxide.[54,55] However, this step generates a catechol that can be subject to bioactivation by oxidizing enzymes, including CYP 450s, to afford *ortho*-quinone derivatives that are highly reactive toward both soft and hard nucleophiles.[55,56] Consequently, the benzo[*d*][1,3]dioxole element is considered to be a structural alert because it can be associated with drug−drug interactions, metabolic activation, and toxicities that includes hepatotoxicity.[55] For example, despite its relatively low clinical dose of 10−50 mg, the antidepressant paroxetine (**76**) is metabolized by CYP 2D6 in a fashion that leads to inhibition of the enzyme, inhibiting both its own metabolism and that of other drugs that are cleared by CYP 2D6.[57]
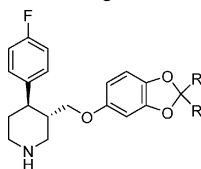
76: R = H (paroxetine)
77: R = D (CPT-347)

An appreciation of these problems has prompted the design of 1,3-benzodioxole replacements that would abrogate this

metabolic pathway while preserving the physicochemical properties requisite for biological activity.[58] Deuteration of the methylene moiety represents the most conservative isosteric substitution that can slow this metabolic process while preserving biological activity and has been successful in the context of CPT-347 (**77**), a deuterated derivative of **76**.[59] However, fluorination offers a more definitive solution, although the effects on biological potency are less predictable with increases, decreases and minimal changes described that show dependence on the specific target or chemotype within a target.[4,60−66] The fluorinated camptothecin analogue **78** was specifically designed to increase metabolic stability over the hydrogen-substituted prototype, a structural modification that resulted in improved exposure following oral administration of the compound as its prodrug **79**.[60] Lumacaftor (VX-809, **80**), which improves trafficking of the cystic fibrosis transmembrane regulator (CFTR) ΔF508 mutant and has been approved by the FDA for the treatment of cystic fibrosis, is a CYP inducer rather than an inhibitor and subject to limited metabolism, which involves oxidation and glucuronidation.[65] JNJ-42165279 (**81**) is a clinically evaluated, mechanism-based inhibitor of fatty acid amide hydrolase (FAAH) for which the 2,2-difluorobenzo[*d*][1,3]dioxole heterocycle was observed to be metabolically stable.[66]
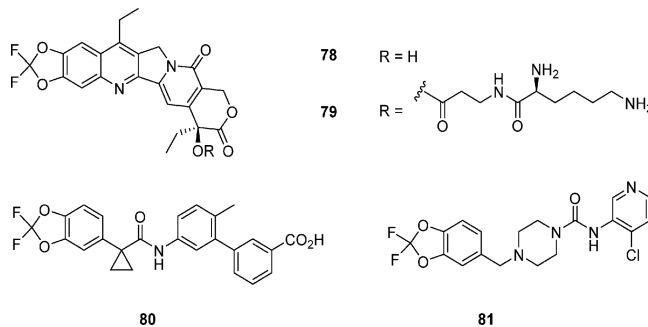
FLUORINATION OF ALKYL GROUPS AND CONFORMATIONAL EFFECTS

In this section, the effects of fluorinating alkyl moieties proximal to a range of functional groups that can lead to an influence on the conformation of a molecule are discussed.
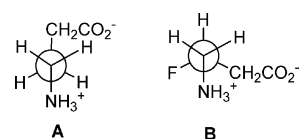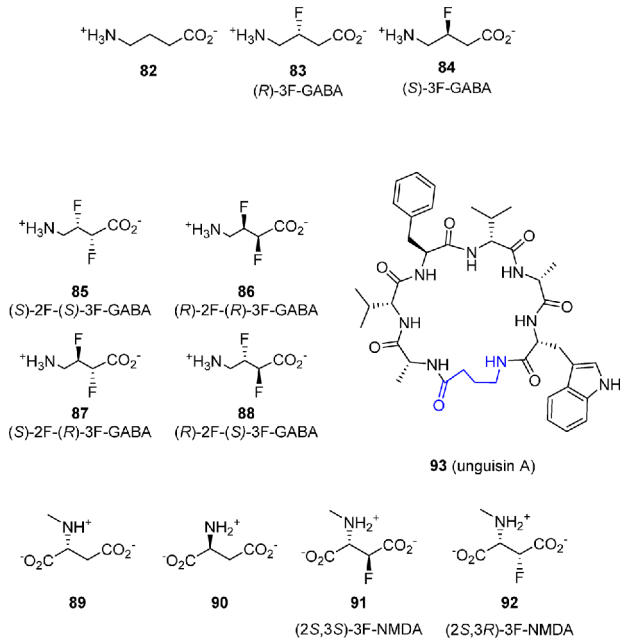
Fluorine for Hydrogen in Alkyl Groups Proximal to Amines. The substitution of hydrogen attached to sp^3 carbon atoms by fluorine can influence the properties of a molecule significantly in a fashion that is dependent upon the nature of proximal functionality. The gauche effect between fluorine and substituents on the adjacent carbon atom can be an effective approach to influencing the conformation of a molecule.[67] The calculated energetic preferences for the gauche conformation of a series of 2-substituted, 1-fluoroethane derivatives are compiled in Table 9, and this phenomenon has been taken advantage of to probe aspects of molecular recognition.[67] Thus, the conformations of 3-F GABA **83** and **84**,[68] the 2,3-difluoro GABA analogues **85−88**,[69] and 3-fluoro-*N*-methyl-D-aspartate (NMDA) derivatives **91** and **92**[70] have been analyzed in order to illuminate aspects of the bound conformation of their progenitors **82** and **89**, respectively, while the conformation of the GABA element in the

**Table 9. Calculated Stabilization Energies Favoring a Gauche Relationship in 2-Substituted 1-Fluoroethane**

	stabilization energy (kcal/mol)
F	0.5−1.0
OH	1.0−2.0
OAc	1.6
NHAc	1.8
NH_2	0.9−1.0
NH_3^+	5.8

macrocyclic heptapeptide unguisin A (**93**), which is isolated from the marine fungus *Emericella unguis*, has been probed by incorporating **85−88**.[71] The design principle behind these studies relies upon a gauche interaction between fluorine and the ammonium moiety to favor a specific conformation that is used to probe cognate receptors and, in the case of GABA, recognition by the transaminase. For 2,3-difluoro GABA, a gauche interaction between the two fluorine atoms provides an additional element of stereocontrol in addition to the gauche preference of the fluorine/ammonium elements.

Fluorine was introduced at the 3-postion of GABA (**82**) and the individual enantiomers (*R*)-3-F-GABA (**83**) and (*S*)-3-F-GABA (**83**) evaluated as ligands for the $GABA_A$ and $GABA_C$ receptors.[68] Because the cloned $GABA_A$ receptor failed to distinguish between **83** and **84**, the extended conformation A depicted in Figure 3, in which the two key functionalities are in an antiperiplanar arrangement that is available to both enantiomers, was considered to represent the bound topology. However, both the $GABA_C$ receptor and the transaminase favored **83**, suggesting that conformer B depicted in Figure 3 is that recognized by these proteins because that topographical arrangement is a conformation disfavored by **84**.[68] Evaluation of the difluoro homologues **85−88** revealed that **85** was a more potent ligand for the $GABA_C$ receptor than either $GABA_A$ or $GABA_B$, while **86** exhibited dual $GABA_A/GABA_C$ binding.[69] Interestingly, while both **85** and **86** adopted an extended, zigzag conformation, they elicited very different effects at the $GABA_C$ receptor, with **85** an agonist while **86** acted as an antagonist.


82

83
(*R*)-3F-GABA

84
(*S*)-3F-GABA

85
(*S*)-2F-(*S*)-3F-GABA

86
(*R*)-2F-(*R*)-3F-GABA

87
(*S*)-2F-(*R*)-3F-GABA

88
(*R*)-2F-(*S*)-3F-GABA

93 (unguisin A)

89

90

91
(2*S*,3*S*)-3F-NMDA

92
(2*S*,3*R*)-3F-NMDA

Figure 3. Preferred conformation of **82** at the $GABA_A$ receptor (A) and the $GABA_C$ receptor and the transaminase enzyme (B) deduced from an evaluation of **83** and **84**.

The preferred conformations of **91** and **92**, fluoro-substituted derivatives of NMDA (**89**) which acts as an agonist at a subset of receptors that recognize glutamic acid (**90**), were analyzed by ¹H- and ¹⁹F-NMR, which revealed that **91** adopted the conformation depicted in Figure 4.[70] However, the precise conformation
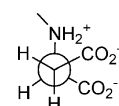
Figure 4. Proposed active conformation of NMDA at the GluN2A and GluN2B receptors after analysis of **91** and **92**.

of **92** could not be determined, although one conformation was ruled out and density functional theory (DFT) calculations suggested that of the other two conformations, the one reflecting the arrangement depicted in Figure 4 was not favored. The (2*S*,3*S*)-isomer **91** evoked currents at GluN2A and GluN2B receptors expressed in *Xenopus laevis* oocytes that were indicative of agonistic activity, while **92** was silent. As consequence, it was suggested that the active conformation is as depicted in Figure 4, a conclusion consistent with the conformation of **89** at the closely related GluN2D receptor in the cocrystal structure.[70]

Fluorine for Hydrogen in Alkyl Groups Proximal to Amides. The replacement of a hydrogen on a carbon atom *β*- to an amide nitrogen with fluorine can affect biological activity in a positive or negative fashion, a function of modulating conformational preferences due to the influence of a gauche effect between these substituents.[67] This is elegantly exemplified in the context of proline-containing ligands where fluorine is introduced at the C-4 position of the ring. *N*-Acetyl proline methyl ester (**94**) exhibits a preference for the Cγ-endo conformation (Figure 5A) that is reinforced by the introduction of a 4-(*S*)-fluoro substituent in **95** (Figure 5B), while the 4-(*R*)-fluoro derivative **96** favors the Cγ-exo conformer presented in Figure 5C.[72] The *trans*-(*Z*) topology of the amide moieties in **94−96** is also favored, attributed to a stabilizing interaction between the oxygen of the tertiary amide and the exocyclic C═O carbon atom. This phenomenon is viewed as the donation of electron density from the nonbonded electrons of the amide C═O to the π* orbital of the adjacent CO_2Me (or CO·NHR) substituent, which confers a detectable element of pyramidalization to the electron accepting C═O moiety (Figure 6).[73]

94

95

96
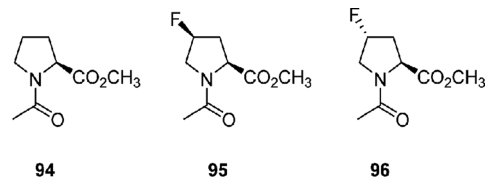
The effect of C-4 fluorination of a pyrrolidine ring on biological activity has been illustrated in the context of both DPP-4 and fibroblast activation protein (FAP) inhibitors where in each case the proline moiety is installed at P_1 and the nitrile engages with the active site serine of the protease in a Pinner-type reaction to reversibly form a stable iminoether.[74,75] In the series of
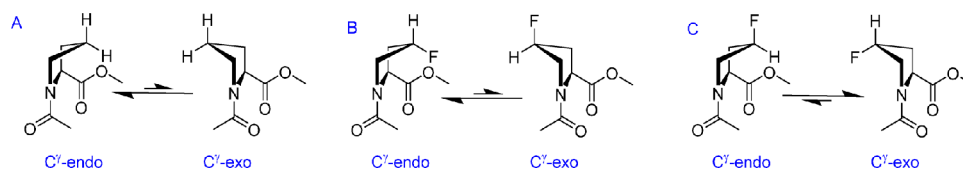
Figure 5. Conformational preferences of *N*-acetyl-proline methyl ester (**94**) (A), *N*-acetyl-4-(*R*)-fluoro-L-proline methyl ester (**95**) (B), and *N*-acetyl-4-(*S*)-fluoro-L-proline methyl ester (**96**) (C).
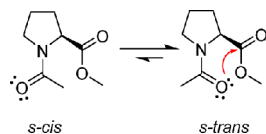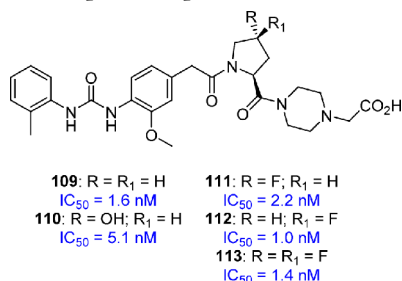

Figure 6. Acetamide conformation of **94** depicting an n → π* interaction.

DPP-4 inhibitors **97**−**100**, the *cis*-4-F-(*S*)-isomer **98** was 450-fold more potent than the *trans*-4-F-(*R*)-isomer **99**, SAR points that cannot be attributed to a steric effect because the 4,4-difluoro homologue **100** fully retained the potent enzyme inhibitory activity of the prototype **97** (Table 10). The *cis*-(*S*)-4-fluoro substituent stabilizes the C$^\gamma$-endo pucker, while the *trans*-(*R*)-4-fluoro isomer stabilizes the C$^\gamma$-exo pucker (Figure 5), and it is this phenomenon that is believed to underlie the observed SARs. These observations were reproduced in the FAP inhibitors **102**−**104**, where the effects of fluorination and the preferred absolute configuration are identical to those observed with **97** and **98** (Table 10).[75]

However, the SARs for fluorination of a proline moiety installed at P$_2$ of the series of thrombin inhibitors **105**−**108** reflected the opposite preference to that observed with the P$_1$ moiety of DPP-4 and FAP inhibitors.[76] In this series, the *trans*-4-(*R*)-fluoro isomer **106** was 300-fold more potent than the *cis*-4-(*S*)-fluoro isomer **107**, while the 4,4-difluoro analogue **108** was 6-fold less potent than the hydrogen prototype **105** (Table 11).

The effects of fluorination of a proline ring do not always manifest as an influence on potency. In the series of VLA-4 antagonists **109**−**113**, all three fluorinated compounds **111**−**112** exhibited potency comparable to the parent **109** and the 4-(*R*)-hydroxy derivative **110**, indicative of considerable tolerance for substitution at this region of the pharmacophore.[77]

109: R = R$_1$ = H
IC$_{50}$ = 1.6 nM
110: R = OH; R$_1$ = H
IC$_{50}$ = 5.1 nM

111: R = F; R$_1$ = H
IC$_{50}$ = 2.2 nM
112: R = H; R$_1$ = F
IC$_{50}$ = 1.0 nM
113: R = R$_1$ = F
IC$_{50}$ = 1.4 nM

Fluorine for Hydrogen in Alkyl Groups Proximal to Fluorine. An understanding of the conformational preferences of alkanes in which hydrogen atoms have selectively been replaced by fluorine can confer advantageous effects that may be useful in drug design (Figure 7).[78−81] The C−C−C bond angle of the R−CF$_2$−R moiety widens to ∼118°, while the F−C−F angle is narrowed to ∼104° relative to normal tetrahedral carbon bond angles, which can manifest as a Thorpe−Ingold effect (Figure 7A).[78] When CF$_2$ moieties are introduced in a 1,4 relationship to an alkyl chain, dipole−dipole interactions and the relief of steric buttressing favors an extended conformation (Figure 7B). Vicinal difluoroalkanes adopt a gauche conformation that overrides the unfavorable C−F dipole−dipole alignment and, as a consequence,

confers increased polarity to a molecule.[79,80] For 1,3-difluoroalkanes, the conformational preferences are dictated by favorable dipole−dipole alignment, with the preferred conformation depicted in Figure 7D estimated to be 3.3 kcal/mol lower in energy than that in which the C−F dipoles project in the same direction.

The conformational effects of fluorination patterning have been examined in the stearic acid derivatives **114** and **115** and the substituted palmitic acids **116**−**118**.[78] The higher melting point of the (±)-*threo*-isomer **115** (86−88 °C) compared to the (±)-*erythro*-configured **114** (67−69 °C) was attributed to the ability of **115** to adopt an elongated form stabilized by F−F gauche interactions that project the alkyl moieties in an antiperiplanar arrangement, thereby minimizing unfavorable steric interactions and facilitating improved crystal packing.[78b] In contrast, the two conformations of the (±)-*erythro*-isomer **114** that are stabilized by F−F gauche interactions also place the alkyl chains in a gauche relationship, while the conformation with the alkyl chains antiperiplanar sacrifices the F−F gauche effects. The melting point of **118** (89.9 °C) was higher than palmitic acid (62.5 °C) and **116** (62.9 °C), while **117** was isolated as an amorphous solid that could not be obtained in crystalline form.[78a] Single crystal X-ray structures of **116** and **118** revealed extended, zigzag-type conformations that presumably facilitate crystal packing, while the amorphous nature of **117** was attributed to repulsive intramolecular effects associated with the pattern of fluorination that lead to disorder.

114
mp = 67-69°C

115
mp = 86-88°C

116
mp = 62.9°C

117
amorphous

118
mp = 89.9°C
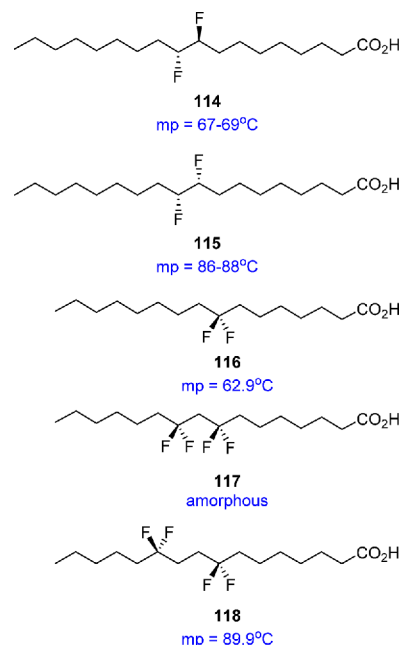
An example of the application of fluorination patterning to conformational control is provided by a detailed analysis of the solid state and solution conformations of a series of trifluorinated 1,3-diphenylpropane derivatives.[80] Uniquely, the all-*anti* isomer **119** was found to adopt a conformation that placed the two aryl rings in a topography that mimicked those of the preferred

Table 10. SARs for the 4-Substituted Pyrrolidine-2-nitrile-Based Inhibitors of DPP-4 (97−100) and FAP (101−104)
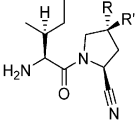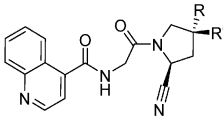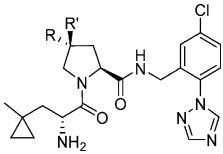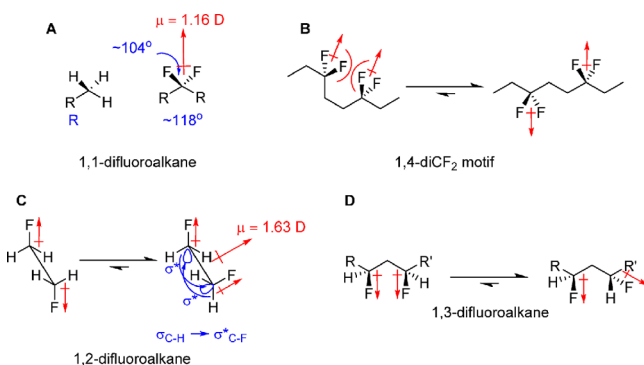

	R	R'	DPP-4 IC$_{50}$ (nM)		R	R'	FAP IC$_{50}$ (nM)
97	H	H	1.5	**101**	H	H	10.3
98	H	F	0.6	**102**	H	F	3.3
99	F	H	290	**103**	F	H	1,000
100	F	F	0.8	**104**	F	F	3.2

Table 11. SARs Associated with 4-Fluorination of the Inhibitors of Thrombin 105−108

	R	R'	thrombin K_i (nM)
105	H	H	0.6
106	F	H	0.37
107	H	F	110
108	F	F	3.6

Figure 7. Geometry of 1,1-difluoroalkanes (A), the 1,4-di-CF$_2$ motif (B), and conformational preferences for 1,2-difluoro- (C) and 1,3-difluoro-alkanes (D).

conformation calculated for 2-benzyl-2,3-dihydrobenzofuran (**120**). This provides an interesting example of how isosterism at the level of atom replacements (F for H) can translate into potential higher order bioisosteric relationships.
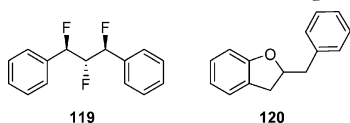
The effects of the fluorination pattern of alkyl side chains on the physicochemical properties of a molecule has been evaluated in the structurally homologous 3-propyl-1*H*-indoles **121−126** and 3-butyl-1*H*-indole derivatives **127−129** compiled in Table 12.[81] The experimental results revealed interesting effects of the pattern of fluorine substitution in the propyl series **121−126**, with the vicinal difluoro derivative **125** less lipophilic than its geminal

difluoro isomer **123**, reflected in the lower measured value of Log *P*. These properties translated into a more than 8-fold increase in aqueous solubility compared to the parent alkane **121** despite the addition of the two slightly more lipophilic fluorine atoms (Table 12). This result was attributed to the gauche interaction between the two fluorine atoms of **125** favoring a conformation that projects the C−F dipoles in a similar direction, reflected in the higher dipole moment of 1.63 *D* compared to 1.16 *D* for the geminal arrangement in **123**. For the butyl series **127−129**, the vicinal difluoro-substituted compound **129** was less lipophilic than the geminal-substituted analogues **127** and **128**, which translated into modestly higher aqueous solubility. Indeed, the Log *P* value measured for **129** was only slightly higher than that for the vicinally substituted homologue **125** despite the presence of the additional CH$_2$ moiety, providing some instruction on how to deploy fluorine to advantageously modulate physical properties. The metabolic stability of the compounds in liver microsomal preparations was also evaluated, and while there appeared to be some enhancement associated with increased fluorination, the results were less than definitive.[81]

A practical consequence of the effect of a considered deployment of fluorine patterning on the solubility of a compound can be appreciated by comparing the properties of the homologous *Mycobacterium tuberculosis* (Mtb) inhibitors **130** and **131**.[82] While both compounds are effective Mtb inhibitors that act by an unknown mechanism, the aqueous solubility of the CF$_2$H-substituted compound **131** was more than 20-fold higher than the CF$_3$ homologue **130** despite a modest increase in the measured value of Log *P*.
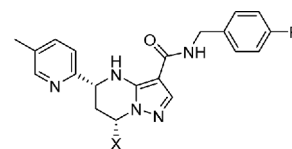
130: X= CF$_3$
MIC = 440 nM
measured Log *P* = 4.4
solubility = 9 μM

131: X = CHF$_2$
MIC = 600 nM
measured Log *P* = 4.6
solubility = 212 μM

■ REPLACING HYDROGEN BY FLUORINE IN AROMATIC RINGS

Aryl Fluoride Derivatives and Metabolism. The judicious substitution of a hydrogen atom in aromatic and heteroaromatic rings by a fluorine atom can exert a significant impact on the properties of a molecule that are of beneficial interest in both drug design and development. An early focus of the introduction

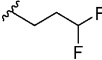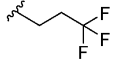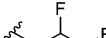**Table 12. Physicochemical Data Associated with the Series Fluorinated 3-Alkyl Indole Derivatives 121−129**
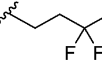

R					
	121	**122**	**123**	**124**	**125**
E_{solv} (kcal/mol)	-6.7	-9.4 to -9.8	-10.1 to -10.4	-8.8	-12.3 to -12.6
Log P*	3.3	2.8	2.9	3.1	2.5
solubility (μM)	200			30	>1720
R					* Log P data were determined experimentally
	126	**127**	**128**	**129**	
Log P*	2.8	3.1	3.0	2.8	
solubility (μM)	820	182	115	277	
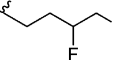
Table 13. HCV GT-1b Replicon Inhibitory Activity of NS5B Inhibitors 133−136

	133	134	135	136
R				
EC$_{50}$ GT-1b replicon (μM)	0.11	0.016	>50	5

of fluorine to aromatic rings was as a tactic to slow metabolism, although fluorinated rings are still subject to metabolic modification by CYP 450 enzymes and fluorine has been shown to undergo the NIH shift.[83] A particularly interesting and complex example of metabolism associated with a fluorophenyl ring is provided by the hepatitis C virus (HCV) NS5B polymerase inhibitor tegobuvir (**132**), which was discovered using a phenotypic cell-based screen.[84a] The fluorination pattern of this chemotype is a critical determinant of antiviral activity, illustrated by the SAR associated with **133−136** (Table 13), which were only understood as the result of a careful mechanistic analysis.[84b,c] Resistance mapping with **132** identified the NS5B polymerase as the antiviral target in the cell-based screen, but the compound was not a direct inhibitor of the enzyme in biochemical assays.[84b] Western blotting analysis of replicon cells treated with **132** revealed the presence of both the natural NS5B polymerase protein and a related protein with a molecular mass that was 820 Da higher. The modified NS5B protein represented the addition of one molecule of a metabolite of **132** that had lost one fluorine atom and acquired GSH. The antiviral activity associated with **132** was reversed by CYP 450 inhibitors, and this activity was subsequently narrowed to CYP 1A1 as the activating enzyme. The proposed metabolic pathway presented in Scheme 4 relies upon metabolism of **132** to the intermediate epoxide **137**, which readily loses fluoride in a

process presumably assisted by an electronic interaction with the imidazo[4,5-c]pyridine heterocycle, leading to the generation of the enone **139**. This molecule offers two electrophilic sites that can react with GSH, with pathways A and B leading to the putative metabolites **140** and **141**. However, GSH attack at the more hindered site outlined by pathway C would generate a molecule that retains electrophilicity and is capable of reacting with either GSH or a cysteine residue of the HCV NS5B protein. While the identity of the reactive cysteine in HCV NS5B was not definitively determined, Cys$_{366}$ was suggested as a potential candidate because it is proximal to the active site of the enzyme, and compounds that react with this residue are documented as inhibitors of the enzyme.[84b,d]
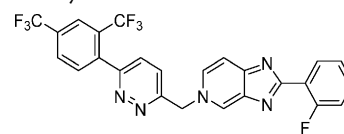
132 (tegobuvir)

Aryl Fluorides: Membrane Permeability and P-gp Recognition. Substitution of a hydrogen atom by fluorine to introduce an intramolecular interaction with a pendent N−H has been exploited to enhance membrane permeability following the seminal observations made with the two series of inhibitors of the coagulation enzyme factor Xa (FXa) summarized in Table 14.[85]
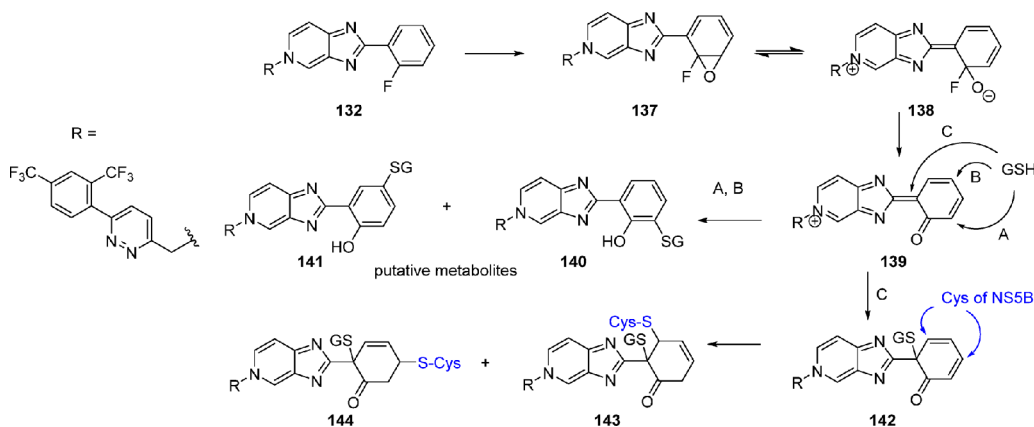
Scheme 4. Metabolism of 132

Table 14. Caco-2 Cell Permeability Values Associated with the Two Series of FXa Inhibitors 145−148 and 149−151

	R	R′	Caco-2 permeability		R′	Caco-2 permeability
145	CH_3	H	1.20×10^{-6} cm/s	149	H	0.82×10^{-6} cm/s
146	CH_3	F	3.14×10^{-6} cm/s	150	F	7.41×10^{-6} cm/s
147	CF_3	H	3.38×10^{-6} cm/s	151	CN	$<0.1 \times 10^{-6}$ cm/s
148	CF_3	F	4.86×10^{-6} cm/s			

Caco-2 cell permeability was improved by substituting the hydrogen atom *ortho-* to the anilide N−H, illustrated by comparing the MMPs **145/146**, **147/148**, and **149/150**. These observations were attributed to an electrostatic interaction between the F atom and the proximal N−H that shields the H-bond donor properties, important to both passive permeability and recognition by P-gp.[86,87] That the effect was not a function of the electron withdrawing properties of the substituent was illustrated by the poor membrane permeability associated with the linear nitrile moiety incorporated into **151**. This structural motif is well-represented in the medicinal chemistry literature and is particularly prevalent in kinase inhibitors.[4a]

This phenomenon is not restricted to anilides but is also observed in benzamide derivatives and the presence of a proximal fluorine atom to interact with these H-bond donating functionalites are common in drug candidates, particularly kinase inhibitors. The effect of intramolecular interactions of this nature has been explored more explicitly by comparing the permeability properties in a parallel artificial membrane permeability assay (PAMPA) of 27 MMPs of *N*-phenylamides that differ by only a fluorine for hydrogen atom exchange (Figure 8A).[88] In 12 of the 27 cases examined, replacing the *ortho-* hydrogen by a fluorine atom led to an increase in permeability of $\geq +0.3$ log P_e. The alternate arrangement represented by the benzamides depicted
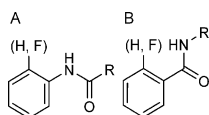
in Figure 8B was also examined by evaluation of 15 MMPs, of which 9/15 exhibited an increase in the permeability coefficient of $\geq +0.3$ log P_e. A simple increase in lipophilicity was not the source of the enhanced membrane permeability because there was no demonstrable effect with *meta*-substituted fluorinated compounds. Moreover, the observation that introducing a fluorine atom had no effect in six out of the total of 42 MMPs examined emphasized the contextual nature of this phenomenon. An analysis of the motifs depicted in Figure 8 in the Cambridge Structural Database (CSD) identified a number of examples where there were close contacts between fluorine atoms and the pendent N−Hs that stabilized the molecular conformation.[88]

Another practical illustration of the value of engaging an NH by a proximal fluorine is provided by observations in the series of β-hydroxyethylamine-based inhibitors of the aspartyl protease β-site amyloid precursor protein cleaving enzyme 1 (BACE-1).[89] The lead inhibitor **152** exhibited potent activity in a cell-based assay, but the brain/plasma ratio following oral administration to rats was low, attributed to P-gp-mediated efflux based on observations of compound performance in a human LLC-PK1 cell line, data that are summarized in Table 15. A potential solution to this problem was probed by introducing structural elements designed to interact with the acetamide N−H because of the known role of exposed N−Hs in P-gp recognition.[87] The methoxy moiety in **154**, which is capable of establishing a conventional intramolecular H-bonding interaction with the N−H, exhibited 2-fold higher permeability and a 5-fold reduced efflux ratio while only modestly (2-fold reduction) affecting potency, data that contrasts with the properties of the iso-butyramide **153**. The *ortho*-fluorobenzamide derivative **155** exhibited similar membrane permeability to **152** but P-gp recognition was reduced

**Figure 8.** Core structures of MMPs of *N*-phenylamides and benzamides examined in a PAMPA.

Table 15. BACE-1 Inhibitory Activity, Membrane Permeability Data, and Efflux Ratios for 152−156

	152	153	154	155	156
R	CH_3	iso-propyl	(methoxy group)	(fluorophenyl group)	(fluoro group)
BACE-1 IC$_{50}$ (nM)	8	144	17	76	29
P$_{app}$ (10^{-6} cm/s)	11	17	23	11	16
efflux ratio in parental LLC-PK1 human cell line	19	16	16	1	2

almost 20-fold based on the efflux ratio, while the data for **156** suggest that an alkyl fluoride can perform similarly. These observations are consistent with an interaction between the fluorine atoms and the N−H along with a reduction in the basicity of the C═O oxygen atom that masks these elements from the external environment and which is believed to compromise P-gp recognition.

These effects were also manifested in the series of cyclic amidine-based BACE-1 inhibitors **157−160** in which the exocyclic NH$_2$ engaged the catalytic residues Asp$_{32}$ and Asp$_{228}$ of this aspartyl protease.[90] The lead compound **157** exhibited limited CNS penetration due, in part, to P-gp-mediated efflux, with a ratio of 12 determined from P$_{app}$ values in Caco-2 cells. The introduction of a fluorine substituent in the peri position ortho- to the amidine carbon atom of **157** reduced the pK$_a$ by 1.3 units from 8.4 to 7.1 in **158**, a structural modification that increased membrane permeability while reducing the efflux ratio by almost 4-fold (Table 16).

Table 16. BACE-1 Inhibition, Membrane Permeability, Efflux Ratio, and pK$_a$ Values for 157−160
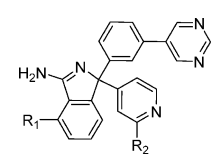
	R$_1$	R$_2$	BACE-1 IC$_{50}$ (nM)	P$_{app}$ (10^{-6} cm/s)	efflux ratio	pK$_a$ of conjugate acid
157	H	H	500	3.4	12	8.4
158	F	H	158	12	3.1	7.1
159	H	CF$_3$	134	0.13	>10	ND
160	F	CF$_3$	241	39	0.6	6.9

In this example, the positive effect on permeability was amplified in the matched pair of homologues **159** and **160**, attributed to a weak interaction between the fluorine atom and one of the hydrogen atoms of the NH$_2$ that reduces the number of H-bond donors available to the environment. In addition, the solvation energy of the fluoro derivative was calculated to be less negative than for the hydrogen analogue, while the combination of electronic and steric effects was proposed to shield the polar nitrogen atom from the environment. In addition to the improvement in permeability and efflux ratio, BACE-1 inhibitory potency was retained for this series and an X-ray cocrystal structure of a close analogue of **160** revealed that the fluorine atom interacted with the carboxylic acid moiety of the catalytic Asp$_{228}$, the side chain hydroxyl of Thr$_{231}$, and three water molecules, with O to F distances that ranged from 2.9 to 3.3 Å.[90]

Aryl Fluorides and Conformation of Proximal Substituents. A fluorine atom ortho- to the NH of an anilide also influences conformation, an effect exploited to illuminate the topology of the pharmacophore associated with the spiroindane-based calcitonin gene-related peptide (CGRP) receptor antagonist **161**, which was evaluated as a potential therapeutic agent for the prevention of migraine attacks.[91] Although the oral bioavailability of **161** was reasonable, the PK profiles of more potent analogues were inferior, attributed to a high polar surface area (PSA) limiting absorption and focusing attention on replacing the central amide moiety with a less polar bioisostere. Modeling studies indicated a preference for coplanarity between the amide and spiroindane cores, with the lowest calculated energies observed at the two topologically divergent conformations of 0° and 180°. The preferred binding topology was probed by separately replacing each of the H atoms ortho- to the anilide by a fluorine to afford **162** and **163**. It was anticipated that these substitutions would stabilize the complementary topologies depicted by the combination of an attractive electrostatic interaction between the N−H and fluorine and repulsive effects between the C═O oxygen and fluorine atoms due to steric and electrostatic considerations. Biological evaluation of isomers **162** and **163** demonstrated a 10-fold difference in CGRP receptor affinity favoring the extended conformation represented by **162**, a hypothesis corroborated by the synthesis of the fused ring compound **164** that constrains the topology in an unambiguous fashion and preserves binding affinity.[91]

161
CGRP K$_i$ = 20 nM

162
CGRP K$_i$ = 55 nM

163
CGRP K$_i$ = 720 nM
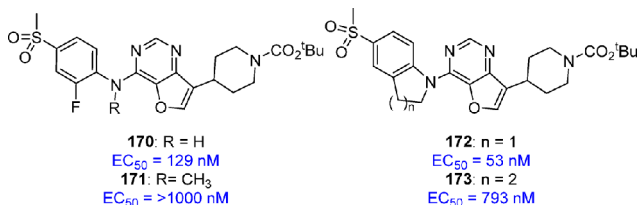

164
CGRP K$_i$ = 17 nM
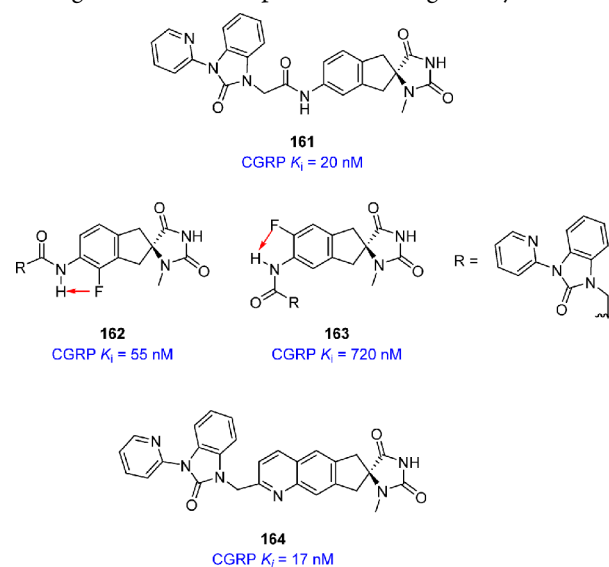
GPR119 agonists have been explored for their potential as a treatment for diabetes because they increase cAMP in in β-cells and stimulate insulin release, mimicking the effects of GLP-1. The introduction of a fluorine atom ortho- to the NH of the

Table 17. hGPR119 Agonistic Activities Associated with 165−169

	R	R′	hGPR119 agonist EC$_{50}$		R	hGPR119 agonist EC$_{50}$
165	H	H	5.8 nM	**168**	H	11.5 nM
166	H	F	0.68 nM	**169**	F	1.5 nM
167	F	H	3.4 nM			

GPR119 agonist **165** afforded **166** with 8-fold improved potency, an effect that was not reproduced by the meta-fluoro analogue **167**, which displayed potency similar to the progenitor (Table 17).[92] A similar SAR observation was made with the pair of related compounds **168** and **169**, leading to the proposal that an intramolecular interaction between the fluorine and the N−H favored a planar conformation. This hypothesis was supported by the much weaker agonist activity associated with the *N*-methyl derivative **171** compared to the hydrogen analogue **170** and inspired the synthesis of bicyclic homologues as functional bioisosteres designed to constrain the preferred topology. The scaffold utilized in this exercise was of particular importance because the indoline **172** was found to be 10-fold more potent than the homologous tetrahydroquinoline **173**.[92]

170: R = H
EC$_{50}$ = 129 nM
171: R= CH$_3$
EC$_{50}$ = >1000 nM

172: n = 1
EC$_{50}$ = 53 nM
173: n = 2
EC$_{50}$ = 793 nM

Aryl Fluorination and Solubility. An interesting observation of the effect of replacing a hydrogen atom ortho- to an anilide N−H by fluorine is provided by the CGRP receptor antagonist **175**, derived from the progenitor **174**.[93] The measured aqueous solubility of **175** was determined to be over 30-fold higher than that of **174**, an observation not well understood, with conjecture focused on the fluorine atom polarizing the adjacent N−H, thereby rendering it a more powerful H-bond donor to promote enhanced solvation. However, this phenomenon may contribute to the poor membrane permeability and oral bioavailability associated with **175**, which led to a focus on intranasal drug delivery for the treatment of migraine.[93]

174: X = H
hCGRP K_i = 0.010 nM
solubility = 15 mg/mL

175: X = F
hCGRP K_i = 0.013 nM
solubility >500 mg/mL
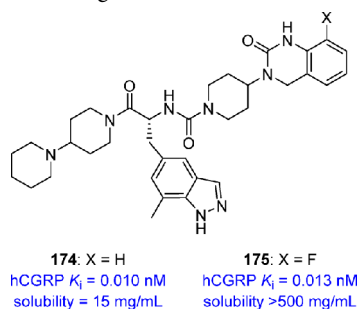
■ **FLUORINE MIMICRY WITH NITROGEN-BASED LONE PAIRS OF ELECTRONS**

Aromatic Fluoride and Azine Mimesis. The similarity of the dipoles of fluorobenzene and azine heterocycles has been recognized as a potential drug design element, and this bioisostere concept has been explored in several settings, with the results

exhibiting a dependence on context.[4g,94−99] The dipole relationships between fluorobenzene and pyridine, 1,2-difluorobenzene and pyridazine, and 1,3-difluorobenzene and pyrimidine are depicted in Figure 9. Using a simpler metaphor of structural
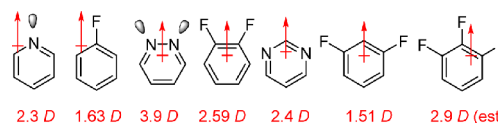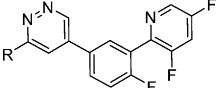

2.3 D   1.63 D   3.9 D   2.59 D   2.4 D   1.51 D   2.9 D (est.)

**Figure 9.** Comparison of the dipole moments and vectors of difluorinated benzenes and azines.

analogy, the electron density associated with the fluorine atoms may be equated with the lone pairs of electrons associated with the heteroatoms of the heterocycles. There are, however, some limitations to the isosteric relationship because the experimental dipole moments determined for fluorobenzenes are less than those measured for the analogous azine heterocycle.[99] Notably, the addition of the third fluorine atom in 1,2,3-trifluorobenzene increases the predicted dipole moment compared to either the 1,2- or 1,3-difluoro isomer, enhancing this aspect of mimicry with pyridine and pyrimidine.[100]

Bioisosterism between an aryl C−F and an azine C−N bond was examined as a means of addressing developability issues in a series of α2/α3 subtype-selective GABA$_A$ agonists, explored as a potential treatment for anxiety.[95] Comparison of the receptor binding data accumulated for the MMPs **176/177** and **178/179** demonstrated effective bioisosterism between a C−F bond and a heterocyclic nitrogen atom in this context (Table 18). Of particular interest, **178** exhibited a poor PK profile due to the formation of the *N*-oxide at the exposed pyridine nitrogen atom in vivo. By replacing the ring nitrogen atom with a C−F moiety in combination with switching the other C−F to a nitrogen atom, both Log *P* and potency were maintained, while the PK profile was improved because the steric encumbrances surrounding the nitrogen atom in **179** interfered with *N*-oxidation. This type of structural isosterism may also be of value as a means of avoiding the CYP inhibition that is often associated with sterically exposed pyridine nitrogen atoms or mitigating susceptibility to aldehyde oxidase-mediated metabolism.

In the related GABA$_A$ agonist **180**, where the imidazo[1,2-*a*]pyrimidine heterocycle functions as an interesting and effective bioisostere of the pyridazine ring of **176−179**, replacement of the nitrogen atom in the six-membered ring with a C−F moiety led to improved potency.[95b] This was illustrated by comparing the profiles of **182** with the pyridine prototype **180** and the C−H analogue **181**, with **182** offering equivalent potency at both the α1 and α3 subtype receptors similar to **180** but with slightly higher efficacy at the α3 receptor and lower efficacy at the α1 subtype (Table 19). In this particular example, this was the targeted biochemical profile. In contemplating the design of **182**,

Table 18. SARs Associated with a Series of GABA$_A$ $\alpha2/\alpha3$ Subtype-Selective Agonists 176−179

	176	177	178	179
R				
GABA$_A$ $\alpha1$ K_i (nM)	0.5	0.1	1.8	1.5
GABA$_A$ $\alpha3$ K_i (nM)	1.4	0.4	6.3	8.5
GABA$_A$ $\alpha5$ K_i (nM)	2.4	0.3	6.0	12.1

Table 19. SARs and Receptor Selectivity Associated with the Series of GABA$_A$ Agonists 180−182
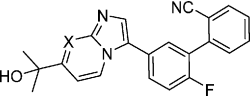
	X	$\alpha1$ K_i (nM)	$\alpha3$ K_i (nM)	$\alpha1$ efficacy (% chlordiazepoxide)	$\alpha3$ efficacy (% chlordiazepoxide)	μ of core (D)
180	N	0.71	0.47	60	79	5.10
181	C−H	4.35	5.16	35	61	3.37
182	C−F	0.20	0.32	34	104	4.52

this study conducted what has probably been the most detailed analysis of C−F/azine bioisosterism. After careful consideration of the calculated and measured physicochemical properties of the abbreviated core heterocycles 183−185 compiled in Table 20,

Table 20. Calculated and Measured Properties for 183−185^a
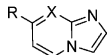
	X	calculated dipole (D)	measured pK_a	measured Log $D_{7.4}$
183	N	3.37 (R = CH$_3$)	4.9 (R = H)	−0.2 (R = H)
184	C−H	5.10 (R = CH$_3$)	6.9 (R = H)	0.8 (R = H)
185	C−F	4.52 (R = CH$_3$)	4.9 (R = H)	0.9 (R = H)

^{a}Structures were built and energy minimized using the Merck Molecular Mechanics Force Field (MMFF). The dipole values were extracted from an AM1 semiempirical calculation.

the C−F derivative 185 was determined to more closely resemble the aza analogue 183 based on dipole and electrostatic potential mapping. Moreover, 183 and 185 express similar pK_a values that are 2 units lower than for the C−H homologue 184, adding further to their functional resemblance; however, the Log $D_{7.4}$ value for 185 is closer to that of 184 than the more polar 183.[95b]

In the MEK inhibitor 186, the fluorine atom ortho- to bromine was observed to engage the backbone N−H of Ser$_{212}$, a stabilizing drug−target interaction that was an important contributor to potency.[96] More conventional H-bond acceptors were explored in the context of the fused heterobicyclic derivatives 187 and 188 where the exposed pyridine and imidazole nitrogen atoms, respectively, interact with the N−H of Ser$_{212}$. This illustrates a bioisosteric relationship between the C−F substituent of 186 and the heterocyclic nitrogen atoms of 187 and 188.[96]
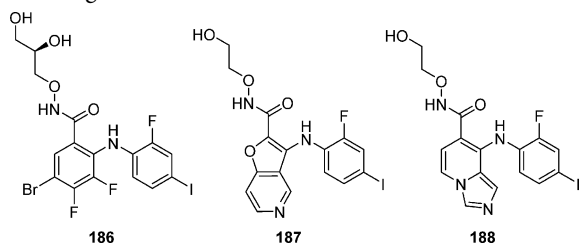
Another example of an aryl C−F mimicking a pyridine atom was observed in a series of CHK1 kinase inhibitors.[97] The lead inhibitor 189, which was discovered using an affinity selection mass spectrometry-based automated ligand identification system screen, exhibited modest selectivity over CDK2 that was iteratively optimized into the more potent and selective pyridine-based inhibitor 190.[97] An X-ray cocrystal structure of 190 with the kinase revealed the important inter- and intramolecular interactions that contributed to the observed inhibitory potency (Figure 10).[97b] The key intermolecular interactions
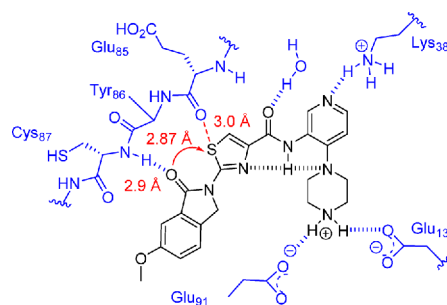
Figure 10. Key interactions between CHK1 kinase and 190 in the cocrystal structure.

were catalogued as H-bonding between the pyridine ring nitrogen atom and the ammonium moiety of Lys$_{38}$ and a H-bond between the amide C=O of the isoindolinone and the N−H of Cys$_{87}$. In addition, there was a close association between the sulfur atom of the thiazole and the backbone C=O oxygen of Glu$_{85}$, which approach each other at a distance of 3.0 Å, less than the 3.32 Å sum of the van der Waals radii for the two atoms and one of the limited number of reported examples of an intermolecular oxygen lone pair to sulfur σ^* interaction.[31] In addition, the planar topography associated with 190 was stabilized by an intramolecular O to S interaction between the isoindolinone amide oxygen and the thiazole sulfur atom which are closer than the van der Waals radii, separated by just 2.87 Å. The potency and selectivity of 190 was matched by the fluorobenzene analogue

191, in which the fluorine atom was suggested to be involved in either a charge−dipole or H-bonding interaction with the side chain ammonium of Lys_{38}.

189
CHK1 IC_{50} = 75 nM
CDK2/CHK1 = 3

190
CHK1 IC_{50} = 1 nM
CDK2/CHK1 = 11,000

191
CHK1 IC_{50} = 4 nM
CDK2/CHK1 = 10,000
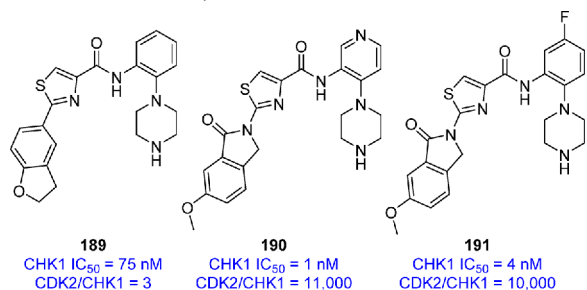
The effective pairing of the difluoro-benzimidazole **192** with cytidine in the context of RNA duplexes inspired an examination of the purine **193** and pyrrolo-pyrimidine **194** as functional mimetics.[98] These structural elements were incorporated as X into the 12-mer RNA 5′-CUU-UUC-XUU-CUU-3′, hybridized with the complementary strands 3′-GAA-AAG-YAA-GAA-5′ that incorporated each of the natural bases at Y and the melting temperatures of the duplexes determined. The results of this study are summarized in Table 21, with ParaFrag similarity scoring indicating that fluorobenzene was 45% similar to pyridine while chlorobenzene was of lower similarity at 27%. Interestingly, the ParaFrag scoring system indicated that in this context, a pyridine N-oxide was 25% similar while pyridone was just 22% similar to pyridine. Although these base pairings were less stable than the natural base pairs, **192** offers a relatively small energy difference compared to the natural bases, suggesting utility as universal base.[98]

192   **193**   **194**
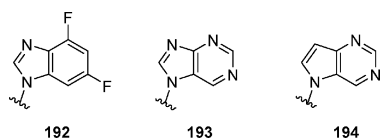
Fluorobenzene-azine bioisosterism has also been assessed in a series of mechanism-based inhibitors **195−204** of cathepsin L although the results were less than definitive.[99] In **195−204**, the (hetero)aryl ring occupies the S_3 pocket of cathepsin L and

$π$-stacking and dipole−dipole interactions were observed between these compounds and the backbone amide bond of Gly_{67}−Gly_{68} of the enzyme (Figure 11). However, while the fluorinated phenyl

195 pK_i = 6.3 **196** pK_i = 6.7 **197** pK_i = 7.0 **198** pK_i = 6.9 **199** pK_i = 6.6
200 pK_i = 6.8 **201** pK_i = 7.0 **202** pK_i = 6.4 **203** pK_i = 6.6 **204** pK_i = 6.8
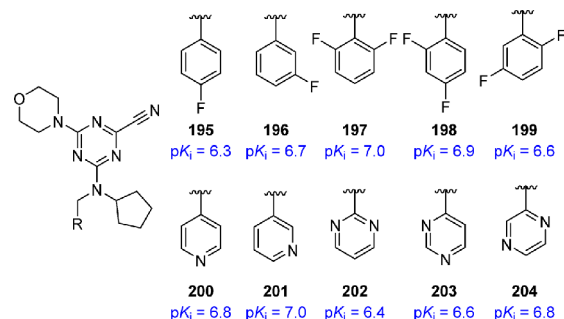
Figure 11. Structures and cathepsin L inhibitory data for **195−204**.

derivatives **195−199** were effective mimics of their matched azine heterocycles **200−204**, there was no clear correlation between the dipole moment of the (hetero)aryl ring and inhibitory potency. This was attributed to the proximity of the adjacent Gly_{68}−Leu_{69} amide bond which adopts a complementary topology to that of Gly_{67}−Gly_{68} such that the dipole is aligned in the opposite direction, believed to be a source of interference with the targeted effect.[99]

Nitrogen Lone Pair Mimesis by an Alkyl Fluoride. An interesting suggestion of isosterism between the piperazine nitrogen atom of the $5HT1_D$ and $5HT1_B$ receptor ligand **205** and the C−F bond of the 4-fluoropiperidine analogue **207** has been invoked to explain the SAR observations.[101] Piperazine **205** is rapidly absorbed in rats, but the piperidine analogue **206** exhibited a poor PK profile attributed to the highly basic nature of the nitrogen atom of this compound. The 4-fluoropiperidine **207** is less basic and displayed a similar in vitro receptor binding profile to **205** and **206** but was associated with much improved absorption in the rat. These observations led to the suggestion that the C−F bond of **207** may be mimicking the unprotonated nitrogen atom of **205** based on electronic considerations and dipole moments, depicted in simplistic terms in Figure 12, although other factors may underlie the observed SAR effects.

Table 21. Melting Temperatures of 5′-CUU-UUC-XUU-CUU-3′ Hybridized with Complementary Strands 3′-GAA-AAG-YAA-GAA-5′

Y				
X	T_m (°C)	T_m (°C)	T_m (°C)	T_m (°C)
(difluoro-phenyl)	27.4	27.3	27.6	27.9
(difluoro-benzimidazole)	28.4	28.7	29.4	29.3
(purine)	34.5	32.2.	35.1	30.8
(pyrrolo-pyrimidine)	35.8	35.0	35.4	33.1

Figure 12. Proposed relationship between a piperazine lone pair of electrons and the fluorine atom of a 4-fluoropiperidine ring.

205
IC$_{50}$ 5HT$_{1D}$ = 0.14 nM
IC$_{50}$ 5HT$_{1B}$ = 11 nM
pK_a = 8.2

206: R = H
IC$_{50}$ 5HT$_{1D}$ = 0.3 nM
IC$_{50}$ 5HT$_{1B}$ = 19 nM
pK_a = 9.7

207: R = F
IC$_{50}$ 5HT$_{1D}$ = 0.9 nM
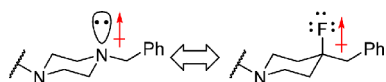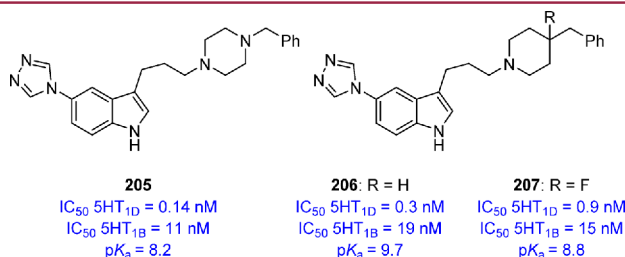IC$_{50}$ 5HT$_{1B}$ = 15 nM
pK_a = 8.8

■ FLOURINATION AND POTENCY

The judicious replacement of a hydrogen atom by fluorine can exert a significant effect on both the potency and specificity of a molecule, and examples where this change either enhances or erodes the potency of a molecule have been described that, perhaps not surprisingly, are dependent upon context. In several examples, the potency-enhancing effects associated with the introduction of fluorine have been traced to intermolecular interactions between the fluorine and the carbon atom of C═O moieties that are characterized as multipolar in nature or to interactions of fluorine with proximal H-bond donors that may have an electrostatic basis.[102] However, other intermolecular interactions and effects involving fluorine atoms of ligands have also been described and are summarized in the next section.

Multipolar and Hydrogen Interactions of Fluorine with Proteins. A detailed mechanistic understanding of how the fluorination of alkyl groups can lead to enhanced potency is provided by **208**−**215**, a series of inhibitors of the binding of mixed lineage leukemia (MLL) to the tumor suppressor protein menin.[103] The fluorination patterns of the two alkyl moieties in **208**−**215** were found to play important roles in modulating potency based on the systematic SAR studies that are compiled in Table 22. In the X-ray cocrystal structure of **211** bound to menin, each of the CF$_3$ moieties were found to engage a backbone C═O of the protein in an orthogonal multipolar interaction. One F atom of the CF$_3$CH$_2$ substituent of **211** is 3.0 Å away from the backbone C═O of His$_{181}$, while a fluorine atom of the CF$_3$ that is bound to the thiadiazole is 3.4 Å away from the C═O of Met$_{322}$. The effect of modulating the thiadiazole substituent was explored in the context of the homologous series **208**−**211**, where fluorination

improved potency over the unsubstituted compound **208**, with the exception of the monofluoromethyl derivative **209**. The CHF$_2$ analogue **210** was found to be equipotent with the CF$_3$ derivative **211**, and both were 9-fold more potent than the CH$_3$ prototype **208**. X-ray cocrystal structures revealed that **208**, **210**, and **211** bound to the protein in a similar fashion and that one of the F atoms of **210** was 3.2 Å from the C═O of Met$_{322}$, while for **211**, the fluorine to C═O carbon distance was 3.4 Å. However, for **209**, the fluorine atom was oriented 38.5° out of the plane of the thiadiazole ring, located 3.7 Å away from the C═O carbon of Met$_{322}$, a distance that was considered to be too remote for a productive multipolar interaction. The conformation of **209** was unanticipated, and a quantum mechanics (QM) analysis suggested that the second fluorine atom of **210** stabilized a conformation that allowed one of the fluorine atoms to engage the C═O of Met$_{322}$. A similar SAR analysis conducted at the benzothienyl alkyl moiety in the context of the thiazolines **212**−**215** revealed that the CH$_2$F analogue **213** was almost 5-fold more potent than the CH$_3$ prototype **212**, while the CF$_2$H analogue **214** offered an additional 4-fold potency improvement and this compound was just 1.5-fold weaker than the CF$_3$ derivative **215**, the optimal compound in this subseries.

These results of this study are consistent with an earlier seminal analysis of cocrystal structures in the Protein Data Bank (PDB), which revealed that fluorine atoms of ligands approached the backbone or side chain C═O moieties of a host protein closely (3.5 Å) and with an appropriate geometry in 16% (442 of the 2559) of the examples evaluated.[102] However, a few examples were highlighted where the effects of fluorine substitution were predicted to be beneficial but the experimental results were not supportive, emphasizing a need to be holistic when assessing the potential for orthogonal multipolar interactions between the fluorine atoms of a ligand and a protein.[102a] This is emphasized by an analysis of 247 matched pairs of compounds differing only by a fluorine for hydrogen exchange and for which there were both X-ray cocrystal structure data for the fluorinated compounds, and the fluorine atom was believed to be engaging in a multipolar interaction with the protein.[102b] In 67% of the examples in this data set, the fluorine was attached to a phenyl ring while the majority of the remaining compounds were CF$_3$ derivatives. The results of the analysis revealed a modest advantage in potency for the fluorinated compounds compared to the hydrogen analogues. After ignoring 79 compounds that were within 2-fold of the 1:1 correlation line as being within experimental error, 123 (73%) of the remainder experienced an increase in potency associated with

Table 22. SARs Associated with Inhibitors 208−215 of the Association of the Tumor Suppressor Protein Menin with MLL

	R	IC$_{50}$ (nM)		R	IC$_{50}$ (nM)
208	CH$_3$	779	**212**	CH$_3$	1200
209	CH$_2$F	1653	**213**	CH$_2$F	260
210	CHF$_2$	82	**214**	CHF$_2$	65
211	CF$_3$	92	**215**	CF$_3$	46

fluorine substitution while the other 27% exhibited a reduction in potency of more than 2-fold. The average improvement in the pIC_{50} value of the fluorinated compounds amounted to 0.36 log units, which translates to a free energy of binding advantage of approximately 0.5 kcal/mol. This reflects a modest but beneficial effect of fluorine substitution on potency that did not appear to be a function of increased lipophilicity; however, because the changes in both parameters were similar in magnitude, the effect on lipophilic ligand efficiency ($pIC_{50} - \mathrm{Log}\ P$) was neutral.[102b]

A fluorine for hydrogen substitution in the benzamidine-based thrombin inhibitor **216** led to a 5-fold enhancement of potency for **218**, which was found to be 3-fold more potent than the 4-Cl analogue **217** and 5−10-fold better than the other fluorination patterns probed by **219−222**.[104] An X-ray cocrystal structure provided an explanation for the observed SAR, which noted that the 4-fluoro atom was proximal to both the backbone C=O carbon atom (3.5 Å) and backbone C−H of Asn_{98} (F to N distance = 3.1 Å), as summarized in Figure 13, productive interactions that are not available to either **216** or **217**.
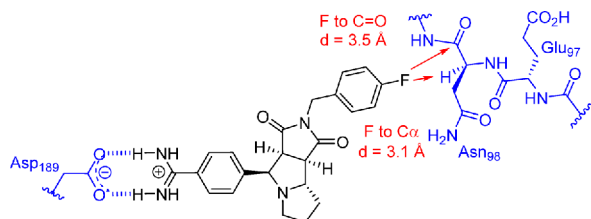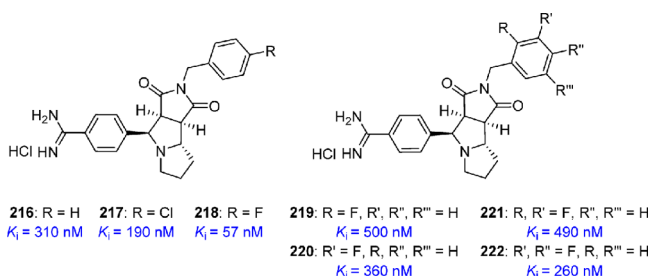

Figure 13. Key interactions between inhibitor **218** and thrombin.

216: R = H   **217**: R = Cl   **218**: R = F   **219**: R = F, R', R'', R''' = H   **221**: R, R', R'', R''' = H
K_i = 310 nM K_i = 190 nM K_i = 57 nM K_i = 500 nM K_i = 490 nM
220: R' = F, R, R'', R''' = H   **222**: R', R'' = F, R, R''' = H
K_i = 360 nM K_i = 260 nM

A more recent example of the importance of fluorination on potency is provided by a series of carbazoles that stabilize the $Tyr_{220}Cys$ mutant of the tumor suppressor protein p53.[105] In this inhibitor series, the CF_3 homologue **224** exhibited 5-fold improved binding affinity compared to the hydrogen-substituted prototype **223**, an observation rationalized by an examination of the X-ray cocrystal structure. As illustrated in Figure 14, each of
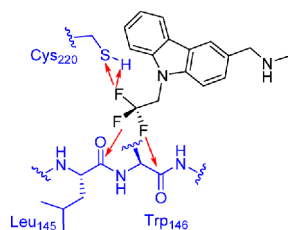

Figure 14. Key drug−target interactions between the CF_3 substituent of **224** and the p53 protein.

the three fluorine atoms of **224** was found to engage the protein, with two establishing multipolar interactions with the backbone C=O moieties of Leu_{145} and Trp_{146} while the third fluorine atom was proximal to the thiol of Cys_{220}, an association attributed

to the combination of weak H-bonding and sulfur σ^* interactions.[105]
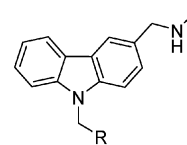
223: R = CH_3
224: R = CF_3

In a series of potent inhibitors of Bruton's tyrosine kinase (BTK), a fluorine scan identified a site for substitution that led to a 10−40-fold enhancement of potency.[106] The effect of fluorination was most effectively exemplified by the comparison of the matched pair of BTK inhibitors **225** and **226** (RN-486), where the introduction of a single fluorine atom increased potency by an order of magnitude.[106a,b] An X-ray cocrystal structure of the ethyl homologue **227**, where the fluorine atom contributed to a remarkable 400-fold increase in potency in a human whole blood (HWB) assay over the hydrogen-substituted prototype **228**, provided some understanding of the SAR observation. The fluorine atom of **227** was observed to be close to the protonated amine of Lys_{430} (3.2 Å), the ortho C−H of Phe_{413} (3.4 Å), and a conserved H_2O molecule (3.4 Å), as captured in Figure 15.[106a]
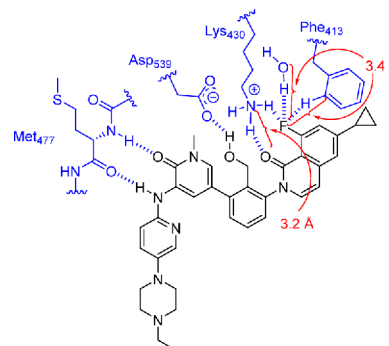
Figure 15. Key drug−target interactions between inhibitor **227** and BTK.

Of note with respect to developability issues, while the cyclopropyl substituent in these analogues replaced a metabolically labile *tert*-butyl element, subsequent studies revealed a metabolic liability associated with the pyridone ring which was susceptible to CYP 450-mediated bioactivation and trapping by GSH, attributed to an initial epoxidation of the C-5,C-6-double bond. This problem was relieved by further optimization in which the pyridone ring was replaced by a pyridazin-3-one heterocycle but not when a pyrazine-2-one was used as the scaffold.[106c]
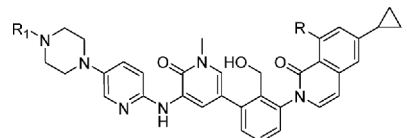
225: R = H; R_1 = CH_3 **227**: R = F; R_1 = CH_2CH_3
BTK K_d = 4 nM   HWB IC_{50} = 4 nM
226: R = F; R_1 = CH_3 **228**: R = H; R_1 = CH_2CH_3
BTK K_d = 0.3 nM   HWB IC_{50} = 1,600 nM

The CF_3 substituent in **230**, an inhibitor of the Q_0 site of the cytochrome bc_1 complex, enhanced potency by an order of magnitude when compared to the CH_3 prototype **229**.[107] An X-ray cocrystal structure of **230** with the chicken enzyme revealed close contacts (2.45−2.98 Å) between the fluorine atoms and two hydrogen atoms of Pro_{270}, three hydrogen atoms of Ile_{146}, and two hydrogen atoms in each of Tyr_{278} and Phe_{274} of the protein.[107]

229
$K_i = 0.75$ nM

230
$K_i = 0.083$ nM
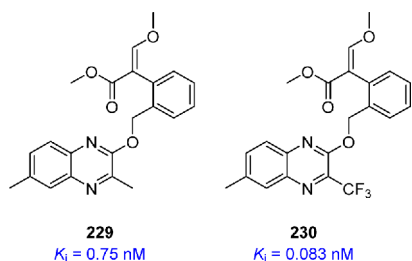
The CF$_3$ Moiety and Tetrel Bonding. A weak but nevertheless interesting interaction between the CF$_3$ moiety and electron rich centers of proteins (CO$_2^-$, amide carbonyl, and the oxygen atoms of serine, threonine, and tyrosine) that involves tetrel (CF$_3$···O) bonding has recently been catalogued.[108] Molecular electrostatic potential (MEP) mapping of perfluorotoluene revealed a π-hole associated with the aromatic ring calculated to be +32.9 kcal/mol and a small region of positive potential at the sp^3 carbon atom that characterizes a σ-hole that was calculated to be +16.9 kcal/mol (Figure 16).[108] The larger

σ-hole:
MEP value = +16.9 kcal/mol

π-hole:
MEP value = +32.9 kcal/mol

Figure 16. Calculated energies of the σ-hole and π-hole associated with perfluorotoluene.
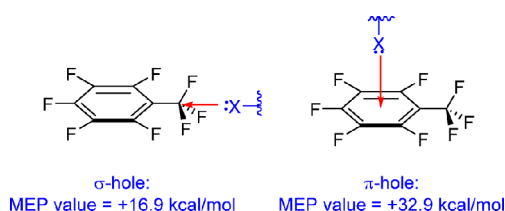
MEP value of the π-hole suggested that the dominant interactions of electron rich species with perfluorotoluene would be at this site, substantiated by calculations of the interaction energies of the π- and σ-holes with NH$_3$, the carbonyl oxygen atom of acetone, formic acid anion, and phenoxide. The geometry of the interaction of electron rich species with the σ-hole associated with the CF$_3$ substituent is highly directional in nature, optimal at an angle of 180° to the Ar-sp^3 carbon bond.

To develop insight into the contribution of this interaction in protein−ligand structures, a search of the PDB was conducted using parametric restraints that required a resolution factor of ≤3.0 Å, a distance between the carbon atom of the CF$_3$ substituent of a ligand and the oxygen atom of the protein of less than 3.37 Å (the sum of the van der Waals radii of the two atoms: 1.7 Å for C and 1.52 Å for O) and an X−C···O angle of >160°. This process identified eight complexes where the carbon to oxygen distances ranged from 2.59 Å in the case of **231** interacting with the side oxygen atom of Asn$_{97}$ of macrophage migration inhibitory factor to 3.35 Å for the Asp$_{312B}$ side chain carboxylic acid of the Arg$_{140}$Gln mutant of mitochondrial isocitrate dehydrogenase 2 (IDH2) interacting with AGI-6780 (**232**).[109,110a] Two examples were examined in detail as illustrative of the phenomenon: the IDH2 inhibitor AG-221 (**234**) in complex with the enzyme and niflumic acid (**235**) in complex with the NmrA-like family domain containing protein 1 NMRAL1.[109,110b,111] The key aspects of drug−target interactions between **234** and **235** and their protein partners are captured in Figures 17 and 18, respectively. In the case of **234**, the side chain carboxylate of Asp$_{312}$ interacted with the CF$_3$ of the inhibitor, while for **235**, the hydroxyl O atom of Tyr$_{246}$ was the partnering element. It was suggested that a potential indicator of the contribution of tetrel bonding to the interaction of **234** with IDH2 is provided by the profile of the des-CF$_3$ derivative **233** which is 2-fold weaker;
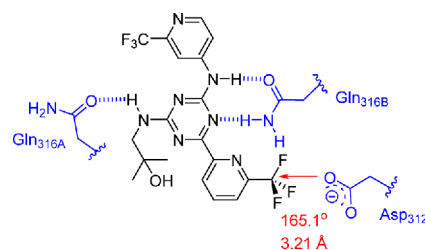
Figure 17. Key interactions between **234** and IDH2 in the cocrystal stucture.[110b]
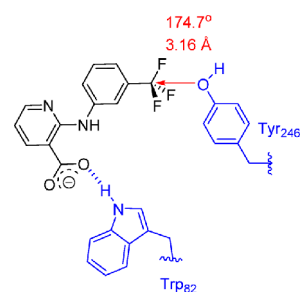
Figure 18. Key interactions between **235** and the NmrA-like family domain containing protein 1 NMRAL1 in the cocrystal complex.[111]

however, because this is data from a cell-based assay, it represents at best an imprecise index.

231 **232**

233: R = H: EC$_{50}$ = 30 nM (cell)
234: R = CF$_3$: EC$_{50}$ = 10-20 nM (cell)

235
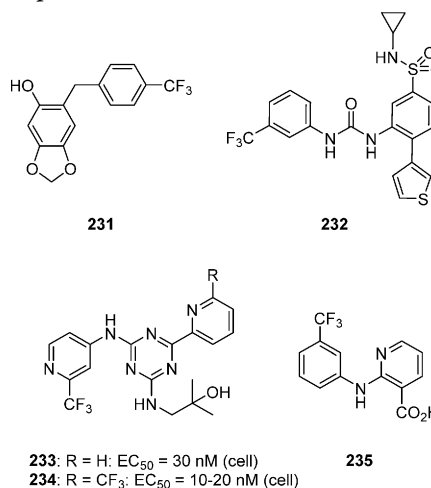
Indomethacin (**236**) is a potent but nonselective inhibitor of the COX-1 and COX-2 enzymes, a profile that can be modified by fluorination of the 2-methyl substituent, illustrated by **237**, which is a selective but 2-fold weaker inhibitor of COX-2 (Table 23).[112] Detailed kinetic studies revealed a K_i for human COX-2 of 13 μM

Table 23. Cyclooxygenase Inhibitory Profile of 236 and Its Fluorinated Homologue 237

	236	**237**
R	CH$_3$	CF$_3$
ovine COX-1 IC$_{50}$	27 nM	>100 μM
mouse COX-2 IC$_{50}$	127 nM	267 nM

for **236** and 1.5 μM for **237**, while studies with a series of site-directed mutant enzymes indicated that the two compounds very likely bound to the enzyme in a similar fashion. Modeling studies suggested that the CF_3 moiety of **237** filled a small hydrophobic pocket in the enzyme in a differential fashion, as detected by differences in inhibitory potency toward mutant COX-2 enzymes. In particular, the inhibitory activity of **237** toward the $Val_{523}Ile$ COX-2 mutant enzyme was reduced by more than 15-fold compared to a smaller 3.7-fold reduction for **236**. However, because in the cocrystal structure Val_{523} is located proximal to the 5-OCH_3 moiety of **236**, the data were interpreted as being the result of the larger CF_3 substituent causing displacement of the heterocyclic core toward the center of the binding pocket. This arrangement was postulated to induce a more significant steric clash between the 5-OCH_3 substituent and the larger isoleucine side chain of the mutant enzyme.[112]

Another example of the introduction of a CF_3 moiety contributing to increased potency is provided by the series of HCV NS3 protease inhibitors **238**−**240**, where both the intrinsic enzyme inhibitory potency and the antiviral activity in cell culture exhibited a dependence on the absolute configuration of the trifluoromethylated carbamate moiety that projects into the S_4 subpocket of the enzyme, data that are summarized in Table 24.[113]

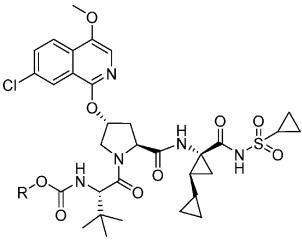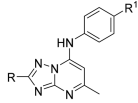**Table 24. SARs Associated with HCV NS3 Protease Inhibitors 238−240** [a]

	R	GT-1a IC$_{50}$ (nM)[†]	GT-1b EC$_{50}$ (nM)[‡]
238	iPr	10	67
239	F$_3$C	8	146
240	F$_3$C	1.3	4.7

[a][†]Biochemical enzyme inhibition assay. [‡]Cell-based HCV replicon assay.

In the absence of cocrystal structure data, rationalization of the observation focused on modeling studies that placed the CF_3 moieties of the two diastereomers in different interactive relationships with the enzyme, with that of **240** suggested to exhibit a closer contact with the protein.

Fluorination patterning has been shown to play an important role in modulating both the potency and species selectivity of triazolopyrimidine-based inhibitors of *Plasmodium falciparum* dihydroorotate dehydrogenase (*Pf* DHODH) that have been probed as therapeutic agents for the treatment of malaria.[114] While the prototype triazolopyrimidine **241** was inactive in both biochemical and cell-based assays, the introduction of a *para*-CH_3 substituent to the phenyl ring afforded the homologue **242** as a compound exhibiting modest inhibitory activity in both assays (Table 25). However, the CF_3 analogue **243** was 15-fold more potent than **242**, while the introduction of a CH_3CH_2 at C-12 (**244**) improved potency by a further 3−5-fold. In these compounds, the aniline N−H engages His_{185} in the active site of the enzyme in a H-bonding interaction that is a source of selectivity toward the malaria enzyme over the human homologue.

Table 25. SARs Associated with Triazolopyrimidine-Based *Pf* DHODH Inhibitors 241−246

	R	R^1	*Pf* DHODH IC$_{50}$ (μM)	*Pf* 3D7 cells EC$_{50}$ (μM)
241 (DSM12)	H	H	>200	>100
242 (DSM97)	H	CH$_3$	4.2	6.4
243 (DSM74)	H	CF$_3$	0.28	0.34
244 (DSM280)	CH$_3$CH$_2$	CF$_3$	0.087	0.058
245 (DSM267)	CH$_3$CF$_2$	CF$_3$	0.038	0.010
246 (DSM265)	CH$_3$CF$_2$	SF$_5$	0.033	0.046

The binding modes of these compounds differ between the two enzymes, with the N−H engaging His_{56}, the residue in the human enzyme equivalent to His_{185}, via the intermediacy of a H_2O molecule. Additional optimization focused in fluorination of the C-12 substituent to give **245** which inhibited *Pf* DHODH with an IC$_{50}$ value of 38 nM and was active in the cell-based assay with an EC$_{50}$ value of 10 nM. The in vitro antimalarial profile of the SF$_5$-containing DSM-265 (**246**) was similar to that of the CF_3 analogue DSM-267 (**245**), and these two compounds offered an optimal compromise between potency and metabolic stability for the series of 4-substituents that were examined. However, in an animal model of infection, **246** offered a potency advantage while a more linear dose-exposure profile was observed in rats, leading to its selection as a candidate for clinical evaluation. The IC$_{50}$ values for *Pf* DHODH inhibition were 33 nM for **246** and 38 nM for **245** and both compounds weak inhibitors of the human enzyme, IC$_{50}$ values >100 μM; however, rodent enzymes were found to be more susceptible, with the IC$_{50}$ values for mouse and rat measured as 2.3 and 2.7 μM, respectively, for **246**, and 24 and 7.2 μM for mouse and rat, respectively, for **245**. Interestingly, the species specificity of inhibition was found to be highly sensitive to the fluorination pattern of the aniline ring with the additional fluorine atoms ortho- to the CF_3 substituent of analogues of **243**−**245** enhancing inhibition of the mammalian enzymes by 5−100-fold. This phenomenon was attributed to an increase in the entropic contribution to binding as a consequence of favorable hydrophobic interactions established between the fluorinated inhibitors and leucine residues in the mammalian enzymes, suggested as evidence that fluorination of a molecule can enhance binding to the lipophilic pockets of proteins.[114]

An unusual effect that was observed when aryl hydrogen atoms were replaced with fluorine is found by comparing the activity profiles of the Aurora A kinase inhibitors **247**−**249**.[115] The monofluoro compound **248** was 2-fold more potent than prototype **247** in both a functional and binding assay, while potency was further enhanced by introducing a fluorine atom to the pyrimidine ring to give **249**. However, the most interesting observation arose from an analysis of X-ray cocrystal structures which revealed substantially different biochemical modes of inhibition for **247** compared to **248** and **249**. In the X-ray cocrystal structure of Aurora A kinase with **247**, the DFG loop was in the active DFG-in conformation, stabilized by an interaction between Asp_{274} and Lys_{162}. Attempts to soak **248** into crystals of Aurora A kinase were unsuccessful, suggesting that binding required changes to the crystal lattice. After developing conditions for cocrystal formation, the X-ray
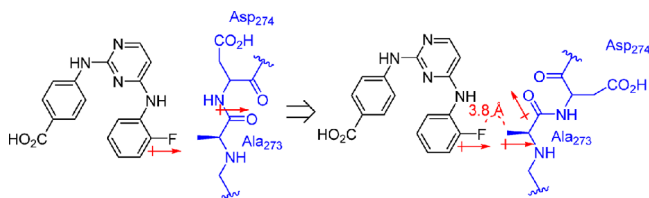
Figure 19. Proposed dipole interactions between **248** and Aurora A kinase leading to a conformational change in the DFG loop of the enzyme.

structures of both **248** and **249** revealed that the DFG loop had flipped to the DFG-out conformation based on rotation about the Ala_{273} amide carbonyl (Figure 19). In this conformation, Asp_{274} was rotated ~100° away from the ATP binding site and there was substantial rearrangement of intramolecular interactions within the protein. This effect on enzyme conformation was also observed with the chloro-, bromo-, and cyano- homologues of **248** but not with the CF_3-, CF_3O-, or phenyl-substituted analogues, arguing against a steric effect as the source. In the cocrystal structure, the fluorine atom was 3.8 Å away from the carbon atom of the CH_3 side chain substituent of Ala_{273}, with the C−F bond aligned almost collinearly with the vector of the $C_\alpha-C_\beta$ bond. For Cl and Br, the measured distances were shorter at 3.4 Å, but the geometry remained collinear. These observations were interpreted in the context of an induction of a dipole in the $C_\alpha-C_\beta$ bond of Ala_{273} by the C−F dipole of the ligand that was transmitted to the amide C=O, thereby facilitating rotation of the peptide backbone, as summarized in Figure 19.
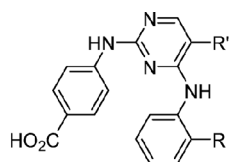
247: R, R' = H
IC_{50} = 10 nM
K_D = 39 nM

248: R = F; R' = H
IC_{50} = 3.7 nM
K_D = 16 nM

249: R, R' = F
IC_{50} = 0.8 nM

## ■ FLUORINE AND THE MODULATION OF THE BASICITY OF AMINES

The high electronegativity associated with a C−F bond has made introduction of fluorine a useful approach to modulate the basicity of proximal amines without introducing additional polarity, with effects that are quantitatively predictable based on the number of fluorine atoms and their connectivity with the nitrogen atom.[116] A careful analysis of the fluorination pattern of a series of tetrahydroisoquinoline-based inhibitors of phenylethanolamine N-methyltransferase (PNMT), the enzyme that methylates norepinephrine to produce epinephrine, led to the identification of compounds with improved selectivity because binding to the α_2 adrenoreceptor subtype was a problem inherent to this chemotype.[117] As summarized in Table 26, the successive introduction of fluorine atoms to the CH_3 moiety of **250** led to stepwise reductions in the basicity of the tetrahydroisoquinoline heterocycle in homologues **251−253**. Fortunately, PNMT inhibitory potency proved to be less sensitive to a reduction in basicity than did binding to the α_2 adrenoreceptor, allowing the sought-after balance of selectivity to be achieved with the CHF_2 derivative **252**.

An interesting application of the effect of modulating amine basicity by replacing a hydrogen atom with a fluorine is found in **255**, a mono-fluoro analogue of the potent μ opioid agonist fentanyl (**254**).[118] The design of **255** explored the hypothesis that peripheral μ opioid receptors are upregulated in painful

**Table 26. Basicity, PNMT Inhibition, and α_2 Adrenoreceptor Affinity for the Tetrahydroisoquinolines 250−253**

	R	pK_a of conjugate acid	K_i PNMT (μM)	K_i α_2 (μM)	PNMT selectivity
250	CH_3	9.29	0.017	1.1	65
251	CH_2F	7.77	0.023	6.4	280
252	CHF_2	6.12	0.094	230	2400
253	CF_3	4.33	3.2	>1000	>310

syndromes and contribute to the sensation of pain. In addition, tissues at sites of damage that produce pain are associated with inflammation and a lower pH, providing a unique environment that could be taken advantage of to modulate the selectivity of action of **254** in a fashion that would spare receptor activation in normal tissues. The hypothesis was based on the understanding that the protonated form of the highly basic **254**, $pK_a > 8$, that predominates at physiological pH is that recognized by the receptor where it engages Asp_{147}. The introduction of a single fluorine atom to the piperidine ring of **254** to afford **255**, evaluated as a mixture of diastereomers, reduced the measured pK_a value to 6.8 and, as such, this compound would be substantially protonated only at pH values that are below those characteristic of normal physiological conditions. Binding experiments conducted in human embryonic kidney cells transfected with the μ opioid receptor indicated that the affinity of **254** was independent of pH with the K_i value at pH = 7.4 = 1.1 nM while **255** bound less potently at physiological pH, K_i = 17.9 nM, than pH = 5.5, K_i = 7.3 nM, and pH = 6.5, K_i = 3.7 nM. This profile would favor binding of **255** to the μ opioid receptor only at lower pH values, providing a measure of selectivity based on local tissue conditions. Thus, **255** was anticipated to activate the μ opioid receptor at the source of pain generation where the pH is believed to be lower than 7.4. In a series of in vivo studies, **255** produced analgesia in rats in an injury-restricted fashion in two different models of inflammatory pain that, in contrast to **254**, was reversed by a peripherally active, non-CNS penetrant μ opioid receptor antagonist. Consistent with the proposed selectivity profile, **255** was devoid of the respiratory depression, sedation, and constipation side effects associated with **254** and exhibited reduced addiction potential as measured by a conditioned place preference evaluation.[118]

254: R = H
255: R = F
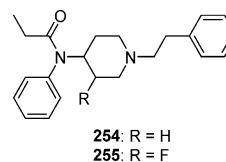
In a series of inhibitors of kinesin spindle protein (KSP), a member of a family of motor proteins that was explored as a mechanism for the treatment of taxane-refractory solid tumors, it was determined that P-gp recognition was sensitive to the basicity of a core piperidine moiety.[119] A pK_a value of 6.5−8.0 was determined to be optimal for maximal efficacy in a tumor cell line by reducing efflux, and this was achieved by both the N-cyclopropyl and N-fluoroethyl derivatives **256** and **257**, respectively. However, **256** displayed time-dependent CYP 450 inhibition in vitro, a known liability of cyclopropyl amines, while evaluation of **257** in vivo revealed toxicity consistent with the release of fluoroacetic acid as a consequence of N-dealkylative metabolism. The solution to this problem was to install a fluorine atom in the

piperidine ring where the effect on pK_a was found to be sensitive to disposition, with the axial compound **258**, which was selected for clinical evaluation, more basic than the equatorial isomer **259**.[119a]

256: R = △
257: R = CH₂CH₂F

258
pK_a = 7.6

259
pK_a = 6.6
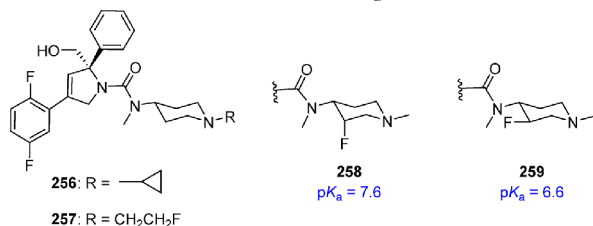
In the structurally related series represented by prototype **260**, modulation of P-gp by fluorination of the primary amine-containing side chain identified both **261** and **262** as satisfactory solutions with efflux ratios of 3 and 5, respectively, compared to the much higher value of 1200 recorded for **260**.[119b]

260: R, R' = H
261: R = CH₂CHF₂; R' = H
262: R = H; R' = CH₂CHF₂

263: R = H
α7 nAChR EC₅₀ = 0.15 μM
Caco-2 efflux ratio 6.9
pK_a = 10.1

264: R = F
α7 nAChR EC₅₀ = 5.8 μM
Caco-2 efflux ratio 0.6
pK_a = 7.6
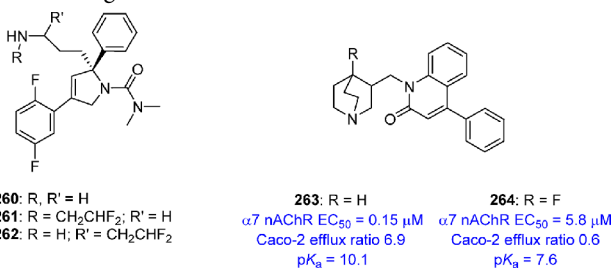
The introduction of a fluorine atom at the bridgehead position of the quinuclidine-based α7-*N*-acetylcholine receptor inhibitor **263** afforded **264**, a compound with a 2.5 unit lower pK_a value that effectively addressed the Caco-2 efflux problem associated with the more basic parent compound.[120] Unfortunately, this structural modification also resulted in a significant erosion in receptor recognition.

Control of basicity is also an approach that has been exploited to modulate the binding of inhibitors to the hERG cardiac potassium channel, a phenomenon that has been associated with the occurrence of arrhythmias in humans, and the induction phospholipidosis, off-target liabilities that have been suggested to possess overlapping pharmacophores.[121] For example, reduction in the electron density and Log *P* value of the pyridine heterocycle of the JAK3 inhibitor **265** was examined as an approach to reducing the affinity of this compound for the hERG channel.[122] As captured in Table 27, the installation of a fluorine atom in the
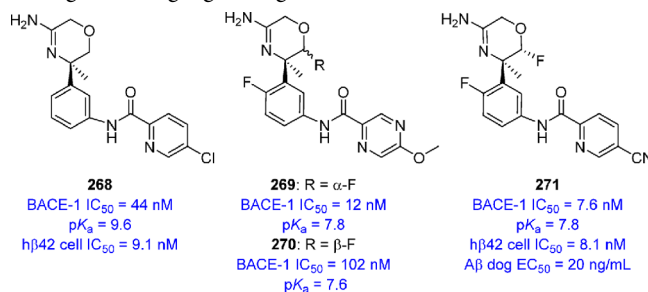
Table 27. JAK3 Inhibitory Potency, hERG Binding, and Calculated Log *P* Values for 265−267

|	R	R′	JAK3 IC₅₀ (nM)	hERG binding (μM)	cLogP
265	H	H	1.3	13.4	2.8
266	F	H	1.7	>100	2.7
267	H	F	0.3	>100	2.7

piperidine ring reduced hERG binding by an order of magnitude without a significant change in the calculated Log *P* value that was accompanied by a 4-fold increase in potency for the (3*S*,4*R*) isomer **267** compared to prototype **265**. The (3*R*,4*R*) isomer **266** was several fold less potent than **267** but was also poorly recognized by the hERG channel.

A fluorine for hydrogen exchange was also taken advantage of as an approach to modulate the basicity of the oxazine-based

BACE-1 inhibitor **268** in order to improve membrane permeability and reduce P-gp-mediated efflux from the CNS compartment.[123] The amino oxazine ring system had been specifically selected as the scaffold to present the key amidine pharmacophore based on calculations conducted a priori that predicted moderate pK_a values. However, the experimental pK_a values revealed the predictions to be inaccurate, with measured values considerably higher than had been anticipated. This was exemplified by the prototype **268** for which the measured pK_a was 9.6, over 3 units higher than the predicted value of 6.4 based on the calculations. After subcutaneous administration to mice, the measured brain levels for **268** were low and the compound was found to be subject to P-gp-mediated efflux in vitro. The introduction of several fluorinated elements to the oxazine ring was contemplated as a means of further refining the basicity, with C-2 selected as the optimal site based on an analysis of the X-ray cocrystal structure where this vector was directed toward the flap residues, offering potential to productively engage the protein. In the event, a simple 2-fluoro substituent proved to be the most effective modification, reducing the pK_a value of the amino oxazine by 1.2−1.4 units. However, potency was shown to be dependent upon the absolute configuration of the newly introduced chiral center because the axial (2*S*)-isomer **270** was less potent and less basic (IC₅₀ = 102 nM, pK_a = 7.6) than the equatorial (2*R*)-isomer **269** (IC₅₀ = 12 nM, pK_a = 7.8). The reduced basicity enhanced the correlation between enzyme inhibitory potency and activity in the cell-based assay, which was attributed to reduced accumulation of compounds in the acidic endosomal compartment where BACE-1 is located. However, **269** exhibited low metabolic stability, and the more stable pyridine nitrile **271** was subsequently selected for evaluation in in vivo studies where a dose-related reduction in Aβ42 levels in CSF was observed, with a 90% decline measured following drug dosing at 2.5 mg/kg to dogs.[123]

268
BACE-1 IC₅₀ = 44 nM
pK_a = 9.6
hβ42 cell IC₅₀ = 9.1 nM

269: R = α-F
BACE-1 IC₅₀ = 12 nM
pK_a = 7.8
270: R = β-F
BACE-1 IC₅₀ = 102 nM
pK_a = 7.6

271
BACE-1 IC₅₀ = 7.6 nM
pK_a = 7.8
hβ42 cell IC₅₀ = 8.1 nM
Aβ dog EC₅₀ = 20 ng/mL

N-CF₃ Derivatives. *N*-Trifluoromethyl amines represent an emerging functionality that compromises the basicity of an amine but have only been cursorily explored as an element in drug design, presumably a function of issues associated with synthetic access.[124] A recent article has described a facile synthesis of *N*-CF₃ derivatives using a mild preparative procedure that is compatible with late-stage functionalization. The developed process relies upon the reaction of an amine with (Me₄N)SCF₃ and AgF in CH₃CN or CH₂Cl₂ and the *N*-CF₃ derivatives of anilines, cyclic amines, and alkyl amines were prepared in good yield using this protocol. Included in the survey was the preparation of **272**−**274** which are the *N*-CF₃ analogues of the PDE-5 inhibitor sildenafil, the antifungal agent terbinafine, and the tricyclic antidepressant amitriptyline, respectively. Unfortunately, these compounds were not evaluated in the appropriate assays to determine if biological activity was preserved or in in vitro assays that would offer insight into drug developability properties and potential issues.[124]

272   **273**   **274**
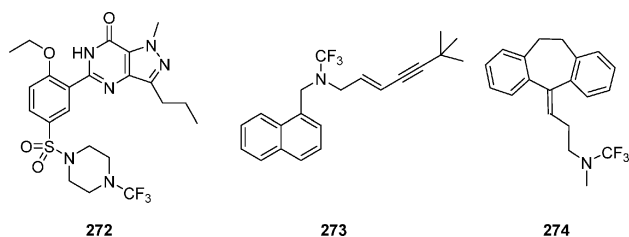
The best documentation of an N-CF₃ derivative that has been assessed biologically in vitro is provided by the quinolone **276**, which was tested in the series of antibacterial assays summarized in Table 28.[125] The inhibitory profile of **276** toward both

Table 28. Antibacterial Activity Associated with the N-CH₃-Substituted Quinolone 275 and Its N-CF₃-Substituted Homologue 276

		Gram-positive		Gram-negative	
	R	*S. aureus* Smith	*St. pneumoniae* type III	*E. coli* NIHJ JC-2	*P. aeruginosa* IID1210
275	CH₃	0.78	3.13	0.05	6.25
276	CF₃	0.39	6.25	0.05	1.56

Gram-positive and Gram-negative bacteria was comparable to the N-CH₃ homologue **275**, with some possible advantage for **276** with respect to inhibition of *P. aeruginosa*.

The purine **277** was prepared as the sole N-CF₃ derivative in a series of Cdk2 inhibitors, and this compound inhibited the enzyme with an IC₅₀ value of 1 μM.[126] Unfortunately, the matching N-CH₃ analogue that would allow a direct comparison was not made but the Cdk2-inhibitory activity of **277** was comparable to similar alkyl-substituted analogues in the broader series.
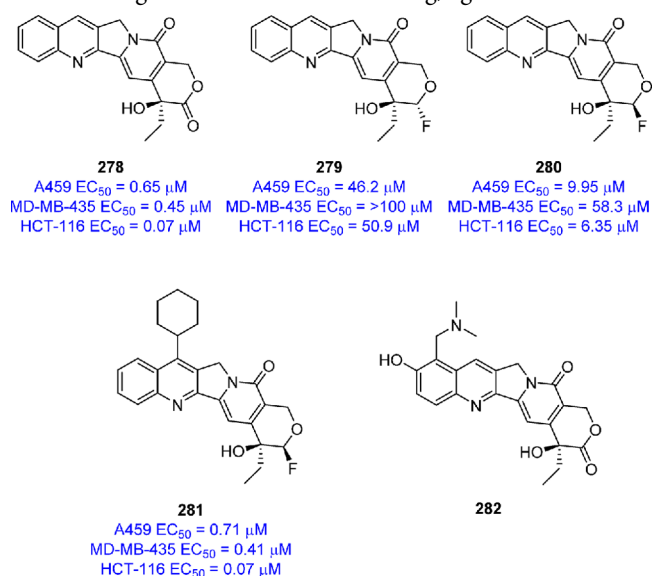

277
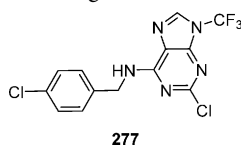
■ FLUORINE AND CARBONYL BIOISOSTERISM

A number of drug design initiatives have sought to take advantage of fluorine-containing functionality as bioisosteres of the carbonyl functionality. However, while there has been some focus on mimicking the amide functionality, which will be discussed later, there are examples of the use of fluorinated elements as bioisosteres of the carbonyl moiety of ketones, lactones, and carboxylic acids. In this section, representative examples are discussed that demonstrate functional bioisosterism in a range of biochemical contexts, with the underlying design principles in some cases supported by X-ray cocrystallographic data.

sp³ C−F as a C=O Bioisostere. Mimicry of C=O by a C−F is a function of the similarity between bond lengths, van der Waals radii and dipoles of the two functionalities and the electronegativity of oxygen and fluorine. A successful application of C=O/C−F bioisosterism can be found in studies with camptothecin (**278**), a naturally occurring alkaloid derivative that potently inhibits topoisomerase I and prevents tumor cell proliferation in vitro with EC₅₀ values of <1 μM.[53b,127] However, in vivo applications of **278** are limited, in part, by the low chemical and metabolic stability associated with the lactone ring

which is hydrolyzed rapidly to the inactive carboxylic acid derivative. Replacing the lactone C=O with an α-fluoro ether moiety was examined as a potential bioisostere based on an appreciation of the similarity of dipoles of the C−F and C=O bonds.[127] The (2R)-isomer **279** was a significantly less potent inhibitor of both topoisomerase I enzyme-mediated relaxation of supercoiled DNA and tumor cell proliferation in vitro than the (2S)-isomer **280**. However, in assays measuring stability in H₂O at pH = 7.4, the fluoro ether ring of **280** was found to offer superior performance when compared to the lactone **278**. Lactone **278** was degraded by >50% after 6 h of incubation compared to a loss of just 4% for **280**, with a similar profile observed in phosphate buffer. The antiproliferative potency of **279** was fully restored to the levels offered by **278** by decoration of the quinolone core, with the C-7 cyclohexyl derivative **281** optimal. This compound demonstrated dose-related inhibition of tumor growth in two xenograft models following IP administration of doses of 2−4 mg/kg, with efficacy comparable to topotecan (**282**), a camptothecin derivative, at a dose of 0.5 mg/kg. Notably, administration of **281** at 2 mg/kg was not associated with the weight loss observed with 0.5 mg/kg doses of **282**.

278
A459 EC₅₀ = 0.65 μM
MD-MB-435 EC₅₀ = 0.45 μM
HCT-116 EC₅₀ = 0.07 μM

279
A459 EC₅₀ = 46.2 μM
MD-MB-435 EC₅₀ = >100 μM
HCT-116 EC₅₀ = 50.9 μM

280
A459 EC₅₀ = 9.95 μM
MD-MB-435 EC₅₀ = 58.3 μM
HCT-116 EC₅₀ = 6.35 μM

281
A459 EC₅₀ = 0.71 μM
MD-MB-435 EC₅₀ = 0.41 μM
HCT-116 EC₅₀ = 0.07 μM

282

Fluoro Alkenes and Aromatic Fluorides as C=O Bioisosteres. Fluoro- and trifluoromethyl-alkenes and chloroalkenes have been proposed as potential amide bioisosteres based on the topological, steric, and electronic relationships illustrated in Figure 20, and some of these structural elements

μ = 3.6 D   μ = 1.4 D   μ = 2.3 D   μ = 0.2 D   μ = 0.1 D   μ = ~1.5 D
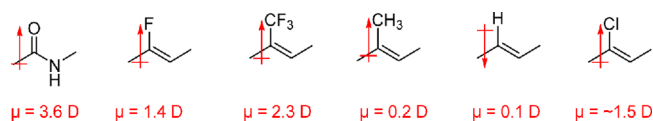
Figure 20. Dipole moments and vectors that illustrate isosterism between an amide moiety and fluorinated alkene derivatives that contrasts with simpler alkenes.

have found application in the design of both small molecule drugs and peptidomimetics.[8,128−132] However, while the geometries are similar, the dipoles associated with the fluorinated and chlorinated olefins are of a lower strength when compared to an amide, more comparable to an aldehyde or ketone, and although the dipole vectors are similarly aligned, DFT calculations indicate that a chloroalkene more closely approximates an amide than a fluoroalkene.[133,134]

Examples of Fluorinated Alkenes As Amide Bioisosteres. An example where a fluoroalkene functions as an effective amide replacement when embedded in a peptidomimetic background is provided by studies with Leu-enkephalin (**283**), a pentapeptide that activates the δ-opioid receptor but fails to produce analgesia in vivo due to poor PK properties.[131] The ester **284** and thioamide **285** retained δ-opioid receptor activity, indicating that a H-bond donor at this site was not essential and inspired the design of the fluoro olefin **286**. The potent activity of **286** confirmed the H-bonding hypothesis, while the weaker receptor binding affinity associated with the simple olefin **287** emphasized the importance of the fluoride atom for effective functional mimicry.

283
K_i = 6.9 ± 2.3 nM
Log $D_{7.4}$ = -0.95

284
K_i = 34 ± 17 nM

286
K_i = 43 ± 14 nM
Log $D_{7.4}$ = -0.11

285
K_i = 47 ± 17 nM

287
K_i = 587 ± 19 nM
Log $D_{7.4}$ = -0.07

288
EC$_{50}$ δ = 5.0 nM
EC$_{50}$ μ = 60 nM
EC$_{50}$ κ >10,000 nM
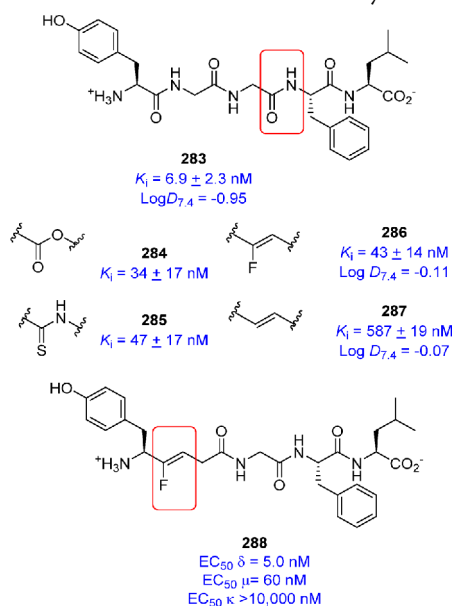
A fluoro alkene was also examined as a replacement for the amide moiety at the Tyr^1–Gly^2 junction as an approach to interfering with metabolism at this site.[132] The Leu-enkephalin analogue **288** demonstrated significant activity toward activating the δ- and μ-opioid receptors stably expressed in CHO cells, although the EC$_{50}$ values were 60- and 45-fold higher, respectively, than for progenitor **283**. However, differentiation was observed at the κ-opioid receptor where the activity of **288** was negligible compared to **283**, which expressed an IC$_{50}$ value of 80 nM.[132]

Both a fluoro- and a chloro-alkene were found to be effective amide mimetics when installed in a 36-residue peptide derived from the amino terminus of human parathyroid hormone (hPTH), where they were incorporated as part of a dipeptide element installed at the amino terminus.[134] Comparison of the matched pairs **289/290** and **291/292** indicates that in this context, the fluoro- and chloro-alkenes performed similarly with respect to binding to the PTH receptor and expression of full intrinsic

activity as measured by cAMP production, with the exception of **289**, which acted as a partial agonist (Table 29).[134b]

A fluoro-olefin was examined as a potential amide bioisostere in DPP-4 inhibitors in an attempt to confer resistance to cleavage by amidases or proteases, with **294** found to be 5-fold less potent than its matched amide **293**, attributed to the weaker dipole associated with the former.[135] However, potency was enhanced by variation of both the P$_1$ moiety and the pattern of substitution on the phenyl ring, with **295** a considerably more potent DPP-4 inhibitor. An X-ray cocrystal structure of **295** bound to the enzyme revealed a similar binding mode to an amide homologue, with the fluorine atom of the bioisostere proximal to the side chain N-Hs of Arg$_{125}$ and Asn$_{710}$, described as a H-bonding interaction.[135]

293
IC$_{50}$ = 0.20 μM

294
IC$_{50}$ = 1.17 μM

295
IC$_{50}$ = 0.2 nM
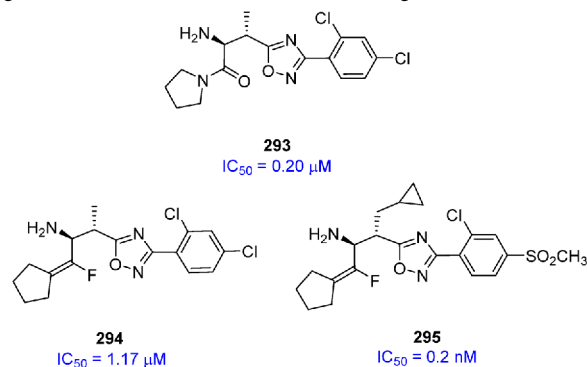
A conformational analysis of the symmetrical and potent HCV NS5A inhibitor daclatasvir (**296**) revealed that the most stable conformers were those stabilized by an intramolecular H-bond between the valine carbonyl oxygen atom and the imidazole N–H (distance = 2.2 Å).[136] This topography resembled that of a γ-turn and inspired the design of a fluoro-alkene amide bioisostere in which both of the valines of **297** were predicted to adopt a similar conformation, with the fluorine to imidazole N–H distance predicted to be 2.29 Å. In contrast, the analogue **298**, in which the conformational constraint associated with the cylcopentane ring of **297** was relaxed, was predicted to exhibit a much lower propensity to adopt a γ-turn topography. In a GT-1b HCV replicon assay, although **297** was several fold weaker than **296**, it still maintained subnanomolar inhibitory potency.[136a] However, in both GT-1a and GT-2a replicons, **297** was substantially (>2500-fold) less active than **296**, demonstrating the heightened sensitivity of these two genotypes to structural changes in the molecule.[136b]

296
GT-1a EC$_{50}$ = 0.050 nM
GT-1b EC$_{50}$ = 0.009 nM
GT-2a EC$_{50}$ = 0.063 nM

297
GT-1a EC$_{50}$ = 189 nM
GT-1b EC$_{50}$ = 0.079 nM
GT-2a EC$_{50}$ = 167 nM

298
GT-1a EC$_{50}$ = 659 nM
GT-1b EC$_{50}$ = 27.3 nM
GT-2a EC$_{50}$ = 3977 nM

Table 29. hPTH Receptor Binding Data for 289−292

A^1-A^2 =

A^1-A^2-Ser^3-Glu-Ile-Gln-Leu-Met-His-Asn^{10}-Leu-Gly-Lys-His-Leu-Asn-Ser-Met-Glu-Arg^{20}-Val-Glu-Trp-Leu-Arg-Lys-Lys-Leu-Gln-Asp^{30}-Val-His-Asn-Phe-Val-Ala-NH$_2$
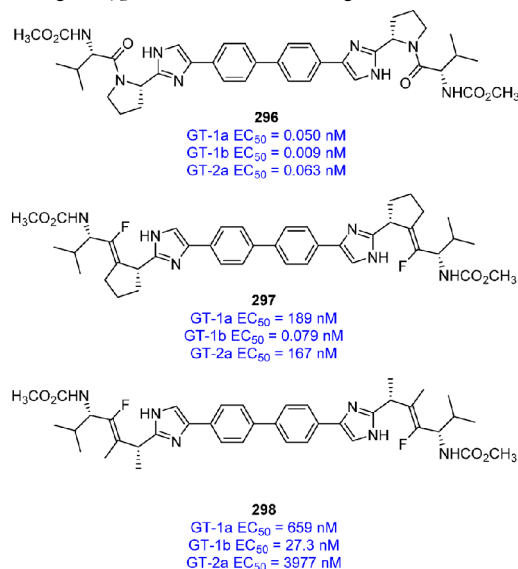
	X	R	binding affinity to opossum kidney (OK-1) cells (pK_D)	cyclic AMP OK1 EC$_{50}$ (nM) (intrinsic activity)
289	F	CH$_3$	8.2	9.1 (0.6)
290	Cl	CH$_3$	8.9	5.5 (1.0)
291	F	iPr	8.9	4.4 (1.0)
292	Cl	iPr	8.9	7.9 (1.0)

The antiviral effects of **298** were of lower potency, lending some support to the fundamental design principle.

Fluorinated olefinic peptide nucleic acids **301** (F-OPAs), patterned after peptide nucleic acids **299** (PNAs), were prepared with adenine, thymidine, and g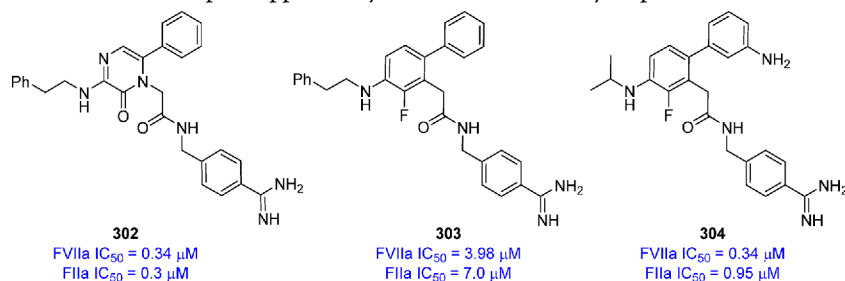uanine as the bases and incorporated into decameric oligomers for evaluation of the stability of the duplexes with complementary strands of DNA.[137] The stability, as determined by T_m values, was dependent upon the location of the nucleotide mimetic in the sequence, and while fully modified F-OPA decamers and pentadecamers formed parallel duplexes with complementary DNA, their stability was lower than either the peptide nucleic acid analogue **299** or OPA analogue **300**.

299
PNA

300
(E)-OPA

301
F-OPA
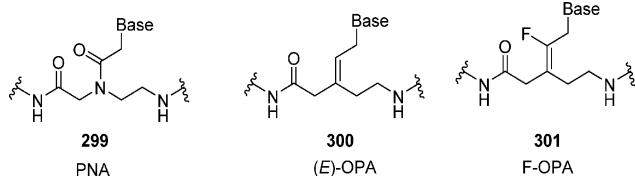
Aromatic Fluorides as C=O Bioisosteres. An aromatic fluoride, which may be viewed as incorporating an embedded alkenyl fluoride, has been shown to effectively substitute for a lactam carbonyl moiety in several biochemical contexts. Prominent examples where a bioisosteric relationship is supported by

302
FVIIa IC$_{50}$ = 0.34 μM
FIIa IC$_{50}$ = 0.3 μM

303
FVIIa IC$_{50}$ = 3.98 μM
FIIa IC$_{50}$ = 7.0 μM

304
FVIIa IC$_{50}$ = 0.34 μM
FIIa IC$_{50}$ = 0.95 μM

X-ray cocrystal structure data have been provided by inhibitors of enzymes in the coagulation cascade, studies that have provided detailed insights into structural emulation.[138,139] Comparison of the MMPs **302** and **303**, which are dual tissue factor VIIa (FVIIa) and thrombin (FIIa) inhibitors and prototype molecules in their respective series, provide an index of the level of functional mimicry, with the fluorophenyl moiety approximately an order of magnitude less potent in both enzyme assays.[138a,b] An X-ray cocrystal of the analogue **304** with FVIIa revealed that the fluorine atom was close to the N−H of Gly$_{216}$ (N to F distance = 3.4 Å) in a fashion that was reminiscent of the H-bond observed between the carbonyl oxygen atom of the amide-based inhibitors (Figure 21).[138] In this structure, the iso-propyl-substituted aniline N−H of **304** donated a H-bond to the backbone C=O of Gly$_{216}$, with the N to O distance measured as 3.4 Å.

Comparison of the data for the matched pair of thrombin inhibitors **305** and **306** suggests the potential for a bioisosteric relationship between the fluorophenyl and pyridine N-oxide moieties although the H-bonding properties of the two elements are considerably different, with the N-oxide moiety the more powerful acceptor.[139b,c,140]
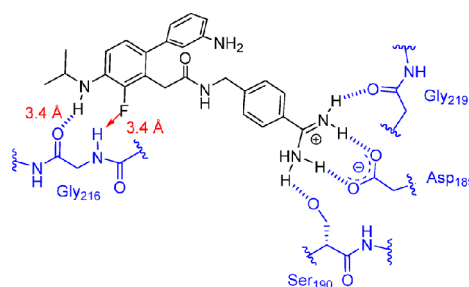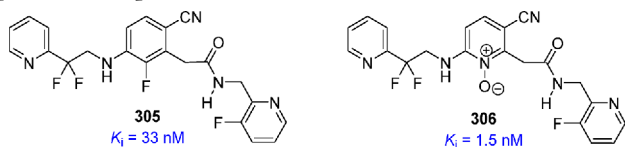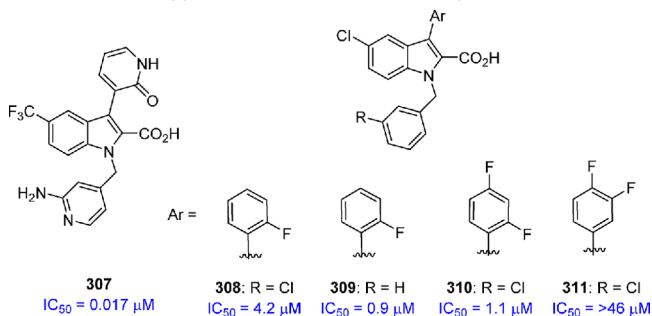

305
K_i = 33 nM

306
K_i = 1.5 nM

Figure 21. Key interactions between and FVIIa and the benzamidine-based inhibitor **304**.

A fluorobenzene motif has also been found to be an effective amide bioisostere when incorporated into allosteric inhibitors of the HCV NS5B RNA-dependent RNA polymerase, with **307** the prototype of the series.[141] The 2-fluoro derivative **309** was a potent inhibitor of NS5B biochemical activity in vitro, a profile that extended to the 2,4-difluoro homologue **310**. However, the des-fluoro analogue **308** and the 3,4-isomer **311** were found to be less potent, data that collectively emphasized the importance of the topology of fluorine patterning and were concordant with the idea that the C−F moieties in **309** and **310** mimic the C=O of **307**. An X-ray cocrystal structure of **309** with the NS5B enzyme revealed that hydrophobic interactions were dominant, with no specific interaction observed between the carboxylate element and the protein (Figure 22). However, the fluorine atom of **309** was close to the backbone NH of Tyr$_{448}$ with a nitrogen to fluorine distance of 2.6 Å, while the hydrogen atom ortho- to the fluorine substituent was 2.9 Å from the backbone carbonyl oxygen atom of Ile$_{447}$, a distance less than the sum of their van der Waals radii that was suggestive of a C−H H-bonding interaction.[140c,141]

307
IC$_{50}$ = 0.017 μM

308: R = Cl
IC$_{50}$ = 4.2 μM

309: R = H
IC$_{50}$ = 0.9 μM

310: R = Cl
IC$_{50}$ = 1.1 μM

311: R = Cl
IC$_{50}$ = >46 μM

In a series of non-ATP competitive MAP kinase kinase 1 (MEK1) inhibitors, the fused pyridone **312** exhibited an IC$_{50}$ value of 38 nM.[142,143] Although clearly not a MMP, the difluorobenzene homologue RO4987655 (**313**) demonstrated high inhibitory potency toward the kinase, and this compound was advanced into phase I clinical trials.[144] An X-ray cocrystal structure of the bromobenzene derivative **314** bound to MEK1 was informative, revealing an intramolecular H-bond between the N−H and the C=O oxygen atom of the hydroxamic acid

ester (Figure 23).[143,144] In addition, there was a halogen bonding interaction between the iodine atom and the backbone carbonyl
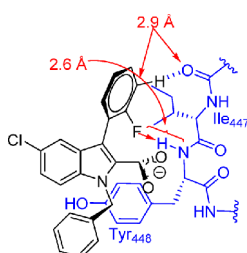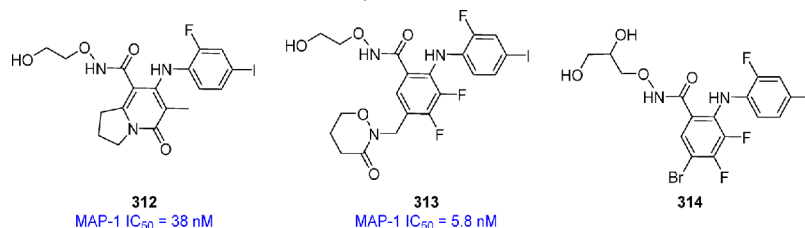
oxygen atom of Val[127] while the 4-fluoro atom was close to the backbone N—H moieties of both Ser[212] and Val[211].

312
MAP-1 IC$_{50}$ = 38 nM

313
MAP-1 IC$_{50}$ = 5.8 nM

314

Figure 22. Key drug−target interactions between **309** and the HCV NS5B polymerase protein.
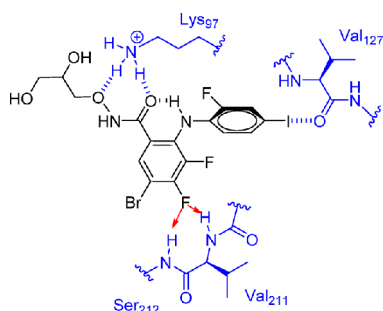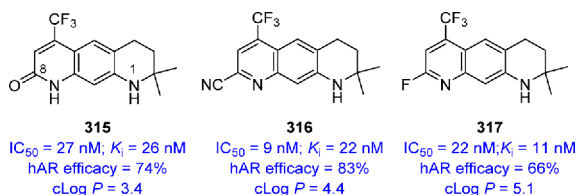

Figure 23. Key drug−target interactions between MEK1 and inhibitor **314**.

Several additional examples where there is evidence of a bioisosteric relationship between the C−F and C=O moieties have been described. In a series of pyridone-based fused tricyclic human androgen receptor (hAR) antagonists of which **315** is representative, examination of the potential of a bioisosteric relationship between the C−F and C=O moieties was adopted as an approach to understand which pyridone tautomer was responsible for the drug−target interactions.[145] The assays for assessing these compounds were based on a primary understanding of hAR binding affinity in a biochemical assay, while functional effects were determined based on inhibition of hAR-dependent transcriptional activity in mammalian CV-1 cells. While 8-amino and 8-alkoxy compounds were much weaker antagonists, small electron withdrawing groups at C-8 were preferred, with nitrile (**316**) and fluorine (**317**) optimal. In this context, there appears to be a bioisosteric relationship between the C=O, C≡N, and C−F moieties, and the data were proposed to support the concept that a H-bond acceptor is

required at this site of the pharmacophore, leading to the suggestion that the active tautomer was that of the pyridone represented in **316** rather than the alternate hydroxy pyridine.[145]

A C−F bond has also been invoked as a C=O isostere in the context of the GABA aminotransferase inhibitors **318** and **319**, where the carboxylic acid moiety was mimicked by a 2,6-difluorophenyl ring.[146] The fluorine patterning in **318** and **319**, which are competitive inhibitors of GABA aminotransferase with K_i values of 11 and 6.3 mM, respectively, enhanced the acidity of the phenolic hydroxyl, which has a pK_a value of 7.12 compared to 9.81 for phenol. The structural overlays presented in Figure 24
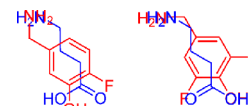
Figure 24. Structural overlays of **82** with **318** and **319** illustrating C−F and C=O mimicry.

were used to illustrate the postulated isosteric relationship between the C−F bond of **318** and **319** and the C=O moiety of the carboxylic acid of **82**.[146]

318
K_i = 11 mM

319
K_i = 6.3 mM
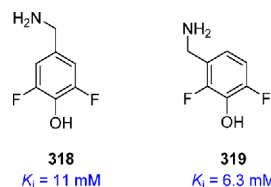
These observations were the basis of the installation of a 2,6-difluorophenol moiety as a potential carboxylic acid bioisostere in a series of carbonic anhydrase inhibitors patterned after the carboxylic acids **320** and **321**.[147] In the analysis of the matched pairs **320**/**321** and **322**/**323**, the 2,6-difluorophenol offered a

315
IC$_{50}$ = 27 nM; K_i = 26 nM
hAR efficacy = 74%
cLog P = 3.4

316
IC$_{50}$ = 9 nM; K_i = 22 nM
hAR efficacy = 83%
cLog P = 4.4

317
IC$_{50}$ = 22 nM; K_i = 11 nM
hAR efficacy = 66%
cLog P = 5.1

320
IC$_{50}$ = 2.4 μM

321
IC$_{50}$ = 0.39 μM

322
IC$_{50}$ = 87 μM

323: R = H
IC$_{50}$ = 33 μM

324: R = NH$_2$
IC$_{50}$ = 14 μM

325: R = OCH$_3$
IC$_{50}$ = 16 μM

326: R = H
IC$_{50}$ = 5.7 μM

327: R = NH$_2$
IC$_{50}$ = 0.4 μM
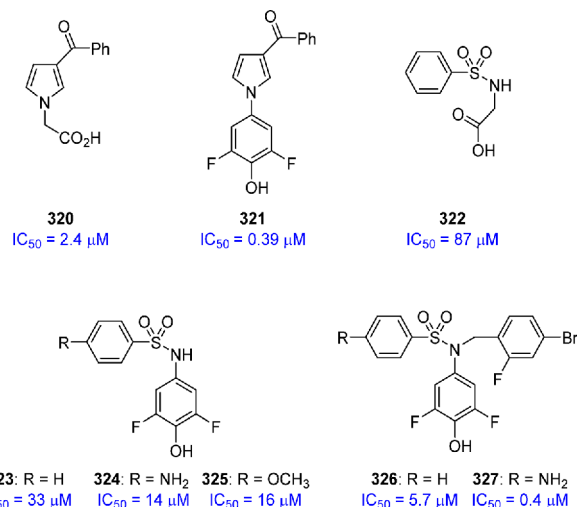
potency advantage that was further modulated by modifying the phenyl ring substituents of **322** (compounds **324** and **325**) or by the introduction of the benzyl moiety, as in **326** and **327**.[147]

Alkenyl Fluoride as an Enol Mimetic. Alkenyl fluorides have also been contemplated as mimics of enol-based intermediates in enzyme-mediated reactions.[148−150] The alkenyl fluorides **329** and **330** were prepared as mimics of the (*Z*) and (*E*) enol forms, respectively, of pregnenolone **328**. These compounds were probed as inhibitors of steroid $C_{17\alpha}$ hydroxylase/$C_{17(20)}$ lyase, which converts progesterone to androstenedione and **328** to dehydroepiandrostene, with extension to potential therapies for prostate cancer and hormone-dependent breast cancer which rely upon the production of androgens and estrogens, respectively.[148] The enol of **328** is thought to be an intermediate in the initial $C_{17\alpha}$ hydroxylation step catalyzed by the dual acting enzyme. Incubation of **329** with cynomolgus monkey testicular $C_{17(20)}$ lyase at a concentration of 1 μM resulted in 49% inhibition of enzymatic activity, with the effect determined to be time-dependent because inhibition after 40 min of preincubation increased to 72%. By way of contrast, **330** was associated with 54% inhibition of $C_{17(20)}$ lyase activity at a concentration of 1 μM but with minimal evidence of time-dependence because the amount of inhibition was relatively constant, measured as 60% after a 40 min preincubation period.[148]

328   **329**   **330**
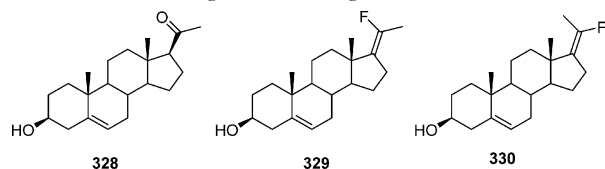
Other steroidal enzyme inhibitors where an alkenyl fluoride has been explored as a transition state mimic are the type I and type II 5α-reductases which convert testosterone (**331**) to the more androgenic dihydrotestosterone (**333**), with the enolate **332** a postulated intermediate (Scheme 5).[149] Finasteride **18** is a potent inhibitor of the type II 5α-reductase, IC_{50} = 1.2 nM but is a more modest inhibitor of the type I enzyme IC_{50} = 650 nM. The alkenyl fluoride **334** inhibited the type II 5α reductase with an IC_{50} value of 480 nM, 400-fold less potently than **18**, and the type I enzyme with an IC_{50} value of 1300 nM, 2-fold weaker than **18**. The alkenyl fluoride **334** was unique in the halogen series because the homologous chloride **335** and bromide **336** were inactive in both assays. In this context, the alkenyl fluoride moiety may be considered reflective of a bioisosteric relationship with both an enolate and an amide.

The α,β-dihydroxyacid dehydratase class of enzyme catalyzes the elimination of water from a dihydroxy acid to produce the enol **337**, which is tautomeric with an α-keto acid, as summarized in Scheme 6.[150] The alkenyl fluoride **338** was prepared as a mimic of **337**, a design principle successful to the extent that this compound inhibited the dehydratase with a K_i/K_m ratio of 0.18,

Scheme 6. Reaction Process Catalyzed by α,β-Dihydroxyacid Dehydratase
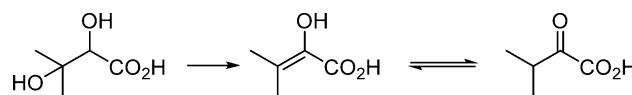
superior in this case to the simpler acrylate **339** and the amide **340**, which was inactive.

337	**338**	**339**	**340**
	K_i/K_m = 0.18	K_i/K_m = 3.6	K_i/K_m = not active
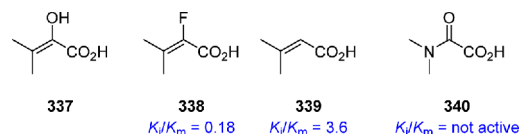
The 1,1-Difluoro Alkene Moiety as a C=O Bioisostere. The fluorine atoms of the 1,1-difluoroalkene moiety have been advocated in C=O mimesis, with the two fluorine atoms approximating the electron density associated with the lone pairs of electrons associated with the oxygen atom, although with similar dipole alignment of 30% lesser magnitude, as summarized in Figure 25.[151]

μ = 2.33 D   μ = 1.38 D
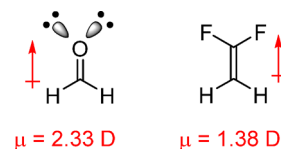
Figure 25. Isosteric relationship between formaldehyde and 1,1-difluoroethylene.

A pioneering examination of a 1,1-difluoroalkene as a C=O mimic was in the design of **341** as a substrate analogue of thymidine diphosphate (TDP)-6-desoxy-L-lyxo-4-hexulose (**342**) which is reduced to TDP-L-rhamnose (**343**) by the action of TDP-L-rhamnose synthase, a pathway summarized in Scheme 7.[152]

Scheme 7. TDP-L-rhamnose Synthase-Catalyzed Reduction of 342 to 343

342   **343**
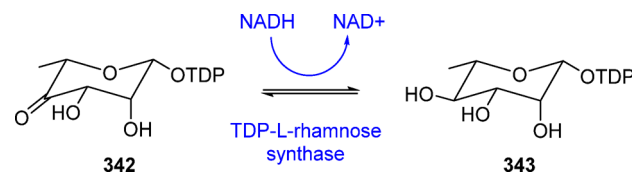
The design premise was based on the underlying electronics of the C=CF₂ moiety acting as a C=O mimic, with the anticipation that the addition of hydride to the olefin would occur with facility and in the same fashion as the addition to the ketone carbonyl. This mode of reaction was expected to generate an intermediate anion on a carbon atom that is adjacent to two fluorine atoms, setting up potentially unfavorable interactions

Scheme 5. Metabolism of 331−333 by Steroid 5α-Reductase

331   **332**   **333**   **334**: X = F
335: X = Cl
336: X= Br
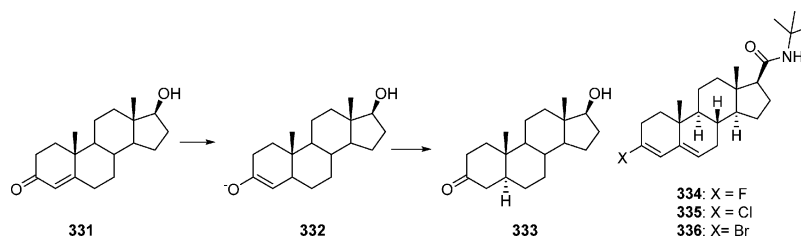
with the fluorine lone pairs that would be destabilizing and precipitate either a structural rearrangement or the loss of fluoride to afford a reactive carbene species.[153]

341
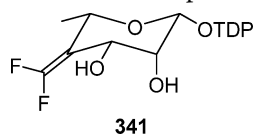
In the event, incubating TDP-L-rhamnose synthase (1 μM) with a 6000-fold excess (6.1 mM) of **341**, evaluated as a 3:1 mixture of α- and β-anomers, revealed that it acted as a poor but nevertheless kinetically competent substrate. However, irreversible inactivation of the enzyme was not observed; rather, the isolated products reflected the loss of one (**344**) or both fluorine atoms (**345**), an observation that was attributed to hydride addition to the exocyclic carbon atom which was favored over the alternative site of attack (Scheme 8). The resulting anion

Scheme 8. Postulated Reaction Pathway of 341 with TDP-L-rhamnose Synthase
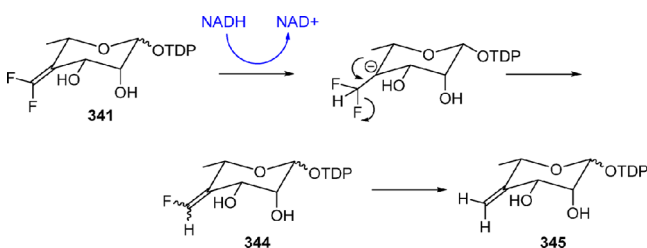
would be expected to decompose by elimination of fluoride, with the initially produced **344** also acting as a substrate for the enzyme, able to engage in a repeat of the reduction cycle that would lead to the completely defluorinated olefin **345**, a process depicted in Scheme 8. Thus, in this context, the difluoro olefin of **341** does indeed act as a mimic of the ketone C=O but reverses the regioselectivity of hydride addition.

A successful application of the 1,1-difluoroethylene moiety as a bioisostere has been in the design of improved derivatives of the antimalarial agent artemisinin (**346**) for which resistance is beginning to emerge.[154,155] The difluorinated alkene **347** was conceived as a more stable derivative of the lactone in **346**, with in vitro potency improved 2-fold compared to the progenitor.[154] Intraperitoneal (IP) administration of **347** to mice infected with *Plasmodium berghei* at a dose of 35.5 μmol/kg for 4 days resulted in no detectable parasitemia on day 4 compared to parasitemia levels of 25% for animals dosed with **346** and 50% for the untreated control group.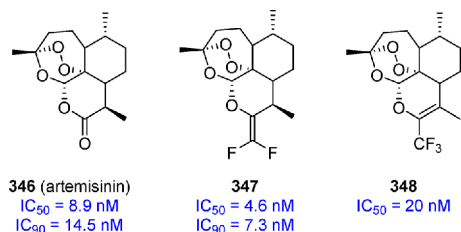[154b] In this setting, a CF_3-alkene moiety is also an effective carbonyl bioisostere, as demonstrated by the potent in vitro antimalarial activity associated with **348**.[154a]

346 (artemisinin)
IC_{50} = 8.9 nM
IC_{90} = 14.5 nM

347
IC_{50} = 4.6 nM
IC_{90} = 7.3 nM

348
IC_{50} = 20 nM

The CF_2 Moiety as a C=O Bioisostere. A CF_2 moiety has been shown to function as an effective ketone bioisostere when installed in analogues of nonimmunosuppressive inhibitors of FK506-binding proteins (FKBPs), members of the immunophilin class of chaperones.[156] The in vitro and in vivo neurotrophic activity exhibited by the immunophilin FK506 (tacrolimus, **349**)

can be recapitulated by nonimmunosuppressive compounds that mimic the FKBP12-binding portion of the macrolide lactone. The design concept explored initially assessed replacing the ketone carbonyl of the prototype molecule **350** with a CF_2 to afford **351**, a compound that performed slightly better as an inhibitor of FKBP12 rotamase activity than the progenitor. The importance of the CF_2 element was underscored by the absence of significant rotamase inhibition by the CH_2 homologue **352**. Chemical stability studies indicated that **351** was stable over 27 h in phosphate-buffered saline/DMSO, alleviating concerns around the benzylic difluoride moiety and particularly its relationship with the electron rich aromatic ring. The optimized molecule **354**, which was patterned as an analogue of V-10367 (**353**), inhibited FKBP12 rotamase activity with a K_i of 19 nM, potency that compared favorably with the 0.3 nM K_i observed for **353** under comparable experimental conditions.[156] An X-ray cocrystal structure of **354** bound to FKB12 indicated that one of the fluorine atoms was close to the hydrogen of Tyr_{26}−OH (F to O distance = 3.18 Å), resembling the H-bonding interaction of the ketone C=O of **353**, while the second fluorine atom interacted with a meta hydrogen of Phe_{36} with an aromatic carbon to fluorine distance of 3.02 Å.[156a]

349
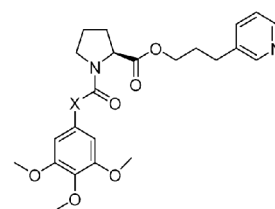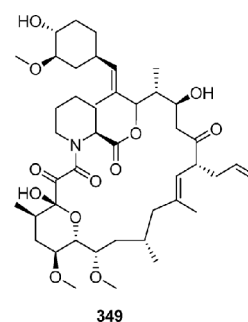
350: X = C=O **351**: X = CF_2 **352**: X = CH_2
K_i = 4.0 μM K_i = 0.87 μM   inactive
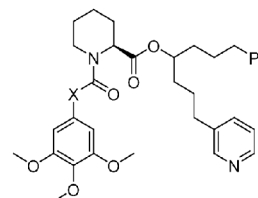
353: X = C=O   **354**: X = CF_2
(V-10367) K_i = 19 nM
K_i = 0.3 nM

The pyrazolo[4,3-*c*]pyridine **355** was characterized as a potent γ-secretase inhibitor that was active in vivo in a wild-type FVB mouse model, reducing brain Aβ40 levels by 25% following an oral dose of 5 mg/kg despite the low oral bioavailability (2.5%) of this compound.[157] However, **355** was labile in liver microsomes, with oxidation of both the ethyl substituents and the methylene that is exocyclic to the pyrazole identified as significant sites of metabolic susceptibility. In addition, the pyrazole ring N atom was subject to rapid glucuronidation, while GSH adducts were formed by a process that involved the direct displacement of the

chlorine substituent on the phenyl ring.[157] Iterative optimization to address these problems led to the identification of the ketone analogue **356**, which was less susceptible to glucuronidation but exhibited poor biological activity in a cell-based assay, despite potent intrinsic enzyme inhibition. This was traced to a chemical degradation pathway that involved elimination of 4-chlorophenylsulfinic acid from these molecules to afford the corresponding hydroxy pyridines **357**. Replacing the ketone C=O with a CF_2 gave a series of compounds from which **358** emerged after further structural manipulation designed to more comprehensively address HLM instability. This compound lowered brain $A\beta40$ by 27% in vivo in a mouse model following oral administration of a dose of 1 mg/kg.[157]

355
IC$_{50}$ (APP) = 0.3 nM
SNC cell EC$_{50}$ = 1 nM

356
IC$_{50}$ (APP) = 0.6 nM
SNC cell EC$_{50}$ = 2 nM

357

358
IC$_{50}$ (APP) = 1.4 nM
SNC cell EC$_{50}$ = 4 nM
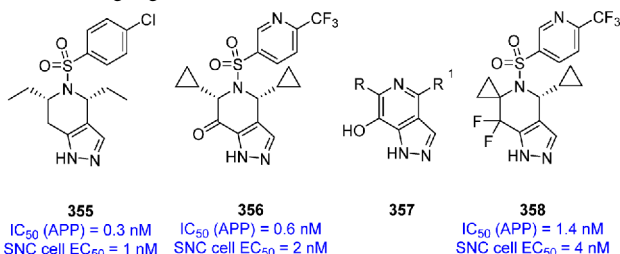
In a series of atypical antipsychotics where the combination of antagonist activity at the dopamine D_2 and serotonin $5HT_{2A}$ receptors with agonist effects at the serotonin $5HT_{1A}$ receptor was sought, the CF_2 moiety in **360** performed similarly to the ketone **359**, an SAR point reproduced in analogues in which the benzothiophene moiety was varied.[158,159]

359: X= C=O
D_2R = 40.5 nM
$5HT_1AR$ = 32.9 nM
$5HT_2AR$ = 44.0 nM

360: X = CF$_2$
D_2R = 3.51 nM
$5HT_1AR$ = 7.09 nM
$5HT_2AR$ = 11.5 nM
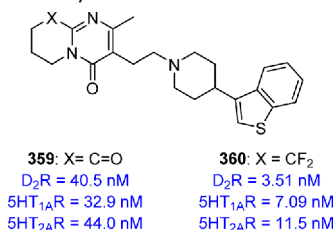
■ FLUORINATED MOTIFS AS AMIDE, SULFONAMIDE, AND UREA MIMETICS

Trifluoroethylamine and Difluoroethylamine Derivatives. The bioisosteric relationship between a trifluoroethylamine moiety and an amide functionality was originally conceived by Zanda who examined its potential in the context of designing peptidomimetics (Figure 26).[159,160] In addition, the plasticity of this structural element was recognized based on its potential to be incorporated either in register within the peptide frame, as depicted in Figure 26B, or in the partially retro-inverted configuration illustrated in Figure 26C.

The fundamental basis for mimicry between the CF_3CH_2NH moiety and the more recently explored CHF_2CH_2NH homologue and an amide is captured in Figure 27 and relies upon both geometrical and electronic considerations.[159] The key C−C−N bond angle of the CF_3CH_2NHR moiety is comparable to that of an amide, while the electron withdrawing effects of the CF_3 moiety reduce the basicity of the amine such that the H-bond
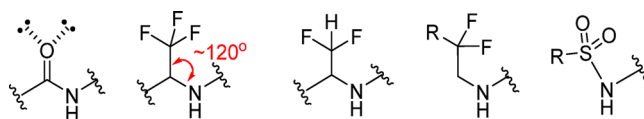
Figure 27. Functional aspects of the mimicry between an amide and a sulfonamide moiety and CF_3CH_2NH and CHF_2CH_2NH.

donating properties of the N−H are more like that of an amide N−H.[159] In addition, the C−F dipoles and electron density are believed to provide some emulation of the amide oxygen lone pairs of electrons. Somewhat analogously, the RCF_2CH_2NH may be viewed as a sulfonamide mimic in which the two fluorine atoms function as metaphors of the sulfone oxygen atoms, with the imprecise topographical relationships between the bonds of the two moieties possibly compensated by the longer C−S and N−S bonds.[159c] These structural elements have the advantage of relieving the topographical constraints imposed by an amide functionality which, in appropriate circumstances, may enhance complementarity with a specific target. While deployment of the CF_3CH_2NH or CHF_2CH_2NH moieties eliminates metabolic sensitivity to amidases, esterases, and proteases, these motifs do introduce a new asymmetric center.

The CF_3CH_2NH moiety has found application as an amide bioisostere beyond incorporation into peptidomimetics, most prominently in mechanism-based inhibitors of the cathepsin family of cysteine protease inhibitors from which the cathepsin K inhibitor odanacatib (**361**) was derived.[161] An analysis of the X-ray cocrystal structures of peptide-based inhibitors of cathepsin K revealed that while the P_1−P_2 amide engaged the protein via H-bonding interactions involving both the N−H and C=O oxygen atom, the P_2−P_3 amide element relied upon a H-bond interaction involving only the N−H as a donor.[161a] This inspired the design of trifluoroethylamine derivatives that would reduce the pK_a of the amine while preserving the H-bond donor attributes. The data presented for **362**−**365** in Table 30 provides

Table 30. SARs Associated with the Series of Cathepsin K Inhibitors 362−365 that Incorporate Potential Amide Bioisosteres at the P_2−P_3 Junction

	R	cathepsin K IC$_{50}$ (nM)	pK_a
362	CF$_3$	0.9	1.3
363	CF$_2$CF$_3$	2.4	1.8
364	CH$_3$	988	6.7
365	CN	30	0.7

key insights into the identification of suitable amide bioisosteres in this series.[161b] The compiled SARs indicate the importance of amine pK_a because the CH$_3$ analogue **364** is 1000-fold less potent than the CF$_3$ derivative **362**; however, the CF$_3$CF$_2$ homologue **363** is somewhat less potent, while the nitrile **365**, which has the

A

B

C

Figure 26. Incorporation of the CF_3CH_2NH motif in a polypeptide backbone in register (B) or in a partially retro-inverted configuration (C) that mimics the amide of a conventional polypeptide (A).

lowest pK_a within this series, is 30-fold weaker than **362**. These results focused attention on the trifluoroethylamine series which w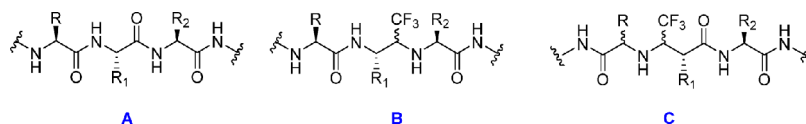as elaborated into the exquisitely potent inhibitor **366**, IC_{50} = 5 pM, a compound that identified the preferred absolute configuration at the trifluoroethylamine asymmetric center because the epimer **367** is almost 1000-fold less potent, IC_{50} = 4.6 nM.[161] However, the basicity associated with the piperazine moiety of **366** led to its accumulation in acidic lysosomes, rising to concentrations where it was able to inhibit cathepsins B, L, and S despite lower intrinsic inhibitory activity toward these proteases, IC_{50} values of 111, 47, and 451 nM, respectively. Consequently, the next phase of iterative compound design focused on structural modifications that avoided overt basicity, accomplished initially with the discovery of **368**, cathepsin K IC_{50} = 0.2 nM, that was cocrystallized with the enzyme.[161] The X-ray data confirmed effective amide emulation, with the trifluoroethylamine N−H engaging the carbonyl oxygen atom of Gly_{66}, while the CF_3 moiety projected into bulk solvent. The structural data also confirmed mechanism-based inhibition, with the nitrile moiety of **368** engaging the catalytic cysteine as a covalent iminothioether (Pinner-type) adduct. Further optimization of **368** focused on modulating the PK profile, with the sulfonamide replaced by a methylsulfone and a fluorine introduced to the isoleucine methine carbon atom to block a site of metabolic hydroxylation. A cyclopropyl moiety at P_1 was installed to reduce susceptibility of the amide toward hydrolysis resulting in **361**, a potent cathepsin K inhibitor, IC_{50} = 0.2 nM, that exhibited good selectivity for this enzyme over cathepsins B (IC_{50} = 1034 nM), L (IC_{50} = 2295 nM) and S (IC_{50} = 60 nM).[161c] Although **361** completed advanced clinical trials as a potential treatment for osteoporosis and bone metastasis, increasing bone mineral density and reducing the risk of fractures in patients, the compound was abandoned by its sponsor prior to the filing of an NDA due to the observation of an increased risk for cardiovascular events associated with drug therapy.[161d]


361
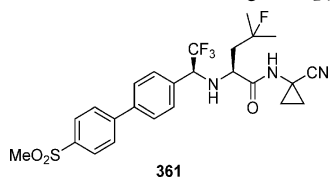
The high crystallinity associated with **361** resulted in low aqueous solubility, a property that contributed to the low (≤10%) oral bioavailability observed after administration of the drug as a suspension to preclinical species.[162] In an effort to address the dissolution-limited bioavailability, the difluoroethylamine analogue **369** was prepared with the anticipation that the enhanced basicity (pK_a increased by ∼1 unit) would facilitate salt formation with sulfonic acids and HCl and lead to reduced lipophilicity, with Log D decreased from 3.53 for

**366**: R = ... **367**: R = ... **368**

369
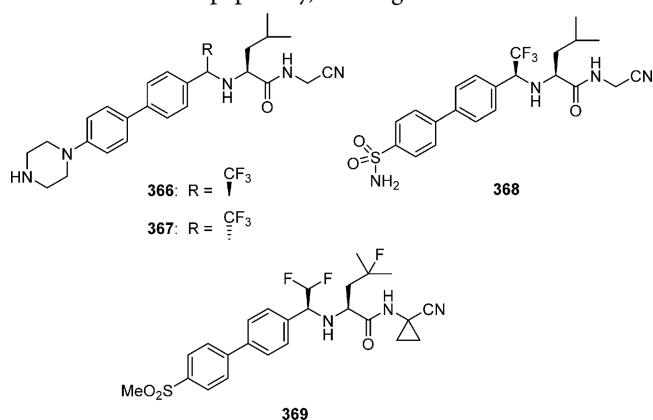
361 to 0.11 for **369**. Compound **369** retained the potent cathepsin K inhibitory activity (IC_{50} = 1 nM) and protease selectivity associated with **361**, while the modified physicochemical properties led to improved oral bioavailability in rats when the compound was administered as a 1% methocel suspension.[162]

A trifluoroethylamine moiety was examined as an amide bioisostere in the design of inhibitors of BACE-1, where a replacement for the anilide in **370** was sought to alleviate concerns about release of the aniline in vivo and its potential to express toxicity after metabolic activation.[164] The drug design process specifically focused on preserving the N−H of the anilide moiety of **370** because this was involved in a critical H-bonding interaction with the C═O oxygen of Gly_{230} of the enzyme based on an X-ray cocrystal structure of a related analogue. It was recognized that the conformational constraint imposed by the planar anilide might be optimized for interaction with Gly_{230} by a benzylamine moiety because it was anticipated to adopt an orthogonal arrangement with respect to the plane of the fluorophenyl ring. Initial derivatization took advantage of a reductive amination protocol to prepare libraries which identified the ethylamine **371** as a modest inhibitor of BACE-1 in a cell-free biochemical assay, IC_{50} = 13.9 μM. However, **371** was considerably more potent in the cell-based screen, which was attributed to concentration of the basic drug in the acidic endosomal compartment where BACE-1 is located. Consequently, further modification focused on modulation of amine basicity, which was accomplished by fluorination (**372**−**377**), as summarized in Table 31. The CF_3-cyclopropane moiety in **377** provided the optimal balance of properties, although further structural manipulation of this chemotype was required in order to surmount a problem associated with problematic CYP 2D6 inhibition. The conformational changes anticipated in the design phase were observed in an X-ray cocrystal structure of **377** with the BACE-1 enzyme, although the compound bound slightly differently in the active site compared to **370** in order to accommodate the altered drug−target vectors. The CF_3 substituent projected into the vestibule of the S_3 pocket, while the cyclopropyl ring filled a lipophilic pocket at the rear of the interface of the S_1 and S_3 pockets. This application provides an illustrative example of the advantage of the CF_3CH_2NH as an amide bioisostere where relief of steric constraint is beneficial.[163]

370
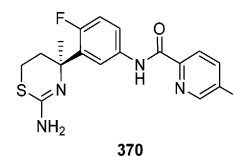
RCF_2CH_2NHR' as a Bioisostere of RSO_2NHR'. While a bioisosteric relationship between the sulfonamide and RCF_2CH_2NH moieties has not been explicitly recognized, inhibitors of the serine protease thrombin provide an example of the potential for this kind of structural metaphor.[139,159c] The X-ray cocrystal structures of thrombin and factor VIIa inhibitors (Figure 21) indicate that the anilide N−Hs of **378** and its analogues **379**−**382** engage with the backbone C═O oxygen atom of Gly_{216} in a H-bonding interaction; however, **378** is a modestly potent inhibitor of thrombin with a K_i value of 1.28 μM (Table 32). The difluoroethylamine **379** is 27-fold more potent, while the pyridine analogue **380** adds a further 6-fold potency increase. In this example, fluorination is of importance because the dimethyl and cyclopropyl derivatives **381** and **382**, respectively, are several fold less potent.[139a] Interestingly, the fluorine atoms were originally introduced as a means of abrogating metabolic modification at the benzylic site rather than for the purpose of structural emulation.[139d]

Table 31. SARs Associated with the BACE-1 Inhibitors 371−377[a]
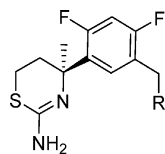
	R	BACE-1 CFA IC$_{50}$ (μM)	BACE-1 WCA* IC$_{50}$ (μM)	MDR Er	Log D	pKa	HLM Cl (mL/min/kg)
371	CH$_3$CH$_2$NH	13.9	0.008	2.0	<-1.5		<8
372	CF$_3$CH$_2$NH	1.31	0.060	1.2	1.0	3.8	12.0
373	CHF$_2$CH$_2$NH	5.89	0.058	3.1	0.3	5.2	13.0
374	CF$_3$CH$_2$CH$_2$NH	54.7	0.400	6.1	0.5	6.0	9.3
375	F$_3$C NH	0.49	0.031	3.6	1.5	4.2	<8.0
376	F$_2$HC NH	0.335	0.012	2.5	0.7	4.2	22.2
377	F$_3$C NH	0.069	0.018	1.5	1.8	2.9	<13

[a]*WCA = whole cell assay.

Table 32. Structure−Activity Relationships for the Thrombin Inhibitors 378−382

	R	K_i (nM)
378		1,280
379		47.1
380		8.6
381		58.0
382		57.0

Comparison of the thrombin inhibitory effects expressed by **383** and **384** illustrates a broad-based application of biosisoster-ism in drug design.[138,139] In these molecules, the oxyguanidine provides a mimetic of the guanidine found in natural substrates but with reduced basicity to facilitate oral delivery, the fluoro-benzene ring of **383** can be viewed as a bioisostere of the cyclic amide of **384** while the difluoroethylamine of **383** functions analogously to the sulfonamide of **384**.

383
K_i = 1.2 nM

384
K_i = 4 nM
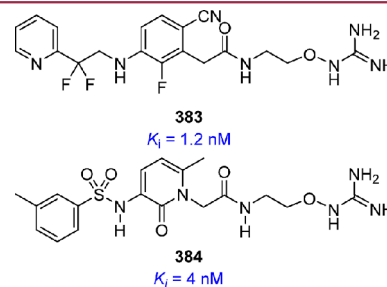
Fluorinated Amines and Mimesis of Imide-like Motifs. The *N*-(2,2,2-trifluoroethyl)methanesulfonamide moiety has found application in the optimization of HCV NS4B and acyl-CoA:monoacylglycerol acyltransferase (MGAT) inhibitors.[164,165] Symmetrical monofluorination of each of the CH$_3$ groups of **385** enhanced potency 3-fold (**386**), but *N*-dealkylative metabolism gave difluoroacetone, a compound associated with significant toxicity, while glutathione adducts resulted from oxidative metabolism of the indole heterocycle (Table 33).[164a,b] Pefluorination of a single CH$_3$ moiety of **385** gave a pair of enantiomers, of which the (*S*)-isomer **387** was 30-fold more potent than the (*R*)-isomer **388**, while the homologues **389** and **390** were less potent. Further optimization gave **391** as a compound that was advanced into clinical trials.[164c]

The MGAT inhibitor **392** was claimed to express an IC$_{50}$ value of <12 nM in a biochemical assay and inhibit MGAT expressed in a Caco-2 cell line with an EC$_{50}$ value of 58 nM, biological effects that translated to a 69% reduction in triacylglycerol absorption in male beagle dogs after an oral dose of 30 mg/kg.[165]

391

392
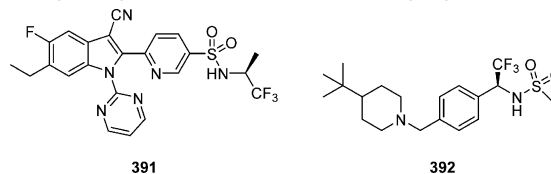
Table 33. Structure−activity Relationships Associated with HCV NS4B Inhibitors

	R	GT-1b HCV replicon EC$_{50}$ (nM)
385	-CH$_2$CH(CH$_3$)	12
386	(CHF$_2$ group)	4
387	(CH-CF$_3$ group)	2
388	(CH-CF$_3$ group)	67
389	(C-CF$_3$ group)	55
390	-CH$_2$CF$_3$	420

There are several higher homologues of the CF$_3$CH$_2$NH moiety that appear to offer opportunity for evaluation as potentially interesting structural metaphors. However, while these have not been the subject of systematic analysis in the context of bioisosteric relationships or the delineation of key physicochemical properties, the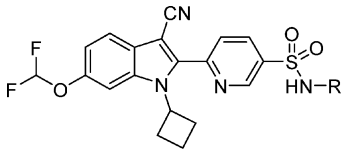re are examples of applications scattered throughout the literature in molecules that, in some cases, have been studied in some detail in a preclinical setting. In this section, I highlight representative examples that demonstrate applications in drug design, and which, if applied in an informed fashion in the appropriate context, may offer interesting benefits.

Inhibition of steroid 5α-reductase enzymatic activity has been shown to be sensitive to amide substitution patterns in a series of azasteroid-based inhibitors, particularly with respect to influencing activity toward the type I enzyme that is only modestly inhibited by **18**.[166] The introduction of the phenyl ring in dutasteride (**393**) is associated with potent type I 5α-reductase inhibition that affords a more balanced 5α-reductase inhibitor than **18** (Table 34). The benzylamine derivative **394** exhibits enhanced potency toward the type 1 enzyme compared to **18**, which is further enhanced by replacement of the CH$_3$ with a second CF$_3$ moiety, as depicted by **395**.[167] This modification removes the chirality associated with **394** and would be expected to enhance the H-bond donating capacity of the amide N−H, although in this example the N−H does not appear to be specifically involved in drug−target interactions.[168]


393

394: R = CH$_3$
395: R = CF$_3$
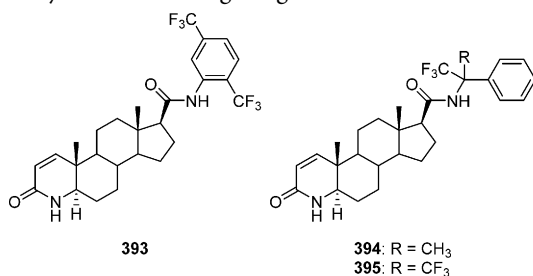
***N*-CH(CF$_3$)$_2$ as a Sulfone Bioisostere.** Diarylsulfonylureas, of which sulofenur (**396**) is the representative prototype, were

Table 34. Inhibition of Steroid 5α-Reductase Enzyme Activity by Aza Steroid Derivatives 18 and 393−395

	steroid 5α-reductase enzyme inhibition IC$_{50}$ (nM)			
	rat prostate	human prostate	human type I	human type II
18	30/32	52/58	470/313[a]	8.5/11.3[a]
393			4[b]	<0.1[b]
394	15	16	36	3.3
395	34	20	3.9	1.8

[a]Data taken from 2 independent assays abstracted from different articles.[166,167] [b]Under the assay conditions used to generate this data, finasteride inhibited the type I and type II enzymes with IC$_{50}$ values of 150 and 0.18 nM, respectively.[166]

discovered as cytotoxic antitumor agents using an in vivo screen conducted in mice implanted subcutaneously with solid tumors, a screening approach developed as an alternative to the more traditional approach of in vitro evaluation using hematopoietic tumor-derived cell lines.[169] Clinical toxicity associated with the metabolic release of 4-chloraniline from **396** led to its replacement by LY295501 (**397**).[170,171] The mode of antitumor action of the sulfonyl ureas is enigmatic but has been attributed, in part, to mitochondrial uncoupling.[170,172] The discovery of **396** stimulated considerable interest in this class of antitumor agent, and one interesting class of cytotoxic agent is provided by **398−400**.[173] The mode of action of **398−400** is equally enigmatic, but one interpretation is that they may be related to the sulfonylureas in a fashion that relies upon a bioisosteric relationship between the (CF$_3$)$_2$CH and SO$_2$ moieties. Unfortunately, MMPs are not available that would allow a more precise comparison. However, that the electron withdrawing effects of the two CF$_3$ substituents influence the proximal urea moiety was indicated by the presence of the isourea tautomer that was observed in polar solvent by ^{1}H NMR spectroscopic analysis.[173a]

396: X = CH$_2$; R = H (sulofenur)
397: X = O, R = Cl (LY295501)

398: R = H
399: R = CH$_3$CH$_2$

400
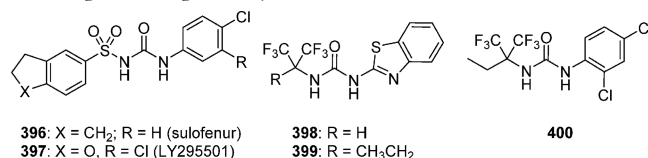
Fluorinated Motifs and Urea Bioisosterism. A careful and detailed theoretical analysis of the isosteric relationship between the urea **401** and fluoro enamide **402** has been conducted that recognizes the close topological similarities depicted in Figure 28.[174] However, while the bond angles and lengths
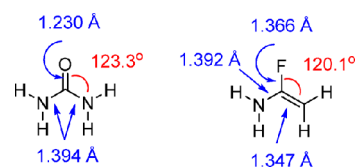
Figure 28. Bond angles and lengths that illustrate topological mimesis between a urea and a fluoroenamide.

show a close and compelling analogy, only *N*-alkyl, *N*-tosyl derivatives were prepared as part of the survey, and although these were shown to be chemically stable under neutral, basic, and acidic conditions, the synthesis of compounds with a free N−H was not described. In addition, there was no discussion of the pK_a value of the N−H in **402** and its homologues. Nevertheless, this motif represents an interesting element for use in drug design, particularly for analogues of ureas that do not possess a free N−H and would thus be more amide-like. However, this moiety has not

been adequately explored despite its potential to also be considered as an amide bioisostere, with functional mimicry potentially extending to the CF$_3$ and CF$_2$H derivatives **403−405**, respectively.
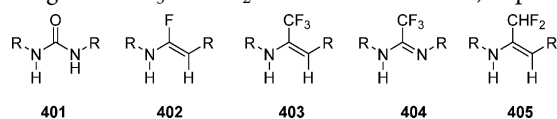
In a series of dopamine D$_2$ partial agonists explored for their potential to treat schizophrenia, the N−H of benzimidazolone of **406** that is distal to the oxyethylamine side chain functioned as a phenol bioisostere.[175] The cyclic urea motif of **406** was effectively mimicked by the 2-trifluoromethyl-substituted benzimidazole **409**, which was 24-fold more potent than the methyl homologue **408** and 54-fold more potent than **407**, the parent molecule of this series, presumably a reflection on the H-bond donating properties.[175c] Further optimization focused on fused pyran derivatives designed to confer conformational restraint, with both **410** and **411** potent ligands for the high affinity dopamine D$_2$ receptor.[175a,d] However, in this chemotype, the 2-trifluoromethyl-substituted benzimidazole was a less effective mimic of the urea of **410** and amide of **411**, with 15−40-fold lower affinity, for which speculation focused on an effect of ring fusion on the preferred tautomeric state of **412**.[175d]
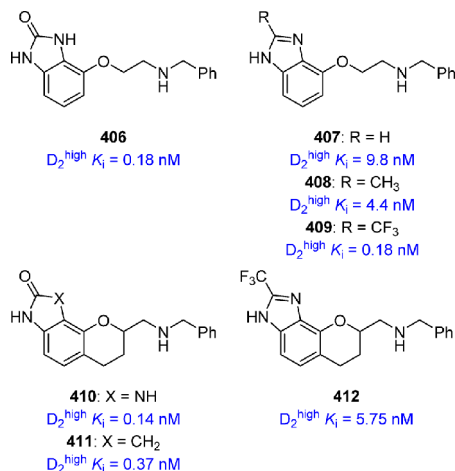
Fluoroamides and Urea Bioisosterism. α-Fluoromethyl and α,α-difluoromethyl secondary amides preferentially adopt a conformation in which the C−F and C=O bonds are aligned in a trans-relationship that is favored by both dipole interactions and reinforced by an electrostatic interaction between the fluorine atom and the amide N−H (Figure 29).[176−178] Indeed,

Figure 29. Calculated conformational preferences for α-fluoromethyl and α,α-difluoromethyl secondary amides.

this phenomenon has been exploited to illuminate the topography of the vanilloid receptor (TRPV1) agonist activity of capsaicin (**413**) by synthesizing and evaluating the α-fluorinated

enantiomers **414** and **415**.[179] The similar performance of **414** and **415** as agonists at the TRPV1 receptor led to the conclusion that the bound form was the extended conformation depicted in Figure 30A that is accessible to both enantiomers rather than the alternative topography presented in Figure 30B.[179]
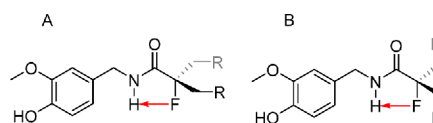
Figure 30. Conformational preferences of the α-fluorinated enantiomers of **413** designed to illuminate the bound conformation.
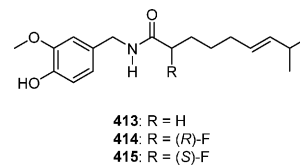
However, there are circumstances where this inherent preference can be overridden in favor of the gauche conformation, which for a simple $\al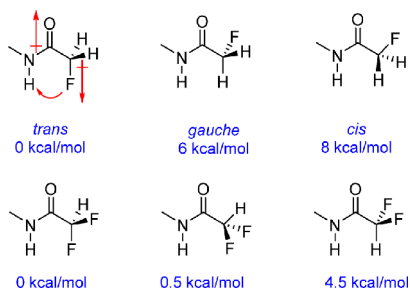pha$-fluoromethyl amide has been calculated to be ~6 kcal/mol higher in energy than the trans conformer, while for the α,α-difluoromethyl homologue the energy of the conformation that places the C−H and N−H in a syn relationship is ~4.5 kcal/mol higher (Figure 31).[180] Under these circumstances, α-fluoromethylamides and, particularly, α,α-difluoromethylamides, offer an opportunity to function as urea mimetics, as illustrated by the solid state structure of **416** which crystallizes in the conformation shown, stabilized by close contacts between both the N−H and C−H hydrogen atoms and the pendent carbamate oxygen atom. The bistrifluoromethylamide **417** and monotrifluoromethylamide **418** behave in a similar fashion, with the C−H to oxygen H-bond in **418** shorter than that in **417**, reflecting the poorer H-bond donor effects of this motif, anticipated based on the differences in electron withdrawing effects and polarizability.[180a] These molecules adopt conformations comparable to that observed with the thiourea **419**, and fluorinated acetanilides have been exploited with some success as organocatalysts based on the anticipation that they would recapitulate the effects of ureas and urea mimics.[180,181] However, the α-fluoro derivatives are more active catalysts than the α,α-difluoro analogues, perhaps surprising based on the calculated H-bond strengths which have been estimated to be ~3.0 kcal/mol for the α-fluoro derivatives and ~4.0 kcal/mol for the bis-CF$_3$ amides, with the latter more capable of overcoming the natural bias toward a conformation in which the F and amide and C=O are in a trans-periplanar arrangement.[181]

These motifs have found only very limited application in drug design presumably a function, in part, of concern for the release of difluoroacetic acid and fluoroacetic acid in vivo. However, an interesting example where the fluorination pattern of an amide moiety exerted an effect on ligand−protein interactions is provided by the disaccharide derivatives **420−423** which bind to the lectin wheat germ agglutinin (WGA), although in this example urea isosterism is not a basis.[182] The mono- and difluoroacetamides **421** and **422**, respectively, bind more tightly to WGA based on NMR analyses than the acetamide **420** and, particularly, the trifluoroacetamide **423**. These data were interpreted in the context of a productive C−H to π interaction between a C−H of the acetamide moiety and the phenol ring of a tyrosine residue of WGA. The electron withdrawing effects of fluorine substitution
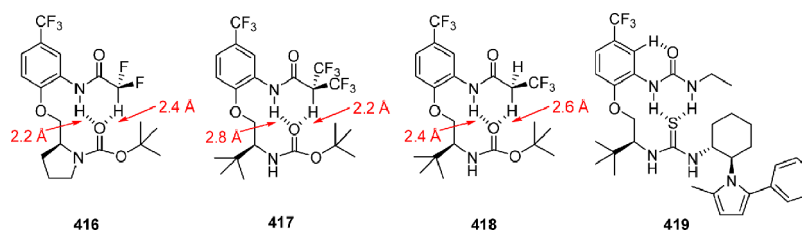
Figure 31. Topologies and bond lengths associated with α-fluoro-substituted amides **416**−**418** and urea **419** in the solid state.

in **421** and particularly **422** polarize the C−H bond, thereby enhancing this interaction. The importance of the effect is underscored by **423**, which cannot engage in this kind of interaction and exhibits an order of magnitude lower affinity for WGA than **422**.[182]

420: R = CH$_3$
K_D = 190 μM

421: R = CH$_2$F
K_D = 150 μM

422: R = CHF$_2$
K_D = 50 μM

423: R = CF$_3$
K_D = 650 μM

Halogenated amide analogues of melatonin (**424**) and ago-melatine (**426**) have revealed interesting structure−activity relationsh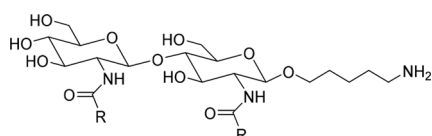ips that indicate the importance of the fluorination pattern on binding affinity (Table 35).[183] The CF$_3$ amide **429** derived

Table 35. Structure−Activity Relationships Associated with Melatonin Agonists

	MT$_1$ (pK_i)	MT$_2$ (pK_i)
424	9.34	9.02
425	9.7[a]	
426	~10	~10
427	8.21	9.40
428	10.27	9.07
429	8.24	8.75
430	8.30	8.75
431	14.3	7.62

[a]Data from an assay assessing binding to cell membranes using ligands that do not distinguish the receptor subtypes[183a]

from **426** shows reduced affinity but similar receptor selectivity, while the CH$_2$F homologue **427** exhibits 10-fold selectivity for the MT$_2$ receptor subtype. In contrast, the CHF$_2$ amide is 10-fold selective for MT$_1$ receptor and retains the potency of **426**, a profile analogous to that of the urea **431**, while the balanced profile and reduced potency of the CHCl$_2$ amide **430** illustrates the importance of selecting the correct halogen.[183]

424: R = CH$_3$
425: R = CF$_3$

426: R = CH$_3$ **429**: R = CF$_3$
427: R = CH$_2$F   **430**: R = CHCl$_2$
428: R = CHF$_2$ **431**: R = NHCH$_2$CH$_2$CH$_3$
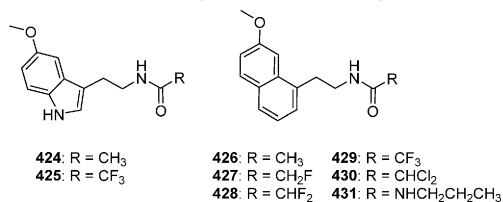
■ C−F AS A CARBINOL (C−OH) MIMIC

C−F as a C−OH Bioisostere in Nucleoside Analogues.
Replacing the hydroxyl substituents and hydrogen atoms of the ribose ring of nucleosides with fluorine has been extensively explored, with gemcitabine (**432**), the HBV inhibitor clevudine (**433**), and the HCV inhibitor sofosbuvir (**434**), a phosphoramidate prodrug, the most prominent clinically approved fluorinated nucleoside derivatives.[184−187] The introduction of fluorine atoms to the ribose ring has a complex influence on the shape of a nucleoside analogue, with antiperiplanar effects, dipole−dipole, anomeric, and gauche interactions contributing to the overall conformational bias, while interactions between fluorine atoms and a pendent C−H of the ribose or the base can also play a role. Consequently, the outcome is dependent upon the specific topological arrangement of functionality and their stereochemical relationships, with complexity heightened by the potentially selective effect on recognition by kinases and viral polymerases. For example, a 2′-α-fluoro substituent in a 3′-deoxy ribose favors a north conformation of the ribose ring while 2′-β-fluoro substitution prefers the south conformation but less strongly, although this preference can be reinforced by a 3′-α-fluoro substituent (Figure 32). Because HIV-1 reverse transcriptase is believed to

2'-α-F
north conformation preferred

2'-β-F
south conformation preferred

2'-β-F, 3'-α-F
south conformation preference reinforced by the 3'-F
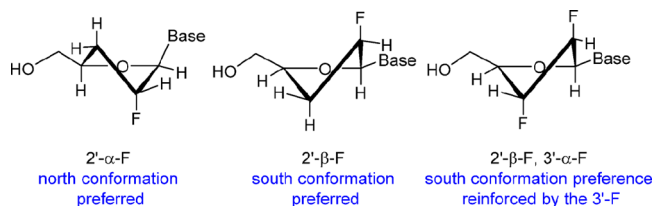
Figure 32. Preferred conformation of a 2′-α-fluoro-substituted ribose compared with a 2′-β-fluoro substituted isomer and a 2′-β, 2′-α-difluoro-substituted ribose ring.

recognize nucleotides adopting the south conformation, 2′-α-fluoro substitution leads to inactive antiretroviral agents.[188] This contrasts with the effect of 2′-β-fluoro-substitution on ribose topography, which has been shown to preferentially adopt the south conformation.[189]

432

433

434

435
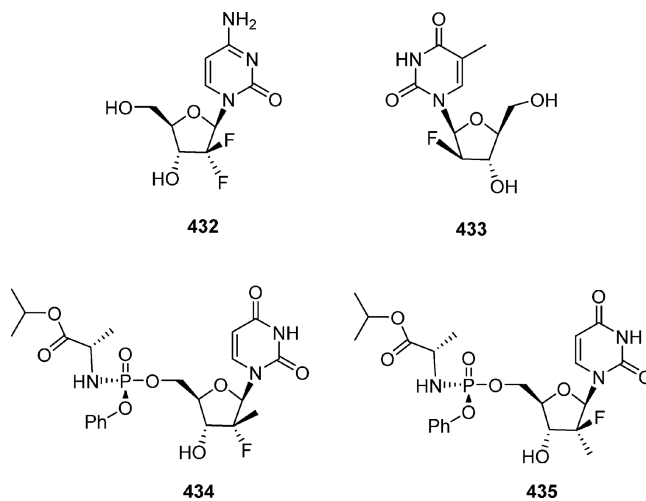
The importance of the correct fluorination patterning is most effectively illustrated by the poor HCV inhibitory activity associated with **435**, the 2′-β-fluoro analogue of **434**.[190] The 2′-fluorine atom of **434** mimics the effects of the 2′-hydroxyl of **436**, while **435** mimics that of **437**. While conformational preferences may contribute to these observations, specific interactions with the HCV NS5B polymerase also play a role because it is sensitive to the identity of the 2′-α- and 2′-β-substituents, critical ribose recognition elements for Ser$_{282}$ of the enzyme.[187b] While the fluoride of **434** lacks the H-bond donating properties of the hydroxyl of **436** (Figure 33A) and binding leads to a
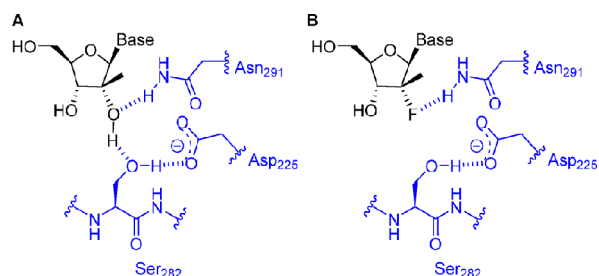
Figure 33. Key H-bonding interactions between a 2′-methyl ribose moiety (**436**) and the 2′-fluoro-2′-methyl homologue that is the ribose hallmark of **434**.

disturbance in the interaction network associated with the 2′-hydoxyl, it appears to be capable of interacting with a side chain N−H of Asn$_{291}$ (Figure 33B), and although the K_m is higher, this nucleotide is able to align correctly for incorporation into the growing RNA chain.[187b]
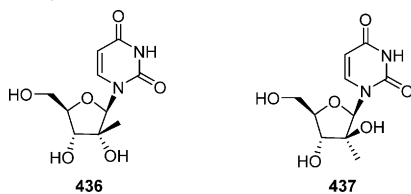
However, there are limits to the bioisosteric relationship between a 2′-fluoro and a 2′-hydroxyl substituent in the context of RNA. While the use of fluorinated RNA is common in siRNA and aptamers as a means of stabilizing the RNA, incorporation into RNA:DNA hybrids has been found to be poorly efficacious toward activating mammalian RNaseH.[191]

Collagen is the most abundant protein in animals, amounting to ~30% of the total protein content of humans and ~75% of the weight of human skin. The polypeptide chains of collagen are comprised of approximately 300 repeats of the triplet sequence XYG in which X is often an L-Pro residue while Y is frequently a 4-(R)-hydroxy-L-proline (**438**, Hyp) residue.[192] These sequences contribute to both the structure and stability of collagen chains, which adopt tightly wound triple helices that are organized into fibrils conferred with considerable tensile strength. The hydroxyl moiety of Hyp is known to contribute to the properties and stability of collagen but its precise function has been esoteric in nature, initially attributed to either its H-bonding properties or an effect on stabilizing *trans*-peptide bonds along the backbone. However, studies with 4-fluoroproline (**439**) as a bioisosteric substitute for the Hyp residue **438** indicate that the predominant effect of 4-substition is to influence the conformation of the pyrrolidine ring of proline, with both the 4-(R)-hydroxy and 4-(R)-fluoro substituents favoring a C^γ-exo conformer as depicted in Figures 5B.[192]

The antibiotic pristinamycin II$_B$ (**440**), which incorporates D-proline and inhibits protein synthesis by acting on bacterial ribosomes, suffers from dehydration at acidic and basic pH to give a conjugated trienone, which is inactive as an antibacterial agent.[193] To identify structural modifications that would address this problem, reduction of the ketone to an alcohol was explored, with the result that both inhibition in a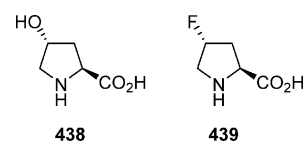 cell-free translational assay and antibacterial activity were preserved with the (R)-isomer **441** (Table 36). In contrast, the (S)-alcohol **442** was 120-fold

Table 36. SARs Associated with 440 and Its Analogues

	R	poly(U) IC$_{50}$ (μM)	MIC (IP8203) (μg/mL)
440	C=O	0.1	4
441	(R)-CHOH	0.05	1
442	(S)-CHOH	6	32
443	(R)-CHF	0.06	0.25
444	(S)-CHF	0.5	8

less potent in the cell free translation assay and 8-fold less potent as an antibacterial agent. These structure−activity observations were recapitulated with the (R)- and (S)-fluorides **443** and **444**, respectively, with the former exhibiting potency similar to **441**, while **444** was 10-fold more potent than **442** in the protein translation assay and 4-fold improved in the antibacterial assay.[193]

Fluorinated Motifs and Alcohol/Thiol Bioisosterism. Fluorine has played a role in the design of bioisosteres of alcohols and thiols where the CHF$_2$ moiety has been exploited as a H-bond donor while replacing a C−OH with a C−F relies upon the ramifications of dipole mimicry.

The intramolecular interaction between the CHF$_2$ moiety of the pyrazole-based fungicide **445** and the adjacent C=O has been characterized as H-bonding in nature based on IR and ^{1}H NMR data.[194] The energy of the intramolecular interaction in **445** has been estimated to be ~1.0 kcal/mol based on a distance of 2.4 Å, which calibrates the CHF$_2$ moiety as a relatively weak H-bond donor compared to more traditional functionalities which are typically associated with energies of 2−15 kcal/mol. Nevertheless, this interaction appears to be important to the fungicidal activity of **445**, which is a consequence of inhibiting

445

446 fluxapyroxad

447 sedaxane

448 isopyrazam

449
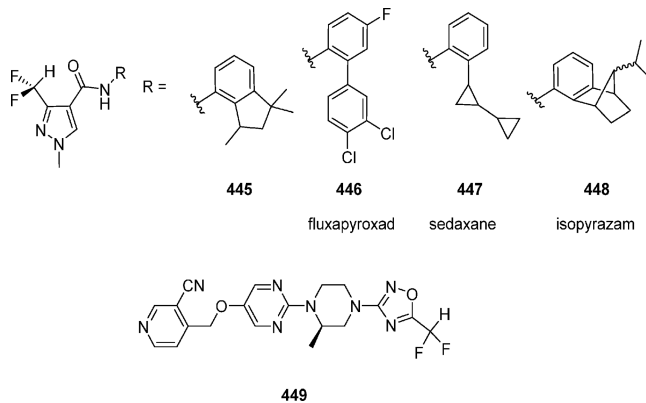
fungal succinate dehydrogenase because the CF_3 homologue, which is absent the H-bond donor, exhibits weaker biological effects.[194,195] The 3-(difluoromethyl)-1-methyl-1H-pyrazole-4-carboxamide moiety is a common structural element in a range of fungicides, including fluxapyroxad (**446**), sedexane (**447**), and isopyrazam (**448**).[195] More recently, intermolecular H-bonds have been observed between the CHF_2 moiety and the nitrile of an adjacent molecule in the single-crystal X-ray structure of the oxadiazole derivative **449**, with the key bond angle and length captured in Figure 34.[196]

Figure 34. Intermolecular H-bond observed in the single-crystal X-ray structure of oxadiazole **449**.

Perhaps the most compelling application of the CHF_2 moiety as a H-bond donor is provided by **452**, an inhibitor of HCV NS3 protease in which the difluoro-Abu was designed as a mimic of the cysteine residue found at the P_1 site of natural substrates, with the structural similarity illustrated in simplistic fashion in Figure 35.[197a] The design of this compound was inspired by the
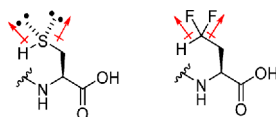
Figure 35. Illustration of the functional mimicry between RSH and RCF_2H in P_1 residues incorporated into **450** and **452**.

earlier observations with the pyrazole **445**, and **452** was found to be equipotent with the Cys analogue **450**, indicative of good functional emulation. Satisfactory bioisosterism was further emphasized by the 20-fold reduced potency observed with the Ala analogue **451**, reflecting the importance of the presence of the H-bond donor in **452**.

450: R = SH   **451**: R = CH_3 **452**: R = CHF_2
K_i = 40 nM K_i = 700 nM K_i = 30 nM

The presence of an intermolecular interaction between the CHF_2 moiety and the HCV NS3 protein was confirmed with X-ray cocrystal structures of the smaller inhibitors **453** and **454**, both of which formed a mimic of the tetrahedral reaction intermediate by the addition of the catalytic Ser_{139} hydroxyl to the activated carbonyl moiety that is a hallmark of these compounds.[197b] The X-ray structures indicated that the hydrogen atom of the CF_2H element donated a H-bond to the backbone C=O of Lys_{136}, w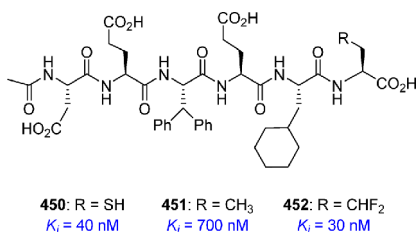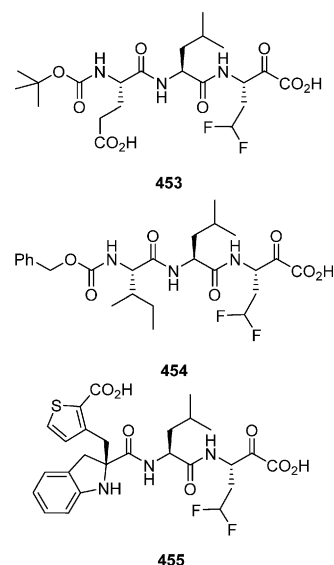hile one fluorine atom was close to the C-4 hydrogen atom of the phenyl ring of Phe_{154}, suggestive of a weak C−H to fluorine H-bonding interaction. The H-bond lengths measured for the CF_2H moiety were ∼2.57 and ∼2.9 Å, at the upper end of the preferred distance but consistent with the 2.9 Å suggested for C−H to oxygen interactions with aromatic ring donors.[139c,197b]

453

454

455

However, in the X-ray cocrystal structure of the related α-keto acid **455** bound to HCV NS3, the carbon atom of the CHF_2 was found to be 6.28 Å away from the backbone C=O of Lys_{136} and 4.08 Å away from the backbone C=O oxygen atom of Leu_{135}.[197c] The 4.08 Å distance represents a C−H to OH-bond that is probably above the preferred limit, so while not ideal, it was nevertheless considered to play a role in drug−target interactions.[139,198] These observations reflect significant differences between this complex and those obtained with **453** and **454** because with **455**, the serine hydroxyl approached the activated C=O from the opposite face to that typically observed with serine proteases. This arrangement resulted in the carboxylate moiety rather than the hemiketal oxygen atom occupying the oxyanion hole. The difluoromethyl side chain fitted snugly into the S_1 pocket with one of the fluorine atoms proximal (3.34 Å) to the C-4 hydrogen atom of the thiophene ring, viewed as a form of hydrophobic collapse that may preorient the molecule for presentation to the protease in its extended conformation.

The direct translation of this Cys mimic to the P_1 element of tripeptide-based inhibitors derived from asunaprevir (**456**) was unsuccessful, with the naturally configured **457** found to be 900-fold less potent in the GT-1a enzyme assay than **456**, while the unnatural isomer **458** was a further 2-fold weaker and demonstrated poor inhibition in the GT-1b replicon (Table 37).[199] This SAR point was mirrored by the des-fluoro derivatives **459** and **460**, which were poor enzyme inhibitors, observations that demonstrated the importance of the cyclopropane moiety at P_1 of **456**. However, replacing the vinyl substituent of **456** with a CHF_2 afforded the potent inhibitor **461**, with activity dependent on configuration because **462** was an order of magnitude weaker in the enzyme assay. The unique attributes of the CHF_2 substituent in this setting were underscored by the 10-fold loss in potency observed with the des-fluoro derivative **463** and the fully fluorinated homologue **464**, while projecting the CHF_2 moiety further from the core, as in **465**, also led to reduced potency. In this analogue, the presence of the fluorine atoms incurred a small but negative impact compared to the simple ethyl derivative **466**. An X-ray cocrystal structure of **451** with HCV NS3 protease revealed a close approximation of the hydrogen atom of the CF_2H moiety to the backbone carbonyl of Leu_{155} at a distance that was consistent with a H-bonding interaction.[199]

The importance of the CHF_2-substituted cyclopropyl moiety identified with **461** in HCV NS3 protease inhibitor design is reflected in the incorporation of this structural element in the

Table 37. SARs Associated with the HCV NS3 Protease Inhibitors 456−466
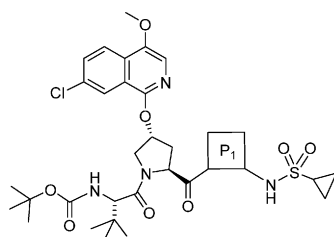
	P$_1$	GT-1a enzyme inhibition IC$_{50}$ (nM)	GT-1b replicon inhibition EC$_{50}$ (nM)
456		1	6
457		976	509
458		2,479	>1,000
459		3,079	>1,000
460		7,970	>1,000
461		1	7.6
462		12	58.9
463		13	64
464		17	125
465		14	31
466		5	16

potent inhibitors glecaprevir (**467**) and voxilaprevir (**468**), both of which express pan-genotypic activity and each of which has been approved for marketing by the FDA as part of a drug combination regimen.[200,201]

467 (glecaprevir) **468** (voxilaprevir)
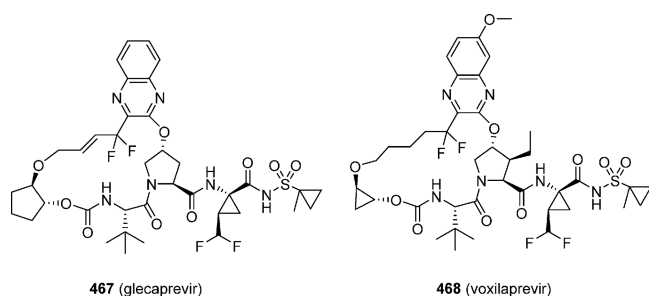
Lysophosphatidic acid (LPA) **469** interacts with four GPCR receptors designated as LPA_{1-4} and also acts as an agonist for the nuclear hormone receptor peroxisome proliferator-activated receptor-γ (PPARγ). However, the propensity of LPA to rearrange by acyl migration inspired the design of the difluorinated LPA analogue **470** in which the terminal primary alcohol has been replaced by a difluoromethyl moiety.[202] While **470** failed to interact with LPA_{1-3} receptors, this compound stimulated the PPARγ receptor as detected by luciferase expression in CV-1 cells transfected with the enzyme under control of a PPARγ-responsive element, demonstrating the contextual nature of bioisosterism and the limits of functional mimicry.

469 **470**

R = $C_{15}H_{31}$ or $C_{17}H_{33}$
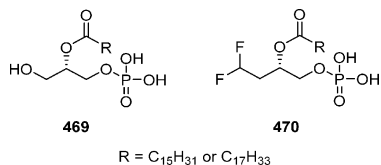
The bioisosteric relationship between the $CHCF_2$ and OH moieties has been extended to hydroxamic acids where incorporation of an $N-CHCF_2$ element functioned as an effective mimic in the context of the 5-lipoxygenase inhibitors **471** and **472**.[203]

471 **472**
5-LOX IC_{50} = 4.9 μM 5-LOX IC_{50} = 5.0 μM
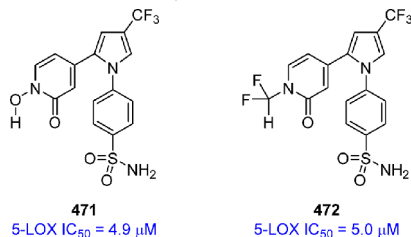
■ CF$_2$ AS A BIOISOSTERE OF AN OXYGEN ATOM

CF$_2$ and Phosphate/Pyrophosphate Mimicry. The CF$_2$ moiety has been explored extensively as a mimic of an oxygen atom in a variety of structural backgrounds in which the C−F bond is considered to be a mimic of the one of the lone pairs of electrons of oxygen. A seminal example is provided by studies of phosphate chemistry where a phosphonate is frequently employed as a bioisostere. However, this substitution leads to lower acidity compared to a phosphate, which can result in poor functional emulation (Tables 38 and 39). The data compiled in Table 37 illustrates the significant differences between the acid dissociation constants for pyrophosphate (**473**) and the CH$_2$ analogue **474**.[204,205] While the CCl$_2$ homologue **475** reduces the pK_a values compared to **474**, fluorination offers a superior effect, with the CF$_2$ derivative **476** the optimal mimic with respect to reproducing the acidity of **473**. Indeed, the electron withdrawing properties of fluorine are such that, in this context, monofluoro substitution (**474**) is as effective at modulating the acidity as two chlorine atoms.

The recognition that the physical properties, bond angles, and bond lengths of difluoromethylenephosphonate render it an

Table 38. pK_a Data for Pyrophosphate (473) and Its Carbon Analogues 474−478

	473	474	475	476	477	478
X	O	CH_2	CCl_2	CF_2	CHF	$C(OH)_2$
pK_a2	2.36	2.87		<2.6	<2.7	
pK_a3	5.77	7.45	6.11	5.80	6.15	5.81
pK_a4	8.22	10.96	9.78	8.00	9.35	8.42

effective mimic of phosphate has led to its widespread adoption in the design of inhibitors of phosphatases that are of physiological relevance (Figure 36).[206−208] The synthesis of **479** as a building block for the construction of nonhydrolyzable tyrosine phosphate mimics for use in the design of phosphatase inhibitors was followed by the development of **480** as a mimic of phosphorylated serine, motifs that have been extended to sphingomyelin and other naturally occurring phosphate elements.[209−211]

The difluoromethylenephosphonate **481** inhibited PTP1B with an IC_{50} value of 120 nM, was active in a cell-based assay with an EC_{50} = 1.2 μM, and exhibited 13% oral bioavailability in the rat, with a C_{max} of 35 μM, plasma exposure that reduced glucose levels in rat and mouse models after single oral doses of 30 and 10 mg/kg, respectively.[212] The furan carboxylate of **482** was introduced to engage a H_2O molecule observed in the active site of *Yersinia pestis* outer protein H (YopH) phosphatase, and this compound was a potent inhibitor, IC_{50} = 190 nM, that reduced intracellular *Yersinia pestis* replication by 9-fold at 10 μM, a concentration below that where cytotoxicity was seen.[213] The phosphopeptidomimetic **483** targeted the Src homology 2 (SH2) domain of signal transducer and activator of transcription 6 (STAT6) and blocked phosphorylation of Tyr$_{641}$ of STAT6 in intact Beas-2B cells when introduced as its bis-pivaloyloxymethyl prodrug at concentrations of 1−10 μM.[214]

479 **480** **481**

482 **483**
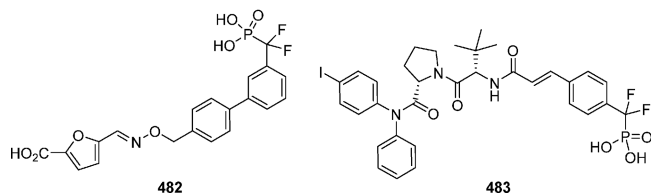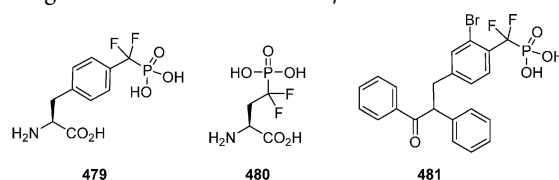
The difluoromethylenephosphonate **485** was designed as an analogue of sphingomyelin (**484**) that inhibited *Bacillus cereus* sphingomyelinase with an IC_{50} value of 57 μM, 2-fold more potent than the des-fluoro analogue.[215]

484 **485**
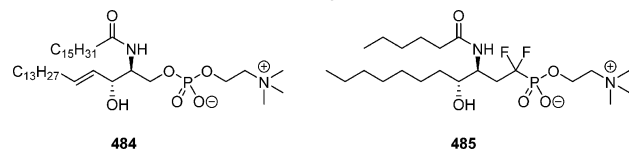
CF$_2$ as an Oxygen Bioisostere in Sulfonic Acids and Sulfonamides. The effects of fluorination α- to sulfonic acids and sulfonamides has been examined in the context of inhibition of steroid sulfatases, protein phosphatases, and carbonic

Table 39. pK_a2 Values for a Homologous Series of Phosphonic Acid Derivatives Compared to the Phosphate Phenyl Ester

	PhOP(O)(OH)$_2$	PhCH$_2$P(O)(OH)$_2$	PhCH(F)P(O)(OH)$_2$	PhCF$_2$P(O)(OH)$_2$
pK_a2	6.22	7.72	6.60	5.71

pK_a for R$_2$ = H	6.4	7.6	5.4

Figure 36. Geometric parameters for the phosphate, phosphonate, and difluoromethylenephosphonate moieties.

Table 40. Carbonic Anhydrase Inhibitor Activity Associated with Sulfonamides 500−504

		IC$_{50}$ (nM)	pK_a
500	PhCH$_2$SO$_2$NH$_2$	630	10.5
501	PhCHFSO$_2$NH$_2$	220	8.8
502	PhCF$_2$SO$_2$NH$_2$	58	7.7
503	CH$_3$SO$_2$NH$_2$	650	10.8
504	CF$_3$SO$_2$NH$_2$	<2	6.3

anhydrase.[216−220] Steroid sulfatase (STS) catalyzes the hydrolytic desulfation of steroid-based sulfate derivatives to afford the free phenols. Estrogen sulfate (**486**) and estrone sulfate (**487**) are substrates for STS, and the former is believed to act as a reservoir for the production of estrogen in breast tumors, suggesting this enzyme as a potential therapeutic target.[217] Sulfonates have been evaluated as STS inhibitors but were poorly active, with **488** representative, K_i = 600 μM.[216a] This was not attributed to an effect on the pK_a relative to the sulfate moiety; rather, the sulfate O atom was considered to be important for interacting with the enzyme. Fluorination of the benzylic carbon atom of **488** gave **489**, which was 5-fold more potent and exhibited competitive inhibition kinetics in contrast to the mixed inhibition kinetic profile observed with **488**. These potency observations were reproduced in the sulfonamide homologues **490** and **491**, where α-fluorination enhanced inhibitory potency by 4-fold, although in this example both compounds exhibited mixed inhibitory kinetics.[216b] Interestingly, the potency of **491** increased with pH, with the K_i 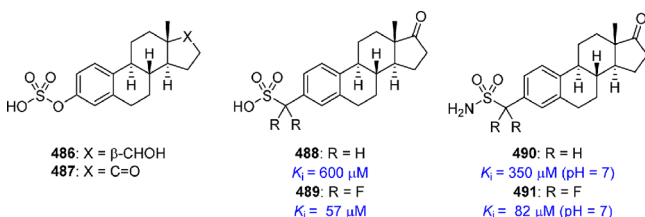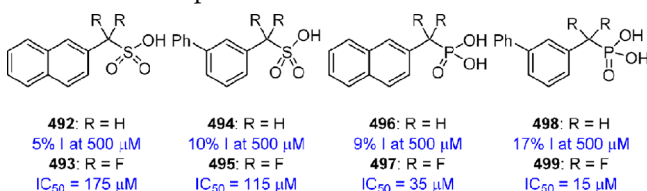value = 28 μM at pH = 8.8 while that of the sulfonate **489** decreased, shifting 2-fold from 73 μM at pH = 7 to 147 μM at pH = 8.8, an observation attributed to the effect of ionization of the sulfonamide.

prototype **500**, while the monofluoro derivative **501** fell between these bookends (Table 40). The effect was more dramatic when comparing the activity of methylsulfonamide **503** with its CF$_3$ congener **504**, where the SARs reflected a close correlation between potency and pK_a value that was consistent with the more potent inhibitors being those more ionized at neutral pH.[220]

CF$_2$ as an Oxygen Bioisostere in Heterocycles. The morpholine heterocycle has long been a staple of drug design when a moderately basic ring system is required because the introduction of the oxygen atom into piperidine reduces the pK_a by 2.6 units compared to piperidine (Table 41).[221] Other

Table 41. Experimentally Measured pK_a Values for the Conjugate Acids of a Series of Heterocyclic Amines

pK_a	11.1	8.5	8.6	9.0	5.4	9.4	8.5

486: X = β-CHOH
487: X = C=O

488: R = H
K_i = 600 μM
489: R = F
K_i = 57 μM

490: R = H
K_i = 350 μM (pH = 7)
491: R = F
K_i = 82 μM (pH = 7)

Difluoromethylsulfonates have also been probed as PTP1B phosphatase inhibitors where α-fluorination resulted in increased potency in two series, as illustrated by comparing data for the MMPs **492/493** and **494/495**.[218] Perhaps not surprisingly for a monoionic species, **493** and **495** were less potent PTP1B phosphatase inhibitors than the phosphonate homologues **497** and **499**, where α-fluorination also enhanced potency over the unsubstituted compound **496** and **498**.[218]

492: R = H
5% I at 500 μM
493: R = F
IC$_{50}$ = 175 μM

494: R = H
10% I at 500 μM
495: R = F
IC$_{50}$ = 115 μM

496: R = H
9% I at 500 μM
497: R = F
IC$_{50}$ = 35 μM

498: R = H
17% I at 500 μM
499: R = F
IC$_{50}$ = 15 μM

Carbonic anhydrase is a Zn^{2+}-dependent enzyme that exhibits affinity for primary sulfonamide moieties which coordinate to the metal.[219] Fluorination α- to the sulfonamide moiety led to a progressive increase in potency, with difluoro(phenyl)-methanesulfonamide (**502**) 10-fold more potent than the

electron withdrawing elements that exert a similar effect but offer a range of lipophilicities include sulfur substitution, with thiomorpholine dioxide the most powerful of this series that reduces the pK_a of piperidine by a more substantial 5.7 units.[222−224] Dual fluorination at the 4-position of piperidine modulates the pK_a to the same extent as morpholine but offers ∼2.5 units of increased lipophilicity accompanied by a 70% reduction in PSA, providing a useful heterocycle when physicochemical properties are being optimized. As a consequence, 4,4-difluoropiperidine has been explored extensively by medicinal chemists; however, only a synopsis of the applications is presented in the following section which also highlights examples where biochemical emulation is poor.

The morpholine derivative **505** is a potent inhibitor of the class 3 tyrosine kinase macrophage colony-stimulating factor-1 receptor (FMS) but was poorly stable in HLM, with just 5.2% of the parent remaining after 10 min of incubation.[225] In contrast, the difluoropiperidine analogue **506** fully retained the enzyme inhibitory properties of **505** while offering enhanced metabolic stability in HLM, with 83% of the parent drug remaining intact after 10 min of incubation. A similar relative profile was seen when the compounds were incubated in RLM. In the selective cannabinoid CB$_2$ agonist series represented by **507−510**, the parent piperidine **507** and 4,4-difluorinated homologue **509** offered potency superior to the more polar morpholine **508** and, particularly, the thiomorpholine dioxide **510**, a reflection of the lipophilic nature of the receptor binding site.[226] However, while

potency increased in parallel with lipophilicity in this series, rat clearance was higher for **507** and **509** compared to **508**, while **510** was too weakly active to qualify for testing, indicating a need to carefully balance physicochemical properties.

505: X = O
IC$_{50}$ = 1.3 nM

506: X = CF$_2$
IC$_{50}$ = 1.7 nM

507 X = CH$_2$
K_i = 6 nM (86%)

508: X = O
K_i = 75 nM (76%)

509: X = CF$_2$
K_i = 15 nM (83%)

510: X = SO$_2$
K_i = 600 nM (89%)
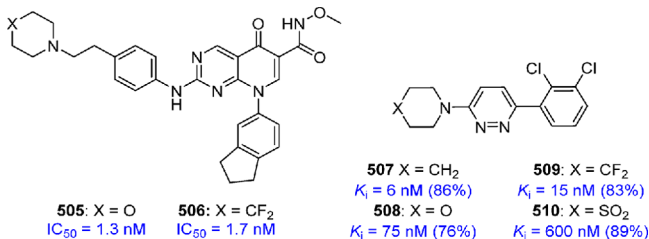
The 4,4-difluoropiperidine moiety of **512** was an effective replacement for the morpholine heterocycle in **511** in a series of histamine-3 receptor inverse agonists, with both compounds exhibiting comparable affinity for the human receptor.[227] The prototype **511** was also a potent rat H$_3$ receptor ligand that exhibited high selectivity over the hERG channel (21% inhibition at 10 μM) and CYP inhibition (IC$_{50}$ > 30 μM) while presenting good metabolic stability in mouse, rat, dog, monkey, and human LMs ($t_{1/2}$ > 40 min), high Caco-2 cell permeability, and low plasma protein binding. However, the in vivo clearance of **511** in the rat was very high and the molecule was extensively distributed to tissues, with a high volume of distribution, a large brain to plasma ratio, and an extended brain residence time. The fluorinated piperidine **512** exhibited acceptable metabolic stability in vitro but, unfortunately, exhibited a short 30 min $t_{1/2}$ in vivo.

511: X = O
hHR$_3$ K_i = 5.4 nM

512: X = CF$_2$
hHR$_3$ K_i = 11 nM

513: X = CH$_2$
SYK pIC$_{50}$ = 7.5; pK_a = 10.0

514: X = O
SYK pIC$_{50}$ = 7.2; pK_a = 7.7

515: X = CF$_2$
SYK pIC$_{50}$ = 8.4; pK_a = 7.9
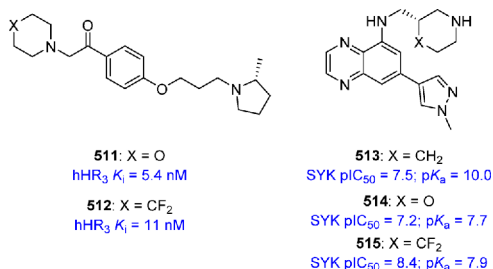
Careful modulation of the pK_a of the SYK inhibitors **513**−**515** was of importance to the PK profile of these molecules.[228] Although the potency of **515** was an order of magnitude better than the morpholine compound **514** while maintaining mild basicity relative to **513**, in this series the morpholine heterocycle ultimately offered the optimal compromise of good oral bioavailability and efficacy in a rat Arthus model. However, **514** was genotoxic in an Ames mutagenicity assay, and **515** proved to be an inadequate substitute because its exposure in vivo was lower than for **514**, attributed to higher clearance.

An interesting application of CF$_2$/O isosterism is provided by the development of the melanin concentrating hormone receptor 1 (MCHR1) inhibitor **518**, which was advanced into clinical trials as a phosphate prodrug of the alcohol for the treatment of obesity.[229] While the oxetane **516** showed high plasma exposure in rats following PO dosing, the compound was ineffective at inducing weight loss in a 4 day diet-induced obese (DIO) rat study, attributed to low brain and plasma concentrations at 20 h postdose. Reversion to the cyclobutane analogue **517** as a means of increasing lipophilicity provided an avenue forward but further modification to **518** was required in order to slow metabolism. This compound had adequate metabolic stability in rat LMs and when dosed as the glycine ester prodrug at a dose of 10 mg/kg, high plasma (4.5 μM) and brain (11.3 μM) levels were observed at the 8 h time point, reflecting a brain to plasma ratio of 2.5.

Administration of a phosphate prodrug of **518** to DIO rats at a dose of 0.3 mg/kg resulted in a 5% weight loss, and this compound exhibited no evidence of the hepatobiliary lesions that had been seen with earlier compounds in the series when administered daily to rats at doses of up to 100 mg/kg for 30 days.[229]

516: X = O
K_i = 8.7 nM

517: X = CH$_2$
K_i = 9.8 nM

518: X = CF$_2$
K_i = 16.9 nM

519

520
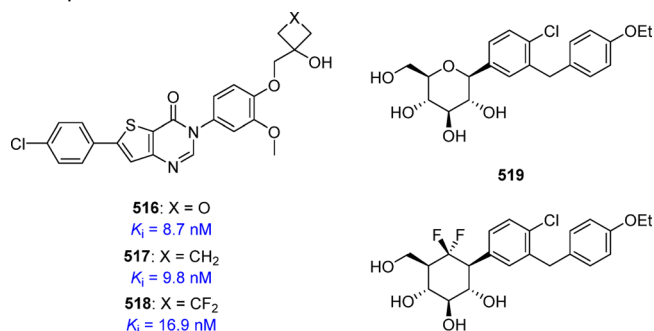
A CF$_2$ moiety appears to be an acceptable substitute for ether oxygen atom of the sodium−glucose cotransporter-2 (SGLT$_2$) inhibitor dapagliflozin (**519**), with **520** claimed to exhibit a longer duration of glucosuria in vivo in rats.[230a] This work complements studies that successfully replaced the C-4 carbinol of **519** with a gem-fluoromethylene moiety.[231b]

However, there are a number of examples where a gem-difluoromethyl moiety has been found to be an inadequate substitute for a heterocyclic oxygen atom in a biochemical setting. For example, the 4,4-difluoropiperidine **522** derived from **521**, an antagonist of the dopamine D$_4$ receptor, exhibits several-fold lower binding affinity than the morpholine-based prototype.[231] In another example, the morpholine ring of the PI3K α, γ, and δ inhibitor **523** was uniquely active compared to the 4,4-difluoropiperidine analogue **524** and the thiomorpholine dioxide **525**.[232]

521 (ML398)
IC$_{50}$ = 130 nM
K_i = 36 nM

522
IC$_{50}$ = 760 nM
K_i = 210 nM

523: X = O
IC$_{50}$ = 19/31/3 nM

524: X = CF$_2$
IC$_{50}$ = >50 nM at all 3

525: X = SO$_2$
IC$_{50}$ =>50 nM at all 3

IC$_{50}$ values refer to PI3Kα, γ and δ, respectively
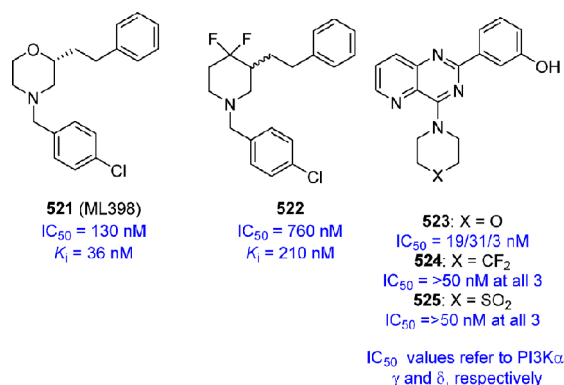
ArCF$_2$CH$_3$ and ArOR Bioisosterism. The difluoroethyl moiety has been advocated as a bioisostere of an aromatic CH$_3$O substituent based on the structural metaphor depicted in Figure 37, with recognition that the conformational preferences
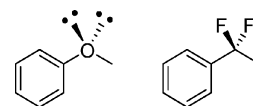
Figure 37. Proposed isosterism between anisole and (1,1-difluoroethyl)benzene.

of the two substituents may be quite different, although the difluoroalkyl substituent may be conformationally flexible.[233,234] An example where a 1,1-difluoroethyl substituent offered advantage is found in the series of inhibitors of the kidney urea

Table 42. SARs and Metabolic Stability of 526−529, Inhibitors of the Kidney Urea Transporter UT-B

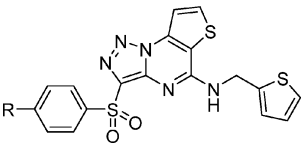|	R	IC$_{50}$ (nM)	% remaining in RLMs
526	CH$_3$O	104	6
527	CF$_3$O	1110	95
528	CH$_3$CH$_2$	11	<5
529	CH$_3$CF$_2$	14	96

transporter UT-B represented by 526−529 captured in Table 42.[235] While the OCH$_3$ derivative 526 exhibited good potency, metabolic stability in rat liver microsomes was very poor and fluorination of the methyl group was not found to be a viable option to solve this problem because 527 suffered a 10-fold loss in potency, although metabolic stability improved dramatically. The ethyl derivative 528 restored potency but metabolic stability was also inadequate, a problem ultimately solved by introducing the 1,1-difluoroethyl substituent, with 529 offering an excellent compromise of targeted properties.

In the series of Takeda G-protein-coupled receptor 5 (TGR5) agonists 530−534 compiled in Table 43, a CF$_2$CH$_3$ substituent

Table 43. SARs and Metabolic Stability of TGR5 Agonists 530−534
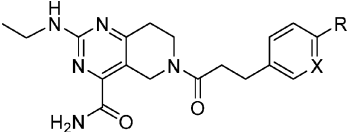
|	R	X	induced human TGR5 EC$_{50}$ (nM)	CL$_{int}$ human (μL/min/mg)
530	OCH$_3$	CH	137	96
531	OCF$_3$	CH	2.3	184
532	CH$_2$CH$_3$	CH	9.2	238
533	CF$_2$CH$_3$	CH	2.7	211
534	CF$_2$CH$_3$	N	43	18

offered increased metabolic stability in human liver microsomes when paired with the pyridine heterocycle, as configured in 534.[236] The OCH$_3$ derivative 530 offered poor agonist potency, but this was improved by the introduction of substituents that lowered the constraint toward coplanarity, with OCF$_3$ (531), CH$_2$CH$_3$ (532), and CF$_2$CH$_3$ (533) substantially more potent. However, metabolic stability in HLM was an issue for 530−533, solved by the pyridine analogue 534, which has a lower E Log D

value, although this was accompanied by some reduction of intrinsic agonist potency. Nevertheless, 531 was the compound selected for more advanced in vivo studies.[236]

■ FLUORINATED ALKOXY MOIETIES AND MIMESIS

Conformational Aspects of Fluorinated Alkoxy Moieties. A probe of the CSD confirmed previous literature observations that in the absence of dual ortho substitution, Ar-OCH$_3$ prefers a coplanar arrangement of the aromatic ring and the O−CH$_3$ bond favored by ∼3 kcal/mol (Figure 38).[237−239] This is a consequence of rehybridization of the oxygen atom to allow overlap with the unsaturated ring which overcomes allylic 1,3-strain. In contrast, Ar-OCF$_3$ favors (by ∼0.5 kcal/mol) a conformation in which the O−CF$_3$ bond is orthogonal to the plane of the aromatic ring, attributed to the reduced electronic overlap between the now electron deficient oxygen atom and the aromatic system that allows allylic 1,3-strain to dominate, furthered by the increased size of fluorine compared to hydrogen. In addition, a hyperconjugative interaction in which one of the lone pairs of electrons on the oxygen atom donates into one of the C−F σ* orbitals is believed to contribute to stabilizing the orthogonal topography. An assessment of the Ar-OCHF$_2$ substituent revealed no strong preference for a specific conformation although the analysis was based on only 22 examples in the CSD. However, in two cases examined more closely, the C(Ar)−C(Ar)−O−C torsion angle was close to 90°, but the fluorine atoms adopted an *endo−exo* arrangement in one example and an *endo−endo* topography in the other. Thus, fluorination of the alkyl moiety of alkyl phenol ethers allows the aryl substituent to function conformationally as mimic of an alkyl substituent.

Developability Aspects of Fluorinated Alkoxy Moieties. Fluorination of the alkyl moiety of phenol ethers has been explored broadly in drug design, and replacing the OCH$_3$ of anisole derivatives with an OCF$_3$ is a common tactic in drug design that is often focused on enhancing metabolic stability based on the premise of mitigating O-demethylation. However, this tactic is not always successful in increasing metabolic stability, dependent upon the potential for alternative sites of metabolism to become a dominant path. This phenomenon has been explored in some detail based on an analysis of MMPs examining the effect of substituting OCH$_3$ by both OCF$_3$ and the less common OCHF$_2$ on metabolic stability, lipophilicity, membrane permeability, and conformation.[237a] The successive replacement of hydrogen by fluorine in anisole leads to a progressive but nonlinear increase in cLog P values, with increments of 0.17, 0.27, and 0.66 for a total of 1.1 log units, accompanied by an increase in MW of 54 for the OCF$_3$ derivative. Measured Log D values confirmed the increased lipophilicity which ranged from 0.3 to 1.3 units for an OCF$_3$ for OCH$_3$ change while an OCHF$_2$ reduced Log D by 0.3−0.7 log units compared to OCF$_3$.
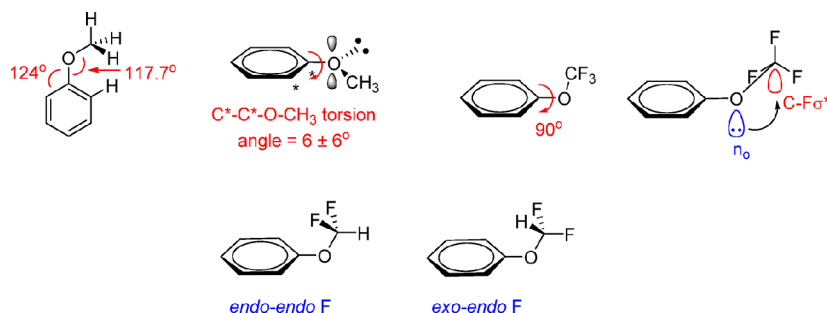
Figure 38. Conformational aspects of anisole, PhOCF$_3$, and PhOCHF$_2$.

However, the analysis of 439 MMPs where the only difference was a OCF_3 for OCH_3 substitution indicated that this change had no clear advantage with respect to improving metabolic stability in HLM. Moreover, the analysis revealed a significant difference in favor of OCH_3 (70% of the MMPs) substitution toward improving passive membrane permeability. The comparison of $OCHF_2$ with OCF_3 was based on 149 MMPs and indicated that although there were compound-specific effects, there was a small overall advantage for $OCHF_2$. In the membrane permeability assay, a $OCHF_2$ for OCF_3 substitution showed improved permeability in 67% of cases examined. This was attributed to the $OCHF_2$ moiety being able to adopt an *endo−endo* conformation that is similar in lipophilicity to OCF_3, attributed to cancellation of bond polarities, while the *endo−exo* state is more hydrophilic due to a 3-fold increase in polarity, which may explain the reduced Log D values. In a comparison between $OCHF_2$ and OCH_3, the former is more lipophilic by 0.2−0.6 log units, and in the HLM MMP analysis, the $OCHF_2$ substituent showed an advantage over OCH_3 that was statistically significant. However, in the membrane permeability comparison, the OCH_3 derivatives were in general more permeable than their $OCHF_2$ analogues when the parent molecule fell into the high or low permeability bin, while in the midrange bin, the two moieties were similarly permeable. The conclusion from this study was that $OCHF_2$ offers advantage over both OCH_3 and OCF_3 during optimization as a means of balancing lipophilicity and molecular weight, conferring improved metabolic stability without compromising membrane permeability.[237a] Nevertheless, there are examples where fluorination of an anisole moiety has a positive effect on metabolic stability, illustrated by comparisons within the series of corticotropin releasing factor-1 (CRF-1) inhibitors **535−538** compiled in Table 44.[240]

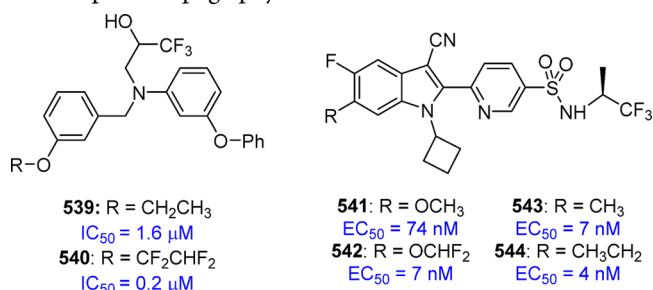**Table 44. Binding Potency and Metabolic Stability of a Series CRF-1 Inhibitors**
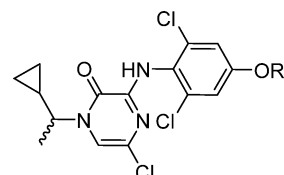
	R	CH_3/CF_3 configuration	CRF-1 IC_{50} (nM)	intrinsic clearance in HLM (mL/min/kg)
535	CH_3	R	1.1	130
536	CF_3	R	6.5	30
537	CHF_2	R	0.46	22
538	CHF_2	S	1.0	62

In this series, replacing the OCH_3 of **535**, a site of metabolic lability, with either OCF_3 (**536**) or $OCHF_2$ (**537**), led to reduced intrinsic clearance in HLM although there was sensitivity to the absolute configuration at the cyclopropyl ethyl substituent with the (*S*)-isomer **538** metabolically less stable.

Fluorination of Alkyl Phenyl Ethers and Conformation. An example where influencing the conformation of an alkyl phenyl ether by fluorination may have played a role in modulating potency is provided by the cholesteryl ester transfer protein (CETP) inhibitors **539** and **540**, where the latter is 8-fold more potent than the former.[241] In another example, the SAR associated with the HCV NS4B inhibitors **541−544** suggested that an orthogonal projection of the C-6 substituent was important for HCV GT-1b replicon inhibition because the methoxy

derivative **541** was 10-fold less potent than substituents that favor a noncoplanar topography.[164c]

539: R = CH_2CH_3
IC_{50} = 1.6 μM
540: R = CF_2CHF_2
IC_{50} = 0.2 μM

541: R = OCH_3
EC_{50} = 74 nM
542: R = $OCHF_2$
EC_{50} = 7 nM

543: R = CH_3
EC_{50} = 7 nM
544: R = CH_3CH_2
EC_{50} = 4 nM

■ FLUORINE AS A NITRILE BIOISOSTERE

The similarity of the biochemical profiles of **316** and **317** provide an example of a bioisosteric relationship between fluorine and the nitrile moiety.[145] Bioisosterism between these substituents has also been proposed in the context of the series of dual $5HT_{1A}$ agonists and 5-HT reuptake inhibitors **545−550**.[242] An analysis of MEPs and dipole moments of 5-cyano- and 5-fluoro-substituted indoles confirmed the potential for a bioisosteric relationship, with the C−F more similar to a C−CN moiety than a C−Cl bond because the MEP maps and dipole vector for the 5-chloroindole were more similar to the parent. In the event, the fluoro and cyano MMPs **546/548** and **549/550** profiled similarly in the binding and reuptake assays, while the 5-chloro-substituted analogue **547** of **548** was markedly less potent and behaved more like the parent compound **545** in the reuptake inhibition assay.[242] The two benzodioxole analogues **549** and **550** showed similar efficacy in vivo in the ultrasonic vocalization test as a measure of in vivo $5-HT_{1A}$ antagonism, and although subsequent studies focused on the nitrile series, the 5-fluoro analogues performed in a very similar fashion where comparisons were made. These studies culminated in the identification of viladozone (**551**), which was approved as an antidepressant by the FDA in 2011; however, the 5-fluoro analogue **552** presented an analogous profile in a range of assays, confirming the C−F/C−CN isosterism in this context.

545: X = H
$5HT_{1A}$ IC_{50} = 8 nM
5HT reuptake IC_{50} = 10 nM
546: X = F
$5HT_{1A}$ IC_{50} = 5 nM
5HT reuptake IC_{50} = 1 nM

547: X = Cl
$5HT_{1A}$ IC_{50} = 40 nM
5HT reuptake IC_{50} = 20 nM
548: X = CN
$5HT_{1A}$ IC_{50} = 1 nM
5HT reuptake IC_{50} = 0.4 nM

549: X= CN
$5HT_{1A}$ IC_{50} = 0.7 nM
5HT reuptake IC_{50} = 0.6 nM
550: X = F
$5HT_{1A}$ IC_{50} = 4 nM
5HT reuptake IC_{50} = 1 nM

551: R = CN (viladozone)
$5HT_{1A}$ = 0.2 nM
5HT reuptake IC_{50} = 0.5 nM
552: R = F
$5HT_{1A}$ = 3.0 nM
5HT reuptake IC_{50} = 0.3 nM
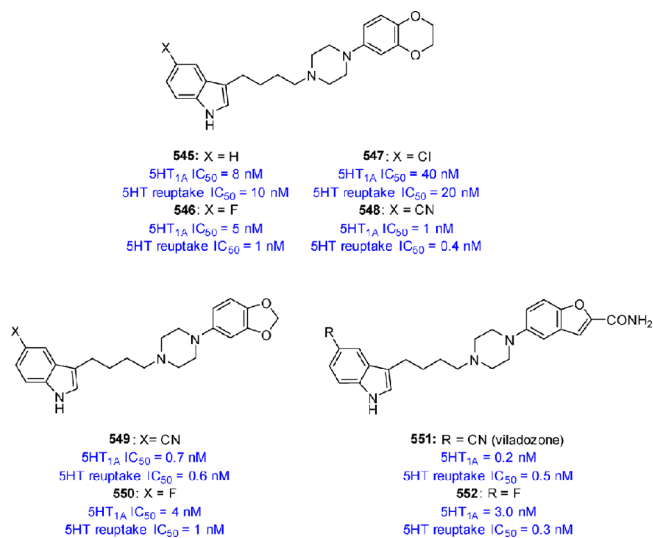
■ THE SF_5 MOIETY

DSM-265 (**246**) is first SF_5-containing drug to enter clinical trials and the in vitro comparison between **246** and **245** suggests a potential bioisosteric relationship between the SF_5 and CF_3 substituents (Table 25). Indeed, the SF_5 moiety has been viewed as a

Table 45. Comparison of the Electron Withdrawing (σ_p), Lipophilicity (π), and Substituent Dipole (μ) Values for the *tert*-Butyl, Nitro, SO$_2$CH$_3$, and a Series of Fluorinated Substituents[244a]

	σ_p	π	μ (D)*
t-Bu	-0.20	1.98	+0.52
NO$_2$	0.78	-0.28	-4.13
CF$_3$	0.54	0.88	-2.61
SF$_5$	0.68	1.23	-3.44
SCF$_3$	0.51	1.44	-2.50
SO$_2$CH$_3$	0.72	-1.63	-4.75
SO$_2$CF$_3$	0.93	0.55	
CF(CF$_3$)$_2$	0.53		-2.68
C(CF$_3$)$_3$	0.55		
SO$_2$CF$_2$CF$_2$CF$_3$	1.07		
SO$_2$CH(CF$_3$)$_2$	1.08		
SO$_2$C(CF$_3$)$_3$	1.11		
S(=CF$_3$)(=N-SO$_2$CF$_3$)	1.28		
S(=O)(CF$_3$)(NH)	0.84		
S(=O)$_2$(CF$_3$)(=N-SO$_2$CF$_3$)	1.39		
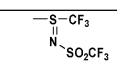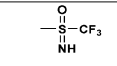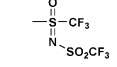
[a]*A negative value indicates that the negative end of the dipole vector is toward the substituent.

"super CF$_3$ group"; however, these two substituents are quite different in shape, size, lipophilicity, and electron withdrawing properties, as captured by the data summarized in Table 45.[243,244] The SF$_5$ substituent is larger in volume than a CF$_3$ but smaller than a *tert*-butyl moiety and possesses an octahedral geometry that presents a pyramidal electron density that is quite different from the tetrahedral shape of CF$_3$, where the electron density is presented as an inverted cone (Figure 39).[243,245] The SF$_5$ moiety

Figure 39. Comparison of the shapes of the CF$_3$ and SF$_5$ substituents.

is a more powerful electron withdrawing substituent than CF$_3$ but similar to SO$_2$CH$_3$ and NO$_2$ and may be considered to be a peripheral member of the family of "superacceptor" substituents that resemble sulfones in which fluorine has a prominent presence, with the key parameters also captured in Table 45.[246] The SF$_5$ substituent is more lipophilic than either a CH$_3$SO$_2$ or a CF$_3$SO$_2$ substituent, thereby conferring good membrane permeability while being metabolically stable and chemically robust.

Medicinal chemistry applications of the SF$_5$ moiety have largely been limited by a lack of convenient synthetic access to suitable building blocks, but considerable progress has been made toward developing new methodology, and this substituent is beginning to be explored in a variety of settings, although still most typically as a homologue of the CF$_3$ substituent.[4a,247] In the series of *Trypanosoma cruzi* trypanothione reductase inhibitors **553−555**, the CF$_3$- and SF$_5$-substituted compounds **553** and **554**, respectively, offered comparable potency and a modest advantage over the *tert*-butyl derivative **555**.[248] However, a kinetic analysis indicated that while **553** was a competitive inhibitor, both **554** and **555** exhibited a mixed competitive−uncompetitive kinetic profile. Compound **554** was docked into the active site of *Trypanosoma cruzi* trypanothione reductase with the orientation guided by X-ray cocrystal structures obtained with closely related structures, and the key interactions proposed are depicted in Figure 40. The comparable binding affinity of the
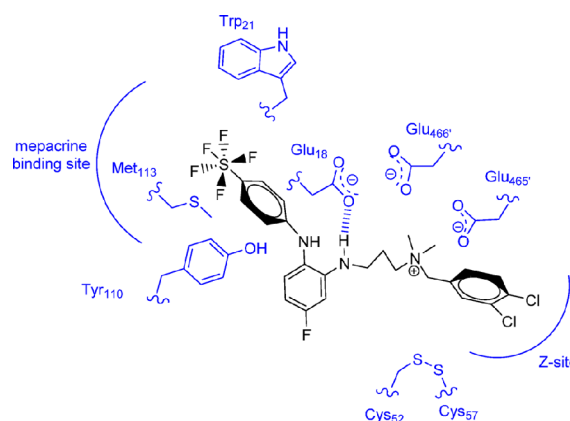
Figure 40. Proposed drug−target interactions between **554** and *T. cruzi* trypanothione reductase based on docking of the ligand into the active site of the enzyme.

bulkier inhibitor **554** compared to the smaller CF$_3$ derivative **553** was attributed to the stronger electron withdrawing nature of the SF$_5$ substituent that might potentially lead to an increase in the strength of the T-shaped interaction of the attached phenyl ring with the electron-rich Trp$_{21}$, Tyr$_{110}$, and Met$_{113}$ residues of the enzyme.[248]
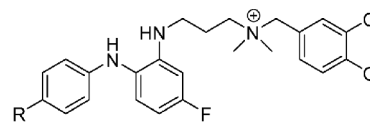
553: R = CF$_3$ **554**: R = SF$_5$ **555**: R = C(CH$_3$)$_3$
K_{ic} = 24 μM K_{ic} = 28 μM K_{ic} = 84 μM

In the matched pair of cannabinoids **556** and **557**, the SF$_5$ derivative **557** exhibited a modest 2-fold increased potency at CB$_1$ receptors, while in the thymidine phosphorylase inhibitors **558** and **559**, there is a 4-fold advantage for the SF$_5$ substituent in **559** compared to the CF$_3$ prototype **558**.[249,250] The antidepressant drug fluoxetine (**560**) is a selective serotonin reuptake inhibitor that also demonstrates affinity for several serotonin receptors.[251] The SF$_5$-substituted analogue **561** exhibited reduced binding to 5HT$_{2a}$ and 5HT$_{2c}$ receptors compared to **560** but had comparable affinity for 5HT$_{2b}$ receptors. In the case of fenfluramine (**562**), the SF$_5$ analogue **563** exhibited 10-fold higher affinity for 5HT$_{2b}$ and 5HT$_6$ receptors than the progenitor.[251]

556: R = CF$_3$
CB$_1$ K$_i$ = 26.5 nM
557: R = SF$_5$
CB$_1$ K$_i$ = 11.2 nM

558: R = CF$_3$
IC$_{50}$ = 1.3 μM
559: R = SF$_5$
IC$_{50}$ = 0.36 μM

560: R = CF$_3$
561: R = SF$_5$

562: R = CF$_3$
563: R = SF$_5$
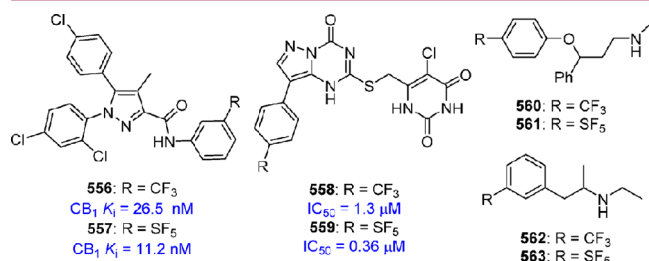
The SF$_5$ moiety continues to be of contemporary interest as a substituent in drug design with the Mtb inhibitor **565** profiling similarly to the CF$_3$ analogue **564**, although protein binding was higher for the former compound (99.7%) than the latter (99.1%).[252] The oxindole derivatives **566** and **567** have been profiled as kinase inhibitors that express cytotoxicity toward the T47D cancer cell line with EC$_{50}$ values of 490 and 350 nM, respectively.[253] While modeling studies were utilized in the design of **566** and **567**, examples of where the SF$_5$ substituent confers a specific advantage based on its unique shape and electronic properties remain to be described.

564: R = CF$_3$
565: R = SF$_5$

566: R = 5-SF$_5$
567: R = 6-SF$_5$
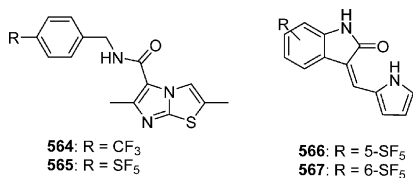
■ CONCLUSION

The unique properties of fluorine continue to reveal itself through the creative application of this unusual element in drug design, with recognition of its potential for mimicking a number of functionalities established as a prominent attribute of this interesting element. The small size of fluorine coupled with the high C−F bond strength has inspired its extensive application as a bioisosteric replacement for the hydrogen atom, particularly with respect to modulating the metabolism and conformation of a molecule. However, the electronic properties of a C−F bond have allowed it to effectively mimic carbonyl, hydroxyl, or nitrile functionality in circumstances that are often very much dependent on context. Thus, specific emulation of these functionalities is often based more on a bioisosteric rather than an isosteric relationship, which can add an element of unpredictability to their application in drug design. The powerful electron withdrawing properties of this electronegative element influence the basicity of proximal amines to an extent that can render an amide mimetic. Moreover, the partial fluorination of methyl groups can lead to polarization of a C−H bond that allows it to function as a H-bond donor that although weaker than more established donors has been shown to be of importance in drug−target interactions. The development of new synthetic methodologies continues to provide facile and effective access to new structural elements containing fluorine that, in turn, are contributing to a deeper understanding of the element and stimulating new applications that often have bioisosterism as an underlying basis. The many examples illustrated in this synopsis reflect the creativity of the medicinal chemistry community at large and anticipate the continued development and application of fluorine in drug design.

■ AUTHOR INFORMATION

Corresponding Author
*Phone: (609) 252-6195. E-mail: Nicholas.meanwell@bms.com.

ORCID ◎
Nicholas A. Meanwell: 0000-0002-8857-1515

Biography
Nicholas A. Meanwell received his Ph.D. degree from the University of Sheffield and conducted postdoctoral studies at Wayne State University before joining Bristol-Myers Squibb in 1982. He has been associated with the discovery of BMY-433771, an inhibitor of respiratory syncytial virus fusion, the HIV-1 attachment inhibitor prodrug fostemsavir, the HIV-1 maturation inhibitor BMS-955176, and the marketed HCV inhibitors asunaprevir (NS3, Sunvepra), daclatasvir (NS5A, Daklinza), and beclabuvir (NS5B). He is the co-recipient of a 2014 PhRMA Research and Hope Award for Biopharmaceutical Industry Research and a 2017 ACS Heroes of Chemistry Award. He was the recipient of the 2015 Philip S. Portoghese Medicinal Chemistry Lectureship Award and was inducted into the ACS Division of Medicinal Chemistry Hall of Fame in 2015.

■ ACKNOWLEDGMENTS

■ ABBREVIATIONS USED

AML, acute myeloid leukemia; BACE-1, β-site amyloid precursor protein cleaving enzyme 1; BCP, [1.1.1]-bicyclopentane; BTK, Bruton's tyrosine kinase; Cdk, cyclin-dependent kinase; CETP, cholesteryl ester transfer protein; CFTR, cystic fibrosis transmembrane regulator; CGRP, calcitonin gene-related peptide; CRF-1, corticotropin releasing factor-1; CSD, Cambridge Structural Database; CYP, cytochrome P enzyme; DFT, density functional theory; DHODH, dihydroorotate dehydrogenase; DIO, diet-induced obese; DPP-4, dipeptidyl peptidase-4; ET, endothelin; FAAH, fatty acid amide hydrolase; FAP, fibroblast activation protein; FKBP, FK506-binding protein; FLT3, FMS-like tyrosine kinase 3; F-OPA, fluorinated olefinic peptide nucleic acid; FXa, factor Xa; GABA, γ-aminobutyric acid; GSH, glutathione; hAR, human androgen receptor; hBRS-3, human bombesin receptor subtype-3; HCV, hepatitis C virus; HIV-1, human immunodeficiency virus-1; HLM, human liver microsomes; hPTH, human parathyroid hormone; 5-HT, 5-hydroxytryptamine (serotonin); Hyp, 4-(R)-hydroxy-L-proline; IDH2, isocitrate dehydrogenase 2; IV, intravenous; LM, liver microsomes; MCHR1, melanin concentrating hormone receptor 1; MEK1, MAP kinase kinase 1; MEP, molecular electrostatic potential; MGAT, acyl-CoA:monoacylglycerol acyltransferase; MI, metabolite intermediate; MMP, matched molecular pairs; Mtb, *Mycobacterium tuberculosis*; MW, molecular weight; NMDA, N-methyl-D-aspartate; PAMPA, parallel artificial membrane permeability assay; PDB, Protein Data Bank; *Pf*, *Plasmodium falciparum*; P-gp, P-glycoprotein; PI3Kα, phosphatidylinositol-3 kinase-α; PNMT, phenylethanolamine N-methyltransferase; PPARγ, peroxisome proliferator-activated receptor-γ; PSA, polar surface area; QM, quantum mechanics; RLM, rat liver microsomes; SAR, structure−activity relationship; STS,

steroid sulfatase; TGR5, Takeda G-protein-coupled receptor 5; WGA, wheat germ agglutinin

■ REFERENCES

(1) (a) Thornber, C. W. Isosterism and molecular modification in drug design. *Chem. Soc. Rev.* **1979**, *8*, 563–580. (b) Lipinski, C. A. Bioisosterism in drug design. *Annu. Rep. Med. Chem.* **1986**, *21*, 283–291. (c) Patani, G. A.; LaVoie, E. J. Bioisosterism: a rational approach in drug design. *Chem. Rev.* **1996**, *96*, 3147–3176. (d) Wermuth, C. G. Similarity in drugs: reflections on analogue design. *Drug Discovery Today* **2006**, *11*, 348–354. (e) Lima, L. M.; Barreiro, E. J. Bioisosterism: a useful strategy for molecular modification in drug design. *Curr. Med. Chem.* **2005**, *12*, 23–49. (f) Meanwell, N. A. Synopsis of some recent tactical applications of bioisosteres in drug design. *J. Med. Chem.* **2011**, *54*, 2529–2591.

(2) (a) Moir, J. Suggestions for a new atomic theory. *J. Chem. Metal. Mining Soc. S. Africa* **1909**, *9* (334–343), 392–393. (b) Langmuir, I. Isomorphism, isosterism and covalence. *J. Am. Chem. Soc.* **1919**, *41*, 1543–1559.

(3) Fried, J.; Sabo, E. F. 9α-Fluoro derivatives of cortisone and hydrocortisone. *J. Am. Chem. Soc.* **1954**, *76*, 1455–1456.

(4) (a) Gillis, E. P.; Eastman, K. J.; Hill, M. D.; Donnelly, D. J.; Meanwell, N. A. Applications of fluorine in medicinal chemistry. *J. Med. Chem.* **2015**, *58*, 8315–8359. (b) Zhu, W.; Wang, J.; Wang, S.; Gu, Z.; Aceña, J. L.; Izawa, K.; Liu, H.; Soloshonok, V. A. Recent advances in the trifluoromethylation methodology and new CF$_3$-containing drugs. *J. Fluorine Chem.* **2014**, *167*, 37–54. (c) Hodgetts, K. J.; Combs, K. J.; Elder, A. M.; Harriman, G. C. The role of fluorine in the discovery and optimization of CNS agents: modulation of drug-like properties. *Annu. Rep. Med. Chem.* **2010**, *45*, 429–448. (d) Purser, S.; Moore, P. R.; Swallow, S.; Gouverneur, V. Fluorine in medicinal chemistry. *Chem. Soc. Rev.* **2008**, *37*, 320–330. (e) Hagmann, W. K. The many roles for fluorine in medicinal chemistry. *J. Med. Chem.* **2008**, *51*, 4359–4369. (f) Böhm, H. J.; Banner, D.; Bendels, S.; Kansy, M.; Kuhn, B.; Müller, K.; Obst-Sander, U.; Stahl, M. Fluorine in medicinal chemistry. *ChemBioChem* **2004**, *5*, 637–643. (g) Müller, K.; Faeh, C.; Diederich, F. Fluorine in pharmaceuticals: looking beyond intuition. *Science* **2007**, *317*, 1881–1886. (h) Shah, P.; Westwell, A. D. The role of fluorine in medicinal chemistry. *J. Enzyme Inhib. Med. Chem.* **2007**, *22*, 527–540. (i) Maienfisch, P.; Hall, R. G. The importance of fluorine in the life science industry. *Chimia* **2004**, *58*, 93–99.

(5) (a) Zhou, Y.; Wang, J.; Gu, Z.; Wang, S.; Zhu, W.; Aceña, J. L.; Soloshonok, V. A.; Izawa, K.; Liu, H. Next generation of fluorine-containing pharmaceuticals, compounds currently in phase II–III clinical trials of major pharmaceutical companies: new structural trends and therapeutic areas. *Chem. Rev.* **2016**, *116*, 422–518. (b) Wang, J.; Sánchez-Roselló, M.; Aceña, J. L.; del Pozo, C.; Sorochinsky, A. E.; Fustero, S.; Soloshonok, V. A.; Liu, H. Fluorine in pharmaceutical industry: fluorine-containing drugs introduced to the market in the last decade (2001–2011). *Chem. Rev.* **2014**, *114*, 2432–2506. (c) Ilardi, E. A.; Vitaku, E.; Njardarson, J. T. Data-mining for sulfur and fluorine: an evaluation of pharmaceuticals to reveal opportunities for drug design and discovery. *J. Med. Chem.* **2014**, *57*, 2832–2842.

(6) (a) Jeschke, P. The unique role of fluorine in the design of active ingredients for modern crop protection. *ChemBioChem* **2004**, *5*, 570–589. (b) Jeschke, P. The unique role of halogen substituents in the design of modern agrochemicals. *Pest Manage. Sci.* **2010**, *66*, 10–27. (c) Fujiwara, T.; O'Hagan, D. Successful fluorine-containing herbicide agrochemicals. *J. Fluorine Chem.* **2014**, *167*, 16–29. (d) Jeschke, P. Latest generation of halogen-containing pesticides. *Pest Manage. Sci.* **2017**, *73*, 1053–1056.

(7) (a) Liang, T.; Neumann, C. N.; Ritter, T. Introduction of fluorine and fluorine-containing functional groups. *Angew. Chem., Int. Ed.* **2013**, *52*, 8214–8264. (b) Yang, X.; Wu, T.; Phipps, R. J.; Toste, F. D. Advances in catalytic enantioselective fluorination, mono-, di-, and trifluoromethylation, and trifluoromethylthiolation reactions. *Chem. Rev.* **2015**, *115*, 826–870. (c) Ahrens, T.; Kohlmann, J.; Ahrens, M.; Braun, T. Functionalization of fluorinated molecules by transition metal-mediated C–F bond activation to access fluorinated building blocks.

Chem. Rev. **2015**, *115*, 931–972. (d) Nenajdenko, V. G.; Muzalevskiy, V. M.; Shastin, A. V. Polyfluorinated ethanes as versatile fluorinated C2-building blocks for organic synthesis. *Chem. Rev.* **2015**, *115*, 973–1050. (e) Yerien, D. E.; Barata-Vallejo, S.; Postigo, A. Difluoromethylation reactions of organic compounds. *Chem. - Eur. J.* **2017**, *23*, 14676–14701.

(8) (a) O'Hagan, D. Understanding organofluorine chemistry. An introduction to the C–F bond. *Chem. Soc. Rev.* **2008**, *37*, 308–319. (b) Mikami, K.; Itoh, Y.; Yamanaka, M. Fluorinated carbonyl and olefinic compounds: basic character and asymmetric catalytic reactions. *Chem. Rev.* **2004**, *104*, 1–16.

(9) Clark, T.; Murray, J. S.; Lane, P.; Politzer, P. Why are dimethyl sulfoxide and dimethyl sulfone such good solvents? *J. Mol. Model.* **2008**, *14*, 689–697.

(10) (a) Park, K. B.; Kitteringham, N. R. Effects of fluorine substitution on drug metabolism: pharmacological and toxicological implications. *Drug Metab. Rev.* **1994**, *26*, 605–643. (b) Murphy, C. D.; Sandford, G. Recent advances in fluorination techniques and their anticipated impact on drug metabolism and toxicity. *Expert Opin. Drug Metab. Toxicol.* **2015**, *11*, 589–599.

(11) (a) Meanwell, N. A. Improving drug candidates by design: a focus on physicochemical properties as a means of improving compound disposition and safety. *Chem. Res. Toxicol.* **2011**, *24*, 1420–1456. (b) Meanwell, N. A. Improving drug design: an update on recent applications of efficiency metrics, strategies for replacing problematic elements, and compounds in nontraditional drug space. *Chem. Res. Toxicol.* **2016**, *29*, 564–616.

(12) Huchet, Q. A.; Kuhn, B.; Wagner, B.; Kratochwil, N. A.; Fischer, H.; Kansy, M.; Zimmerli, D.; Carreira, E. M.; Müller, K. Fluorination patterning: a study of structural motifs that impact physicochemical properties of relevance to drug discovery. *J. Med. Chem.* **2015**, *58*, 9041–9060.

(13) Pettersson, M.; Hou, X.; Kuhn, M.; Wager, T. T.; Kauffman, G. W.; Verhoest, P. R. Quantitative assessment of the impact of fluorine substitution on P-glycoprotein (P-gp) mediated efflux, permeability, lipophilicity, and metabolic stability. *J. Med. Chem.* **2016**, *59*, 5284–5296.

(14) Bott, F.; Field, L. D.; Sternhell, S. Steric effects. A study of a rationally designed system. *J. Am. Chem. Soc.* **1980**, *102*, 5618–5626.

(15) (a) Lunazzi, L.; Mancinelli, M.; Mazzanti, A.; Lepri, S.; Ruzziconi, R.; Schlosser, M. Rotational barriers of biphenyls having heavy heteroatoms as ortho substituents: experimental and theoretical determination of steric effects. *Org. Biomol. Chem.* **2012**, *10*, 1847–1855. (b) de Riggi, I.; Virgili, A.; de Moragas, M.; Jaime, C. Restricted rotation and NOE transfer: a conformational study of some substituted (9-anthry1)carbinol derivatives. *J. Org. Chem.* **1995**, *60*, 27–31. (c) Belot, V.; Farran, D.; Jean, M.; Albalat, M.; Vanthuyne, N.; Roussel, C. Steric scale of common substituents from rotational barriers of N-(o-substituted aryl)thiazoline-2-thione atropisomers. *J. Org. Chem.* **2017**, *82*, 10188–10200. (d) Soloshonok, V. A.; Kukhar, V. P.; Galushko, S. V.; Svistunova, N. Y.; Avilov, D. V.; Kuz'mina, N. A.; Raevski, N. I.; Struchkov, Y. T.; Pysarevsky, A. P.; Belokon, Y. N. General method for the synthesis of enantiomerically pure β-hydroxy-α-amino acids, containing fluorine atoms in the side chains. Case of stereochemical distinction between methyl and trifluoromethyl groups. X-ray crystal and molecular structure of the nickel (II) complex of (2S,3S)-2-(trifluoromethyl)threonine. *J. Chem. Soc., Perkin Trans. 1* **1993**, 3143–3155. (e) Soloshonok, V. A.; Avilov, D. V.; Kukhar, V. P.; Tararov, V. I.; Saveleva, T. F.; Churkina, T. D.; Ikonnikov, N. S.; Kochetkov, K. A.; Orlova, S. A.; Pysarevsky, A. P.; Struchkov, Y. T.; Raevski, N. I.; Belokon, Y. N. Asymmetric aldol reactions of chiral Ni (II)-complex of glycine with aliphatic aldehydes. Stereodivergent synthesis of syn-(2S)- and syn-(2R)-β-alkylserines. *Tetrahedron: Asymmetry* **1995**, *6*, 1741–1756. (f) Soloshonok, V. A.; Kacharov, A. D.; Avilov, D. V.; Ishikawa, K.; Nagashima, N.; Hayashi, T. Transition metal/base-catalyzed aldol reactions of isocyanoacetic acid derivatives with prochiral ketones, a straightforward approach to stereochemically defined α, α -disubstituted-β-hydroxy-α-amino acids. 1. Scope and limitations. *J. Org. Chem.* **1997**, *62*, 3470–3479.

(16) Jagodzinska, M.; Huguenot, F.; Candiani, G.; Zanda, M. Assessing the bioisosterism of the trifluoromethyl group with a protease probe. *ChemMedChem* 2009, 4, 49−51.

(17) Shaughnessy, M. J.; Harsanyi, A.; Li, J.; Bright, T.; Murphy, C. D.; Sandford, G. Targeted fluorination of a nonsteroidal anti-inflammatory drug to prolong metabolic half-life. *ChemMedChem* 2014, 9, 733−736.

(18) Stepan, A. F.; Mascitti, V.; Beaumont, K.; Kalgutkar, A. S. Metabolism-guided drug design. *MedChemComm* 2013, 4, 631−652.

(19) Dossetter, A. G. A matched molecular pair analysis of in vitro human microsomal metabolic stability measurements for methylene substitution or replacements - identification of those transforms more likely to have beneficial effects. *MedChemComm* 2012, 3, 1518−1525.

(20) (a) Stalford, A. C.; Maggs, J. L.; Gilchrist, T. L.; Park, B. K. The metabolism of 16-fluoroestradiols *in vivo*: chemical strategies for restricting the oxidative biotransformations of an estrogen receptor imaging agent. *Steroids* 1997, 62, 750−776. (b) Diana, G. D.; Rudewicz, P.; Pevear, D. C.; Nitz, T. J.; Aldous, S. C.; Aldous, D. J.; Robinson, D. T.; Draper, T.; Dutko, F. J.; Aldi, C.; Gendron, G.; Oglesby, R. C.; Volkots, D. L.; Reurnan, M.; Bailey, T. R.; Czerniak, R.; Block, T.; Roland, R.; Oppermand, J. Picornavirus inhibitors: trifluoromethyl substitution provides a global protective effect against hepatic metabolism. *J. Med. Chem.* 1996, 38, 1355−1371. (c) DeGoey, D. A.; Chen, H.-J.; Cox, P. B.; Wendt, M. D. Beyond the rule of 5: lessons learned from AbbVie's drugs and compound collection. *J. Med. Chem.* 2017, DOI: 10.1021/acs.jmedchem.7b00717.

(21) (a) Ojima, I. Strategic incorporation of fluorine into taxoid anticancer agents for medicinal chemistry and chemical biology studies. *J. Fluorine Chem.* 2017, 198, 10−23. (b) Kuznetsova, L.; Sun, L.; Chen, J.; Zhao, X.; Seitz, J.; Das, M.; Li, Y.; Veith, J. M.; Pera, P.; Bernacki, R. J.; Xia, S.; Horwitz, S. B.; Ojima, I. Synthesis and biological evaluation of novel 3′-difluorovinyl toxoids. *J. Fluorine Chem.* 2012, 143, 177−188. (c) Ehrlichová, M.; Ojima, I.; Chen, J.; Václavíková, R.; Němcová-Fürstová, V.; Vobořilová, J.; Šimek, P.; Horský, S.; Souček, P.; Kovář, J.; Brabec, M.; Gut, I. Transport, metabolism, cytotoxicity and effects of novel taxanes on the cell cycle in MDA-MB-435 and NCI/ADR-RES cells. *Naunyn-Schmiedeberg's Arch. Pharmacol.* 2012, 385, 1035−1048.

(22) Mascitti, V.; Stevens, B. D.; Choi, C.; McClure, K. F.; Guimarães, C. R. W.; Farley, K. A.; Munchhof, M. J.; Robinson, R. P.; Futatsugi, K.; Lavergne, S. Y.; Lefker, B.; Cornelius, A. P.; Bonin, P. D.; Kalgutkar, A. S.; Sharma, R.; Chen, Y. Design and evaluation of a 2-(2,3,6-trifluorophenyl)acetamide derivative as an agonist of the GPR119 receptor. *Bioorg. Med. Chem. Lett.* 2011, 21, 1306−1309.

(23) Barnes-Seeman, D.; Beck, J.; Springer, C. Fluorinated compounds in medicinal chemistry: recent applications, synthetic advances and matched-pair analysis. *Curr. Top. Med. Chem.* 2014, 14, 855−864.

(24) Barnes-Seeman, D.; Jain, M.; Bell, L.; Ferreira, S.; Cohen, S.; Chen, X.-H.; Amin, J.; Snodgrass, B.; Hatsis, P. Metabolically stable *tert*-butyl replacement. *ACS Med. Chem. Lett.* 2013, 4, 514−516.

(25) Westphal, M. V.; Wolfstädter, B. T.; Plancher, J.-M.; Gatfield, J.; Carreira, E. M. Evaluation of *tert*-butyl isosteres: case studies of physicochemical and pharmacokinetic properties, efficacies, and activities. *ChemMedChem* 2015, 10, 461−469.

(26) Chao, Q.; Sprankle, K. G.; Grotzfeld, R. M.; Lai, A. G.; Carter, T. A.; Velasco, A. M.; Gunawardane, R. N.; Cramer, M. D.; Gardner, M. F.; James, J.; Zarrinkar, P. P.; Patel, H. K.; Bhagwat, S. S. Identification of *N*-(5-*tert*-butyl-isoxazol-3-yl)-*N'*-{4-[7-(2-morpholin-4-yl-ethoxy)-imidazo-[2,1-*b*][1,3]benzothiazol-2-yl]phenyl}urea dihydrochloride (AC220), a uniquely potent, selective, and efficacious FMS-like tyrosine kinase-3 (FLT3) inhibitor. *J. Med. Chem.* 2009, 52, 7808−7816.

(27) Sanga, M.; James, J.; Marini, J.; Gammon, G.; Hale, C.; Li, J. An open-label, single-dose, phase I study of the absorption, metabolism, and excretion of quizartinib, a highly selective and potent FLT3 tyrosine kinase inhibitor, in healthy male subjects, for the treatment of acute myeloid leukemia. *Xenobiotica* 2017, 47, 856−869.

(28) Liu, G.; Abraham, S.; Liu, X.; Xu, S.; Rooks, A. M.; Nepomuceno, R.; Dao, A.; Brigham, D.; Gitnick, D.; Insko, D. E.; Gardner, M. F.; Zarrinkar, P. P.; Christopher, R.; Belli, B.; Armstrong, R. C.; Holladay, M. W. Discovery and optimization of a highly efficacious class of 5-aryl-2-aminopyridines as FMS-like tyrosine kinase 3 (FLT3) inhibitors. *Bioorg. Med. Chem. Lett.* 2015, 25, 3436−3441.

(29) Sebhat, I. K.; Franklin, C.; Lo, M. M.-C.; Chen, D.; Jewell, J. P.; Miller, R.; Pang, J.; Palyha, O.; Kan, Y.; Kelly, T. M.; Guan, X.-M.; Marsh, D. J.; Kosinski, J. A.; Metzger, J. M.; Lyons, K.; Dragovic, J.; Guzzo, P. R.; Henderson, A. J.; Reitman, M. L.; Nargund, R. P.; Wyvratt, M. J.; Lin, L. S. Discovery of MK-5046, a potent, selective bombesin receptor subtype-3 agonist for the treatment of obesity. *ACS Med. Chem. Lett.* 2011, 2, 43−47.

(30) Furet, P.; Guagnano, V.; Fairhurst, R. A.; Imbach-Weese, P.; Bruce, I.; Knapp, M.; Fritsch, C.; Blasco, F.; Blanz, J.; Aichholz, R.; Hamon, J.; Fabbro, D.; Caravatti, G. Discovery of NVP-BYL719 a potent and selective phosphatidylinositol-3 kinase alpha inhibitor selected for clinical evaluation. *Bioorg. Med. Chem. Lett.* 2013, 23, 3741−3748.

(31) (a) Beno, B. R.; Yeung, K.-S.; Bartberger, M. D.; Pennington, L. D.; Meanwell, N. A. A survey of the role of noncovalent sulfur interactions in drug design. *J. Med. Chem.* 2015, 58, 4383−4438. (b) Zhang, X.; Gong, Z.; Li, J.; Lu, T. Intermolecular sulfur···oxygen interactions: theoretical and statistical investigations. *J. Chem. Inf. Model.* 2015, 55, 2138−2153.

(32) Rowbottom, M. W.; Faraoni, R.; Chao, Q.; Campbell, B. T.; Lai, A. G.; Setti, E.; Ezawa, M.; Sprankle, K. G.; Abraham, S.; Tran, L.; Struss, B.; Gibney, M.; Armstrong, R. C.; Gunawardane, R. N.; Nepomuceno, R. R.; Valenta, I.; Hua, H.; Gardner, M. F.; Cramer, M. D.; Gitnick, D.; Insko, D. E.; Apuy, J. L.; Jones-Bolin, S.; Ghose, A. K.; Herbertz, T.; Ator, M. A.; Dorsey, B. D.; Ruggeri, B.; Williams, M.; Bhagwat, S.; James, J.; Holladay, M. W. Identification of 1-(3-(6,7-dimethoxyquinazolin-4-yloxy)phenyl)-3-(5-(1,1,1-trifluoro-2-methylpropan-2-yl)isoxazol-3-yl)urea hydrochloride (CEP-32496), a highly potent and orally efficacious inhibitor of V-RAF murine sarcoma viral oncogene homologue B1 (BRAF) V600E. *J. Med. Chem.* 2012, 55, 1082−1105.

(33) Pettersson, M.; Johnson, D. S.; Humphrey, J. M.; Butler, T. W.; am Ende, C. W.; Fish, B. A.; Green, M. E.; Kauffman, G. W.; Mullins, P. B.; O'Donnell, C. J.; Stepan, A. F.; Stiff, C. M.; Subramanyam, C.; Tran, T. P.; Cooper Vetelino, B.; Yang, E.; Xie, L.; Bales, K. R.; Pustilnik, L. R.; Steyn, S. J.; Wood, K. M.; Verhoest, P. R. Design of pyridopyrazine-1,6-dione γ-secretase modulators that align potency, MDR efflux ratio, and metabolic stability. *ACS Med. Chem. Lett.* 2015, 6, 596−601.

(34) Mukherjee, P.; Pettersson, M.; Dutra, J. K.; Xie, L.; am Ende, C. W. Trifluoromethyl oxetanes: synthesis and evaluation as a *tert*-butyl isostere. *ChemMedChem* 2017, 12, 1574−1577.

(35) (a) Kim, D.; Wang, L.; Beconi, M.; Eiermann, G. J.; Fisher, M. H.; He, H.; Hickey, G. J.; Kowalchick, J. E.; Leiting, B.; Lyons, K.; Marsilio, F.; McCann, M. E.; Patel, R. A.; Petrov, A.; Scapin, G.; Patel, S. B.; Roy, R. S.; Wu, J. K.; Wyvratt, M. J.; Zhang, B. B.; Zhu, L.; Thornberry, N. A.; Weber, A. E. (2*R*)-4-Oxo-4-[3-(trifluoromethyl)-5,6-dihydro[1,2,4]-triazolo[4,3-*a*]pyrazin-7(8*H*)-yl]-1-(2,4,5-trifluorophenyl)butan-2-amine: a potent, orally active dipeptidyl peptidase IV inhibitor for the treatment of type 2 diabetes. *J. Med. Chem.* 2005, 48, 141−151. (b) Kim, D.; Kowalchick, J.E.; Edmondson, S. D.; Mastracchio, A.; Xu, J.; Eiermann, G. J.; Leiting, B.; Wu, J. K.; Pryor, K. D.; Patel, R. A.; He, H.; Lyons, K. A.; Thornberry, N. A.; Weber, A. E. Triazolopiperazine-amides as dipeptidyl peptidase IV inhibitors: close analogs of JANUVIA (sitagliptin phosphate). *Bioorg. Med. Chem. Lett.* 2007, 17, 3373−3377. (c) Thornberry, N. A.; Weber, A. E. Discovery of JANUVIA (Sitagliptin), a selective dipeptidyl peptidase IV inhibitor for the treatment of type 2 diabetes. *Curr. Top. Med. Chem.* 2007, 7, 557−568.

(36) Mayer, S. C.; Kreft, A. F.; Harrison, B.; Abou-Gharbia, M.; Antane, M.; Aschmies, S.; Atchison, K.; Chlenov, M.; Cole, D. C.; Comery, T.; Diamantidis, G.; Ellingboe, J.; Fan, K.; Galante, R.; Gonzales, C.; Ho, D. M.; Hoke, M. E.; Hu, Y.; Huryn, D.; Jain, U.; Jin, M.; Kremer, K.; Kubrak, D.; Lin, M.; Lu, P.; Magolda, R.; Martone, R.; Moore, W.; Oganesian, A.; Pangalos, M. N.; Porte, A.; Reinhart, P.; Resnick, L.; Riddell, D. R.; Sonnenberg-Reines, J.; Stock, J. R.; Sun, S.-C.; Wagner, E.; Wang, T.; Woller, K.; Xu, Z.; Zaleska, M. M.; Zeldis, J.; Zhang, M.; Zhou, H.; Jacobsen, J. S. Discovery of begacestat, a notch-1-sparing γ-secretase inhibitor for the treatment of Alzheimer's disease. *J. Med. Chem.* 2008, 51, 7348−7351.

(37) Floyd, D. M.; Stein, P.; Wang, Z.; Liu, J.; Castro, S.; Clark, J. A.; Connelly, M.; Zhu, F.; Holbrook, G.; Matheny, A.; Sigal, M. S.; Min, J.; Dhinakaran, R.; Krishnan, S.; Bashyum, S.; Knapp, S.; Guy, R. K. Hit-to-lead studies for the antimalarial tetrahydroisoquinolone carboxanilides. *J. Med. Chem.* **2016**, *59*, 7950–7962.

(38) Selnick, H. G.; Liverton, N. J.; Baldwin, J. J.; Butcher, J. W.; Claremon, D. A.; Elliott, J. M.; Freidinger, R. M.; King, S. A.; Libby, B. E.; McIntyre, C. J.; Pribush, D. A.; Remy, D. C.; Smith, G. R.; Tebben, A. J.; Jurkiewicz, N. K.; Lynch, J. J.; Salata, J. J.; Sanguinetti, M. C.; Siegl, P. K. S.; Slaughter, D. E.; Vyas, K. Class III antiarrhythmic activity in vivo by selective blockade of the slowly activating cardiac delayed rectifier potassium current I_{Ks} by (*R*)-2-(2,4-trifluoromethyl)-*N*-[2-oxo-5-phenyl-1-(2,2,2-trifluoroethyl)-2,3-dihydro-1*H*-benzo[*e*][1,4]diazepin-3-yl]acetamide. *J. Med. Chem.* **1997**, *40*, 3865–3868.

(39) (a) Tohnishi, M.; Nishimatsu, T.; Motoba, K.; Hirooka, T.; Seo, A. Development of a novel insecticide, flubendiamide. *J. Pestic. Sci.* **2010**, *35*, 490–491. (b) Nakao, T.; Banba, S. Broflanilide: a meta-diamide insecticide with a novel mode of action. *Bioorg. Med. Chem.* **2016**, *24*, 372–377.

(40) Swaminathan, S.; Siddiqui, A. U.; Pinkerton, F. D.; Gerst, N.; Wilson, W. K.; Schroepfer, G. J. Inhibitors of sterol synthesis: 3*β*-hydroxy-25,26,26,26,27,27,27-heptafluoro-5*α*-cholestan-15-one, an analog of a potent hypocholesterolemic agent in which its major metabolism is blocked. *Biochem. Biophys. Res. Commun.* **1994**, *201*, 168–173.

(41) Lepri, S.; Goracci, L.; Valeri, A.; Cruciani, G. Metabolism study and biological evaluation of bosentan derivatives. *Eur. J. Med. Chem.* **2016**, *121*, 658–670.

(42) (a) Thangavelu, B.; Bhansali, P.; Viola, R. E. Elaboration of a fragment library hit produces potent and selective aspartate semi-aldehyde dehydrogenase inhibitors. *Bioorg. Med. Chem.* **2015**, *23*, 6622–6631. (b) Thangavelu, B.; Mutthamsetty, V.; Wang, Q.; Viola, R. E. Design and optimization of aspartate *N*-acetyltransferase inhibitors for the potential treatment of Canavan disease. *Bioorg. Med. Chem.* **2017**, *25*, 870–885.

(43) Kees, K. L.; Fitzgerald, J. J., Jr.; Steiner, K. E.; Mattes, J. F.; Mihan, B.; Tosi, T.; Mondoro, D.; McCaleb, M. L. New potent antihyperglycemic agents in db/db mice: synthesis and structure-activity relationship studies of (4-substituted benzyl)(trifluoromethyl)-pyrazoles and -pyrazolones. *J. Med. Chem.* **1996**, *39*, 3920–3928.

(44) (a) Rose, T. E.; Morisseau, C.; Liu, J.-Y.; Inceoglu, B.; Jones, P. D.; Sanborn, J. R.; Hammock, B. D. 1-Aryl-3-(1-acylpiperidin-4-yl)urea inhibitors of human and murine soluble epoxide hydrolase: structure-activity relationships, pharmacokinetics, and reduction of inflammatory pain. *J. Med. Chem.* **2010**, *53*, 7067–7075. (b) Lee, K. S. S.; Liu, J.-Y.; Wagner, K. M.; Pakhomova, S.; Dong, H.; Morisseau, C.; Fu, S. H.; Yang, J.; Wang, P.; Ulu, A.; Mate, C. A.; Nguyen, L. V.; Hwang, S. H.; Edin, M. L.; Mara, A. A.; Wulff, H.; Newcomer, M. E.; Zeldin, D. C.; Hammock, B. D. Optimized inhibitors of soluble epoxide hydrolase improve in vitro target residence time and in vivo efficacy. *J. Med. Chem.* **2014**, *57*, 7016–7030.

(45) Atouioual, B.; Hagmann, L.; Jung, P. M. J.; Lamy, E.; Winkler, T. Atropisomerism about a heptafluoroisopropyl to aryl bond in 5-amino-4-heptafluoroisopropyl indazole. *Tetrahedron Lett.* **2008**, *49*, 5403–5404.

(46) (a) Dieckhaus, C. M.; Thompson, C. D.; Roller, S. G.; Macdonald, T. L. Mechanisms of idiosyncratic drug reactions: the case of felbamate. *Chem.-Biol. Interact.* **2002**, *142*, 99–117. (b) Kapetanovic, I. M.; Torchin, C. D.; Strong, J. M.; Yonekawa, W. D.; Lu, C.; Li, A. P.; Dieckhaus, C. M.; Santos, W. L.; Macdonald, T. L.; Sofia, R. D.; Kupferberg, H. J. Reactivity of atropaldehyde, a felbamate metabolite in human liver tissue in vitro. *Chem.-Biol. Interact.* **2002**, *142*, 119–134. (c) Popović, M.; Nierkens, S.; Pieters, R.; Uetrecht, J. Investigating the role of 2-phenylpropenal in felbamate-induced idiosyncratic drug reactions. *Chem. Res. Toxicol.* **2004**, *17*, 1568–1576.

(47) Parker, R. J.; Hartman, N. R.; Roecklein, B. A.; Mortko, H.; Kupferberg, H. J.; Stables, J.; Strong, J. M. Stability and comparative metabolism of selected felbamate metabolites and postulated

fluorofelbamate metabolites by post-mitochondrial suspensions. *Chem. Res. Toxicol.* **2005**, *18*, 1842–1848.

(48) (a) Kupferberg, H. J.; Macdonald, T. L.; Dieckhaus, C. M.; Perhach, J. L.; Sofia, R. D. Fluorofelbamate: pharmacodynamic and metabolic profile of a potent anticonvulsant. *Epilepsia* **2000**, *41* (Suppl 7), 214. (b) Mazarati, A. M.; Sofia, R. D.; Wasterlain, C. G. Anticonvulsant and antiepileptogenic effects of fluorofelbamate in experimental status epilepticus. *Seizure* **2002**, *11*, 423–430.

(49) (a) Roecklein, B. A.; Sacks, H. J.; Mortko, H.; Stables, J. Fluorofelbamate. *Neurotherapeutics* **2007**, *4*, 97–101. (b) Bialer, M. New antiepileptic drugs that are second generation to existing antiepileptic drugs. *Expert Opin. Invest. Drugs* **2006**, *15*, 637–647.

(50) Xu, S.; Zhu, B.; Teffera, Y.; Pan, D. E.; Caldwell, C. G.; Doss, G.; Stearns, R. A.; Evans, D. C.; Beconi, M. G. Metabolic activation of fluoropyrrolidine dipeptidyl peptidase-IV inhibitors by rat liver microsomes. *Drug Metab. Dispos.* **2005**, *33*, 121–130.

(51) (a) Edmondson, S. D.; Mastracchio, A.; Mathvink, R. J.; He, J.; Harper, B.; Park, Y. J.; Beconi, M.; Di Salvo, J.; Eiermann, G. J.; He, H.; Leiting, B.; Leone, J. F.; Levorse, D. A.; Lyons, K.; Patel, R. A.; Patel, S. B.; Petrov, A.; Scapin, G.; Shang, J.; Roy, R. S.; Smith, A.; Wu, J.K.; Xu, S.; Zhu, B.; Thornberry, N. A.; Weber, A. E. (2*S*,3*S*)-3-Amino-4-(3,3-difluoropyrrolidin-1-yl)-*N*,*N*-dimethyl-4-oxo-2-(4-[1,2,4]triazolo[1,5-*a*]-pyridin-6-ylphenyl)butanamide: a selective *α*-amino amide dipeptidyl peptidase IV inhibitor for the treatment of type 2 diabetes. *J. Med. Chem.* **2006**, *49*, 3614–3627. (b) Sharma, R.; Sun, H.; Piotrowski, D. W.; Ryder, T. F.; Doran, S. D.; Dai, H.; Prakash, C. Metabolism, excretion, and pharmacokinetics of (3,3-difluoropyrrolidin-1-yl)-((2*S*,4*S*)-4-(4-(pyrimidin-2-yl)piperazin-1-yl)pyrrolidin-2-yl)-metha-none, a dipeptidyl peptidase inhibitor, in rat, dog and human. *Drug Metab. Dispos.* **2012**, *40*, 2143–2161.

(52) Tremblay, M.; Bethell, R. C.; Cordingley, M. G.; Deroy, P.; Duan, J.; Duplessis, M.; Edwards, P. J.; Faucher, A. M.; Halmos, T.; James, C. A.; Kuhn, C.; Lacoste, J. E.; Lamorte, L.; LaPlante, S. R.; Malenfant, É.; Minville, J.; Morency, L.; Morin, S.; Rajotte, D.; Salois, P.; Simoneau, B.; Tremblay, S.; Sturino, C. F. Identification of benzofurano-[3,2-*d*]pyrimidin-2-ones, a new series of HIV-1 nucleotide-competing reverse transcriptase inhibitors. *Bioorg. Med. Chem. Lett.* **2013**, *23*, 2775–2780.

(53) (a) Meyer, A.; Imming, P. Benzylisoquinoline alkaloids from the papaveraceae: the heritage of Johannes Gadamer (1867–1928). *J. Nat. Prod.* **2011**, *74*, 2482–2487. (b) Sriram, D.; Yogeeswari, P.; Thirumurugan, R.; Ratan Bal, T. R. Camptothecin and its analogues: a review on their chemotherapeutic potential. *Nat. Prod. Res.* **2005**, *19*, 393–412. (c) Olsen, L. R.; Grillo, M. P.; Skonberg, C. Constituents in kava extracts potentially involved in hepatotoxicity: a review. *Chem. Res. Toxicol.* **2011**, *24*, 992–1002.

(54) Murray, M. Mechanisms of inhibitory and regulatory effects of methylenedioxyphenyl compounds on cytochrome P450-dependent drug oxidation. *Curr. Drug Metab.* **2000**, *1*, 67–84.

(55) (a) Kalgutkar, A. S.; Gardner, I.; Obach, R. S.; Shaffer, C. L.; Callegari, E.; Henne, K. R.; Mutlib, A. E.; Dalvie, D. K.; Lee, J. S.; Nakai, Y.; O'Donnell, J. P.; Boer, J.; Harriman, S. P. A comprehensive listing of bioactivation pathways of organic functional groups. *Curr. Drug Metab.* **2005**, *6*, 161–225. (b) Stepan, A. F.; Walker, D. P.; Bauman, J.; Price, D. A.; Baillie, T. A.; Kalgutkar, A. S.; Aleo, M. D. Structural alert/reactive metabolite concept as applied in medicinal chemistry to mitigate the risk of idiosyncratic drug toxicity: a perspective based on the critical examination of trends in the top 200 drugs marketed in the United States. *Chem. Res. Toxicol.* **2011**, *24*, 1345–1410.

(56) Bolton, J. L.; Trush, M. A.; Penning, T. M.; Dryhurst, G.; Monks, T. J. Role of quinones in toxicology. *Chem. Res. Toxicol.* **2000**, *13*, 135–160.

(57) (a) Hemeryck, A.; De Vriendt, C. A.; Belpaire, F. M. Metoprolol-paroxetine interaction in human liver microsomes: stereoselective aspects and prediction of the in vivo interaction. *Drug Metab. Dispos.* **2001**, *29*, 656–663. (b) Zhao, S. X.; Dalvie, D. K.; Kelly, J. M.; Soglia, J. R.; Frederick, K. S.; Smith, E. B.; Obach, R. S.; Kalgutkar, A. S. NADPH-dependent covalent binding of [³H]-paroxetine to human liver microsomes and S-9 fractions: identification of an electrophilic quinone

metabolite of paroxetine. *Chem. Res. Toxicol.* **2007**, *20*, 1649−1657. (c) Bertelsen, K. M.; Venkatakrishnan, K.; von Moltke, L. L.; Obach, R. S.; Greenblatt, D. J. Apparent mechanism-based inhibition of human CYP 2D6 in vitro by paroxetine: comparison with fluoxetine and quinidine. *Drug Metab. Dispos.* **2003**, *31*, 289−293.

(58) (a) Anzali, S.; Mederski, W. W. K. R.; Osswald, M.; Dorsch, D. 1. Endothelin antagonists: search for surrogates of methylendioxyphenyl by means of a kohonen neural network. *Bioorg. Med. Chem. Lett.* **1998**, *8*, 11−16. (b) Iyengar, R. R.; Lynch, J. K.; Mulhern, M. M.; Judd, A. S.; Freeman, J. C.; Gao, J.; Souers, A. J.; Zhao, G.; Wodka, D.; Falls, H. D.; Brodjian, S.; Dayton, B. D.; Reilly, R. M.; Swanson, S.; Su, Z.; Martin, R. L.; Leitz, S. T.; Houseman, K. A.; Diaz, G.; Collins, C. A.; Sham, H. L.; Kym, P. R. An evaluation of 3,4-methylenedioxy phenyl replacements in the aminopiperidine chromone class of MCHr1 antagonists. *Bioorg. Med. Chem. Lett.* **2007**, *17*, 874−878. (c) Bardelle, C.; Barlaam, B.; Brooks, N.; Coleman, T.; Cross, D.; Ducray, R.; Green, I.; Lambert-van der Brempt, C.; Olivier, A.; Read, J. Inhibitors of the tyrosine kinase EphB4. Part 3: identification of non-benzodioxole-based kinase inhibitors. *Bioorg. Med. Chem. Lett.* **2010**, *20*, 6242−6245. (d) Orr, S. T. M.; Ripp, S. L.; Ballard, T. E.; Henderson, J. L.; Scott, D. O.; Obach, R. S.; Sun, H.; Kalgutkar, A. S. Mechanism-based inactivation (MBI) of cytochrome P450 enzymes: structure−activity relationships and discovery strategies to mitigate drug−drug interaction risks. *J. Med. Chem.* **2012**, *55*, 4896−4933. (e) Crawford, J. J.; Kenny, P. W.; Bowyer, J.; Cook, C. R.; Finlayson, J. E.; Heyes, C.; Highton, A. J.; Hudson, J. A.; Jestel, A.; Krapp, S.; Martin, S.; MacFaul, P. A.; McDermott, B. P.; McGuire, T. M.; Morley, A. D.; Morris, J. J.; Page, K. M.; Rosenbrier Ribeiro, L.; Sawney, H.; Steinbacher, S.; Smith, C.; Dossetter, A. G. Pharmacokinetic benefits of 3,4-dimethoxy substitution of a phenyl ring and design of isosteres yielding orally available cathepsin K inhibitors. *J. Med. Chem.* **2012**, *55*, 8827−8837.

(59) Uttamsingh, V.; Gallegos, R.; Liu, J. F.; Harbeson, S. L.; Bridson, G. W.; Cheng, C.; Wells, D. S.; Graham, P. B.; Zelle, R.; Tung, R. Altering metabolic profiles of drugs by precision deuteration: reducing mechanism-based inhibition of CYP2D6 by paroxetine. *J. Pharmacol. Exp. Ther.* **2015**, *354*, 43−54.

(60) (a) Vasudevan, A.; Wodka, D.; Verzal, M. K.; Souers, A. J.; Gao, J.; Brodjian, S.; Fry, D.; Dayton, B.; Marsh, K. C.; Hernandez, L. E.; Ogiela, C. A.; Collins, C. A.; Kym, P. R. Synthesis and evaluation of 2-amino-8-alkoxy quinolines as MCHr1 antagonists. Part 2. *Bioorg. Med. Chem. Lett.* **2004**, *14*, 4879−4882. (b) Nuzzi, A.; Fiasella, A.; Ortega, J. A.; Pagliuca, C.; Ponzano, S.; Pizzirani, D.; Mandrup Bertozzi, S.; Ottonello, G.; Tarozzo, G.; Reggiani, A.; Bandiera, T.; Bertozzi, F.; Piomelli, D. Potent *α*-amino-*β*-lactam carbamic acid ester as NAAA inhibitors. Synthesis and structure-activity relationship (SAR) studies. *Eur. J. Med. Chem.* **2016**, *111*, 138−159.

(61) (a) Guo, Z.; Zhu, Y.-F.; Gross, T. D.; Tucci, F. C.; Gao, Y.; Moorjani, M.; Connors, P. J., Jr.; Rowbottom, M. W.; Chen, Y.; Struthers, R. S.; Xie, Q.; Saunders, J.; Reinhart, G.; Chen, T. K.; Killam Bonneville, A. L.; Chen, C. Synthesis and Structure-activity relationships of 1-arylmethyl-5-aryl-6-methyluracils as potent gonadotropin-releasing hormone receptor antagonists. *J. Med. Chem.* **2004**, *47*, 1259−1271. (b) Lynch, J. K.; Freeman, J. C.; Judd, A. S.; Iyengar, R.; Mulhern, M.; Zhao, G.; Napier, J. J.; Wodka, D.; Brodjian, S.; Dayton, B. D.; Falls, D.; Ogiela, C.; Reilly, R. M.; Campbell, T. J.; Polakowski, J. S.; Hernandez, L.; Marsh, K. C.; Shapiro, R.; Knourek-Segel, V.; Droz, B.; Bush, E.; Brune, M.; Preusser, L. C.; Fryer, R. M.; Reinhart, G. A.; Houseman, K.; Diaz, G.; Mikhail, A.; Limberis, J. T.; Sham, H. L.; Collins, C. A.; Kym, P. R. Optimization of chromone-2-carboxamide melanin concentrating hormone receptor 1 antagonists: assessment of potency, efficacy, and cardiovascular safety. *J. Med. Chem.* **2006**, *49*, 6569−6584.

(62) Malamas, M. S.; Erdei, J.; Gunawan, I.; Barnes, K.; Johnson, M.; Hui, Y.; Turner, J.; Hu, Y.; Wagner, E.; Fan, K.; Olland, A.; Bard, J.; Robichaud, A. J. Aminoimidazoles as potent and selective human *β*-secretase (BACE1) inhibitors. *J. Med. Chem.* **2009**, *52*, 6314−6323.

(63) Rose, W. C.; Marathe, P. H.; Jang, G. R.; Monticello, T. M.; Balasubramanian, B. N.; Long, B.; Fairchild, C. R.; Wall, M. E.; Wani, M. C. Novel fluoro-substituted camptothecins: in vivo antitumor activity,

reduced gastrointestinal toxicity and pharmacokinetic characterization. *Cancer Chemother. Pharmacol.* **2006**, *58*, 73−85.

(64) Trachsel, D.; Hadorn, M.; Baumberger, F. Synthesis of fluoro analogues of 3,4-(methylenedioxy)amphetamine (MDA) and its derivatives. *Chem. Biodivers.* **2009**, *6*, 2115−2135.

(65) (a) Van Goor, F.; Hadida, S.; Grootenhuis, P. D. J.; Burton, B.; Stack, J. H.; Straley, K. S.; Decker, C. J.; Miller, M.; McCartney, J.; Olson, E. R.; Wine, J. J.; Frizzell, R. A.; Ashlock, M.; Negulescu, P. A. Correction of the F508del-CFTR protein processing defect in vitro by the investigational drug VX-809. *Proc. Natl. Acad. Sci. U. S. A.* **2011**, *108*, 18843−18848. (b) Deeks, E. D. Lumacaftor/ivacaftor: a review in cystic fibrosis. *Drugs* **2016**, *76*, 1191−1201.

(66) Keith, J. M.; Jones, W. M.; Tichenor, M.; Liu, J.; Seierstad, M.; Palmer, J. A.; Webb, M.; Karbarz, M.; Scott, B. P.; Wilson, S. J.; Luo, L.; Wennerholm, M. L.; Chang, L.; Rizzolio, M.; Rynberg, R.; Chaplan, S. R.; Breitenbucher, J. G. Preclinical characterization of the FAAH inhibitor JNJ-42165279. *ACS Med. Chem. Lett.* **2015**, *6*, 1204−1208.

(67) Buissonneaud, D. Y.; van Mourik, T.; O'Hagan, D. A DFT study on the origin of the fluorine gauche effect in substituted fluoroethanes. *Tetrahedron* **2010**, *66*, 2196−2202.

(68) (a) Deniau, G.; Slawin, A. M. Z.; Lebl, T.; Chorki, F.; Issberner, J. P.; van Mourik, T.; Heygate, J. M.; Lambert, J. J.; Etherington, L. A.; Sillar, K. T.; O'Hagan, D. Synthesis, conformation and biological evaluation of the enantiomers of 3-fluoro-*γ*-aminobutyric acid ((*R*)- and (*S*)-3F-GABA): an analogue of the neurotransmitter GABA. *Chem-BioChem* **2007**, *8*, 2265−2274. (b) Yamamoto, I.; Deniau, G. P.; Gavande, N.; Chebib, M.; Johnston, G. A. R.; O'Hagan, D. Agonist responses of (*R*)- and (*S*)-3-fluoro-*γ*-aminobutyric acids suggest an enantiomeric fold for GABA binding to GABAC receptors. *Chem. Commun.* **2011**, *47*, 7956−7958. (c) Clift, M. D.; Ji, H.; Deniau, G. P.; O'Hagan, D.; Silverman, R. B. Enantiomers of 4-amino-3-fluorobutanoic acid as substrates for *γ*-aminobutyric acid aminotransferase. Conformational probes for GABA binding. *Biochemistry* **2007**, *46*, 13819−13828. (d) Crittenden, D. L.; Chebib, M.; Jordan, M. J. T. A quantitative structure-activity relationship investigation into agonist binding at GABAC receptors. *J. Mol. Struct.: THEOCHEM* **2005**, *755*, 81−89.

(69) (a) Hunter, L.; Jolliffe, K. A.; Jordan, M. J. T.; Jensen, P.; MacQuart, R. B. Synthesis and conformational analysis of *α*,*β*-difluoro-*γ*-amino acid derivatives. *Chem. - Eur. J.* **2011**, *17*, 2340−2343. (b) Yamamoto, I.; Jordan, M. J. T.; Gavande, N.; Doddareddy, M. R.; Chebib, M.; Hunter, L. The enantiomers of syn-2,3-difluoro-4-aminobutyric acid elicit opposite responses at the GABA C receptor. *Chem. Commun.* **2012**, *48*, 829−831.

(70) Chia, P. W.; Livesey, M. R.; Slawin, A. M. Z.; Van Mourik, T.; Wyllie, D. J. A.; O'Hagan, D. 3-Fluoro-N-methyl-D-aspartic acid (3F-NMDA) stereoisomers as conformational probes for exploring agonist binding at NMDA receptors. *Chem. - Eur. J.* **2012**, *18*, 8813−8819.

(71) Hu, X. G.; Thomas, D. S.; Griffith, R.; Hunter, L. Stereoselective fluorination alters the geometry of a cyclic peptide: exploration of backbone-fluorinated analogues of unguisin A. *Angew. Chem., Int. Ed.* **2014**, *53*, 6176−6179.

(72) Hodges, J. A.; Raines, R. T. Stereoelectronic effects on collagen stability: the dichotomy of 4-fluoroproline diastereomers. *J. Am. Chem. Soc.* **2003**, *125*, 9262−9263.

(73) (a) Jakobsche, C. E.; Choudhary, A.; Miller, S. J.; Raines, R. T. n→*π** Interaction and n)(*π* Pauli repulsion are antagonistic for protein stability. *J. Am. Chem. Soc.* **2010**, *132*, 6651−6653. (b) Newberry, R. W.; VanVeller, B.; Guzei, I. A.; Raines, R. T. n→*π** Interactions of amides and thioamides: implications for protein stability. *J. Am. Chem. Soc.* **2013**, *135*, 7843−7846. (c) Kamer, K. J.; Choudhary, A.; Raines, R. T. Intimate interactions with carbonyl groups: dipole-dipole or n→*π**? *J. Org. Chem.* **2013**, *78*, 2099−2103.

(74) Fukushima, H.; Hiratate, A.; Takahashi, M.; Saito, M.; Munetomo, E.; Kitano, K.; Saito, H.; Takaoka, Y.; Yamamoto, K. Synthesis and structure−activity relationships of potent 3- or 4-substituted-2-cyanopyrrolidine dipeptidyl peptidase IV inhibitors. *Bioorg. Med. Chem.* **2004**, *12*, 6053−6061.

(75) Jansen, K.; Heirbaut, L.; Verkerk, R.; Cheng, J. D.; Joossens, J.; Cos, P.; Maes, L.; Lambeir, A.-M.; De Meester, I.; Augustyns, K.; Van

der Veken, P. Extended structure–activity relationship and pharmacokinetic investigation of (4-quinolinoyl)glycyl-2-cyanopyrrolidine inhibitors of fibroblast activation protein (FAP). *J. Med. Chem.* **2014**, *57*, 3053−3074.

(76) Staas, D. D.; Savage, K. L.; Sherman, V. L.; Shimp, H. L.; Lyle, T. A.; Tran, L. O.; Wiscount, C. M.; McMasters, D. R.; Sanderson, P. E. J.; Williams, P. D.; Lucas, B. J., Jr.; Krueger, J. A.; Lewis, S. D.; White, R. B.; Yu, S.; Wong, B. K.; Kochansky, C. J.; Anari, M. R.; Yan, Y.; Vacca, J. P. Discovery of potent, selective 4-fluoroproline-based thrombin inhibitors with improved metabolic stability. *Bioorg. Med. Chem.* **2006**, *14*, 6900−6916.

(77) Chiba, J.; Takayama, G.; Takashi, T.; Yokoyama, M.; Nakayama, A.; Baldwin, J. J.; McDonald, E.; Moriarty, K. J.; Sarko, C. R.; Saionz, K. W.; Swanson, R.; Hussain, Z.; Wong, A.; MachinagA, N. Synthesis, biological evaluation, and pharmacokinetic study of prolyl-1-piperazinyl-acetic acid and prolyl-4-piperidinylacetic acid derivatives as VLA-4 antagonists. *Bioorg. Med. Chem.* **2006**, *14*, 2725−2746.

(78) (a) Wang, Y.; Callejo, R.; Slawin, A. M. Z.; O'Hagan, D. The difluoromethylene (CF₂) group in aliphatic chains: synthesis and conformational preference of palmitic acids and nonadecane containing CF₂ groups. *Beilstein J. Org. Chem.* **2014**, *10*, 18−25. (b) Tavasli, M.; O'Hagan, D.; Pearson, C.; Petty, M. C. The fluorine gauche effect. Langmuir isotherms report the relative conformational stability of (±)-*erythro*- and (±)-*threo*-9,10-difluorostearic acids. *Chem. Commun.* **2002**, 1226−1227.

(79) (a) O'Hagan, D. Organofluorine chemistry: synthesis and conformation of vicinal fluoromethylene motifs. *J. Org. Chem.* **2012**, *77*, 3689−3699. (b) Wu, D.; Tian, A.; Sun, H. Conformational properties of 1,3-difluoropropane. *J. Phys. Chem. A* **1998**, *102*, 9901−9905. (c) Hunter, L.; Kirsch, P.; Slawin, A. M. Z.; O'Hagan, D. Synthesis and structure of stereoisomeric multivicinal hexafluoroalkanes. *Angew. Chem., Int. Ed.* **2009**, *48*, 5457−5460.

(80) Scheidt, F.; Selter, P.; Santschi, N.; Holland, M. C.; Dudenko, D. V.; Daniliuc, C.; Mück-Lichtenfeld, C.; Hansen, M. R.; Gilmour, R. Emulating natural product conformation by cooperative, non-covalent fluorine interactions. *Chem. - Eur. J.* **2017**, *23*, 6142−6149.

(81) Huchet, Q. A.; Kuhn, B.; Wagner, B.; Kratochwil, N. A.; Fischer, H.; Kansy, M.; Zimmerli, D.; Carreira, E. M.; Müller, K. Fluorination patterning: a study of structural motifs that impact physicochemical properties of relevance to drug discovery. *J. Med. Chem.* **2015**, *58*, 9041−9060.

(82) Yokokawa, F.; Wang, G.; Chan, W. L.; Ang, S. H.; Wong, J.; Ma, I.; Rao, S. P. S.; Manjunatha, U.; Lakshminarayana, S. B.; Herve, M.; Kounde, C.; Tan, B. H.; Thayalan, P.; Ng, S. H.; Nanjundappa, M.; Ravindran, S.; Gee, P.; Tan, M.; Wei, L.; Goh, A.; Chen, P.-Y.; Lee, K. S.; Zhong, C.; Wagner, T.; Dix, I.; Chatterjee, A. K.; Pethe, K.; Kuhen, K.; Glynne, R.; Smith, P.; Bifani, P.; Jiricek, J. Discovery of tetrahydropyr-azolopyrimidine carboxamide derivatives as potent and orally active antitubercular agents. *ACS Med. Chem. Lett.* **2013**, *4*, 451−455.

(83) Koerts, J.; Soffers, A. E. M. F.; Vervoort, J.; De Jager, A.; Rietjens, I. M. C. M. Occurrence of the NIH shift upon the cytochrome P450-catalyzed in vivo and in vitro aromatic ring hydroxylation of fluorobenzenes. *Chem. Res. Toxicol.* **1998**, *11*, 503−512.

(84) (a) Shih, I.-h.; Vliegen, I.; Peng, B.; Yang, H.; Hebner, C.; Paeshuyse, J.; Purstinger, G.; Fenaux, M.; Tian, Y.; Mabery, E.; Qi, X.; Bahador, G.; Paulson, M.; Lehman, L. S.; Bondy, S.; Tse, W.; Reiser, H.; Lee, W. A.; Schmitz, U.; Neyts, J.; Zhong, W. Mechanistic characterization of GS-9190 (tegobuvir), a novel nonnucleoside inhibitor of hepatitis C virus NS5B polymerase. *Antimicrob. Agents Chemother.* **2011**, *55*, 4196−4203. (b) Hebner, C. M.; Han, B.; Brendza, K. M.; Nash, M.; Sulfab, M.; Tian, Y.; Hung, M.; Fung, W.; Vivian, R. W.; Trenkle, J.; Taylor, J.; Bjornson, K.; Bondy, S.; Liu, X.; Link, J.; Neyts, J.; Sakowicz, R.; Zhong, W.; Tang, H.; Schmitz, U. The HCV non-nucleoside inhibitor tegobuvir utilizes a novel mechanism of action to inhibit NS5B polymerase function. *PLoS One* **2012**, *7*, e39163. (c) Leivers, M.; Miller, J. F.; Chan, S. A.; Lauchli, R.; Liehr, S.; Mo, W.; Ton, T.; Turner, E. M.; Youngman, M.; Falls, J. G.; Long, S.; Mathis, A.; Walker, J. Imidazopyridazine hepatitis C virus polymerase inhibitors. Structure-activity relationship studies and the discovery of a novel, traceless

prodrug mechanism. *J. Med. Chem.* **2014**, *57*, 1964−1975. (d) Powers, J. P.; Piper, D. E.; Li, Y.; Mayorga, V.; Anzola, J.; Chen, J. M.; Jaen, J. C.; Lee, G.; Liu, J.; Peterson, M. G.; Tonn, G. R.; Ye, Q.; Walker, N. P. C.; Wang, Z. SAR and mode of action of novel non-nucleoside inhibitors of hepatitis C NS5b RNA polymerase. *J. Med. Chem.* **2006**, *49*, 1034−1046.

(85) Pinto, D. J. P.; Orwat, M. J.; Wang, S.; Fevig, J. M.; Quan, M. L.; Amparo, E.; Cacciola, J.; Rossi, K. A.; Alexander, R. S.; Smallwood, A. M.; Luettgen, J. M.; Liang, L.; Aungst, B. J.; Wright, M. R.; Knabb, R. M.; Wong, P. C.; Wexler, R. R.; Lam, P. Y. S. Discovery of 1-[3-(aminomethyl)phenyl]-*N*-[3-fluoro-2′-(methylsulfonyl)-[1,1′-biphen-yl]-4-yl]-3-(trifluoromethyl)-1*H*-pyrazole-5-carboxamide (DPC423), a highly potent, selective, and orally bioavailable inhibitor of blood coagulation factor Xa. *J. Med. Chem.* **2001**, *44*, 566−578.

(86) Alex, A.; Millan, D. S.; Perez, M.; Wakenhut, F.; Whitlock, G. A. Intramolecular hydrogen bonding to improve membrane permeability and absorption in beyond rule of five chemical space. *MedChemComm* **2011**, *2*, 669−674.

(87) (a) Hitchcock, S. A. Structural modifications that alter the P-glycoprotein efflux properties of compounds. *J. Med. Chem.* **2012**, *55*, 4877−4895. (b) Desai, P. V.; Raub, T. J.; Blanco, M. J. How hydrogen bonds impact P-glycoprotein transport and permeability. *Bioorg. Med. Chem. Lett.* **2012**, *22*, 6540−6548.

(88) (a) Dalvit, C.; Vulpetti, A. Intermolecular and intramolecular hydrogen bonds involving fluorine atoms: implications for recognition, selectivity, and chemical properties. *ChemMedChem* **2012**, *7*, 262−272. (b) Dalvit, C.; Invernizzi, C.; Vulpetti, A. Fluorine as a hydrogen-bond acceptor: experimental evidence and computational calculations. *Chem. - Eur. J.* **2014**, *20*, 11058−11068.

(89) Weiss, M. M.; Williamson, T.; Babu-Khan, S.; Bartberger, M. D.; Brown, J.; Chen, K.; Cheng, Y.; Citron, M.; Croghan, M. D.; Dineen, T. A.; Esmay, J.; Graceffa, R. F.; Harried, S. S.; Hickman, D.; Hitchcock, S. A.; Horne, D. B.; Huang, H.; Imbeah-Ampiah, R.; Judd, T.; Kaller, M. R.; Kreiman, C. R.; La, D. S.; Li, V.; Lopez, P.; Louie, S.; Monenschein, H.; Nguyen, T. T.; Pennington, L. D.; Rattan, C.; San Miguel, T.; Sickmier, E. A.; Wahl, R. C.; Wen, P. H.; Wood, S.; Xue, Q.; Yang, B. H.; Patel, V. F.; Zhong, W. Design and preparation of a potent series of hydroxyethylamine containing *β*-secretase inhibitors that demonstrate robust reduction of central *β*-amyloid. *J. Med. Chem.* **2012**, *55*, 9009−9024.

(90) Swahn, B.-M.; Kolmodin, K.; Karlström, S.; von Berg, S.; Söderman, P.; Holenz, J.; Berg, S.; Lindström, J.; Sundström, M.; Turek, D.; Kihlström, J.; Slivo, C.; Andersson, L.; Pyring, D.; Rotticci, D.; Öhberg, L.; Kers, A.; Bogar, K.; von Kieseritzky, F.; Bergh, M.; Olsson, L.-L.; Janson, J.; Eketjäll, S.; Georgievska, B.; Jeppsson, F.; Fälting, J. Design and synthesis of *β*-site amyloid precursor protein cleaving enzyme (BACE1) inhibitors with in vivo brain reduction of *β*-amyloid peptides. *J. Med. Chem.* **2012**, *55*, 9346−9361.

(91) Bell, I. M.; Bednar, R. A.; Fay, J. F.; Gallicchio, S. N.; Hochman, J. H.; McMasters, D. R.; Miller-Stein, C.; Moore, E. L.; Mosser, S. D.; Pudvah, N. T.; Quigley, A. G.; Salvatore, C. A.; Stump, C. A.; Theberge, C. R.; Wong, B. K.; Zartman, C. B.; Zhang, X. F.; Kane, S. A.; Graham, S. L.; Vacca, J. P.; Williams, T. M. Identification of novel, orally bioavailable spirohydantoin CGRP receptor antagonists. *Bioorg. Med. Chem. Lett.* **2006**, *16*, 6165−6169.

(92) Koshizawa, T.; Morimoto, T.; Watanabe, G.; Watanabe, T.; Yamasaki, N.; Sawada, Y.; Fukuda, T.; Okuda, A.; Shibuya, K.; Ohgiya, T. Optimization of a novel series of potent and orally bioavailable GPR119 agonists. *Bioorg. Med. Chem. Lett.* **2017**, *27*, 3249−3253.

(93) Degnan, A. P.; Chaturvedula, P. V.; Conway, C. M.; Cook, D. A.; Davis, C. D.; Denton, R.; Han, X.; Macci, R.; Mathias, N. R.; Moench, P.; Pin, S. S.; Ren, S. X.; Schartman, R.; Signor, L. J.; Thalody, G.; Widmann, K. A.; Xu, C.; Macor, J. E.; Dubowchik, G. M. Discovery of (*R*)-4-(8-fluoro-2-oxo-1,2-dihydroquinazolin-3(4*H*)-yl)-*N*-(3-(7-methyl-1*H*-in-dazol-5-yl)-1-oxo-1-(4-(piperidin-1-yl)piperidin-1-yl)propan-2-yl)-piperidine-1-carboxamide (BMS-694153): a potent antagonist of the human calcitonin gene-related peptide receptor for migraine with rapid and efficient intranasal exposure. *J. Med. Chem.* **2008**, *51*, 4858−4861.

(94) Razgulin, A. V.; Mecozzi, S. Binding properties of aromatic carbon-bound fluorine. *J. Med. Chem.* **2006**, *49*, 7902−7906.

(95) (a) Lewis, R. T.; Blackaby, W. P.; Blackburn, T.; Jennings, A. S. R.; Pike, A.; Wilson, R. A.; Hallett, D. J.; Cook, S. M.; Ferris, P.; Marshall, G. R.; Reynolds, D. S.; Sheppard, W. F. A.; Smith, A. J.; Sohal, B.; Stanley, J.; Tye, S. J.; Wafford, K. A.; Atack, J. R. A pyridazine series of α2/α3 subtype selective GABAₐ agonists for the treatment of anxiety. *J. Med. Chem.* 2006, 49, 2600−2610. (b) Humphries, A. C.; Gancia, E.; Gilligan, M. T.; Goodacre, S.; Hallett, D.; Merchant, K. J.; Thomas, S. R. 8-Fluoroimidazo[1,2-*a*]pyridine: synthesis, physicochemical properties and evaluation as a bioisosteric replacement for imidazo[1,2-*a*]pyrimidine in an allosteric modulator ligand of the GABAₐ receptor. *Bioorg. Med. Chem. Lett.* 2006, 16, 1518−1522.

(96) (a) Robarge, K. D.; Lee, W.; Eigenbrot, C.; Ultsch, M.; Wiesmann, C.; Heald, R.; Price, S.; Hewitt, J.; Jackson, P.; Savy, P.; Burton, B.; Choo, E. F.; Pang, J.; Boggs, J.; Yang, A.; Yang, X.; Baumgardner, M. Structure based design of novel 6,5 heterocbicyclic mitogen-activated protein kinase kinase (MEK) inhibitors leading to the discovery of imidazo[1,5-*a*]pyrazine G-479. *Bioorg. Med. Chem. Lett.* 2014, 24, 4714−4723.

(97) (a) Huang, X.; Cheng, C. C.; Fischmann, T. O.; Duca, J. S.; Yang, X.; Richards, M.; Shipps, G. W., Jr. Discovery of a novel series of CHK1 kinase inhibitors with a distinctive hinge binding mode. *ACS Med. Chem. Lett.* 2012, 3, 123−128. (b) Huang, X.; Cheng, C. C.; Fischmann, T. O.; Duca, J. S.; Richards, M.; Tadikonda, P. K.; Reddy, P. A.; Zhao, L.; Siddiqui, M. A.; Parry, D.; Davis, N.; Seghezzi, W.; Wiswell, D.; Shipps, G. W., Jr. Structure-based design and optimization of 2-aminothiazole-4-carboxamide as a new class of CHK1 inhibitors. *Bioorg. Med. Chem. Lett.* 2013, 23, 2590−2594.

(98) (a) Koller, A. N.; Božilović, J.; Engels, J. W.; Gohlke, H. Aromatic N versus aromatic F: bioisosterism discovered in RNA base pairing interactions leads to a novel class of universal base analogs. *Nucleic Acids Res.* 2010, 38, 3133−3146. (b) Gohlke, H.; Božilović, J.; Engels, J. W. Synthesis and properties of fluorinated nucleobases in DNA and RNA. *Mol. Medicine Med. Chem.* 2012, 6, 3−32.

(99) (a) Giroud, M.; Harder, M.; Kuhn, B.; Haap, W.; Trapp, N.; Schweizer, W. B.; Schirmeister, T.; Diederich, F. Fluorine scan of inhibitors of the cysteine protease human cathepsin L: dipolar and quadrupolar effects in the π-stacking of fluorinated phenyl rings on peptide amide bonds. *ChemMedChem* 2016, 11, 1042−1047. (b) Giroud, M.; Ivkovic, J.; Martignoni, M.; Fleuti, M.; Trapp, N.; Haap, W.; Kuglstatter, A.; Benz, J.; Kuhn, B.; Schirmeister, T.; Diederich, F. Inhibition of the cysteine protease human cathepsin L by triazine nitriles: amide···heteroarene π-stacking interactions and chalcogen bonding in the S3 pocket. *ChemMedChem* 2017, 12, 257−270.

(100) Császár, P.; Császár, A. On the dipole moments of fluorobenzenes by quantum chemical methods. *J. Mol. Struct.: THEOCHEM* 1984, 110, 405−407.

(101) van Niel, M. B.; Collins, I.; Beer, M. S.; Broughton, H. B.; Cheng, S. K. F.; Goodacre, S. C.; Heald, A.; Locker, K. L.; MacLeod, A. M.; Morrison, D.; Moyes, C. R.; O'Connor, D.; Pike, A.; Rowley, M.; Russell, M. G. N.; Sohal, B.; Stanton, J. A.; Thomas, S.; Verrier, H.; Watt, A. P.; Castro, J. L. Fluorination of 3-(3-(piperidin-1-yl)propyl)indoles and 3-(3-(piperazin-1-yl)propyl)indoles gives selective human 5-HT1ᴅ receptor ligands with improved pharmacokinetic profiles. *J. Med. Chem.* 1999, 42, 2087−2104.

(102) (a) Paulini, R.; Müller, K.; Diederich, F. Orthogonal multipolar interactions in structural chemistry and biology. *Angew. Chem., Int. Ed.* 2005, 44, 1788−1805. (b) Xing, L.; Keefer, C.; Brown, M. F. Fluorine multipolar interaction: towards elucidating its energetics in binding recognition. *J. Fluorine Chem.* 2017, 198, 47−53.

(103) (a) Shi, A.; Murai, M. J.; He, S.; Lund, G.; Hartley, T.; Purohit, T.; Reddy, G.; Chruszcz, M.; Grembecka, J.; Cierpicki, T. Structural insights into inhibition of the bivalent menin-MLL interaction by small molecules in leukemia. *Blood* 2012, 120, 4461−4469. (b) Pollock, J.; Borkin, D.; Lund, G.; Purohit, T.; Dyguda-Kazimierowicz, E.; Grembecka, J.; Cierpicki, T. Rational design of orthogonal multipolar interactions with fluorine in protein−ligand complexes. *J. Med. Chem.* 2015, 58, 7465−7474. (c) Grembecka, J.; He, S.; Shi, A.; Purohit, T.; Muntean, A. G.; Sorenson, R. J.; Showalter, H. D.; Murai, M. J.; Belcher, A. M.; Hartley, T.; Hess, J. L.; Cierpicki, T. Menin-MLL inhibitors reverse oncogenic activity of MLL fusion proteins in leukemia. *Nat.*

Chem. Biol. 2012, 8, 277−284. (d) Borkin, D.; Pollock, J.; Kempinska, K.; Purohit, T.; Li, X.; Wen, B.; Zhao, T.; Miao, H.; Shukla, S.; He, M.; Sun, D.; Cierpicki, T.; Grembecka, J. Property focused structure-based optimization of small molecule inhibitors of the protein−protein interaction between menin and mixed lineage leukemia (MLL). *J. Med. Chem.* 2016, 59, 892−913.

(104) (a) Olsen, J. A.; Banner, D. W.; Seiler, P.; Obst-Sander, U.; D'Arcy, A.; Stihle, M.; Müller, K.; Diederich, F. A fluorine scan of thrombin inhibitors to map the fluorophilicity/fluorophobicity of an enzyme active site: evidence for C-F···C═O interactions. *Angew. Chem., Int. Ed.* 2003, 42, 2507−2511. (b) Olsen, J. A.; Banner, D. W.; Seiler, P.; Wagner, B.; Tschopp, T.; Obst-Sander, U.; Kansy, M.; Müller, K.; Diederich, F. Fluorine interactions at the thrombin active site: protein backbone fragments H-Cα-C═O comprise a favorable C-F environment and interactions of C-F with electrophiles. *ChemBioChem* 2004, 5, 666−675. (c) Schweizer, E.; Hoffmann-Röder, A.; Olsen, J. A.; Seiler, P.; Obst-Sander, U.; Wagner, B.; Kansy, M.; Banner, D. W.; Diederich, F. Multipolar interactions in the D pocket of thrombin: large differences between tricyclic imide and lactam inhibitors. *Org. Biomol. Chem.* 2006, 4, 2364−2375.

(105) Bauer, M. R.; Jones, R. N.; Baud, M. G. J.; Wilcken, R.; Boeckler, F. M.; Fersht, A. R.; Joerger, A. C.; Spencer, J. Harnessing fluorine-sulfur contacts and multipolar interactions for the design of p53 mutant Y220C rescue drugs. *ACS Chem. Biol.* 2016, 11, 2265−2274.

(106) (a) Lou, Y.; Sweeney, Z. K.; Kuglstatter, A.; Davis, D.; Goldstein, D. M.; Han, X.; Hong, J.; Kocer, B.; Kondru, R. K.; Litman, R.; McIntosh, J.; Sarma, K.; Suh, J.; Taygerly, J.; Owens, T. D. Finding the perfect spot for fluorine: Improving potency up to 40-fold during a rational fluorine scan of a Bruton's tyrosine kinase (BTK) inhibitor scaffold. *Bioorg. Med. Chem. Lett.* 2015, 25, 367−371. (b) Lou, Y.; Han, X.; Kuglstatter, A.; Kondru, R. K.; Sweeney, Z. K.; Soth, M.; McIntosh, J.; Litman, R.; Suh, J.; Kocer, B.; Davis, D.; Park, J.; Frauchiger, S.; Dewdney, N.; Zecic, H.; Taygerly, J. P.; Sarma, K.; Hong, J.; Hill, R. J.; Gabriel, T.; Goldstein, D. M.; Owens, T. D. Structure-based drug design of RN486, a potent and selective Bruton's tyrosine kinase (BTK) Inhibitor, for the treatment of rheumatoid arthritis. *J. Med. Chem.* 2015, 58, 512−516. (c) Lou, Y.; Lopez, F.; Jiang, Y.; Han, X.; Brotherton, C.; Billedeau, R.; Gabriel, S.; Gleason, S.; Goldstein, D. M.; Hilgenkamp, R.; Kocer, B.; Orzechowski, L.; Tan, J.; Wovkulich, P.; Wen, B.; Fry, D.; Di Lello, P.; Chen, L.; Zhang, F.-j.; Fretland, J.; Nangia, A.; Yang, T.; Owens, T. D. Mitigation of reactive metabolite formation for a series of 3-amino-2-pyridone inhibitors of Bruton's tyrosine kinase (BTK). *Bioorg. Med. Chem. Lett.* 2017, 27, 632−635.

(107) Hao, G.-F.; Wang, F.; Li, H.; Zhu, X.-L.; Yang, W.-C.; Huang, L.-S.; Wu, J.-W.; Berry, E. A.; Yang, G.-F. Computational discovery of picomolar Qₒ site inhibitors of cytochrome bc₁ complex. *J. Am. Chem. Soc.* 2012, 134, 11168−11176.

(108) García-LLinás, X.; Bauzá, A.; Seth, S. K.; Frontera, A. Importance of R-CF₃●●●O tetrel bonding interactions in biological systems. *J. Phys. Chem. A* 2017, 121, 5371−5376.

(109) Cisneros, J. A.; Robertson, M. J.; Valhondo, M.; Jorgensen, W. L. Irregularities in enzyme assays: the case of macrophage migration inhibitory factor. *Bioorg. Med. Chem. Lett.* 2016, 26, 2764−2767.

(110) (a) Wang, F.; Travins, J.; DeLaBarre, B.; Penard-Lacronique, V.; Schalm, S.; Hansen, E.; Straley, K.; Kernytsky, A.; Liu, W.; Gliser, C.; Yang, H.; Gross, S.; Artin, E.; Saada, V.; Mylonas, E.; Quivoron, C.; Popovici-Muller, J.; Saunders, J. O.; Salituro, F. G.; Yan, S.; Murray, S.; Wei, W.; Gao, Y.; Dang, L.; Dorsch, M.; Agresta, S.; Schenkein, D. P.; Biller, S. A.; Su, S. M.; de Botton, S.; Yen, K. E. Targeted inhibition of mutant IDH2 in leukemia cells induces cellular differentiation. *Science* 2013, 340, 622−626. (b) Yen, K.; Travins, J.; Wang, F.; David, M. D.; Artin, E.; Straley, K.; Padyana, A.; Gross, S.; DeLaBarre, B.; Tobin, E.; Chen, Y.; Nagaraja, R.; Choe, S.; Jin, L.; Konteatis, Z.; Cianchetta; Saunders, J. O.; Salituro, F. G.; Quivoron, C.; Opolon, P.; Bawa, O.; Saada, O.; Paci, A.; Broutin, S.; Bernard, O. A.; de Botton, S.; Marteyn, B. S.; Pilichowska, M.; Xu, Y. X.; Fang, C.; Jiang, F.; Wei, W.; Jin, S.; Silverman, L.; Liu, W.; Yang, H.; Dang, L.; Dorsch, M.; Penard-Lacronique, V.; Biller, S. A.; Su, S.-S. M. AG-221, A first-in-class therapy

targeting acute myeloid leukemia harboring oncogenic IDH2 mutations. *Cancer Discovery* **2017**, 7, 478−493.

(111) Bhatia, C.; Yue, W. W.; Niesen, F.; Pilka, E.; Ugochukwu, E.; Savitsky, P.; Hozjan, V.; Roos, A. K.; Filippakopoulos, P.; Von Delft, F.; Heightman, T.; Arrowsmith, C.; Weigelt, J.; Edwards, A.; Bountra, C.; Opperman, U. 2WM3: Crystal structure of NmrA-like family domain containing protein 1 in complex with niflumic acid. *Protein Data Bank*, **2009**, DOI: 10.2210/pdb2wm3/pdb.

(112) Blobaum, A. L.; Uddin, Md. J.; Felts, A. S.; Crews, B. C.; Rouzer, C. A.; Marnett, L. J. The 2′-trifluoromethyl analogue of indomethacin is a potent and selective COX-2 inhibitor. *ACS Med. Chem. Lett.* **2013**, 4, 486−490.

(113) Sun, L.-Q.; Mull, E.; Zheng, B.; D'Andrea, S.; Zhao, Q.; Wang, A. X.; Sin, N.; Venables, B. L.; Sit, S.-Y.; Chen, Y.; Chen, J.; Cocuzza, A.; Bilder, D. M.; Mathur, A.; Rampulla, R.; Chen, B.-C.; Palani, T.; Ganesan, S.; Arunachalam, P. N.; Falk, P.; Levine, A.; Chen, C.; Friborg, J.; Yu, F.; Hernandez, D.; Sheaffer, A. K.; Knipe, J. O.; Han, Y.-H.; Schartman, R.; Donoso, M.; Mosure, K.; Sinz, M. W.; Zvyaga, T.; Rajamani, R.; Kish, K.; Tredup, J.; Klei, H. E.; Gao, Q.; Ng, A.; Mueller, L.; Grasela, D. M.; Adams, S.; Loy, J.; Levesque, P. C.; Sun, H.; Shi, H.; Sun, L.; Warner, W.; Li, D.; Zhu, J.; Wang, Y.-K.; Fang, H.; Cockett, M. I.; Meanwell, N. A.; McPhee, F.; Scola, P. M. Discovery of a potent acyclic, tripeptidic, acyl sulfonamide inhibitor of hepatitis C virus NS3 protease as a back-up to asunaprevir with the potential for once-daily dosing. *J. Med. Chem.* **2016**, 59, 8042−8060.

(114) (a) Phillips, M. A.; Gujjar, R.; Malmquist, N. A.; White, J.; El Mazouni, F.; Baldwin, J.; Rathod, P. K. Triazolopyrimidine-based dihydroorotate dehydrogenase inhibitors with potent and selective activity against the malaria parasite, Plasmodium falciparum. *J. Med. Chem.* **2008**, 51, 3649−3653. (b) Gujjar, R.; Marwaha, A.; El Mazouni, F.; White, J.; White, K. L.; Creason, S.; Shackleford, D. M.; Baldwin, J.; Charman, W. N.; Buckner, F. S.; Charman, S.; Rathod, P. K.; Phillips, M. A. Identification of a metabolically stable triazolopyrimidine-based dihydroorotate dehydrogenase inhibitor with antimalarial activity in mice. *J. Med. Chem.* **2009**, 52, 1864−1872. (c) Deng, X.; Gujjar, R.; El Mazouni, F.; Kaminsky, W.; Malmquist, N. A.; Goldsmith, E. J.; Rathod, P. K.; Phillips, M. A. Structural plasticity of malaria dihydroorotate dehydrogenase allows selective binding of diverse chemical scaffolds. *J. Biol. Chem.* **2009**, 284, 26999−27009. (d) Coteron, J. M.; Marco, M.; Esquivias, J.; Deng, X.; White, K. L.; White, J.; Koltun, M.; El Mazouni, F.; Kokkonda, S.; Katneni, K.; Bhamidipati, R.; Shackleford, D. M.; Angulo-Barturen, I.; Ferrer, S. B.; Jiménez-Díaz, M. B.; Gamo, F.-J.; Goldsmith, E. J.; Charman, W. N.; Bathurst, I.; Floyd, D.; Matthews, D.; Burrows, J. N.; Rathod, P. K.; Charman, S. A.; Phillips, M. A. Structure-guided lead optimization of triazolopyrimidine-ring substituents identifies potent *Plasmodium falciparum* dihydroorotate dehydrogenase inhibitors with clinical candidate potential. *J. Med. Chem.* **2011**, 54, 5540−5561. (e) Deng, X.; Kokkonda, S.; El Mazouni, F.; White, J.; Burrows, J. N.; Kaminsky, W.; Charman, S. A.; Matthews, D.; Rathod, P. K.; Phillips, M. A. Fluorine modulates species selectivity in the triazolopyrimidine class of Plasmodium falciparum dihydroorotate dehydrogenase inhibitors. *J. Med. Chem.* **2014**, 57, 5381−5394. (f) Phillips, M. A.; Lotharius, J.; Marsh, K.; White, J.; Dayan, A.; White, K. L.; Njoroge, J. W.; El Mazouni, F.; Lao, Y.; Kokkonda, S.; Tomchick, D. R.; Deng, X.; Laird, T.; Bhatia, S. N.; March, S.; Ng, C. L.; Fidock, D. A.; Wittlin, S.; Lafuente-Monasterio, M.; Benito, F. J.; Alonso, L. M.; Martinez, M. S.; Jimenez-Diaz, M. B.; Bazaga, S. F.; Angulo-Barturen, I.; Haselden, J. N.; Louttit, J.; Cui, Y.; Sridhar, A.; Zeeman, A. M.; Kocken, C.; Sauerwein, R.; Dechering, K.; Avery, V. M.; Duffy, S.; Delves, M.; Sinden, R.; Ruecker, A.; Wickham, K. S.; Rochford, R.; Gahagen, J.; Iyer, L.; Riccio, E.; Mirsalis, J.; Bathhurst, I.; Rueckle, T.; Ding, X.; Campo, B.; Leroy, D.; Rogers, M. J.; Rathod, P. K.; Burrows, J. N.; Charman, S. A. A long-duration dihydroorotate dehydrogenase inhibitor (DSM265) for prevention and treatment of malaria. *Sci. Transl. Med.* **2015**, 7 (296), 296ra111. (g) Phillips, M. A.; White, K. L.; Kokkonda, S.; Deng, X.; White, J.; El Mazouni, F.; Marsh, K.; Tomchick, D. R.; Manjalanagara, K.; Rudra, K. R.; Wirjanata, G.; Noviyanti, R.; Price, R. N.; Marfurt, J.; Shackleford, D. M.; Chiu, F. C. K. M.; Campbell, M.; Jimenez-Diaz, M. B.; Ferrer Bazaga, S.; Angulo-Barturen, I.; Santos

Martinez, M.; Lafuente-Monasterio, M.; Kaminsky, W.; Silue, K.; Zeeman, A.-M.; Kocken, C.; Leroy, D.; Blasco, B.; Rossignol, E.; Rueckle, T.; Matthews, D.; Burrows, J. N.; Waterson, D.; Palmer, M. J.; Rathod, P. K.; Charman, S. A. A triazolopyrimidine-based dihydroorotate dehydrogenase inhibitor with improved drug-like properties for treatment and prevention of malaria. *ACS Infect. Dis.* **2016**, 2, 945−957.

(115) Martin, M. P.; Zhu, J.-Y.; Lawrence, H. R.; Pireddu, R.; Luo, Y.; Alam, R.; Ozcan, S.; Sebti, S. M.; Lawrence, N. J.; Schönbrunn, E. A novel mechanism by which small molecule inhibitors induce the DFG flip in Aurora A. *ACS Chem. Biol.* **2012**, 7, 698−706.

(116) (a) Clark, J.; Perrin, D. D. Prediction of the strengths of organic bases. *Q. Rev., Chem. Soc.* **1964**, 18, 295−320. (b) Morgenthaler, M.; Schweizer, E.; Hoffmann-Röder, A.; Benini, F.; Martin, R. E.; Jaeschke, G.; Wagner, B.; Fischer, H.; Bendels, S.; Zimmerli, D.; Schneider, J.; Diederich, F.; Kansy, M.; Müller, K. Predicting and tuning physicochemical properties in lead optimization: amine basicities. *ChemMedChem* **2007**, 2, 1100−1115.

(117) Grunewald, G. L.; Seim, M. R.; Lu, J.; Makboul, M.; Criscione, K. R. Application of the Goldilocks effect to the design of potent and selective inhibitors of phenylethanolamine N-methyltransferase: balancing pK_a and steric effects in the optimization of 3-methyl-1,2,3,4-tetrahydroisoquinoline Inhibitors by β-fluorination. *J. Med. Chem.* **2006**, 49, 2939−2952.

(118) Spahn, V.; Del Vecchio, G.; Labuz, D.; Rodriguez-Gaztelumendi, A.; Massaly, N.; Temp, J.; Durmaz, V.; Sabri, P.; Reidelbach, M.; Machelska, H.; Weber, M.; Stein, C. A nontoxic pain killer designed by modeling of pathological receptor conformations. *Science* **2017**, 355, 966−969.

(119) (a) Cox, C. D.; Coleman, P. J.; Breslin, M. J.; Whitman, D. B.; Garbaccio, R. M.; Fraley, M. E.; Buser, C. A.; Walsh, E. S.; Hamilton, K.; Schaber, M. D.; Lobell, R. B.; Tao, W.; Davide, J. P.; Diehl, R. E.; Abrams, M. T.; South, V. J.; Huber, H. E.; Torrent, M.; Prueksaritanont, T.; Li, C.; Slaughter, D. E.; Mahan, E.; Fernandez-Metzler, C.; Yan, Y.; Kuo, L. C.; Kohl, N. E.; Hartman, G. D. Kinesin spindle protein (KSP) inhibitors. 9. Discovery of (2S)-4-(2,5-difluorophenyl)-N-[(3R,4S)-3-fluoro-1-methylpiperidin-4-yl]-2-(hydroxymethyl)-N-methyl-2-phenyl-2,5-dihydro-1H-pyrrole-1-carboxamide (MK-0731) for the treatment of taxane-refractory cancer. *J. Med. Chem.* **2008**, 51, 4239−4252. (b) Cox, C. D.; Breslin, M. J.; Whitman, D. B.; Coleman, P. J.; Garbaccio, R. M.; Fraley, M. E.; Zrada, M. M.; Buser, C. A.; Walsh, E. S.; Hamilton, K.; Lobell, R. B.; Tao, W.; Abrams, M. T.; South, V. J.; Huber, H. E.; Kohl, N. E.; Hartman, G. D. Kinesin spindle protein (KSP) inhibitors. Part V: discovery of 2-propylamino-2,4-diaryl-2,5-dihydropyrroles as potent, water-soluble KSP inhibitors, and modulation of their basicity by β-fluorination to overcome cellular efflux by P-glycoprotein. *Bioorg. Med. Chem. Lett.* **2007**, 17, 2697−2702.

(120) McDonald, I. M.; Mate, R. A.; Zusi, F. C.; Huang, H.; Post-Munson, D. J.; Ferrante, M. A.; Gallagher, L.; Bertekap, R. L., Jr.; Knox, R. J.; Robertson, B. J.; Harden, D. G.; Morgan, D. G.; Lodge, N. J.; Dworetzky, S. I.; Olson, R. E.; Macor, J. E. Discovery of a novel series of quinolone α7 nicotinic acetylcholine receptor agonists. *Bioorg. Med. Chem. Lett.* **2013**, 23, 1684−1688.

(121) Sun, H.; Xia, M.; Shahane, S. A.; Jadhav, A.; Austin, C. P.; Huang, R. Are hERG channel blockers also phospholipidosis inducers? *Bioorg. Med. Chem. Lett.* **2013**, 23, 4587−4590.

(122) Nakajima, Y.; Inoue, T.; Nakai, K.; Mukoyoshi, K.; Hamaguchi, H.; Hatanaka, K.; Sasaki, H.; Tanaka, A.; Takahashi, F.; Kunikawa, S.; Usuda, H.; Moritomo, A.; Higashi, Y.; Inami, M.; Shirakami, S. Synthesis and evaluation of novel 1H-pyrrolo[2,3-b]pyridine-5-carboxamide derivatives as potent and orally efficacious immunomodulators targeting JAK3. *Bioorg. Med. Chem.* **2015**, 23, 4871−4883.

(123) Rombouts, F. J. R.; Tresadern, G.; Delgado, O.; Martínez-Lamenca, C.; Van Gool, M.; García-Molina, A.; Alonso de Diego, S. A.; Oehlrich, D.; Prokopcova, H.; Alonso, J. M.; Austin, N.; Borghys, H.; Van Brandt, S.; Surkyn, M.; De Cleyn, M.; Vos, A.; Alexander, R.; Macdonald, G.; Moechars, D.; Gijsen, H.; Trabanco, A. A. 1,4-Oxazine β-secretase 1 (BACE1) inhibitors: from hit generation to orally bioavailable brain penetrant leads. *J. Med. Chem.* **2015**, 58, 8216−8235.

(124) Scattolin, T.; Deckers, K.; Schoenebeck, F. Efficient synthesis of trifluoromethyl amines through a formal umpolung strategy from the bench-stable precursor (Me₄N)SCF₃. *Angew. Chem., Int. Ed.* **2017**, *56*, 221−224.

(125) Asahina, Y.; Araya, I.; Iwase, K.; Iinuma, F.; Hosaka, M.; Ishizaki, T. Synthesis and antibacterial activity of the 4-quinolone-3-carboxylic acid derivatives having a trifluoromethyl group as a novel *N*-1 substituent. *J. Med. Chem.* **2005**, *48*, 3443−3446.

(126) Schow, S. R.; Mackman, R. L.; Blum, C. L.; Brooks, E.; Horsma, A. G.; Joly, A.; Kerwar, S. S.; Lee, G.; Shiffman, D.; Nelson, M. G.; Wang, X.; Wick, M. M.; Zhang, X.; Lum, R. T. Synthesis and activity of 2,6,9-trisubstituted purines. *Bioorg. Med. Chem. Lett.* **1997**, *7*, 2697−2702.

(127) Miao, Z.; Zhu, L.; Dong, G.; Zhuang, C.; Wu, Y.; Wang, S.; Guo, Z.; Liu, Y.; Wu, S.; Zhu, S.; Fang, K.; Yao, J.; Li, J.; Sheng, C.; Zhang, W. A new strategy to improve the metabolic stability of lactone: discovery of (20*S*,21*S*)-21-fluorocamptothecins as novel, hydrolytically stable topoisomerase I inhibitors. *J. Med. Chem.* **2013**, *56*, 7902−7910.

(128) Wipf, P.; Henninger, T. C.; Geib, S. J. Methyl- and (trifluoromethyl)alkene peptide isosteres: synthesis and evaluation of their potential as β-turn promoters and peptide mimetics. *J. Org. Chem.* **1998**, *63*, 6088−6089.

(129) (a) Urban, J. J.; Tillman, B. G.; Cronin, W. A. Fluoroolefins as peptide mimetics: a computational study of structure, charge distribution, hydration, and hydrogen bonding. *J. Phys. Chem. A* **2006**, *110*, 11120−11129. (b) Drouin, M.; Paquin, J.-F. Recent progress in the racemic and enantioselective synthesis of monofluoroalkene-based dipeptide isosteres. *Beilstein J. Org. Chem.* **2017**, *13*, 2637−2658. (c) Drouin, M.; Hamel, J.-F.; Paquin, J.-F. Synthesis of monofluoroalkenes: a leap forward. *Synthesis* **2018**.

(130) Couve-Bonnaire, S.; Cahard, D.; Pannecoucke, X. Chiral dipeptide mimics possessing a fluoroolefin moiety: a relevant tool for conformational and medicinal studies. *Org. Biomol. Chem.* **2007**, *5*, 1151−1157.

(131) Nadon, J.-F.; Rochon, K.; Grastilleur, S.; Langlois, G.; Dao, T. T. H.; Blais, V.; Guérin, B.; Gendron, L.; Dory, Y. L. Synthesis of Gly-ψ[(*Z*)CF═CH]-Phe, a fluoroalkene dipeptide isostere, and its incorporation into a Leu-enkephalin peptidomimetic. *ACS Chem. Neurosci.* **2017**, *8*, 40−49.

(132) Karad, S. N.; Pal, M.; Crowley, R. S.; Prisinzano, T. E.; Altman, R. A. Synthesis and opioid activity of Tyr¹-Ψ(*Z*)CF═CH]-Gly² and Tyr¹-Ψ(*S*)/(*R*)CF₃CH-NH]-Gly² Leu enkephalin fluorinated peptidomimetics. *ChemMedChem* **2017**, *12*, 571−576.

(133) Rogers, M. T. The electric moments of some unsaturated aldehydes, ethers and halogen compounds. *J. Am. Chem. Soc.* **1947**, *69*, 1243−1246.

(134) (a) Kobayakawa, T.; Narumi, T.; Tamamura, H. Remote stereoinduction in the organocuprate-mediated allylic alkylation of allylic gem-dichlorides: highly diastereoselective synthesis of (*Z*)-chloroalkene dipeptide isosteres. *Org. Lett.* **2015**, *17*, 2302−2305. (b) Waelchli, R.; Gamse, R.; Bauer, W.; Lier, E.; Feyen, J. H. M. Dipeptide mimetics can substitute for the receptor activation domain resulting in highly potent analogues of hPTH(1−36) fragment. *Bioorg. Med. Chem. Lett.* **1996**, *6*, 1151−1156. (c) Kobayakawa, T.; Matsuzaki, Y.; Hozumi, K.; Nomura, W.; Nomizu, M.; Tamamura, H. Synthesis of a Chloroalkene dipeptide isostere-containing peptidomimetic and its biological application. *ACS Med. Chem. Lett.* **2018**, *9*, 6−10.

(135) Edmondson, S. D.; Wei, L.; Xu, J.; Shang, J.; Xu, S.; Pang, J.; Chaudhary, A.; Dean, D. C.; He, H.; Leiting, B.; Lyons, K. A.; Patel, R. A.; Patel, S. B.; Scapin, G.; Wu, J. K.; Beconi, M. G.; Thornberry, N. A.; Weber, A. E. Fluoroolefins as amide bond mimics in dipeptidyl peptidase IV inhibitors. *Bioorg. Med. Chem. Lett.* **2008**, *18*, 2409−2413.

(136) (a) Chang, W.; Mosley, R. T.; Bansal, S.; Keilman, M.; Lam, A. M.; Furman, P. A.; Otto, M. J.; Sofia, M. J. Inhibition of hepatitis C virus NS5A by fluoro-olefin based γ-turn mimetics. *Bioorg. Med. Chem. Lett.* **2012**, *22*, 2938−2942. (b) Belema, M.; Lopez, O. D.; Bender, J. A.; Romine, J. L.; St. Laurent, D. R.; Langley, D. R.; Lemm, J. A.; O'Boyle, D. R., II; Sun, J.-H.; Wang, C.; Fridell, R. A.; Meanwell, N. A. The discovery and development of hepatitis C virus NS5A replication complex inhibitors. *J. Med. Chem.* **2014**, *57*, 1643−1672.

(137) Hollenstein, M.; Leumann, C. J. Fluorinated olefinic peptide nucleic acid: synthesis and pairing properties with complementary DNA. *J. Org. Chem.* **2005**, *70*, 3205−3217.

(138) (a) Parlow, J. J.; Case, B. L.; Dice, T. A.; Fenton, R. L.; Hayes, M. J.; Jones, D. E.; Neumann, W. L.; Wood, R. S.; Lachance, R. M.; Girard, T. J.; Nicholson, N. S.; Clare, M.; Stegeman, R. A.; Stevens, A. M.; Stallings, W. C.; Kurumbail, R. G.; South, M. S. Design, parallel synthesis, and crystal structures of pyrazinone antithrombotics as selective inhibitors of the tissue factor VIIa complex. *J. Med. Chem.* **2003**, *46*, 4050−4062. (b) Parlow, J. J.; Stevens, A. M.; Stegeman, R. A.; Stallings, W. C.; Kurumbail, R. G.; South, M. S. Synthesis and crystal structures of substituted benzenes and benzoquinones as tissue factor VIIa inhibitors. *J. Med. Chem.* **2003**, *46*, 4297−4312. (c) Parlow, J. J.; Kurumbail, R. G.; Stegeman, R. A.; Stevens, A. M.; Stallings, W. C.; South, M. S. Synthesis and X-ray crystal structures of substituted fluorobenzene and benzoquinone inhibitors of the tissue factor VIIa complex. *Bioorg. Med. Chem. Lett.* **2003**, *13*, 3721−3725. (d) Parlow, J. J.; Kurumbail, R. G.; Stegeman, R. A.; Stevens, A. M.; Stallings, W. C.; South, M. S. Design, synthesis, and crystal structure of selective 2-pyridone tissue factor VIIa inhibitors. *J. Med. Chem.* **2003**, *46*, 4696−4701.

(139) (a) Lee, L.; Kreutter, K. D.; Pan, W.; Crysler, C.; Spurlino, J.; Player, M. R.; Tomczuk, B.; Lu, T. 2-(2-Chloro-6-fluorophenyl)-acetamides as potent thrombin inhibitors. *Bioorg. Med. Chem. Lett.* **2007**, *17*, 6266−6269. (b) Kreutter, K. D.; Lu, T.; Lee, L.; Giardino, E. C.; Patel, S.; Huang, H.; Xu, G.; Fitzgerald, M.; Haertlein, B. J.; Mohan, V.; Crysler, C.; Eisennagel, S.; Dasgupta, M.; McMillan, M.; Spurlino, J. C.; Huebert, N. D.; Maryanoff, B. E.; Tomczuk, B. E.; Damiano, B. P.; Player, M. R. Orally efficacious thrombin inhibitors with cyanofluorophenylacetamide as the P2 motif. *Bioorg. Med. Chem. Lett.* **2008**, *18*, 2865−2870. (c) Nantermet, P. G.; Burgey, C. S.; Robinson, K. A.; Pellicore, J. M.; Newton, C. L.; Deng, J. M.; Selnick, H. G.; Lewis, S. D.; Lucas, B. J.; Krueger, J. A.; Miller-Stein, C.; White, R. B.; Wong, B.; McMasters, D. R.; Wallace, A. A.; Lynch, J. J., Jr.; Yan, Y.; Chen, Z.; Kuo, L.; Gardell, S. J.; Shafer, J. A.; Vacca, J. P.; Lyle, T. A. P2 pyridine N-oxide thrombin inhibitors: a novel peptidomimetic scaffold. *Bioorg. Med. Chem. Lett.* **2005**, *15*, 2771−2775. (d) Burgey, C. S.; Robinson, K. A.; Lyle, T. A.; Sanderson, P. E. J.; Lewis, S. D.; Lucas, B. J.; Krueger, J. A.; Singh, R.; Miller-Stein, C.; White, R. B.; Wong, B.; Lyle, E. A.; Williams, P. D.; Coburn, C. A.; Dorsey, B. D.; Barrow, J. C.; Stranieri, M. T.; Holahan, M. A.; Sitko, G. R.; Cook, J. J.; McMasters, D. R.; McDonough, C. M.; Sanders, W. M.; Wallace, A. A.; Clayton, F. C.; Bohn, D.; Leonard, Y. M.; Detwiler, T. J., Jr.; Lynch, J. J., Jr.; Yan, Y.; Chen, Z.; Kuo, L.; Gardell, S. J.; Shafer, J. A.; Vacca, J. P. Metabolism-directed optimization of 3-aminopyrazinone acetamide thrombin inhibitors. Development of an orally bioavailable series containing P1 and P3 pyridines. *J. Med. Chem.* **2003**, *46*, 461−473.

(140) (a) Laurence, C.; Brameld, K. A.; Graton, J.; Le Questel, J.-Y.; Renault, E. The pKBHX database: toward a better understanding of hydrogen-bond basicity for medicinal chemists. *J. Med. Chem.* **2009**, *52*, 4073−4086. (b) Kenny, P. W.; Montanari, C. A.; Prokopczyk, I. M.; Ribeiro, J. F.; Sartori, G. R. Hydrogen bond basicity prediction for medicinal chemistry design. *J. Med. Chem.* **2016**, *59*, 4278−4288. (c) Pierce, A. C.; Sandretto, K. L.; Bemis, G. W. Kinase inhibitors and the case for CH···O hydrogen bonds in protein-ligand binding. *Proteins: Struct., Funct., Genet.* **2002**, *49*, 567−576.

(141) Anilkumar, G. N.; Lesburg, C. A.; Selyutin, O.; Rosenblum, S. B.; Zeng, Q.; Jiang, Y.; Chan, T.-Y.; Pu, H.; Vaccaro, H.; Wang, L.; Bennett, F.; Chen, K. X.; Duca, J.; Gavalas, S.; Huang, Y.; Pinto, P.; Sannigrahi, M.; Velazquez, F.; Venkatraman, S.; Vibulbhan, B.; Agrawal, S.; Butkiewicz, N.; Feld, B.; Ferrari, E.; He, Z.; Jiang, C.-k.; Palermo, R. E.; Mcmonagle, P.; Huang, H.-C.; Shih, N.-Y.; Njoroge, G.; Kozlowski, J. A. I. Novel HCV NS5B polymerase inhibitors: discovery of indole 2-carboxylic acids with C3-heterocycles. *Bioorg. Med. Chem. Lett.* **2011**, *21*, 5336−5341.

(142) Adams, M. E.; Wallace, M. B.; Kanouni, T.; Scorah, N.; O'Connell, S. M.; Miyake, H.; Shi, L.; Halkowycz, P.; Zhang, L.; Dong, Q. Design and synthesis of orally available MEK inhibitors with potent

in vivo antitumor efficacy. *Bioorg. Med. Chem. Lett.* **2012**, *22*, 2411−2414.

(143) (a) Isshiki, Y.; Kohchi, Y.; Iikura, H.; Matsubara, Y.; Asoh, K.; Murata, T.; Kohchi, M.; Mizuguchi, E.; Tsujii, S.; Hattori, K.; Miura, T.; Yoshimura, Y.; Aida, S.; Miwa, M.; Saitoh, R.; Murao, N.; Okabe, H.; Belunis, C.; Janson, C.; Lukacs, C.; Schück, V.; Shimma, N. Design and synthesis of novel allosteric MEK inhibitor CH4987655 as an orally available anticancer agent. *Bioorg. Med. Chem. Lett.* **2011**, *21*, 1795−1801. (b) Leijen, S.; Middleton, M. R.; Tresca, P.; Kraeber-Bodéré, F.; Dieras, V.; Scheulen, M. E.; Gupta, A.; Lopez-Valverde, V.; Xu, Z. X.; Rueger, R.; Tessier, J. J.; Shochat, E.; Blotner, S.; Naegelen, V. M.; Schellens, J. H.; Eberhardt, W. E. Phase I dose-escalation study of the safety, pharmacokinetics, and pharmacodynamics of the MEK inhibitor RO4987655 (CH4987655) in patients with advanced solid tumors. *Clin. Cancer Res.* **2012**, *18*, 4794−4805.

(144) Ohren, J. F.; Chen, H.; Pavlovsky, A.; Whitehead, C.; Zhang, E.; Kuffa, P.; Yan, C.; McConnell, P.; Spessard, C.; Banotai, C.; Mueller, W. T.; Delaney, A.; Omer, C.; Sebolt-Leopold, J.; Dudley, D. T.; Leung, I. K.; Flamme, C.; Warmus, J.; Kaufman, M.; Barrett, S.; Tecle, H.; Hasemann, C. A. Structures of human MAP kinase kinase 1 (MEK1) and MEK2 describe novel noncompetitive kinase inhibition. *Nat. Struct. Mol. Biol.* **2004**, *11*, 1192−1197.

(145) Kong, J. W.; Hamann, L. G.; Ruppar, D. A.; Edwards, J. P.; Marschke, K. B.; Jones, T. K. Effects of isosteric pyridone replacements in androgen receptor antagonists based on 1,2-dihydro- and 1,2,3,4-tetrahydro-2,2-dimethyl-6-trifluoromethyl-8-pyridono[5,6-g]-quinolones. *Bioorg. Med. Chem. Lett.* **2000**, *10*, 411−414.

(146) Qiu, J.; Stevenson, S. H.; O'Beirne, M. J.; Silverman, R. B. 2,6-Difluorophenol as a bioisostere of a carboxylic acid: bioisosteric analogues of γ-aminobutyric acid. *J. Med. Chem.* **1999**, *42*, 329−332.

(147) (a) Nicolaou, I.; Zika, C.; Demopoulos, V. J. [1-(3,5-Difluoro-4-hydroxyphenyl)-1*H*-pyrrol-3-yl]phenylmethanone as a bioisostere of a carboxylic acid aldose reductase inhibitor. *J. Med. Chem.* **2004**, *47*, 2706−2709. (b) Alexiou, P.; Demopoulos, V. J. A diverse series of substituted benzenesulfonamides as aldose reductase inhibitors with antioxidant activity: design, synthesis, and in vitro activity. *J. Med. Chem.* **2010**, *53*, 7756−7766. (c) Kotsampasakou, E.; Demopoulos, V. J. Synthesis of derivatives of the keto-pyrrolyl-difluorophenol scaffold: some structural aspects for aldose reductase inhibitory activity and selectivity. *Bioorg. Med. Chem.* **2013**, *21*, 869−873.

(148) (a) Burkhart, J. P.; Weintraub, P. M.; Gates, C. A.; Resvick, R. J.; Vaz, R. J.; Friedrich, D.; Angelastro, M. R.; Bey, P.; Peet, N. P. Novel steroidal vinyl fluorides as inhibitors of steroid C$_{17(20)}$ lyase. *Bioorg. Med. Chem.* **2002**, *10*, 929−934. (b) Corina, D. L.; Miller, S. L.; Wright, J. N.; Akhtar, M. The mechanism of cytochrome P-450 dependent C-C bond cleavage: studies on 17α-hydroxylase-I7,20-lyase. *J. Chem. Soc., Chem. Commun.* **1991**, 782−783.

(149) Li, X.; Singh, S. M.; Luu-The, V.; Côté, J.; Laplante, S.; Labrie, F. Vinyl fluoride as a mimic of the 'intermediate' enol form in the 5α-reductase transformation: synthesis and in vitro activity of (*N*-1′, 1′-dimethylethyl)-3-haloandrost-3,5-diene-17β-carboxamides. *Bioorg. Med. Chem.* **1996**, *4*, 55−60.

(150) Pirrung, M. C.; Ha, H.-J.; Holmes, C. P. Purification and inhibition of spinach αβ,-dihydroxyacid dehydratase. *J. Org. Chem.* **1989**, *54*, 1543−1548. (b) Pirrung, M. C.; Holmes, C. P.; Horowitz, D. M.; Nunn, D. S. Mechanism and stereochemistry of a α,β,-dihydroxyacid dehydratase. *J. Am. Chem. Soc.* **1991**, *113*, 1020−1025.

(151) Dixon, D. A.; Fukunaga, T.; Smart, B. E. Geometries and energies of the fluoroethylenes. *J. Am. Chem. Soc.* **1986**, *108*, 1585−1588.

(152) Leriche, C.; He, X.; Chang, C.-w. T.; Liu, H.-w. Reversal of the apparent regiospecificity of NAD(P)H-dependent hydride transfer: the properties of the difluoromethylene group, a carbonyl mimic. *J. Am. Chem. Soc.* **2003**, *125*, 6348−6349.

(153) Bickelhaupt, F. M.; Hermann, H. L.; Boche, G. α-Stabilization of carbanions: fluorine is more effective than the heavier halogens. *Angew. Chem., Int. Ed.* **2006**, *45*, 823−826.

(154) (a) Bégué, J.-P.; Bonnet-Delpon, D. Fluoroartemisinins: metabolically more stable antimalarial artemisinin derivatives. *Chem-*

MedChem **2007**, *2*, 608−624. (b) Magueur, G.; Crousse, B.; Ourévitch, M.; Bonnet-Delpon, D.; Bégué, J.-P. Fluoro-artemisinins: when a gem-difluoroethylene replaces a carbonyl group. *J. Fluorine Chem.* **2006**, *127*, 637−642.

(155) (a) Tu, Y. Artemisinin- a gift from traditional Chinese medicine to the world (Nobel lecture). *Angew. Chem., Int. Ed.* **2016**, *55*, 10210−10226. (b) Ashley, E. A.; Dhorda, M.; Fairhurst, R. M.; Amaratunga, C.; Lim, P.; Suon, S.; Sreng, S.; Anderson, J. M.; Mao, S.; Sam, B.; Sopha, C.; Chuor, C. M.; Nguon, C.; Sovannaroth, S.; Pukrittayakamee, S.; Jittamala, P.; Chotivanich, K.; Chutasmit, K.; Suchatsoonthorn, C.; Runcharoen, R.; Hien, T. T.; Thuy-Nhien, N. T.; Thanh, N. V.; Phu, N. H.; Htut, Y.; Han, K.-T.; Aye, K. H.; Mokuolu, O. A.; Olaosebikan, R. R.; Folaranmi, O. O.; Mayxay, M.; Khanthavong, M.; Hongvanthong, B.; Newton, P. N.; Onyamboko, M. A.; Fanello, C. I.; Tshefu, A. K.; Mishra, N.; Valecha, N.; Phyo, A. P.; Nosten, F.; Yi, P.; Tripura, R.; Borrmann, S.; Bashraheil, M.; Peshu, J.; Faiz, M. A.; Ghose, A.; Hossain, M. A.; Samad, R.; Rahman, M. R.; Hasan, M. M.; Islam, A.; Miotto, O.; Amato, R.; MacInnis, B.; Stalker, J.; Kwiatkowski, D. P.; Bozdech, Z.; Jeeyapant, A.; Cheah, P. Y.; Sakulthaew, T.; Chalk, J.; Intharabut, B.; Silamut, K.; Lee, S. J.; Vihokhern, B.; Kunasol, C.; Imwong, M.; Tarning, J.; Taylor, W. J.; Yeung, S.; Woodrow, C. J.; Flegg, J. A.; Das, D.; Smith, J.; Venkatesan, M.; Plowe, C. V.; Stepniewska, K.; Guerin, P. J.; Dondorp, A. M.; Day, N. P.; White, N. J.; Tracking Resistance to Artemisinin Collaboration. Spread of artemisinin resistance in *Plasmodium falciparum* malaria. *N. Engl. J. Med.* **2014**, *371*, 411−423.

(156) (a) Dubowchik, G. M.; Vrudhula, V. M.; Dasgupta, B.; Ditta, J.; Chen, T.; Sheriff, S.; Sipman, K.; Witmer, M.; Tredup, J.; Vyas, D. M.; Verdoorn, T. A.; Bollini, S.; Vinitsky, A. 2-Aryl-2,2-difluoroacetamide FKBP12 ligands: synthesis and X-ray structural studies. *Org. Lett.* **2001**, *3*, 3987−3990. (b) Bollini, S.; Herbst, J. J.; Gaughan, G. T.; Verdoorn, T. A.; Ditta, J.; Dubowchik, G. M.; Vinitsky, A. High-throughput fluorescence polarization method for identification of FKBP12 ligands. *J. Biomol. Screening* **2002**, *7*, 526−530.

(157) Ye, X. M.; Konradi, A. W.; Smith, J.; Aubele, D. L.; Garofalo, A. W.; Marugg, J.; Neitzel, M. L.; Semko, C. M.; Sham, H. L.; Sun, M.; Truong, A. P.; Wu, J.; Zhang, H.; Goldbach, E.; Sauer, J.-M.; Brigham, E. F.; Bova, M.; Basi, G. S. Discovery of a novel sulfonamide-pyrazolopiperidine series as potent and efficacious γ-secretase inhibitors (Part II). *Bioorg. Med. Chem. Lett.* **2010**, *20*, 3502−3506.

(158) Xiamuxi, H.; Wang, Z.; Li, J.; Wang, Y.; Wu, C.; Yang, F.; Jiang, X.; Liu, Y.; Zhao, Q.; Chen, W.; Zhang, J.; Xie, Y.; Hu, T.; Xu, M.; Guo, S.; Akber Aisa, H.; He, Y.; Shen, J. Synthesis and biological investigation of tetrahydropyridopyrimidinone derivatives as potential multi-receptor atypical antipsychotics. *Bioorg. Med. Chem.* **2017**, *25*, 4904−4916.

(159) (a) Zanda, M. Trifluoromethyl group: an effective xenobiotic function for peptide backbone modification. *New J. Chem.* **2004**, *28*, 1401−1411. (b) Sani, M.; Volonterio, A.; Zanda, M. The trifluoroethyl-amine function as peptide bond replacement. *ChemMedChem* **2007**, *2*, 1693−1700. (c) Brusoe, A. T.; Hartwig, J. F. Palladium-catalyzed arylation of fluoroalkylamines. *J. Am. Chem. Soc.* **2015**, *137*, 8460−8468.

(160) (a) Volonterio, A.; Bellosta, S.; Bravin, F.; Bellucci, M. C.; Bruche, L.; Colombo, G.; Malpezzi, L.; Mazzini, S.; Meille, S. V.; Meli, M.; Ramirez de Arellano, C.; Zanda, M. Synthesis, structure and conformation of partially-modified retro- and retro-inverso Ψ[NHCH-(CF₃)]Gly peptides. *Chem. - Eur. J.* **2003**, *9*, 4510−4522. (b) Molteni, M.; Pesenti, C.; Sani, M.; Volonterio, A.; Zanda, M. Fluorinated peptidomimetics: synthesis, conformational and biological features. *J. Fluorine Chem.* **2004**, *125*, 1735−1743. (c) Molteni, M.; Bellucci, M. C.; Bigotti, S.; Mazzini, S.; Volonterio, A.; Zanda, M. Ψ[CH(CF₃)NH]Gly-peptides: synthesis and conformation analysis. *Org. Biomol. Chem.* **2009**, *7*, 2286−2296.

(161) (a) Black, W. C.; Bayly, C. I.; Davis, D. E.; Desmarais, S.; Falgueyret, J.-P.; Leger, S.; Li, C. S.; Massé, F.; McKay, D. J.; Palmer, J. T.; Percival, M. D.; Robichaud, J.; Tsou, N.; Zamboni, R. Trifluoroethyl-amines as amide isosteres in inhibitors of cathepsin K. *Bioorg. Med. Chem. Lett.* **2005**, *15*, 4741−4744. (b) Li, C. S.; Deschenes, D.; Desmarais, S.; Falgueyret, J.-P.; Gauthier, J. Y.; Kimmel, D. B.; Léger, S.; Massé, F.; McGrath, M. E.; McKay, D. J.; Percival, M. D.; Riendeau, D.; Rodan, S. B.; Thérien, M.; Truong, V.-L.; Wesolowski, G.; Zamboni, R.;

Black, W. C. Identification of a potent and selective non-basic cathepsin K inhibitor. *Bioorg. Med. Chem. Lett.* **2006**, *16*, 1985−1989. (c) Gauthier, J. Y.; Chauret, N.; Cromlish, W.; Desmarais, S.; Duong, L.T.; Falgueyret, J.-P.; Kimmel, D. B.; Lamontagne, S.; Leger, S.; LeRiche, T.; Li, C. S.; Massé, F.; McKay, D. J.; Nicoll-Griffith, D. A.; Oballa, R. M.; Palmer, J. T.; Percival, M. D.; Riendeau, D.; Robichaud, J.; Rodan, G. A.; Rodan, S. B.; Seto, C.; Therien, M.; Truong, V.-L.; Venuti, M. C.; Wesolowski, G.; Young, R. N.; Zamboni, R.; Black, W. C. The discovery of odanacatib (MK-0822), a selective inhibitor of cathepsin K. *Bioorg. Med. Chem. Lett.* **2008**, *18*, 923−928. (d) Mullard, A. Merck & Co. drops osteoporosis drug odanacatib. *Nat. Rev. Drug Discovery* **2016**, *15*, 669.

(162) Isabel, E.; Mellon, C.; Boyd, M. J.; Chauret, N.; Deschênes, D.; Desmarais, S.; Falgueyret, J. P.; Gauthier, J. Y.; Khougaz, K.; Lau, C. K.; Léger, S.; Levorse, D. A.; Li, C. S.; Massé, F.; Percival, M. D.; Roy, B.; Scheigetz, J.; Thérien, M.; Truong, V. L.; Wesolowski, G.; Young, R. N.; Zamboni, R.; Black, W. C. Difluoroethylamines as an amide isostere in inhibitors of cathepsin K. *Bioorg. Med. Chem. Lett.* **2011**, *21*, 920−923.

(163) Butler, C. R.; Ogilvie, K.; Martinez-Alsina, L.; Barreiro, G.; Beck, E. M.; Nolan, C. E.; Atchison, K.; Benvenuti, E.; Buzon, L.; Doran, S.; Gonzales, C.; Helal, C. J.; Hou, X.; Hsu, M.-H.; Johnson, E. F.; Lapham, K.; Lanyon, L.; Parris, K.; O'Neill, B. T.; Riddell, D.; Robshaw, A.; Vajdos, F.; Brodney, M. A. Aminomethyl-derived beta secretase (BACE-1) inhibitors: engaging Gly230 without an anilide functionality. *J. Med. Chem.* **2017**, *60*, 386−402.

(164) (a) Chen, G.; Ren, H.; Turpoff, A.; Arefolov, A.; Wilde, R.; Takasugi, J.; Khan, A.; Almstead, N.; Gu, Z.; Komatsu, T.; Freund, C.; Breslin, J.; Colacino, J.; Hedrick, J.; Weetall, M.; Karp, G. M. Discovery of N-(4′-(indol-2-yl)phenyl)sulfonamides as novel inhibitors of HCV replication. *Bioorg. Med. Chem. Lett.* **2013**, *23*, 3942−3946. (b) Zhang, X.; Zhang, N.; Chen, G.; Turpoff, A.; Ren, H.; Takasugi, J.; Morrill, C.; Zhu, J.; Li, C.; Lennox, W.; Paget, S.; Liu, Y.; Almstead, N.; Njoroge, F. G.; Gu, Z.; Komatsu, T.; Clausen, V.; Espiritu, C.; Graci, J.; Colacino, J.; Lahser, F.; Risher, N.; Weetall, M.; Nomeir, A.; Karp, G. M. Discovery of novel HCV inhibitors: synthesis and biological activity of 6-(indol-2-yl)pyridine-3-sulfonamides targeting hepatitis C virus NS4B. *Bioorg. Med. Chem. Lett.* **2013**, *23*, 3947−3953. (c) Zhang, N.; Zhang, X.; Zhu, J.; Turpoff, A.; Chen, G.; Morrill, C.; Huang, S.; Lennox, W.; Kakarla, R.; Liu, R.; Li, C.; Ren, H.; Almstead, N.; Venkatraman, S.; Njoroge, F. G.; Gu, Z.; Clausen, V.; Graci, J.; Jung, S. P.; Zheng, Y.; Colacino, J. M.; Lahser, F.; Sheedy, J.; Mollin, A.; Weetall, M.; Nomeir, A.; Karp, G.M. Structure−activity relationship (SAR) optimization of 6-(indol-2-yl)pyridine-3-sulfonamides: identification of potent, selective, and orally bioavailable small molecules targeting hepatitis C (HCV) NS4B. *J. Med. Chem.* **2014**, *57*, 2121−2135.

(165) Fernandez, M. C.; Gonzalez-Garcia, M. R.; Liu, B.; Pfeifer, L. A. Phenyl Methanesulfonamide Derivatives Useful as MGAT-2 Inhibitors. World Patent Application WO-2013/112323 A1, Aug. 1, 2013.

(166) Frye, S. V.; Haffner, C. D.; Maloney, P. R.; Hiner, R. N.; Dorsey, G. F.; Noe, R. A.; Unwalla, R. J.; Batchelor, K. W.; Bramson, H. N.; Stuart, J. D.; Schweiker, S. L.; van Arnold, J.; Bickett, D. M.; Moss, M. L.; Tian, G.; Lee, F. W.; Tippin, T. K.; James, M. K.; Grizzle, M. K.; Long, J. E.; Croom, D. K. Structure-activity relationships for inhibition of type 1 and 2 human 5α-reductase and human adrenal 3β-hydroxy-Δ5-steroid dehydrogenase/3-keto-Δ5-steroid isomerase by 6-azaandrost-4-en-3-ones: optimization of the C17 substituent. *J. Med. Chem.* **1995**, *38*, 2621−2627.

(167) (a) di Salle, E.; Briatico, G.; Giudici, D.; Ornati, G.; Zaccheo, T.; Buzzetti, F.; Nesi, M.; Panzeri, A. Novel aromatase and 5α-reductase inhibitors. *J. Steroid Biochem. Mol. Biol.* **1994**, *49*, 289−294. (b) Giudici, D.; Briatico, G.; Cominato, C.; Zaccheo, T.; Ihelè, C.; Nesi, M.; Panzeri, A.; di Salle, E. FCE 28260, a new 5α-reductase inhibitor: in vitro and in vivo effects. *J. Steroid Biochem. Mol. Biol.* **1996**, *58*, 299−305. (c) di Salle, E.; Giudici, D.; Radice, A.; Zaccheo, T.; Ornati, G.; Nesi, M.; Panzeri, A.; Délos, S.; Martin, P. M. PNU 157706, a novel dual type I and II 5α-reductase inhibitor. *J. Steroid Biochem. Mol. Biol.* **1998**, *64*, 179−186. (d) Basileo, G.; Breda, M.; James, C. A. Determination of PNU-157706, a new dual inhibitor of 5α-reductase, in rat plasma by high-performance liquid chromatography with ultraviolet detection. *J. Chromatogr., Biomed. Appl.* **1998**, *719*, 191−197.

(168) (a) Drury, J. E.; Di Costanzo, L.; Penning, T. M.; Christianson, D. W. Inhibition of human steroid 5α-reductase (AKR1D1) by finasteride and structure of the enzyme-inhibitor complex. *J. Biol. Chem.* **2009**, *284*, 19786−19790. (b) Karnsomwan, W.; Rungrotmongkol, T.; De-Eknamkul, W.; Chamni, S. chamni, S. In silico prediction of human steroid 5α-reductase type II. *Med. Chem. Res.* **2016**, *25*, 1049−1056.

(169) (a) Howbert, J. J.; Grossman, C. S.; Crowell, T. A.; Rieder, B. J.; Harper, R. W.; Kramer, K. E.; Tao, E. V.; Aikins, J.; Poore, G. A. Novel agents effective against solid tumors: the diarylsulfonylureas. Synthesis, activities, and analysis of quantitative structure-activity relationships. *J. Med. Chem.* **1990**, *33*, 2393−2407. (b) Mohamadi, F.; Spees, M. M.; Grindey, G. B. Sulfonylureas: a new class of cancer chemotherapeutic agents. *J. Med. Chem.* **1992**, *35*, 3012−3016.

(170) (a) Houghton, P. J.; Houghton, J. A. Antitumor diarylsulfonylureas: novel agents with unfulfilled promise. *Invest. New Drugs* **1996**, *14*, 271−280. (b) Owa, T.; Nagasu, T. Novel sulfonamide derivatives for the treatment of cancer. *Expert Opin. Ther. Pat.* **2000**, *10*, 1725−1740. (c) Pasello, G.; Urso, L.; Conte, P.; Favaretto, A. Effects of sulfonylureas on tumor growth: a review of the literature. *Oncologist* **2013**, *18*, 1118−1125.

(171) Forouzesh, B.; Takimoto, C. H.; Goetz, A.; Diab, S.; Hammond, L. A.; Smetzer, L.; Schwartz, G.; Gazak, R.; Callaghan, J. T.; Von Hoff, D. D.; Rowinsky, E. K. A Phase I and pharmacokinetic study of ILX-295501, an oral diarylsulfonylurea, on a weekly for 3 weeks every 4-week schedule in patients with advanced solid malignancies. *Clin. Cancer Res.* **2003**, *9*, 5540−5549.

(172) (a) Toth, J. E.; Grindey, G. B.; Ehlhardt, W. J.; Ray, J. E.; Boder, G. B.; Bewley, J. R.; Klingerman, K. K.; Gates, S. B.; Rinzel, S. M.; Schultz, R. M.; Weir, L. C.; Worzalla, J. F. Sulfonimidamide analogs of oncolytic sulfonylureas. *J. Med. Chem.* **1997**, *40*, 1018−1025. (b) Chern, J. W.; Leu, Y. L.; Wang, S. S.; Jou, R.; Lee, C. F.; Tsou, P. C.; Hsu, S. C.; Liaw, Y. C.; Lin, H. M. Synthesis and cytotoxic evaluation of substituted sulfonyl-N-hydroxyguanidine derivatives as potential antitumor agents. *J. Med. Chem.* **1997**, *40*, 2276−2286.

(173) (a) Luzina, E. L.; Popov, A. V. Synthesis and anticancer activity of N-bis(trifluoromethyl)alkyl-N′-thiazolyl and N-bis(trifluoromethyl)-alkyl-N′-benzothiazolyl ureas. *Eur. J. Med. Chem.* **2009**, *44*, 4944−4953. (b) Luzina, E. L.; Popov, A. V. Anticancer activity of N-bis-(trifluoromethyl)alkyl-N′-(polychlorophenyl) and N′-(1,2,4-triazolyl) ureas. *Eur. J. Med. Chem.* **2010**, *45*, 5507−5512. (c) Luzina, E. L.; Popov, A. V. Synthesis, evaluation of anticancer activity and COMPARE analysis of N-bis(trifluoromethyl)alkyl-N′-substituted ureas with pharmacophoric moieties. *Eur. J. Med. Chem.* **2012**, *53*, 364−373.

(174) Métayer, B.; Compain, G.; Jouvin, K.; Martin-Mingot, A.; Bachmann, C.; Marrot, J.; Evano, G.; Thibaudeau, S. Chemo- and stereo-selective synthesis of fluorinated enamides from ynamides in HF/pyridine: second-generation approach to potent ureas bioisosteres. *J. Org. Chem.* **2015**, *80*, 3397−3410.

(175) (a) Mewshaw, R. E.; Marquis, K. L.; Shi, X.; McGaughey, G.; Stack, G.; Webb, M. B.; Abou-Gharbia, M.; Wasik, T.; Scerni, R.; Spangler, T.; Brennan, J. A.; Mazandarani, H.; Coupet, J.; Andree, T. H. New generation dopaminergic agents 4. Exploiting the 2-methyl chroman scaffold. Synthesis and evaluation of two novel series of 2-(aminomethyl)-3,4,7,9-tetrahydro-2H-pyrano [2,3-e]indole and indol-8-one derivatives. *Tetrahedron* **1998**, *54*, 7081−7108. (b) Mewshaw, R. E.; Verwijs, A.; Shi, X.; McGaughey, G. B.; Nelson, j. A.; Mazandarani, H.; Brennan, J. A.; Marquis, K. L.; Coupet, J.; Andree, T. H. New generation dopaminergic agents. 5. Heterocyclic bioisosteres that exploit the 3-OH-N1-phenylpiperazine dopaminergic template. *Bioorg. Med. Chem. Lett.* **1998**, *8*, 2675−2680. (c) Mewshaw, R. E.; Nelson, J. A.; Shah, U. S.; Shi, X.; Mazandarani, H.; Coupet, J.; Marquis, K.; Brennan, J. A.; Andree, T. H. New generation dopaminergic agents. 7. Heterocyclic bioisosteres that exploit the 3-OH-phenoxyethylamine D2 template. *Bioorg. Med. Chem. Lett.* **1999**, *9*, 2593−2598. (d) Mewshaw, R. E.; Zhao, R.; Shi, X.; Marquis, K.; Brennan, J. A.; Mazandarani, H.; Coupet, J.; Andree, T. H. New generation dopaminergic agents. Part 8: heterocyclic bioisosteres that exploit the

7-OH-2-(aminomethyl)chroman D$_2$ template. *Bioorg. Med. Chem. Lett.* **2002**, *12*, 271−274.

(176) Banks, J. W.; Batsanov, A. S.; Howard, J. A. K.; O'Hagan, D.; Rzepa, H. S.; Martin-Santamaria, S. The preferred conformation of α-fluoroamides. *J. Chem. Soc., Perkin Trans. 2* **1999**, 2409−2411.

(177) Olivato, P. R.; Guerrero, S. A.; Yreijo, M. H.; Rittner, R.; Tormena, C. F. Conformational and electronic interaction studies of 2-fluoro-substituted *N,N*-dimethylamides. *J. Mol. Struct.* **2002**, *607*, 87−99.

(178) Briggs, C. R. S.; O'Hagan, D.; Howard, J. A. K.; Yufit, D. S. The C-F bond as a tool in the conformational control of amides. *J. Fluorine Chem.* **2003**, *119*, 9−13.

(179) Winkler, M.; Moraux, T.; Khairy, H. A.; Scott, R. H.; Slawin, A. M. Z.; O'Hagan, D. Synthesis and vanilloid receptor (TRPV1) activity of the enantiomers of α-fluorinated capsaicin. *ChemBioChem* **2009**, *10*, 823−828.

(180) (a) Jones, C. R.; Baruah, P. K.; Thompson, A. L.; Scheiner, S.; Smith, M. D. Can. a C−H···O interaction be a determinant of conformation? *J. Am. Chem. Soc.* **2012**, *134*, 12064−12071. (b) Driver, R. W.; Claridge, T. D. W.; Scheiner, S.; Smith, M. D. Torsional and electronic factors control the C−H···O interaction. *Chem. - Eur. J.* **2016**, *22*, 16513−16521. (c) Koeller, S.; Thomas, C.; Peruch, F.; Deffieux, A.; Massip, S.; Léger, J.-M.; Desvergne, J.-P.; Milet, A.; Bibal, B. α-Halogenoacetanilides as hydrogen-bonding organocatalysts that activate carbonyl bonds: fluorine versus chlorine and bromine. *Chem. - Eur. J.* **2014**, *20*, 2849−2859. (d) Jaun, B.; Seebach, D.; Mathad, R. I. Note: Helix or no helix of β-peptides containing β³hAla(αF) residues? *Helv. Chim. Acta* **2011**, *94*, 355−361. (e) Chekhlov, A. N.; Aksinenko, A. Yu.; Pushin, A. N.; Sokolov, V. B. An unusually strong intramolecular C-H●●●N hydrogen bond in 3-(α-hydroperfluoroisobutyryl)-2-[(α-hydroperfluoroisobutyryl)imino]-1,3-thiazolidine. *Russ. Chem. Bull.* **1995**, *44*, 1531−1532. (f) Chekhlov, A. N. Crystal and molecular structure of 3-(α-hydroperfluoroisobutyryl)-2-[(α-hydroperfluoroisobutyryl)imino]-1,3-thiazolidine with an unusually short intramolecular C-H●●●N hydrogen bond. *Kristallografiya* **1995**, 842−847. (g) Brewitz, L.; Arteaga Arteaga, F.; Yin, L.; Alagiri, K.; Kumagai, N.; Shibasaki, M. Direct catalytic asymmetric Mannich-type reaction of α- and β-fluorinated amides. *J. Am. Chem. Soc.* **2015**, *137*, 15929−15939. (h) Brewitz, L.; Noda, H.; Kumagai, N.; Shibasaki, M. Structural and computational investigation of intramolecular N●●●H interactions in α- and β-fluorinated 7-azaindoline amides. *Eur. J. Org. Chem.* **2017**, DOI: 10.1002/ejoc.201701083.

(181) Jones, C. R.; Dan Pantos, G. D.; Morrison, A. J.; Smith, M. D. Plagiarizing proteins: enhancing efficiency in asymmetric hydrogen-bonding catalysis through positive cooperativity. *Angew. Chem., Int. Ed.* **2009**, *48*, 7391−7394.

(182) Unione, L.; Alcalá, M.; Echeverria, B.; Serna, S.; Ardá, A.; Franconetti, A.; Cañada, F. J.; Diercks, T.; Reichardt, N.; Jiménez-Barbero, J. Fluoroacetamide moieties as NMR spectroscopy probes for the molecular recognition of GlcNAc-containing sugars: modulation of the CH−π stacking interactions by different fluorination patterns. *Chem. - Eur. J.* **2017**, *23*, 3957−3965.

(183) (a) Depreux, P.; Lesieur, D.; Mansour, H. A.; Morgan, P.; Howell, H. E.; Renard, P.; Caignard, D.-H.; Pfeiffer, B.; Delagrange, P.; Guardiola, B.; Yous, S.; Demarque, A.; Adam, G.; Andrieux, J. Synthesis and structure-activity relationships of novel naphthalenic and bioisosteric related amidic derivatives as melatonin receptor ligands. *J. Med. Chem.* **1994**, *37*, 3231−3239. (b) Leclerc, V.; Fourmaintraux, E.; Depreux, P.; Lesieur, D.; Morgan, P.; Howell, H. E.; Renard, P.; Caignard, D.-H.; Pfeiffer, B.; Delagrange, P.; Guardiola-Lemaître, B.; Andrieux, J. Synthesis and structure-activity relationships of novel naphthalenic and bioisosteric related amidic derivatives as melatonin receptor ligands. *Bioorg. Med. Chem.* **1998**, *6*, 1875−1887. (c) Ettaoussi, M.; Sabaouni, A.; Rami, M.; Boutin, J. A.; Delagrange, P.; Renard, P.; Spedding, M.; Caignard, D.-H.; Berthelot, P.; Yous, S. Design, synthesis and pharmacological evaluation of new series of naphthalenic analogues as melatoninergic (MT$_1$/MT$_2$) and serotoninergic 5-HT$_{2C}$ dual ligands (I). *Eur. J. Med. Chem.* **2012**, *49*, 310−323. (d) Zlotos, D. P.; Riad, N. M.; Osman, M. B.; Dodda, B. R.; Witt-Enderby, P. A. Novel

difluoroacetamide analogues of agomelatine and melatonin: probing the melatonin receptors for MT1 selectivity. *MedChemComm* **2015**, *6*, 1340−1344.

(184) Qiu, X.-L.; Xu, X.-H.; Qing, F.-L. Recent advances in the synthesis of fluorinated nucleosides. *Tetrahedron* **2010**, *66*, 789−843.

(185) Noble, S.; Goa, K. L. Gemcitabine. A review of its pharmacology and clinical potential in non-small cell lung cancer and pancreatic cancer. *Drugs* **1997**, *54*, 447−472.

(186) Hui, C. K.; Lau, G.K. K. Clevudine for the treatment of chronic hepatitis B virus infection. *Expert Opin. Invest. Drugs* **2005**, *14*, 1277−1284.

(187) (a) Sofia, M. J.; Bao, S.; Chang, W.; Du, J.; Nagarathnam, D.; Rachakonda, S.; Reddy, P. G.; Ross, B. S.; Wang, P.; Zhang, H.-R.; Bansal, S.; Espiritu, C.; Keilman, M.; Lam, A. M.; Micolochick Steur, H. M.; Niu, C.; Otto, M. J.; Furman, P. A. Discovery of a β-D-2′deoxy-2′-α-fluoro-2′-β-C-methyluridine nucleotide prodrug (PSI-7977) for the treatment of hepatitis c virus. *J. Med. Chem.* **2010**, *53*, 7202−7218. (b) Appleby, T. C.; Perry, J. K.; Murakami, E.; Barauskas, O.; Feng, J.; Cho, A.; Fox, D., III; Wetmore, D. R.; McGrath, M. E.; Ray, A. S.; Sofia, M. J.; Swaminathan, S.; Edwards, T. E. Structural basis for RNA replication by the hepatitis C virus polymerase. *Science* **2015**, *347*, 771−775.

(188) Van Roey, P.; Salerno, J. M.; Chu, C.-K.; Schinazi, R. F. Correlation between preferred sugar ring conformation and activity of nucleoside analogues against human immunodeficiency virus. *Proc. Natl. Acad. Sci. U. S. A.* **1989**, *86*, 3929−3933.

(189) Gore, K. R.; Harikrishna, S.; Pradeepkumar, P. I. Influence of 2′-fluoro versus 2′-O-methyl substituent on the sugar puckering of 4′-C-aminomethyluridine. *J. Org. Chem.* **2013**, *78*, 9956−9962.

(190) Zeng, D.; Zhang, R.; Nie, Q.; Cao, L.; Shang, L.; Yin, Z. Discovery of 2′-α-C-methyl-2′-β-C-fluorouridine phosphoramidate prodrugs as inhibitors of hepatitis C virus. *ACS Med. Chem. Lett.* **2016**, *7*, 1197−1201.

(191) Pallan, P. S.; Prakash, T. P.; de Leon, A. R.; Egli, M. Limits of RNA 2′-OH mimicry by fluorine: crystal structure of bacillus halodurans RNase H bound to a 2′-FRNA:DNA hybrid. *Biochemistry* **2016**, *55*, 5321−5325.

(192) (a) Hinderaker, M. P.; Raines, R. T. An electronic effect on protein structure. *Protein Sci.* **2003**, *12*, 1188−1194. (b) Horng, J.-C.; Raines, R. T. Stereoelectronic effects on polyproline conformation. *Protein Sci.* **2006**, *15*, 74−83. (c) Bretscher, L. E.; Jenkins, C. L.; Taylor, K. M.; DeRider, M. L.; Raines, R. T. Conformational stability of collagen relies on a stereoelectronic effect. *J. Am. Chem. Soc.* **2001**, *123*, 777−778.

(193) Bacqué, E. Influence of fluorination at position 16 of antibacterial pristinamycins II. *Chimia* **2004**, *58*, 128−132.

(194) Erickson, J.; McLoughlin, J. I. Hydrogen bond donor properties of the difluoromethyl group. *J. Org. Chem.* **1995**, *60*, 1626−1631.

(195) (a) Walter, H.; Tobler, H.; Gribkov, D.; Corsi, D. Sedaxane, isopyrazam and solatenol: novel broad-spectrum fungicides inhibiting succinate dehydrogenase (SDH) - synthesis challenges and biological aspects. *Chimia* **2015**, *69*, 425−434. (b) Jeschke, P. Progress of modern agricultural chemistry and future prospects. *Pest Manage. Sci.* **2016**, *72*, 433−455.

(196) Goldberg, K.; Groombridge, S.; Hudson, J.; Leach, A. G.; MacFaul, P. A.; Pickup, A.; Poultney, R.; Scott, J. S.; Svensson, P. H.; Sweeney, J. Oxadiazoles isomers: all bioisosteres are not created equal. *MedChemComm* **2012**, *3*, 600−604.

(197) (a) Narjes, F.; Koehler, K. F.; Koch, U.; Gerlach, B.; Colarusso, S.; Steinkuhler, C.; Brunetti, M.; Altamura, S.; De Francesco, R.; Matassa, V. G. A designed P1 cysteine mimetic for covalent and non-covalent inhibitors of HCV NS3 protease. *Bioorg. Med. Chem. Lett.* **2002**, *12*, 701−704. (b) Di Marco, S.; Rizzi, M.; Volpari, C.; Walsh, M. A.; Narjes, F.; Colarusso, S.; De Francesco, R.; Matassa, V. G.; Sollazzo, M. J. Inhibition of the hepatitis C virus NS3/4A protease: the crystal structures of two protease-inhibitor complexes. *J. Biol. Chem.* **2000**, *275*, 7152−7157. (c) Ontoria, J. M.; Di Marco, S.; Conte, I.; Di Francesco, M. E.; Gardelli, C.; Koch, U.; Matassa, V. G.; Poma, M.; Steinkühler, C.; Volpari, C.; Harper, S. The design and enzyme-bound crystal structure

of indoline based peptidomimetic inhibitors of hepatitis C virus NS3 protease. *J. Med. Chem.* **2004**, *47*, 6443−6446.

(198) (a) Desiraju, G. R. The C-H···O hydrogen bond: structural implications and supramolecular design. *Acc. Chem. Res.* **1996**, *29*, 441−449. (b) Zafrani, Y.; Yeffet, D.; Sod-Moriah, G.; Berliner, A.; Amir, D.; Marciano, D.; Gershonov, E.; Saphier, S. Difluoromethyl bioisostere: examining the "lipophilic hydrogen bond donor" concept. *J. Med. Chem.* **2017**, *60*, 797−804. (c) Sessler, C. D.; Rahm, M.; Becker, S.; Goldberg, J. M.; Wang, F.; Lippard, S. J. CF$_2$H, a hydrogen bond donor. *J. Am. Chem. Soc.* **2017**, *139*, 9325−9332.

(199) Zheng, Z. B.; D'Andrea, S. V.; Sun, L.-Q.; Wang, A. X.; Chen, Y.; Bowsher, M.; Hiebert, S.; Friborg, J.; Falk, P.; Hernandez, D.; Yu, F.; Sheaffer, A. K.; Zhai, G.; Knipe, J. O.; Mosure, K.; Rajamani, R.; Ng, A.; Gao, Q.; Meanwell, N. A.; McPhee, F.; Scola, P. M. Sulfonamide inhibitors of hepatitis C virus NS3 protease bearing a novel P1 cyclopropyl difluoromethyl moiety. *ACS Med. Chem. Lett.*, **2018**,

(200) Lin, C.-W.; Dutta, S.; Asatryan, A.; Chiu, Y.-L.; Wang, H.; Clifton, J., II; Campbell, A.; Liu, W. Pharmacokinetics, safety, and tolerability of single and multiple doses of ABT-493: a first-in-human study. *J. Pharm. Sci.* **2017**, *106*, 645−651.

(201) Rodriguez-Torres, M.; Glass, S.; Hill, J.; Freilich, B.; Hassman, D.; Di Bisceglie, A. M.; Taylor, J. G.; Kirby, B. J.; Dvory-Sobol, H.; Yang, J. C.; An, D.; Stamm, L. M.; Brainard, D. M.; Kim, S.; Krefetz, D.; Smith, W.; Marbury, T.; Lawitz, E. GS-9857 in patients with chronic hepatitis C virus genotype 1−4 infection: a randomized, double-blind, dose-ranging phase 1 study. *J. Viral Hepatitis* **2016**, *23*, 614−622.

(202) (a) Xu, Y.; Prestwich, G. D. Concise synthesis of acyl migration-blocked 1,1-difluorinated analogues of lysophosphatidic acid. *J. Org. Chem.* **2002**, *67*, 7158−7161. (b) Xu, Y.; Qian, L.; Pontsler, A. V.; McIntyre, T. M.; Prestwich, G. D. Synthesis of difluoromethyl substituted lysophosphatidic acid analogues. *Tetrahedron* **2004**, *60*, 43−49.

(203) (a) Chowdhury, M. A.; Abdellatif, K. R. A.; Dong, Y.; Das, D.; Suresh, M. R.; Knaus, E. E. Synthesis of celecoxib analogues possessing an N-difluoromethyl-1,2-dihydropyrid-2-one 5-lipoxygenase pharmacophore: biological evaluation as dual inhibitors of cyclooxygenases and 5-lipoxygenase with anti-inflammatory activity. *J. Med. Chem.* **2009**, *52*, 1525−1529. (b) Yu, G.; Praveen Rao, P. N.; Chowdhury, M. A.; Abdellatif, K. R. A.; Dong, Y.; Das, D.; Velázquez, C. A.; Suresh, M. R.; Knaus, E. E. Synthesis and biological evaluation of N-difluoromethyl-1,2-dihydropyrid-2-one acetic acid regioisomers: dual Inhibitors of cyclooxygenases and 5-lipoxygenase. *Bioorg. Med. Chem. Lett.* **2010**, *20*, 2168−2173.

(204) Romanenko, V. D.; Kukhar, V. P. Fluorinated phosphonates: synthesis and biomedical application. *Chem. Rev.* **2006**, *106*, 3868−3935.

(205) (a) Blackburn, G. M.; Kent, D. E. A novel synthesis of R- and γ-fluoroalkylphosphonates. *J. Chem. Soc., Chem. Commun.* **1981**, 511−513. (b) Blackburn, G. M.; England, D. A.; Kolkmann, F. Monofluoro and difluoro-methylenebisphosphonic acids: isopolar analogues of pyrophosphoric acid. *J. Chem. Soc., Chem. Commun.* **1981**, 930−932.

(206) (a) Chambers, R. D.; O'Hagan, D.; Lamont, R. B.; Jaina, S. C. The difluoromethylenephosphonate moiety as a phosphate mimic: X-ray structure of 2-amino-1,1,-difluoroethylphosphonic acid. *J. Chem. Soc., Chem. Commun.* **1990**, 1053−1054. (b) Nieschalk, J.; Batsanov, A. S.; O'Hagan, D.; Howard, J. A. K. Synthesis of monofluoro- and difluoro-methylenephopshonate analogues of sn-glycerol-3-phosphate as substrates for glycerol-3-phosphate dehydrogenase and the X-ray structure of the fluoromethylenephosphonate moiety. *Tetrahedron* **1996**, *52*, 165−176. (c) O'Hagan, D.; Rzepa, H. S. Some influences of fluorine in bioorganic chemistry. *Chem. Commun.* **1997**, 645−652. (d) Thatcher, G. R. J.; Campbell, A. S. Phosphonates as mimics of phosphate biomolecules: Ab initio calculations on tetrahedral ground states and pentacoordinate intermediates for phosphoryl transfer. *J. Org. Chem.* **1993**, *58*, 2272−2281.

(207) Ivanova, M. V.; Bayle, A.; Besset, T.; Pannecoucke, X.; Poisson, T. New prospects toward the synthesis of difluoromethylated phosphate mimics. *Chem. - Eur. J.* **2016**, *22*, 10284−10293.

(208) (a) Bialy, L.; Waldmann, H. Inhibitors of protein tyrosine phosphatases: next-generation drugs? *Angew. Chem., Int. Ed.* **2005**, *44*, 3814−3839. (b) Combs, A. P. Recent advances in the discovery of competitive protein tyrosine phosphatase 1B inhibitors for the treatment of diabetes, obesity, and cancer. *J. Med. Chem.* **2010**, *53*, 2333−2344.

(209) (a) Smyth, M. S.; Ford, H., Jr.; Burke, T. R., Jr. A general method for the preparation of benzylic R,R-difluorophosphonic acids; non-hydrolyzable mimetics of phosphotyrosine. *Tetrahedron Lett.* **1992**, *33*, 4137−4140. (b) Ivanova, M. V.; Bayle, A.; Besset, T.; Poisson, T.; Pannecoucke, X. Copper-mediated formation of aryl, heteroaryl, vinyl and alkynyl difluoromethylphosphonates: a general approach to fluorinated phosphate mimics. *Angew. Chem., Int. Ed.* **2015**, *54*, 13406−13410. (c) Ivanova, M. V.; Bayle, A.; Besset, T.; Pannecoucke, X.; Poisson, T. Copper-mediated introduction of the CF$_2$PO(OEt)$_2$ motif: scope and limitations. *Chem. - Eur. J.* **2017**, *23*, 17318−17338.

(210) (a) Panigrahi, K.; Eggen, M.; Maeng, J.-H.; Shen, Q.; Berkowitz, D. B. The α,α-difluorinated phosphonate L-pSer-analogue: an accessible chemical tool for studying kinase-dependent signal transduction. *Chem. Biol.* **2009**, *16*, 928−936. (b) Arrendale, A.; Kim, K.; Choi, J. Y.; Li, W.; Geahlen, R. L.; Borch, R. F. Synthesis of a phosphoserine mimetic prodrug with potent 14−3-3 protein inhibitory activity. *Chem. Biol.* **2012**, *19*, 764−771.

(211) (a) Rye, C. S.; Baell, J. B. Phosphate isosteres in medicinal chemistry. *Curr. Med. Chem.* **2005**, *12*, 3127−3141. (b) Elliott, T. S.; Slowey, A.; Ye, Y.; Conway, S. J. The use of phosphate bioisosteres in medicinal chemistry and chemical biology. *MedChemComm* **2012**, *3*, 735−751. (c) Zhang, Y.; Borrel, A.; Ghemtio, L.; Regad, L.; Boije af Gennäs, G.; Camproux, A.-C.; Yli-Kauhaluoma, J.; Xhaard, H. Structural isosteres of phosphate groups in the protein data bank. *J. Chem. Inf. Model.* **2017**, *57*, 499−516.

(212) Dufresne, C.; Roy, P.; Wang, Z.; Asante-Appiah, E.; Cromlish, W.; Boie, Y.; Forghani, F.; Desmarais, S.; Wang, Q.; Skorey, K.; Waddleton, D.; Ramachandran, C.; Kennedy, B. P.; Xu, L.; Gordon, R.; Chan, C. C.; Leblanc, Y. The development of potent non-peptidic PTP-1B inhibitors. *Bioorg. Med. Chem. Lett.* **2004**, *14*, 1039−1042.

(213) Bahta, M.; Lountos, G. T.; Dyas, B.; Kim, S.-E.; Ulrich, R. G.; Waugh, D. S.; Burke, T. R., Jr. Utilization of nitrophenylphosphates and oxime-based ligation for the development of nanomolar affinity inhibitors of the *Yersinia pestis* outer protein H (YopH) phosphatase. *J. Med. Chem.* **2011**, *54*, 2933−2943.

(214) Morlacchi, P.; Mandal, P. K.; McMurray, J. S. Synthesis and in vitro evaluation of a peptidomimetic inhibitor targeting the Src homology 2 (SH2) domain of STAT6. *ACS Med. Chem. Lett.* **2014**, *5*, 69−72.

(215) Hakogi, T.; Yamamoto, T.; Fujii, S.; Ikeda, K.; Katsumura, S. Synthesis of sphingomyelin difluoromethylene analogue. *Tetrahedron Lett.* **2006**, *47*, 2627−2630.

(216) (a) Lapierre, J.; Ahmed, V.; Chen, M.-J.; Ispahany, M.; Guillemette, J. G.; Taylor, S. D. The difluoromethylene group as a replacement for the labile oxygen in steroid sulfates: a new approach to steroid sulfatase inhibitors. *Bioorg. Med. Chem. Lett.* **2004**, *14*, 151−155. (b) Liu, Y.; Ahmed, V.; Hill, B.; Taylor, S. D. Synthesis of a non-hydrolyzable estrone sulfate analogue bearing the difluoromethanesulfonamide group and its evaluation as a steroid sulfatase inhibitor. *Org. Biomol. Chem.* **2005**, *3*, 3329−3335.

(217) (a) Maltais, R.; Poirier, D. Steroid sulfatase inhibitors: a review covering the promising 2000−2010 decade. *Steroids* **2011**, *76*, 929−948. (b) Mostafa, Y. A.; Taylor, S. D. Steroid derivatives as inhibitors of steroid sulfatase. *J. Steroid Biochem. Mol. Biol.* **2013**, *137*, 183−198.

(218) Kotoris, C. K.; Chen, M.-J.; Taylor, S. D. Novel phosphate mimetics for the design of non-peptidyl inhibitors of protein tyrosine phosphatases. *Bioorg. Med. Chem. Lett.* **1998**, *8*, 3275−3280.

(219) Lomelino, C.; McKenna, R. Carbonic anhydrase inhibitors: a review on the progress of patent literature (2011−2016). *Expert Opin. Ther. Pat.* **2016**, *26*, 947−956.

(220) Blackburn, G. M.; Türkmen, H. Synthesis of α-fluoro- and α,α-difluoro-benzenemethanesulfonamides: new inhibitors of carbonic anhydrase. *Org. Biomol. Chem.* **2005**, *3*, 225−226.

(221) Naim, M. J.; Alam, O.; Alam, M. J.; Alam, P.; Shrivastava, N. A review on pharmacological profile of morpholine derivatives. *Int. J. Pharmacol. Pharm. Sci.* **2015**, *3*, 40−51.

(222) Morgenthaler, M.; Schweizer, E.; Hoffmann-Röder, A.; Benini, F.; Martin, R. E.; Jaeschke, G.; Wagner, B.; Fischer, H.; Bendels, S.; Zimmerli, D.; Schneider, J.; Diederich, F.; Kansy, M.; Müller, K. Predicting and tuning physicochemical properties in lead optimization: amine basicities. *ChemMedChem* **2007**, *2*, 1100−1115.

(223) Martin, R. E.; Plancq, B.; Gavelle, O.; Wagner, B.; Fischer, H.; Bendels, S.; Müller, K. Remote modulation of amine basicity by a phenylsulfone and a phenylthio group. *ChemMedChem* **2007**, *2*, 285−287.

(224) Geneste, P.; Hugon, I.; Reminiac, C.; Lamaty, G.; Roque, J. P. The pK_a of substituted 4-piperidones. *Bull. Soc. Chim. Fr.* **1976**, *5−6*, 845−846.

(225) Huang, H.; Hutta, D. A.; Rinker, J. M.; Hu, H.; Parsons, W. H.; Schubert, C.; DesJarlais, R. L.; Crysler, C. S.; Chaikin, M. A.; Donatelli, R. R.; Chen, Y.; Cheng, D.; Zhou, Z.; Yurkow, E.; Manthey, C. L.; Player, M. R. Pyrido[2,3-*d*]pyrimidin-5-ones: a novel class of antiinflammatory macrophage colony-stimulating factor-1 receptor inhibitors. *J. Med. Chem.* **2009**, *52*, 1081−1099.

(226) Gleave, R. J.; Beswick, P. J.; Brown, A. J.; Giblin, G. M. P.; Goldsmith, P.; Haslam, C. P.; Mitchell, W. L.; Nicholson, N. H.; Page, L. W.; Patel, S.; Roomans, S.; Slingsby, B. P.; Swarbrick, M. E. Synthesis and evaluation of 3-amino-6-aryl-pyridazines as selective CB$_2$ agonists for the treatment of inflammatory pain. *Bioorg. Med. Chem. Lett.* **2010**, *20*, 465−468.

(227) (a) Sundar, B. G.; Bailey, T. R.; Dunn, D.; Hostetler, G. A.; Chatterjee, S.; Bacon, E. R.; Yue, C.; Schweizer, D.; Aimone, L. D.; Gruner, J. A.; Lyons, J.; Raddatz, R.; Lesur, B. Novel morpholine ketone analogs as potent histamine H$_3$ receptor inverse agonists with wake activity. *Bioorg. Med. Chem. Lett.* **2012**, *22*, 1546−1549. (b) Zulli, A.; Aimone, L. D.; Mathiasen, J. R.; Gruner, J. A.; Raddatz, R.; Bacon, E. R.; Hudkins, R. L. Substituted phenoxypropyl-(R)-2-methylpyrrolidine aminomethyl ketones as histamine-3 receptor inverse agonists. *Bioorg. Med. Chem. Lett.* **2012**, *22*, 2807−2810.

(228) Garton, N. S.; Barker, M. D.; Davis, R. P.; Douault, C.; Hooper-Greenhill, E.; Jones, E.; Lewis, H. D.; Liddle, J.; Lugo, D.; McCleary, S.; Preston, A. G. S.; Ramirez-Molina, C.; Neu, M.; Shipley, T. J.; Somers, D. O.; Watson, R. J.; Wilson, D. M. Optimisation of a novel series of potent and orally bioavailable azanaphthyridine SYK inhibitors. *Bioorg. Med. Chem. Lett.* **2016**, *26*, 4606−4612.

(229) Ahmad, S.; Washburn, W. N.; Hernandez, A. S.; Bisaha, S.; Ngu, K.; Wang, W.; Pelleymounter, M. A.; Longhi, D.; Flynn, N.; Azzara, A. V.; Rohrbach, K.; Devenny, J.; Rooney, S.; Thomas, M.; Glick, S.; Godonis, H.; Harvey, S.; Zhang, H.; Gemzik, B.; Janovitz, E. B.; Huang, C.; Zhang, L.; Robl, J. A.; Murphy, B. J. Synthesis and antiobesity properties of 6-(4-chlorophenyl)-3-(4-((3,3-difluoro-1-hydroxycyclobutyl)methoxy)-3-methoxyphenyl)thieno[3,2-*d*]-pyrimidin-4(3*H*)-one (BMS-814580): a highly efficacious melanin concentrating hormone receptor 1 (MCHR1) inhibitor. *J. Med. Chem.* **2016**, *59*, 8848−8858.

(230) (a) Deliencourt-Godefroy, G.; Lopes, L. Family of Aryl, Heteroaryl, O-Aryl and O-Heteroaryl Carbasugars. World Patent Application WO 2012/160218, Nov. 29, 2012. (b) Chen, Z.-H.; Wang, R.-W.; Qing, F.-L. Synthesis and biological evaluation of SGLT2 inhibitors: *gem*-difluoromethylenated dapagliflozin analogs. *Tetrahedron Lett.* **2012**, *53*, 2171−2176.

(231) (a) Berry, C. B.; Bubser, M.; Jones, C. K.; Hayes, J. P.; Wepy, J. A.; Locuson, C. W.; Daniels, J. S.; Lindsley, C. W.; Hopkins, C. R. Discovery and characterization of ML398, a potent and selective antagonist of the D$_4$ receptor with *in vivo* activity. *ACS Med. Chem. Lett.* **2014**, *5*, 1060−1064. (b) Witt, J. O.; McCollum, A. L.; Hurtado, M. A.; Huseman, E. D.; Jeffries, D. E.; Temple, K. J.; Plumley, H. C.; Blobaum, A. L.; Lindsley, C. W.; Hopkins, C. R. Synthesis and characterization of a series of chiral alkoxymethyl morpholine analogs as dopamine receptor 4 (D$_4$R) antagonists. *Bioorg. Med. Chem. Lett.* **2016**, *26*, 2481−2488.

(232) Saurat, T.; Buron, F.; Rodrigues, N.; de Tauzia, M.-L.; Colliandre, L.; Bourg, S.; Bonnet, P.; Guillaumet, G.; Akssira, M.; Corlu, A.; Guillouzo, C.; Berthier, P.; Rio, P.; Jourdan, M.-L.; Bénédetti, H.; Routier, S. Design, synthesis, and biological activity of pyridopyrimidine scaffolds as novel PI3K/mTOR dual inhibitors. *J. Med. Chem.* **2014**, *57*, 613−631.

(233) Zhou, Q.; Ruffoni, A.; Gianatassio, R.; Fujiwara, Y.; Sella, E.; Shabat, D.; Baran, P. S. Direct synthesis of fluorinated heteroarylether bioisosteres. *Angew. Chem., Int. Ed.* **2013**, *52*, 3949−3952.

(234) Xue, F.; Li, H.; Delker, S. L.; Fang, J.; Martásek, P.; Roman, L. J.; Poulos, T. L.; Silverman, R. B. Potent, Highly selective, and orally bioavailable *gem*-difluorinated monocationic inhibitors of neuronal nitric oxide synthase. *J. Am. Chem. Soc.* **2010**, *132*, 14229−14238.

(235) Anderson, M. O.; Zhang, J.; Liu, Y.; Yao, C.; Phuan, P.-W.; Verkman, A. S. Nanomolar potency and metabolically stable inhibitors of kidney urea transporter UT-B. *J. Med. Chem.* **2012**, *55*, 5942−5950.

(236) Piotrowski, D. W.; Futatsugi, K.; Warmus, J. S.; Orr, S. T.M.; Freeman-Cook, K. D.; Londregan, A. T.; Wei, L.; Jennings, S. M.; Herr, M.; Coffey, S. B.; Jiao, W.; Storer, G.; Hepworth, D.; Wang, J.; Lavergne, S. Y.; Chin, J. E.; Hadcock, J. R.; Brenner, M. B.; Wolford, A. C.; Janssen, A. M.; Roush, N. S.; Buxton, J.; Hinchey, T.; Kalgutkar, A. S.; Sharma, R.; Flynn, D. A. Identification of tetrahydropyrido[4,3-*d*]pyrimidine amides as a new class of orally bioavailable TGR5 agonists. *ACS Med. Chem. Lett.* **2013**, *4*, 63−68.

(237) (a) Xing, L.; Blakemore, D. C.; Narayanan, A.; Unwalla, R.; Lovering, F.; Denny, R. A.; Zhou, H.; Bunnage, M. E. Fluorine in drug design: a case study with fluoroanisoles. *ChemMedChem* **2015**, *10*, 715−726. (b) Jeschke, P.; Baston, E.; Leroux, F. R. α-Fluorinated ethers as "exotic" entity in medicinal chemistry. *Mini-Rev. Med. Chem.* **2007**, *7*, 1027−1034.

(238) (a) Brameld, K. A.; Kuhn, B.; Reuter, D. C.; Stahl, M. Small molecule conformational preferences derived from crystal structure data. A medicinal chemistry focused analysis. *J. Chem. Inf. Model.* **2008**, *48*, 1−24. (b) Hehre, W. J.; Radom, L.; Pople, J. A. Molecular orbital theory of the electronic structure of organic compounds. XII. Conformations, stabilities, and charge distributions in monosubstituted benzenes. *J. Am. Chem. Soc.* **1972**, *94*, 1496−1504. (c) Anderson, G. M.; Kollman, P. A.; Domelsmith, L. N.; Houk, K. N. Methoxy group nonplanarity in *o*-dimethoxybenzenes. Simple predictive models for conformations and rotational barriers in alkoxyaromatics. *J. Am. Chem. Soc.* **1979**, *101*, 2344−2352.

(239) (a) Kapustin, E. G.; Bzhezovsky, V. M.; Yagupolskii, L. M. Torsion potentials and electronic structure of trifluoromethoxy- and trifluoromethylthiobenzene: an ab initio study. *J. Fluorine Chem.* **2002**, *113*, 227−237. (b) Horne, D. B.; Bartberger, M. D.; Kaller, M. R.; Monenschein, H.; Zhong, W.; Hitchcock, S. A. Synthesis and conformational analysis of α,α-difluoroalkyl heteroaryl ethers. *Tetrahedron Lett.* **2009**, *50*, 5452−5455.

(240) Hartz, R. A.; Ahuja, V. T.; Rafalski, M.; Schmitz, W. D.; Brenner, A. B.; Denhart, D. J.; Ditta, J. L.; Deskus, J. A.; Yue, E. W.; Arvanitis, A. G.; Lelas, S.; Li, Y.-W.; Molski, T. F.; Wong, H.; Grace, J. E.; Lentz, K. A.; Li, J.; Lodge, N. J.; Zaczek, R.; Combs, A. P.; Olson, R. E.; Mattson, R. J.; Bronson, J. J.; Macor, J. E. In vitro intrinsic clearance-based optimization of N^3-phenylpyrazinones as corticotropin-releasing factor-1 (CRF1) receptor antagonists. *J. Med. Chem.* **2009**, *52*, 4161−4172.

(241) (a) Massa, M. A.; Spangler, D. P.; Durley, R. C.; Hickory, B. S.; Connolly, D. T.; Witherbee, B.J.; Smith, M. E.; Sikorski, J. A. Novel heteroaryl replacements of aromatic 3-tetrafluoroethoxy substituents in trifluoro-3-(tertiaryamino)-2-propanols as potent inhibitors of cholesteryl ester transfer protein. *Bioorg. Med. Chem. Lett.* **2001**, *11*, 1625−1628. (b) Reinhard, E. J.; Wang, J. L.; Durley, R. C.; Fobian, Y. M.; Grapperhaus, M. L.; Hickory, B. S.; Massa, M. A.; Norton, M. B.; Promo, M. A.; Tollefson, M. B.; Vernier, W. F.; Connolly, D. T.; Witherbee, B.J.; Melton, M. A.; Regina, K. J.; Smith, M. E.; Sikorski, J. A. Discovery of a simple picomolar inhibitor of cholesteryl ester transfer protein. *J. Med. Chem.* **2003**, *46*, 2152−2168. (c) Mantlo, N. B.; Escribano, A. Update on the discovery and development of cholesteryl ester transfer protein inhibitors for reducing residual cardiovascular risk. *J. Med. Chem.* **2014**, *57*, 1−17.

(242) (a) Heinrich, T.; Böttcher, H.; Gericke, R.; Bartoszyk, G. D.; Anzali, S.; Seyfried, C. A.; Greiner, H. E.; van Amsterdam, C. Synthesis

and structure-activity relationship in a class of indolebutylpiperazines as dual 5-HT$_{1A}$ receptor agonists and serotonin reuptake inhibitors. *J. Med. Chem.* **2004**, *47*, 4684−4692. (b) Heinrich, T.; Böttcher, H.; Bartoszyk, G. D.; Schwartz, H.; Anzali, S.; März, J.; Greiner, H. E.; Seyfried, C. A. Bioisosterism of fluorine and cyano as indole substituents. Theoretical, in vitro and in vivo examination. *Chimia* **2004**, *58*, 143−147.

(243) (a) Altomonte, S.; Zanda, M. Synthetic chemistry and biological activity of pentafluorosulphanyl (SF$_5$) organic molecules. *J. Fluorine Chem.* **2012**, *143*, 57−93. (b) Sowaileh, M. F.; Hazlitt, R. A.; Colby, D. A. Application of the pentafluorosulfanyl group as a bioisosteric replacement. *ChemMedChem* **2017**, *12*, 1481−1490.

(244) (a) Hansch, C.; Leo, A.; Unger, S. H.; Kim, K. H.; Nikaitani, D.; Lien, E. J. Aromatic substituent constants for structure-activity correlations. *J. Med. Chem.* **1973**, *16*, 1207−1216. (b) Hansch, C.; Leo, A.; Taft, R. W. A survey of Hammett substituent constants and resonance and field parameters. *Chem. Rev.* **1991**, *91*, 165−195. (c) Lien, E. J.; Guo, Z.-R.; Li, R.-L.; Su, C.-T. Use of dipole moment as a parameter in drug-receptor interaction and quantitative structure-activity relationship studies. *J. Pharm. Sci.* **1982**, *71*, 641−655.

(245) Du, J.; Hua, G.; Beier, P.; Slawin, A. M. Z.; Woollins, J. D. Single crystal X-ray structural features of aromatic compounds having a pentafluorosulfuranyl (SF$_5$) functional group. *Struct. Chem.* **2017**, *28*, 723−733.

(246) Rouxel, C.; Le Droumaguet, C.; Macé, Y.; Clift, S.; Mongin, O.; Magnier, E.; Blanchard-Desce, M. Octupolar derivatives functionalized with superacceptor peripheral groups: synthesis and evaluation of the electron-withdrawing ability of potent unusual groups. *Chem. - Eur. J.* **2012**, *18*, 12487−12497.

(247) (a) Bowden, R. D.; Comina, P. J.; Greenhall, M. P.; Kariuki, B. M.; Loveday, A.; Philp, D. A new method for the synthesis of aromatic sulfurpentafluorides and studies of the stability of the sulfurpentafluoride group in common synthetic transformations. *Tetrahedron* **2000**, *56*, 3399−3408. (b) Savoie, P. R.; Welch, J. T. Preparation and utility of organic pentafluorosulfanyl-containing compounds. *Chem. Rev.* **2015**, *115*, 1130−1190. (c) von Hahmann, C. N.; Savoie, P. R.; Welch, J. T. Reactions of organic pentafluorosulfanyl-containing compounds. *Curr. Org. Chem.* **2015**, *19*, 1592−1618.

(248) Stump, B.; Eberle, C.; Schweizer, W. B.; Kaiser, M.; Brun, R.; Krauth-Siegel, R. L.; Lentz, D.; Diederich, F. Pentafluorosulfanyl as a novel building block for enzyme inhibitors: trypanothione reductase inhibition and antiprotozoal activities of diarylamines. *ChemBioChem* **2009**, *10*, 79−83.

(249) Altomonte, S.; Baillie, G. L.; Ross, R. A.; Riley, J.; Zanda, M. The pentafluorosulfanyl group in cannabinoid receptor ligands: synthesis and comparison with trifluoromethyl and tert-butyl analogues. *RSC Adv.* **2014**, *4*, 20164−20176.

(250) Sun, L.; Bera, H.; Chui, W. K. Synthesis of pyrazolo[1,5-*a*][1,3,5]triazine derivatives as inhibitors of thymidine phosphorylase. *Eur. J. Med. Chem.* **2013**, *65*, 1−11. (b) Sun, L.; Li, J.; Bera, H.; Dolzhenko, A. V.; Chiu, G. N. C.; Chui, W. K. Fragment-based approach to the design of 5-chlorouracil-linked-pyrazolo[1, 5-*a*][1,3,5]triazines as thymidine phosphorylase inhibitors. *Eur. J. Med. Chem.* **2013**, *70*, 400−410.

(251) Welch, J. T.; Lim, D. S. The synthesis and biological activity of pentafluorosulfanyl analogs of fluoxetine, fenfluramine, and norfenfluramine. *Bioorg. Med. Chem.* **2007**, *15*, 6659−6666.

(252) Moraski, G. C.; Bristol, R.; Seeger, N.; Boshoff, H. I.; Tsang, P. S. Y.; Miller, M. J. Preparation and evaluation of potent pentafluorosulfanyl-substituted anti-tuberculosis compounds. *ChemMedChem* **2017**, *12*, 1108−1115.

(253) Sansook, S.; Ocasio, C. A.; Day, I. J.; Tizzard, G. J.; Coles, S. J.; Fedorov, O.; Bennett, J. M.; Elkins, J. M.; Spencer, J. Synthesis of kinase inhibitors containing a pentafluorosulfanyl moiety. *Org. Biomol. Chem.* **2017**, *15*, 8655−8660.